UNIVERSITAT DE BARCELONA

The Dachsous/Fat/Four-jointed Signalling Coordinates the Uniform Orientation of Planar Cell Alignement in the *Drosophila* Abdominal Epithelium

Federica Mangione

Aquesta tesi doctoral està subjecta a la llicència ***Reconeixement- NoComercial – CompartirIgual 4.0. Espanya de Creative Commons***.

Esta tesis doctoral está sujeta a la licencia ***Reconocimiento - NoComercial – CompartirIgual 4.0. España de Creative*** **Commons.**

This doctoral thesis is licensed under the ***Creative Commons Attribution-NonCommercial-ShareAlike 4.0. Spain License.***

Programa de Doctorado del Departamento de Genética
Facultad de Biología
Universitat de Barcelona (UB)

TESIS DOCTORAL

The Dachsous/Fat/Four-jointed Signalling Coordinates the Uniform Orientation of Planar Cell Alignment in the *Drosophila* Abdominal Epithelium

Memoria presentada por

Federica Mangione

Para optar al grado de

Doctora por la Universitat de Barcelona (UB)

El Director	La Alumna	El Tutor
Dr. Enrique Martin-Blanco	Federica Mangione	Dr. Pedro Martinez

Barcelona, Septiembre 2016

Eadem Mutata Resurgo

Jakob Bernoulli

Acknowledgements

There are many who helped me, in one way or another, in the course of this long and often difficult PhD, and to whom thanks are due.

I thank my supervisor, Enrique, who gave me the opportunity to join his lab and let me working with the wonderful *Drosophila* histoblasts and to give me the freedom to develop this project. Thanks to help me in growing both scientifically and personally.
I also thank the JAE-CSIC for funding my PhD during these years.

Many people have provided me with many helpful suggestions for work or personal improvement and to them I also offer my thanks; Nic Tapon, Pedro Martinez, Jordi Casanova, Antonio Garcia-Bellido, Marco Milan, Florenci Serras among many others.
Special thanks go to David Strutt and Yohanns Bellaiche for kindly providing many of the fly stocks without which my project would have never been possible to carry on.

I'm deeply indebted to Nic Tapon for his extreme generosity and massive support and for giving me the opportunity to continue my scientific career in his Lab.
A special thank goes, also, to my Tutor Pedro for all his help and advices.

Particularly, I want to thank all the people of Enrique's Lab for their friendship and support. Thanks to all of you for all the laughs and funny moments we shared and for making the lab such a pleasant place to stay when we were together.
Maria, Amayra, Sofia, Carla, Ania, Sry, Irene. You know already how important you are for me. Thanks for sustained me in all these years and to be such great friends. Carol y Juanito (Juanation) thanks for all your advises and support. Katerina, thanks for all the laughs and the good time we spent together, including in your beautiful country.
Thanks to Delia, Gaelle, Kyra, Bea, Seb, Julien, Lidia, Anna for the many beers, coffees, lunches, discussions and laughs we had together.

Thanks, also, to the member of Nic's Lab: Tessa, JR, Anna, Max, Birgit, Nicola, Jen, Ieva, JohnW. Tessa, thanks a lot for all your help. Thanks to Mario, MC and George for all the nice Fridays at the PUB.

Special thanks also my family, my grandparents, my parents, my brother, his wife, and my adorable/loved nephews, Dante and Artù.

Luisa, the best friend ever! Thanks a lot for everything!

Most particularly, I thank my beloved Ale, for putting up with me when I have been at my most insufferable, for his deep love and support. Thanks, also, for all your help and assistance with the writing of this Thesis.

To my parents, grandparents and, of course,
to Ale

CONTENTS

INTRODUCTION 1

1. ASYMMETRY AND DIRECTIONALITY IN MORPHOGENESIS 3
2. EPITHELIAL TISSUES: CELL POLARIZATION 4
2.1 ARCHITECTURE AND APICAL-BASAL POLARITY OF EPITHELIAL MONOLAYERS 5
2.2 INTERCELLULAR JUNCTION ORGANIZATION, GEOMETRY AND REMODELLING 6
2. 3 PLANAR POLARITY WITHIN CELLS AND ITS COORDINATION WITH THE BODY AXES 9
3. PLANAR POLARITY PATHWAYS *IN DROSOPHILA* 10
3.1 THE CORE PLANAR POLARITY PATHWAY 11
3.2 THE DACHSOUS/FAT/FOUR-JOINTED PATHWAY 14
3.3 PLANAR POLARITY DURING MORPHOGENESIS 17
4. THE HIPPO PATHWAY *IN DROSOPHILA* 18
5. ORDERED CELL ARRANGEMENT AND PLANAR POLARITY 20
6. THE ABDOMINAL EPITHELIAL MONOLAYER AS A MODEL TO STUDY THE ORIENTATION OF CELL ALIGNMENT AND PLANAR POLARITY 22
6.1 MORPHOGENESIS OF THE ADULT ABDOMINAL EPIDERMIS: THE IMAGINAL HISTOBLASTS. 23
6.2 HISTOBLAST GROWTH AND PROLIFERATION DURING LARVAL AND PRE-PUPA STAGES 23
6.3 HISTOBLAST GROWTH AND EXPANSION DURING PUPATION 24
6.4 HISTOBLAST PATTERNING AND POLARITY DURING PUPATION 27

AIMS 31

MATERIALS AND METHODS 35

1. *DROSOPHILA* HUSBANDRY AND STOCKS MAINTENANCE 36
2. *IN VIVO* IMAGING OF PUPAL DEVELOPMENT 36
2.1 CONFOCAL LASER SCANNING MICROSCOPY (LSM) FOR IMAGE AND TIME-LAPSE ACQUISITION 36
2.2 STAGING PUPAE BEFORE IMAGING 37
2.3. PREPARING PUPAE FOR LIVE IMAGING DURING PUPATION 38
2.4. FOCUSING ON THE AIII SEGMENT 39
3. IMMUNOHISTOCHEMISTRY OF THE PUPAL EPIDERMIS 40
3.1 PREPARATION OF THE ABDOMINAL TISSUE FOR IMMUNOSTAINING 40
3.2. STAINING AND MOUNTING PROTOCOL OF FIXED ABDOMINAL EPITHELIA 40
4. THE GAL4/UAS BINARY SYSTEM 41
5. GENETIC MOSAICS INDUCED BY SITE-SPECIFIC MITOTIC RECOMBINATION 43
5.1. THE FLP/FRT BINARY SYSTEM FOR GENE INACTIVATION 43
5.2. FLP-OUT TO ASSESS AASYMMETRIC LOCALIZATION OF PROTEINS 45
5.3 THE FLP-OUT-GAL4 TECHNIQUE FOR GENE MODULATION 46
5.4. MUTANT ALLELES 47
6. IMAGE ANALYSIS 48
6.1 CELL ORIENTATION DYNAMICS FROM CELL JUNCTION OUTLINES 48
6.2. COMPOSITE CLONE DIAGRAMS 51
6.3 CLONAL ANALYSIS: 2D GEOMETRICAL AND SHAPE PARAMETERS FROM CLONE OUTLINES 51
6.4. CONTACT ANGLE AND CONTACT LENGTH MEASUREMENT 52
21. INTENSITY PROFILES PLOTS 52
7. STATISTICS 53

RESULTS 55

CHAPTER I 59

EPITHELIAL MORPHOGENESIS AND THE UNIFORM AXIAL ORIENTATION OF PLANAR CELL ALIGNMENT (PCA) IN THE MATURE TISSUE 61
1.1 LONG-TERM LIVE IMAGING OF THE ABDOMINAL EPITHELIAL MORPHOGENESIS DURING PUPATION 61
1.2 PROLIFERATION AND INTERCALARY GROWTH DURING EPITHELIAL EXPANSION 63
1.3 CELL-CELL INTERACTIONS INCREASE DURING TISSUE REMODELLING 67
1.4 CELLULAR ARRANGEMENTS AND THE UNIFORM ORIENTATION OF PLANAR CELL ALIGNMENT IN THE MATURE EPITHELIUM 69
1.5 AXIAL ORIENTATION OF PLANAR CELL ALIGNMENT DURING HISTOBLAST EXPANSION AND REMODELING 74
1.6 THE UNIFORM ORIENTATION OF PCA AND PLANAR CELL POLARITY (PCP) IN THE ABDOMINAL EPIDERMIS 79
SYNOPSIS 83

CHAPTER II 85

THE PCP SIGNALLING AND THE AXIAL ORIENTATION OF PCA 87
2.1 DACHSOUS IS EXPRESSED IN OPPOSING GRADIENTS ALONG THE A/P AXIS 87
2.2 FOUR-JOINTED OPPOSITE GRADIENTS DYNAMICS DURING EXPANSION AND REMODELLING 91
2.3 THE EMERGING AXIAL GRADIENT OF FAT 93
2.4 RECIPROCAL CROSS-REGULATION OF DS, FT AND FJ 94
2.5 STRABISMUS EXPRESSION PATTERN AND ITS LATE ASYMMETRY DURING MORPHOGENESIS 102
SYNOPSIS 105

CHAPTER III 107

THE DS/FT/FJ PATHWAY IS REQUIRED TO COORDINATE THE AXIAL UNIFORM ORIENTATION OF PCA 108
3.1 THE UNIFORM ORIENTATION OF PCA IS LOST IN *DS* PUPAE 108
3.2 LOCAL ORIENTATION OF PCA IN *FAT* AND *FOUR-JOINTED* 111
3.3 PERTURBATIONS OF THE DS/FT/FJ SIGNALING AFFECT THE UNIFORM ORIENTATION OF PCA AND REDUCE CELL SHAPE ANISOTROPY. 114
3.3 FAT EXPRESSION AND DACHS LOCALIZATION RESPOND TO PERTURBATIONS IN THE DS/FT/FJ SIGNALING 116
3.4 LOSS OF THE AXIAL UNIFORM ORIENTATION OF PCA CAUSES THE SWIRLING OF TRICHOMES IN *DS* AND *FT* MUTANTS 119
SYNOPSIS 123

CHAPTER IV 125

THE DS/FT/FJ SIGNALING COORDINATES PCA BY ORIENTED CELL-CELL CONTACT ADHESIVENESS 126
4.1 *DS*, *FT*, AND *FJ* CLONES OF CELLS MINIMIZE THE CONTACTS WITH *WT* CELLS WHEN JUXTAPOSED GENETICALLY 126
4.2 THE DIRECTIONAL ACTIVITY OF DS INFLUENCES CELL-CELL INTERACTIONS THROUGHOUT THE A COMPARTMENT 131
4.3 DIFFERENTIAL ADHESIVENESS DRIVES THE AXIAL ORIENTATION OF CELLS 135
4.4 DS/FT/FJ ACTIVITY AUTONOMOUS AND NON-AUTONOMOUS EFFECTS 139
4.5 *DS* AND *FT* CLONES DIFFERENTIALLY INFLUENCE THE ORIENTATION OF TRICHOME POLARITY 141
SYNOPSIS 144

CHAPTER V 147

HIPPO SIGNALING AND THE CONTROL OF GROWTH THROUGH YKI ACTIVITY IN THE *DROSOPHILA* ABDOMINAL EPIDERMIS **148**
5.1 YKI EXPRESSION PATTERN DURING TISSUE EXPANSION AND REMODELLING 148
5.2 *DIAP1* EXPRESSION PATTERN DURING TISSUE EXPANSION AND REMODELLING 150
5.3 *HIPPO* AND THE UPSTREAM CONTROL OF YKI IN THE ABDOMINAL EPITHELIUM 154

DISCUSSION **165**

1. THE UNIFORM ORIENTATION OF HISTOBLAST ALONG THE MAIN A/P AXIS 167
2. THE DS/FT/FJ PATHWAY AND PCA 169
3. EXPRESSION PATTERN DYNAMICS LINK THE DS/FT/FJ PATHWAY TO THE UNIFORM AXIAL ORIENTATION OF THE PCA 169
4. THE ATTAINMENT OF THE UNIFORM ORIENTATION OF PCA REQUIRES THE DS/FT/FJ PATHWAY 173
5. A CELL ADHESION CODE AT THE BASE OF THE ESTABLISHMENT OF PCA 174
6. DS, FT AND FJ MODULATE CELL-CELL CONTACT ALIGNMENTS AND INFLUENCE CELL SHAPE ANISOTROPY 176
7. DOES CELLS/TISSUE GROWTH (THE HIPPO PATHWAY) INFLUENCE PCA ORIENTATION? 179
8. THE DS/FT/FJ PATHWAY INPUTS IN PCA AND PCP 179
9. CONCLUDING REMARKS 181

CONCLUSIONS **183**

BIBLIOGRAPHY **187**

Introduction

Within multicellular organism, mature tissues and organs reach high degrees of order in the arrangement of their constituent cells. During morphogenesis the emergence of long-range order is subjected to multiple and multilevel developmental constrains. Complex series of temporal and spatial instructions must be integrated to account for reproducible and stereotyped mature tissue arrangements. A remarkable example is given by mature epithelial monolayers were cells are ringed together in specific morphologies via cell-cell adhesion and show highly organized planar patterns. Cells in epithelial tissue acquire a precise planar geometry that is often, if not always, unevenly aligned with the tissue axes. Little is still known on the cellular mechanisms governing the axial orientation of cell arrangement.

The research presented in this Thesis addressed this issue through the analysis of the developing pupal abdominal epithelium of *Drosophila melanogaster*.

1. Asymmetry and Directionality in Morphogenesis

The developmental course by which multicellular organisms shape from a single fertilized egg encompasses a diverse array of processes that transforms un-patterned populations of multiplying cells into distinct and specialized tissues and organs with highly organized morphologies.

The achievement of asymmetry is a fundamental process in development and its establishment and modulation are hallmarks in the path to adult organization. Indeed, one of the first tasks an animal embryo has to accomplish is the determination of its antero-posterior (A/P) and dorso-ventral (D/V) axes (Gray et al., 2011).

Symmetry-breaking events can be intrinsic and extrinsic. The establishment of the body axes is intrinsically triggered within the oocyte. For example, in *Drosophila* axes asymmetry is largely specified during the time course of oogenesis as a result of spatial heterogeneities in gene expression and activities (Roth and Lynch, 2009; St Johnston and Nusslein-Volhard, 1992). On the other hand, symmetry breaking can be influenced by spatial heterogeneities in the environment. Most higher plants develop a single major body axis in response to environmental gradients such as light and gravity, developing roots that grow below the ground and stem and leaves above it (Cove et al., 1999).

Beyond the essential role of early asymmetry in animal and plant ontogenesis, the progressive integration of local asymmetries is essential in the establishment of morphological diversity at all levels, tissues, organs and organisms as a whole. Throughout development, this integration is mediated by cell communication involving secreted factors and cell-cell contacts. In the context of multi-cellularity, signals, in the form of secreted (morphogens) or cell-bound molecules, do not act on single cells but on field of cells that first locally and then globally modify their behaviors (Vogg et al., 2016). In this scenario, directionality is essential as geometry is a basic constrain to be assumed during morphogenesis. Morphogenesis relies on the capacity of the cells to sense and transmit signals on a cell-to-cell base in specific directions. Single cells may be intrinsically asymmetric but in community between adjoining cells their asymmetries must harmonize to orient their positions or movements within particular directions in the space through developmental time. Without this sense of directionality most cells within tissues will fail to fulfill their functions (Hale and Strutt, 2015).

2. Epithelial Tissues: Cell polarization

Cell polarity is a form of asymmetry that underlies tissue morphogenesis. When, the cellular asymmetries are persistently and orderly distributed along a particular axis, the cell can be defined as polarized (Cove et al., 1999; Li and Bowerman 2010). In a multicellular context individual cell polarities mirror each other resulting in cell alignments, which orient within spatial coordinates.

Polarization of cell populations or tissues is most evident in the case of epithelia, in which cells develop a stable and contact-mediated asymmetry along their apical-basal axis soon after the onset of embryogenesis. This early polarity does not necessarily need to be oriented with the body axes (Grey et al., 2011).

The epithelia, often structured as monolayers, are essential constituents of multicellular organisms, formed in the first steps of embryogenesis. They sustain the shape the body and all short of morphogenetic movements. They are also structurally and functionally relevant throughout adult life. They line the internal and the external surface of the body, serve as chemical-physical barriers and provide structural support for physiological functions.

Irrespectively of their location within the body, epithelial tissues possess two structural features that are crucial for their function and integrity; their constituent cells exhibit a stable apical-basal (A/B) polarity and they are linked together by intercellular junctions connecting each cell to its immediate neighbors (Fristrom, 1988).

2.1 Architecture and Apical-Basal polarity of epithelial monolayers

Epithelial cells are mainly organized in three-dimensional monolayers. The apical and basal surfaces of these monolayers normally orient in such a way that the apical one faces the external environment (*i.e.* the exterior for the epidermis or the luminal space for tubular epithelia) and the basal one faces the internal organs or body cavities resting on an extracellular basal lamina (Schock and Perrimon, 2002). The epithelial A/B polarity is also reflected in the asymmetric distribution of both cell surface and cytoplasmic components; e.g. nuclei tend to lie basally whereas most of the time the Golgi apparatus positions apically, directing the sorting of vesicular and protein trafficking (Simons and Fuller, 1985). A most important consequence of A/B polarity is the differential distribution of specialized structural domains along the lateral surface of epithelial cells (the z-dimension) (Fig. 1A). The number, organization, components or relative positions of membrane domains may vary across the animal kingdom. However, their functions are highly conserved (Franke et al., 2009). Indeed the sequential deployment of these complexes is intrinsic to the establishment of the polarity.

The lateral domain of each epithelial cell can be broadly subdivided into two different domains, apical-lateral and basal-lateral, with distinct physiological and cellular functions. The apical-lateral surface is divided into a free apical plane and a sub-apical region that keeps defined contacts with neighboring cells. In *Drosophila*, epithelial polarization is established during early embryogenesis when apical and basal cellular domains segregate as a consequence of the assembly of protein complexes at specific positions (Tepass, 2001). The Marginal Zone (MZ), located in the sub-apical region, is defined by the accumulation of two protein complexes, the Crb (Crumbs) complex and the aPKC (atypical protein kinase C) complex which together modulate the localization of Bazooka (Baz, Par-3) (Genevet and Tapon, 2011; Bergstralh and St. Johnston, 2012) (Fig 1B). On the other hand, the basal-lateral domain is subdivided into a basal subdomain mostly involved in sustaining cell-matrix adhesions and a lateral domain providing further cell-cell contacts.

In fully differentiated epithelia, Adherens Junctions (AJs) constitute a circumferential belt located basal to the MZ. Its major function is to establish and maintain the adhesive contacts between cells that are essential for epithelial integrity. The Septate Junctions (SJs), the equivalent of the thigh junctions (TJs) in vertebrates (Bergstralh and St. Johnston, 2012) probably act as permeability barriers (Tepass, 2001). Notably, the relative arrangement of AJs and SJs/TJs typically differs between insect and vertebrate cells. In the former, the AJ usually localizes apically to SJs (Fig 1B), while in vertebrates the opposite is true (Bergstralh and St.

Johnston, 2012). A set of conserved proteins, Disc large (Dlg), lethal giant larvae (Lgl) and Scribble (Scrib) form part of the SJs and have been proposed to form a biochemical complex that controls and refines the segregation of apical and basal-lateral membrane domains (Bilder, 2000a; Bilder, 2000b).

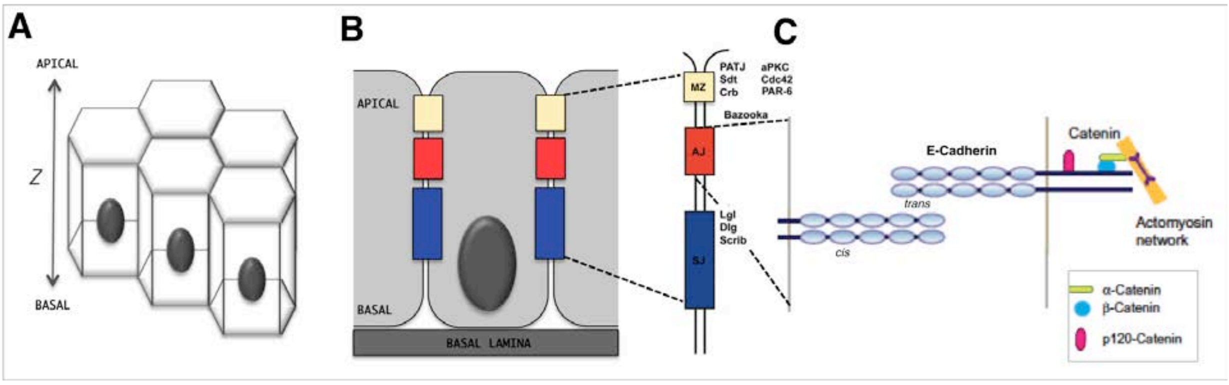

Fig. 1: Epithelial Apical-Basal Polarity. A) The A/B polarity specifies the z-dimension of an epithelium. **B)** (Left) Cartoon showing apical-lateral intercellular junctions in *Drosophila* epithelial cells. Right) zoom in the intercellular junctions and the key regulators of the A/B polarity (Adapted from Bergstralh and St. Johnston, 2012). **C)** Cartoon presenting E-Cadherin mediated cell adhesion at the AJs (Adapted from Priya and Yap, 2015). MZ: Marginal Zone; AJ: Adherens Junction; SJ: Septate Junction.

2.2 Intercellular junction organization, geometry and remodelling

The intercellular connections essential for epithelial tissue integrity, signalling transmission and physiology, are mostly mediated by adhesive molecules locally clustered at the AJs. Classical cadherins are highly conserved trans-membrane receptors of which E-cadherin (DE-Cadherin or *shotgun*, in *Drosophila*) is a universal component of the AJs. Lateral adhesiveness is mediated through E-Cadherins by homophilic interactions linking their extracellular domains amongst neighboring cells (Gumbiner, 2000) (Fig. 1C).

DE-Cadherin at its intracellular domain contains two regions, one binding Armadillo/β-catenin and the other binding to p120 catenin, an important cadherin regulator (Thoreson et al., 2000; Yap et al., 1998). Armadillo/β-catenin acts as an adaptor protein linking cadherins to the actin cytoskeleton via α-catenin directly (Gumbiner 2000; Wheelock and Johnson, 2003) or indirectly through actin-binding proteins (*i.e.* Vinculin). In this way, cell adhesion via classical cadherins couples neighboring cells cortices stabilizing epithelial architecture (Takeichi, 2014).

The simplest classification of epithelia is by cell proportions: a columnar epithelium contains tall cells with extended lateral domains; a cuboidal epithelium contains cells that are as high as they are wide; and a squamous epithelium contains flattened cells with extended apical domains (Davidson, 2012). Cell shape within an epithelium strongly depends on the AJs. E-cadherin-mediated adhesions tend to increase the surface of cell contacts, thus influencing the extent to which cells interact with their neighbors and cell shape (Collinet and Lecuit, 2013). This adhesive input mediated by the classical cadherins is coupled with the cortical actomyosin cytoskeleton linked to the cadherin itself. Although many cytoskeleton components are involved in the generation of cell, and thus tissue shape, including microtubules and intermediate filaments (Booth et al., 2014; Huber et al., 2014), cadherin-based adhesions and their associated contractile actomyosin meshwork appear to play the dominant role (Mao and Baum, 2015).

The geometrical diversity of the cells within epithelial monolayers is remarkable (Fig. 2). Despite this diversity, epithelial cells have a strong tendency to adopt hexagonal geometries (Thomson, 1921; Abbott and Lindenmayer, 1981; Classen et al., 2005). This packing topology can involve highly regular or isodiametric cells, or elongated (anisotropic) ones. Cell adhesion, controlled by the homotypic binding of E-cadherin between adjacent cells, is required for this regular geometrical arrangement, and loss of E-cadherin function results in a failure to establish and/or to maintain the epithelial organization of the tissue. The hexagonal packing is also perturbed when E-cadherin recycling through the endocytic pathway is prevented (Classen et al., 2005).

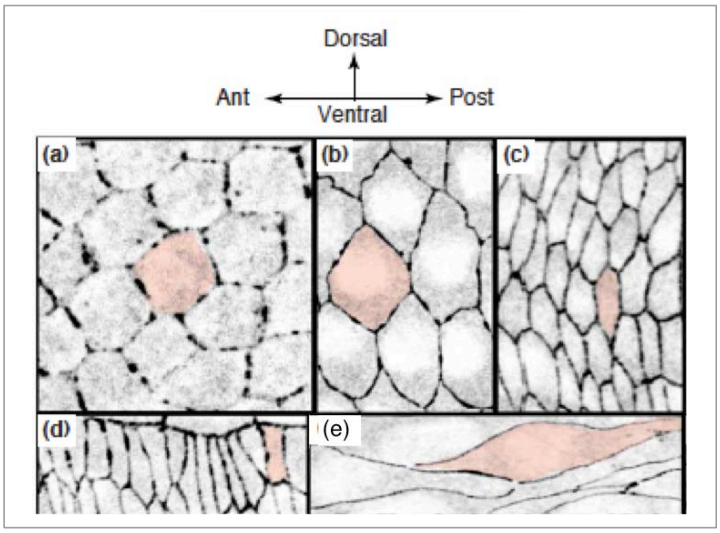

Fig. 2: Epithelial cell shape diversity. Epithelial cells outlined by Armadillo/b-catenin, a marker of AJs, are shown at different stages of a developing *Drosophila* embryo to illustrate the variety of cell shapes**. A-C)** Hexagonal patterns are frequent in early (A) and older (B, C) embryos. The hexagonal shape can be either isodiametric (A, B) or anisotropic (C), and the orientation of the hexagons depends on the tissue (A, B). **D)** Trapezoidal-squared epithelial shapes or elongated and curved shapes **(E)** are more rare. Adapted from Lecuit, 2005.

Besides homophilic interactions, the balance between different adhesive molecules may influence cells arrangements within tissues. A remarkable example is given by the peculiar shape adopted by the cone cells in the ommatidial unit of the Drosophila eye (Carthew, 2005). Differential expression of E- and N-Cadherin within the cone and the surrounding primary pigment cells is required to sculpt their proper shapes (Hayashi and Carthew, 2004) (Fig. 3).

The epithelial cells are remarkably plastic allowing shapes remodelling and positional changes relative to its neighbors while maintaining the integrity of the tissue. This plasticity mainly relies on their capacity to extensively modulate their adhesive contacts at the level of AJs. A classical example is given by the extension of the germ-band during *Drosophila* gastrulation (Zallen and Blankenship, 2008) (Fig. 4). During this process two related types of cell neighbouring exchanges occur; one involving groups of four cells (T1 transitions; Bertet et al., 2004) and another involving an extensive number of cells (Rosette formation; Blankenship et al., 2006). In both cases, the two main actors are the myosin-II, which promote cell cortex contraction, and DE-Cadherin, promoting junction extension (Fig. 4). Notably, the control of the orientation of junctional remodelling in the germ band is linked to the embryonic A/P patterning system (Bertet et al., 2004; Irvine and Wieschaus, 1994; Zallen and Wieschaus, 2004).

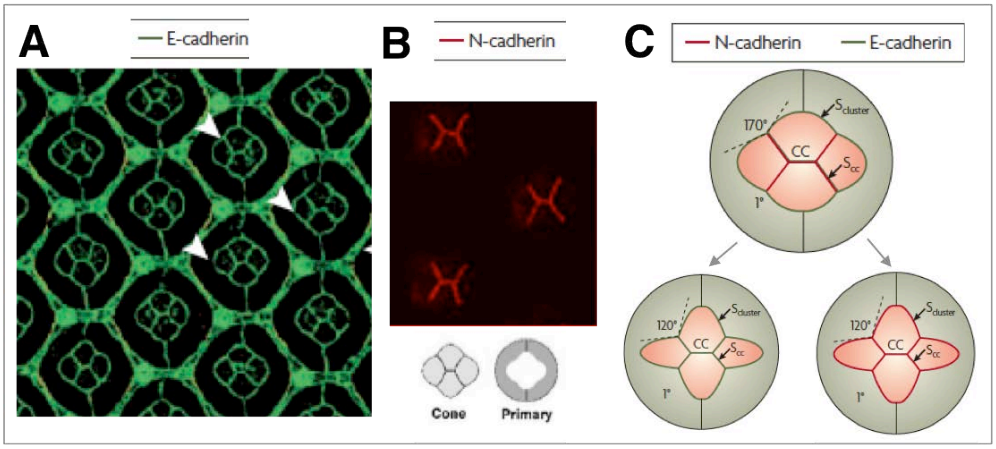

Fig. 3: Differential expression of classical cadherins influence cell shape geometry. A) The fly retinal epithelium is a highly ordered structure. Within each hexagonal ommatidial unit, the cone (arrowheads) and the two surrounding primary pigment cells express E-Cadherin at their AJs. **B)** (Top) N-Cadherin is specifically expressed in the cone cells (CC) junctions. Bottom) Cartoon showing the 4 CC and 2 primary pigment cells per ommatidium. **C**) (Top) CCs adopt a specific conformation in response to N-cadherin high levels (red), whereas all cells express E-cadherin (green). This up-regulation causes a minimization of the surface of the CC cluster ($S_{cluster}$) and an increment of the surface of contact between CCs (S_{cc}). Bottom) When N-cadherin is removed from the CCs (left) or when N-cadherin is overexpressed in all cells (right), cell adhesions become uniform and the surface of the CCs cluster increases and the CCs reduce their surface of contact. The contact angles between CCs get smaller and the geometry of the cluster changes. Adapted from Lecuit and Lenne, 2007; Gemp et al., 2011 and Hayashi and Carthew, 2005.

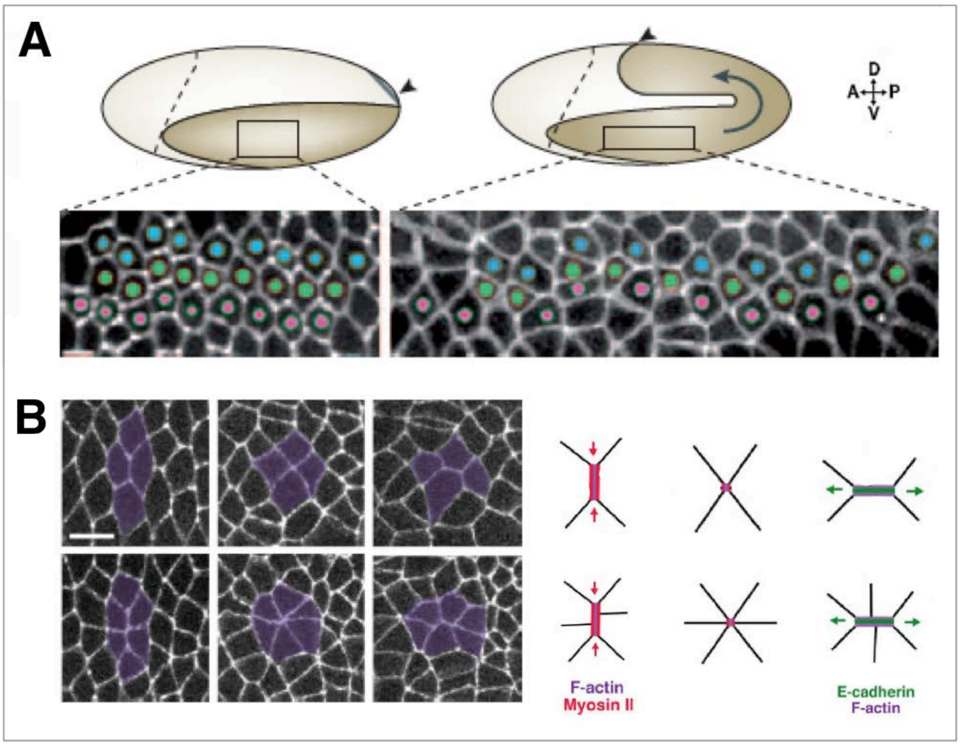

Fig. 4: Cell shape changes driven by junctional remodelling. A) (Top) Schematic diagrams showing the *Drosophila* embryonic epithelium undergoing germ-band extension (GBE). The posterior germ band tip moves towards the anterior-dorsal side of the embryo (arrowheads). Bottom) During GBE, epithelial cells (marked with E-cadherin, and highlighted with colored dots) exchange neighbors in a fast process that takes 30-40 minutes (Adapted from Lecuit and Lenne, 2007). **B)** Top-left) 4-cells undergoing a T1-based cell intercalation. Right) Cartoons of the three sequential steps of T1 transitions. Bottom-left) 6-cells undergoing intercalation through rosette formation. Right) Cartoons showing the three main steps of rosette formation and resolution (Adapted from Blankenship et al., 2006 and Vichas and Zallen, 2011)

2. 3 Planar polarity within cells and its coordination with the body axes

During development most, if not all, epithelial tissues acquire a second polarity axis, which entails cell polarization within the plane of the epithelium (Adler, 2002). This second form of polarity, known as planar cell polarity (PCP) (Nübler-Jung et al., 1987) is robustly coordinated amongst cells (Gao, 2012). The planar coordinates define the polarity axis that orient subcellular structures and allow cells to sense their angular orientations within the plane. PCP is readily apparent in the surface of many mature epithelia and applies to cells with diverse morphologies and physiological functions. e.g. PCP is obvious in the common alignment of fish scales, bird feathers and animal furs, as well as in the arrangement of cilia in internal organs such as the stereocilia bundles in the inner hear (Zallen, 2007; Wu and Mlodzik, 2009) (Fig. 5). In the adult *Drosophila* epidermis, individual and multicellular structures display PCP in the common orientation of trichomes (Fig. 5) and sensory bristles.

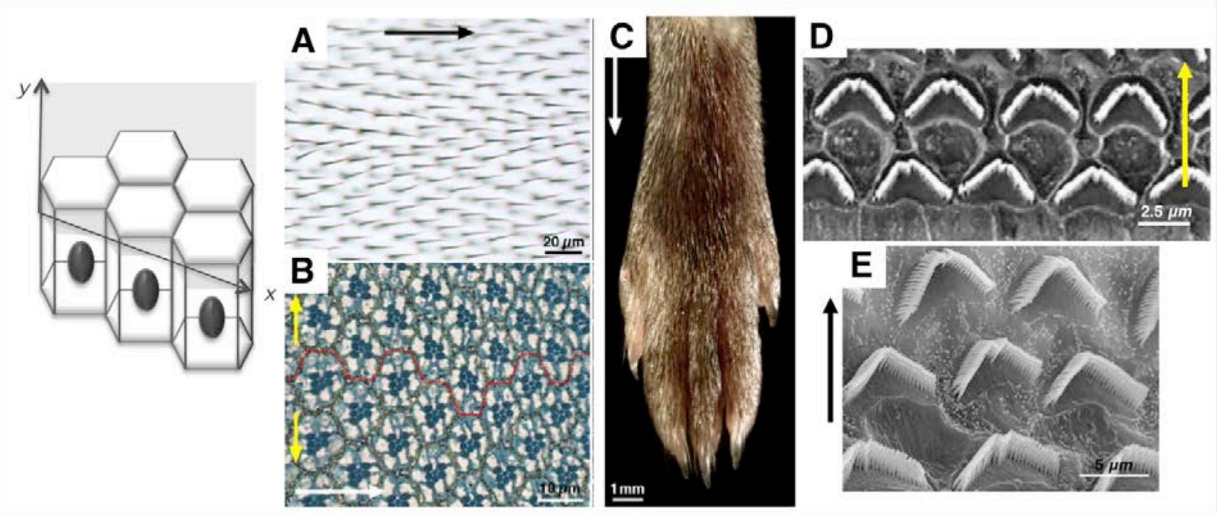

Fig. 5: **PCP in flies, mice and humans.** Left: Cartoon of the planar coordinates x and y for the expression of polarity within the cell and across tissues. **A)** Adult *Drosophila* wing surface. PCP is evident in the organization of trichomes on the proximo-distal (P/D) axis (black arrow). **B)** Sub-apical section through an adult *Drosophila* eye at the dorso-ventral (D/V) midline. The pigmented rhabdomeres (dark blue) of seven photoreceptors are in the centre of each hexagonal ommatidium. Ommatidia show mirror-image symmetry around the D/V midline (broken red line), revealing polarity on the antero-posterior (A-P, white arrow) and D-V (yellow arrows) axes. **C)** Distal end of an adult mouse leg, showing the P/D polarized arrangement of the fur. **D-E)** Scanning electron micrographs (SEMs) of hair bundles in the mouse (D) and in the human cochlea (E). PCP is evident in each cell where stereocilia form regularly organized arrays, with the apex of the stereocilia pointing in one direction (arrows). Adapted from Goodrich and Strutt, 2011 (A-to-C); Curtin et al., 2003 (D) and Schwander et al., 2010 (E).

The angle to which the planar polarity is aligned with the body axis appears to vary from tissue to tissue within the same organism. For instance, on the *Drosophila* dorsal thorax and abdomen both trichomes and bristles point posterior, while in the fly appendages such as the wings they point distally (Struhl et al., 1997a; Casal et al., 2002; Wong and Adler, 1993). What is invariant, however, is the consistent alignment of planar polarities with the body axes.

3. Planar polarity pathways *in Drosophila*

Two major properties are associated with the establishment and robustness of planar polarity: the first is the generation of intracellular asymmetries whose orientation is coordinated with neighbor cells via intercellular contacts. The second property is the concerted ordered alignment of cell polarity with the axis of the tissues, a coupling that, in many cases, has to be achieved among cells located hundreds of diameters apart. Two largely independent signaling pathways have emerged as main conserved cellular systems governing these different but generally linked features of planar polarity: the Core and the Ds/Ft/Fj planar polarity pathways.

3.1 The Core planar polarity pathway

The Core pathway, originally identified in *Drosophila* (for a review see Adler, 2012), comprises six highly conserved proteins whose mutations affect the planar polarity of epithelial cells (Fig. 6). They are recruited to the apical cell surface and subsequently unevenly localized within the apical plane of the epithelia.

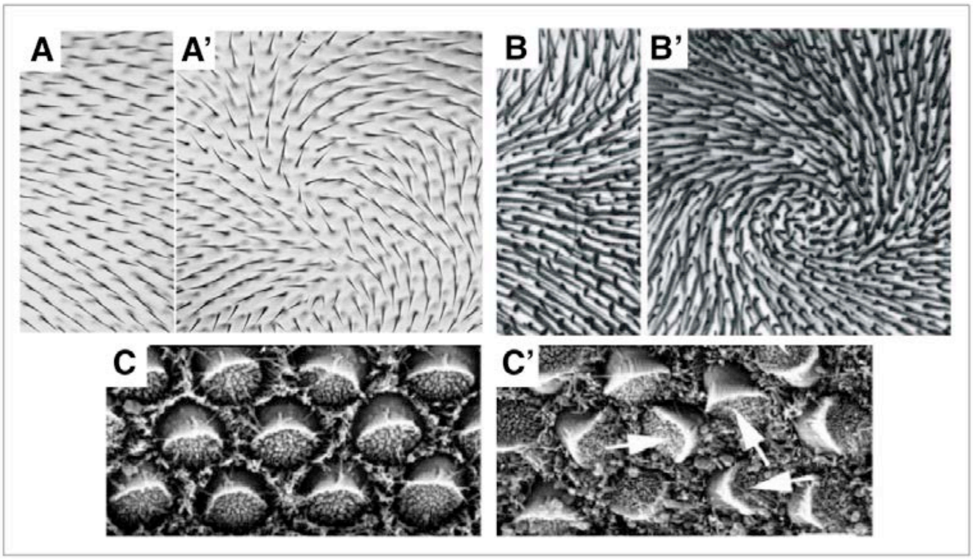

Fig. 6: **Alterations of PCP in Core mutants. A-A')** Trichome orientation in a *wt* (A) and mutant (A') *Drosophila* wing in which Flamingo (Fmi) was upregulated. **B)** Hair follicle orientation in the dorsal surface of a *wt* (B) and a f*rizzled* (*Fz6*$^{-/-}$) mouse paw. C) SEMs of the inner ear of a *wt* mouse (C) and a mouse homozygous for mutations in a vertebrate homologue of *flamingo* (C), called *crash* (*Crsh-/-*). Arrows point to the new polarity axis. Adapted from Takeichi et al., 2000; Wang and Nathans, 2007 (B-B'); Curtis et al., 2003 (C-C').

Three out of the six Core signaling components are trans-membrane proteins that asymmetrically distribute at the level of the AJs. In the wing, Frizzled (Fz) and Strabismus (Stbm, or Van Gogh) localizes at the opposite side of each cell, with Fz localizing distally (Fig. 7) and Stbm localizing proximally.

The atypical cadherin Flamingo (Fmi or Starry Night) localizes to both proximal and distal cell surfaces (Usui et al., 1999; Shimada et al., 2001). Fz associates with the cytoplasmic proteins Dishevelled (Dsh), and Diego (Dgo), which are also enriched distally (Axelrod, 2001; Strutt, 2001; Das et al., 2004), while Prickle (Pk) is enriched proximally, where Stbm preferentially localizes (Tree et al., 2002; Bastock et al., 2003).

The asymmetric segregation of Fz–Dsh–Fmi and Stbm–Pk–Fmi complexes to opposite sides of the cell relies on their mutual intracellular exclusion and their preferential binding affinities between neighboring cells (Fig. 7) (Tree et al., 2002; Chen et al., 2008; Seifert and Mlodzik, 2007; Strutt and Strutt, 2008). Importantly, depletion of any Core component results in a loss of asymmetry of all the others (Strutt and Strutt 2009).

The homophilic adhesion between cells mediated by the atypical cadherin Fmi is essential for the junctional recruitment of Fz and Stbm and the establishment of asymmetric complexes (Chen et al., 2008; Strutt and Strutt, 2008) (Fig. 7). In the wing the asymmetric localization of the Core proteins along the P/D axis is gradually achieved and become stably clustered into polarized complexes just before trichomes form (Classen et al., 2005; Aigouy et al., 2010; Strutt et al., 2011). The Core pathway is required for restricting the site of trichome shooting to the distal most part of the cells (Fig. 7). The trichomes then grow out away from the periphery pointing distally. In mutants defective for the core PCP proteins, wing trichomes initiate from a central location on the apical plane (i.e. actual loss of polarity) and subsequently point in inappropriate directions (Wong and Adler, 1993). Evidences for the instructive role of the Core pathway in polarity establishment comes from its directional non-autonomous effects on trichome polarity (Gubb and García-Bellido, 1982; Vinson and Adler, 1987; Taylor et al., 1998). Groups of cells that lack Fz induce neighboring cells to point their trichomes towards the mutant cells, whereas loss of Stbm causes neighboring cells to point their trichomes away in a directional fashion.

Although the Core pathway is able to locally coordinate polarity between cells, the long-range organization of PCP orientation requires additional inputs, of which one appears to be the Dachsous/Fat/Four-jointed pathway.

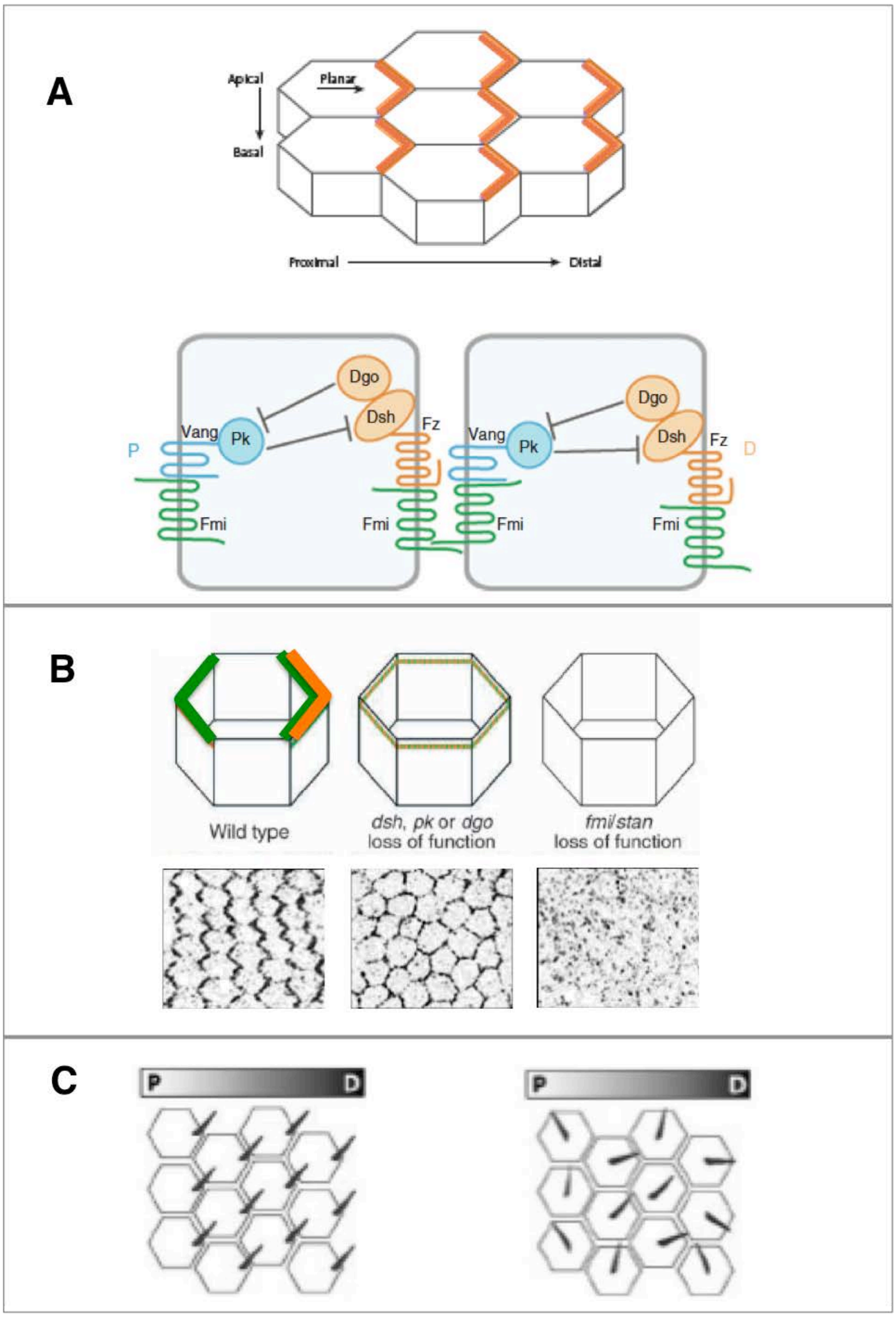
A
Apical
Planar
Basal
Proximal
Distal
Dgo
Dsh
Fz
Vang
Pk
P
D
Fmi
Fmi
Dgo
Dsh
Fz
Vang
Pk
Fmi
Fmi
B
Wild type
dsh, pk or dgo
loss of function
fmi/stan
loss of function
C
P
D
P
D

Fig. 7: **The Core Pathway in *Drosophila*. A)** (Top) Cartoon displaying *Drosophila* wing cells showing the polarization of Fz (orange) prior to trichome eversion. (Bottom) Asymmetric localization of the Core proteins across two wing disc cells: Fz–Dsh–Dgo–Fmi form a complex at the distal edges of cells, while the Vang–Pk–Fmi complex concentrates to proximal edges (from left to right). Fz binds to Stbm/Vang (blue) and this interaction is stabilized by Fmi (green). Dsh and Dgo (orange) physically interact and promote Fz–Dsh signaling antagonizing Pk (blue). **B)** At the top row are represented diagrams depicting the subcellular arrangements of PCP Core pathway components. At the bottom row the actual expression of Fz in the diverse conditions analyzed is presented (Left) *wt* wing cells showing Fmi (green) symmetric expression and Fz (orange) asymmetry. (Centre) Loss of core PCP components such as Dsh, Pk or Dgo blocks the formation of asymmetric P/D complexes resulting in even Fz and Stbm distribution around the cells periphery (*pk* mutants-bottom). (Right) Loss of Fmi largely blocks Fz and Stbm recruitment to the apical periphery (*fmi* mutants-bottom). **C)** Cartoons showing distally pointing trichomes in the *wt* (left) and swirling trichome patterns in mutants of the Core pathway (right). P/D indicates the proximo-distal axis. (Adapted from Hale and Strutt, 2015 (C and Top A); Strutt, 2003 (B); Singh and Mlodzik, 2012 (Bottom A).

3.2 The Dachsous/Fat/Four-jointed pathway

A second conserved signaling pathway also dedicated to the regulation of planar polarity is the Dachsous/Fat/Four-jointed (Ds/Ft/Fj) pathway. Mutants for this pathway randomize trichomes orientations in the *Drosophila* wings amongst other tissues (Fig. 8). The Ds/Ft/Fj pathway, unlike the Core pathway, is not exclusively involved in PCP regulation but it has also been linked to the control of tissue shape and growth control via the Hippo pathway.

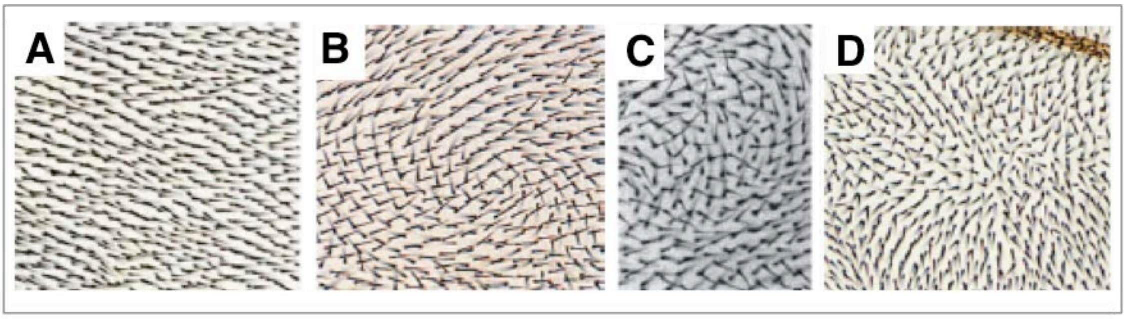

Fig. 8: **Aberrant PCP in the *Drosophila* wing in Ds/Ft/Fj mutants.** Examples of trichomes polarity in *wt* (**A), *ft* (B)**, *ds* **(C)** and in the Core mutant *dsh* **(D)**. Note the whirly polarity pattern of *ft* and *ds* compared to that of *dsh.* Adapted from Matis and Axelrod, 2013 (A, B and D) and Matakatsu and Blair, 2004 (C)

The Ds/Ft/Fj signaling mainly relies on three proteins: two large atypical cadherins, Dachsous and Fat, with 27 and 34 conserved extracellular cadherin domains, through which they heterophilically interact (Matakatsu and Blair, 2004; Saburi and McNeill, 2005) and a Golgi-kinase that phosphorylates specific domains of Ds and Fat as they transit through the Golgi apparatus (Brodsky and Steller, 1996; Ishikawa et al., 2008; Villano and Katz 1995; Zeidler et al. 2000; Strutt et al., 2004). The phosphorylation of Fat and Ds by Fj modulates the strength and stability of Ds/Ft heterodimeric interaction (Fig. 8). (Ishikawa et al., 2008; Hale et al., 2015; Brittle et al., 2010; Simon et al., 2010; Hale et al., 2015). The phosphorylation of Ft by Fj promotes Ft binding ability, while Ds phosphorylation by Fj decreases Ds ability to bind Ft (Brittle et al., 2010; Simon et al., 2010; Hale et al., 2015).

The Ds/Ft/Fj pathway holds all the right characters to be a major contributor to planar polarity establishment: tissue-wide asymmetric expression patterns (long-range) and asymmetric cell-to-cell interactions (Carvajal-Gonzalez and Mlodzik, 2014).

Two of its components, *fj* and *ds* are expressed in largely opposing gradients in the developing wing, eye and the adult abdomen (see Fig. 9) (Yang et al., 2002; Ma et al., 2003; Strutt and Strutt, 2002; Casal et al., 2002; Zeidler et al., 1999 and 2000; Brodsky and Steller 1996, Villano and Katz, 1995). Ft, however, shows a rather uniform expression both in the wing (Fig.

9) and in the eye (Strutt and Strutt 2002; Yang et al., 2002; Ma et al., 2003; Garoia et al., 2000). Its expression in the abdomen is unknown.

The transcriptional gradients of *fj* and *ds* prompt Ds and Ft to generate asymmetric interactions at the cell surface (Yang et al. 2002; Ma et al. 2003; Strutt and Strutt; 2002; Hale et al., 2015) in a way that is not completely understood. Ds and, to a lesser extent, Ft localize asymmetrically across the apical cell junctions (Ambegaonkar et al., 2012; Brittle et al., 2012; Bosveld et al., 2012) where they segregate to opposite cell edges (Fig. 9). Moreover, both in the wing and the eye, the phosphorylation of Ds and Ft by Fj modulates the stability of the interaction between Ds and Ft in a graded fashion (Hale et al., 2015). Overall, in a *fj* mutant background, the Ds/Ft complex is less stable. Expression of mutant forms of Ft or Ds in which the Fj phosphorylation sites were mutated well defines Fj function. Ds mutant interaction with Ft was more stable, while Ft mutant interaction with Ds was less (Hale et al., 2015; Collu and Mlodzik, 2015).

Clones of cells lacking Ds, Ft or Fj activities do not abolish PCP in individual cells either inside or outside the clone but promote opposing non-autonomous effects on the orientation of surrounding *wt* cells. *ft* and *fj* clones induce surrounding cells to “point” toward the clone, whereas *ds* clones reorient trichome polarity away from the mutant patch (Adler et al., 1998; Zeidler et al., 2000; Strutt et al., 2002; Casal et al., 2002 Ma et al., 2003; Lawrence et al., 2004; Casal et al., 2006). These non-autonomous effects on trichome polarity have been also observed in null mutant backgrounds of *fmi* or *fz* in the abdomen (Casal et al., 2006; Lawrence et al., 2007) (see also section 6.4).

The causes of Ds and Ft trichome swirling patterns are not understood (Zhu, 2009). Whether the Ds/Ft/Fj pathway directly influences trichomes growth or guide trichome orientations or alter other cellular features is not known.

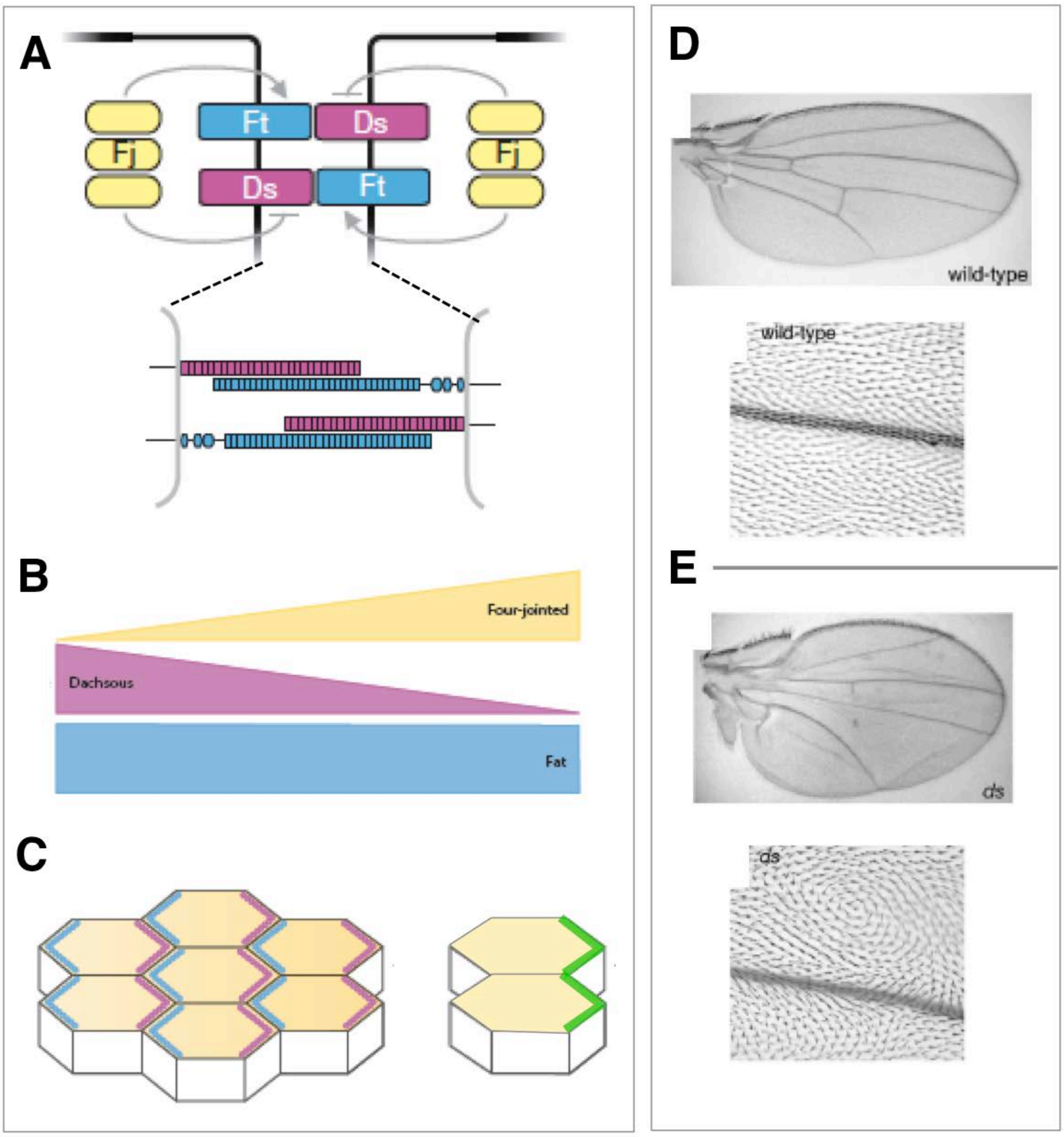

Fig. 9: **The Ds/Ft/Fj planar polarity pathway in *Drosophila*. A)** Ft and Ds are large atypical cadherins whose extracellular domains bind to each other heterophilically across cell membranes. Ft localizes proximally and Ds distally in each cell in the developing wing. Ft/Ds heterodimeric interaction is modulated by the Golgi-kinase Fj. Fj phosphorylates both Ft and Ds, producing opposing effects on Ds and Ft that modulates their interaction. **B)** Ds and Fj are expressed in complementary patterns in developing *Drosophila* tissues; here are shown the opposing gradients of Fj and Ds in the wing. Fj expression is low proximally and high distally opposing Ds. Ft is uniformly expressed. **C)** (Left) the complementary expression patterns of Ds and Fj result in their polarized localization and in the distal accumulation of D (right). **D)** (Top) Wild-type shape of an adult wing. (Bottom) From each cell a distally pointing trichome is generated in wt wings. **E)** (Top) Shape of an adult *ds* wing. Compared to wt, *ds* wings are enlarged in the antero-posterior axis. (Bottom) In *ds* mutant wings, coordination of cell polarity is lost and trichomes form swirling patterns. Adapted from Hale and Strutt, 2015 (A-Top, B-C); Goodrich and Strutt, 2011 (bottom A) and Thomas and Strutt, 2011 (D-E).

While several proteins are known to bind to the intracellular domains of Ft and Ds, the functional downstream effectors of the Ft/Ds pathway mediating PCP are not defined, (Thomas and Strutt, 2011; Sharma and McNeill, 2013; Carvajal-Gonzalez and Mlodzik, 2014). Two genes have been placed genetically downstream of the pathway: the atypical myosin *dachs* (*d*) (Mao et al., 2006), with no homologous in vertebrates, and the conserved transcriptional co-repressor *atrophin* (*atro* or *grunge*) (Fanto et al., 2013). D localizes asymmetrically in the wing (Fig. 9), eye and thorax cells in a Ds/Ft-dependent manner (Mao et al., 2006; Brittle et al., 2012; Bosveld et al., 2012; Ambegaonkar et al., 2012) and in clones lacking Ft or overexpressing Ds, D is strongly recruited to clone boundaries (Mao et al., 2006; Brittle et al., 2012; Bosveld et al., 2016). Whether D is recruited directly by Ds or indirectly through the action of Ds and Ft heterodimers is unclear. A potential function for Dachs in PCP establishment is elusive, mainly because its loss of function phenotype is very mild. The transcriptional co-repressor Atro does not show sign of asymmetric localization. However, *atro* loss-of-function mutant tissues do show cell non-autonomous polarity defects that resemble the loss of *ft* in the wing and in the eye (Fanto et al., 2003; Zhang et al., 2002). Atro physically interacts with the C-terminus of Ft; however, over-expression of a Ft construct lacking this domain is sufficient to rescue most *ft* phenotypes in the wing disc (Matakatsu and Blair, 2012) suggesting that other effectors rather than *atro* would be involved. Thus, the functional significance of Atro binding to Ft is unclear.

3.3 Planar Polarity during Morphogenesis

How PCP is achieved during morphogenesis in proliferating tissues and which are the roles of the Ds/Ft/Fj pathway in these processes and in tissue shape are open issues. In imaginal tissues in *Drosophila,* this problem has been mainly analyzed in two different models, the reshaping of the wing and the scutellum.

In the wing the trichome polarity emerges at the end of pupal morphogenesis (Turner and Adler, 1993; Wong and Adler 1993) and its preceded by the polarization of Core pathway components along the P/D axis (Strutt, 2001). Importantly, the orientation of the asymmetric localization of Core proteins (Classen et al., 2005; Sagner et al., 2012) is modulated during the remodelling of the pupal wing and is dynamically reoriented to finally align with the P/D axis as the hinge contracts mid-way through the pupal period (Aigouy et al., 2010; Merkel et al., 2014). Cells in the wing blade engage in a series of dynamic activities including the orientation of cell divisions, transient elongations, and polarized neighbors exchanges that promote the lengthening and narrowing of the tissue (Aigouy et al., 2010). Severing the hinge abolishes the cell elongation and disrupts the orientation of cell divisions and polarized rearrangements. This process is affected in Ds mutants and it has been then proposed that Ds couples the extrinsic mechanical forces generated by the hinge contraction to individual cells behaviour, specifically oriented division (Baena-Lopez et al, 2005; Mao et al., 2011) and transient cells elongation (Aigouy et al., 2010). The function of D in this process has not been tested yet. Alternatively it has been suggested that Ds may mediate the polarized transport of Fz along the P/D axis as, in Ds mutants, the orientation of the cortical microtubules in the pupal wing is affected (Shimada et al., 2006; Harumoto et al., 2010). Yet, this effect would be most probably indirect, as the intracellular domain of Ds does not contain catenin-binding domains that could link directly its function to the cortical cytoskeleton and no molecular bridges have been yet described for such interaction. Indeed, the distal wing gets polarized prior to hinge contraction (Aigouy et al., 2010) and does not display any obvious microtubule polarity (Harumoto et al., 2010).

In the thoracic scutellum, the shaping of the tissue correlates with strong asymmetries of D localization, which itself responds to the opposite gradients of *fj* and *ds* (Bosveld et al., 2012). The polarized Ds would recruit D and together they will modulate oriented cell rearrangements (but not division orientations) shaping the scutellum increasing junctional tension (Bosveld et al., 2012). In this context, the possible effects of the Ds/Ft/Fj pathway in the expression of planar polarity have not been evaluated yet.

4. The Hippo pathway *in Drosophila*

Extensive proliferation and cell growth are characteristics of epithelial tissue morphogenesis that must be tightly controlled in space and time for the achievement of proper morphologies and optimal physiological functions. The well-conserved Hippo pathway has emerged as a key cellular signalling for growth control (Harvey et al. 2003; Jia et al., 2003; Pantalacci et al., 2003; Udan et al., 2003; Wu et al., 2003; Huang et al., 2005). At the core of the pathway are two kinases, Hippo (Hpo) and Warts (Wts) and the transcriptional co-activator Yorkie (Yki). Hpo phosphorylates and activates Wts (Justice et al., 1995; Xu et al., 1995), which in turn phosphorylates and inactivates Yki (Huang et al., 2005; Dong et al., 2007). Yki positively regulates the expression of a wide range of genes involved in promoting cell growth, survival, proliferation and migration by binding and activating the transcription factor Scalloped (Sd) (Goulev et al. 2008; Wu et al. 2008; Zhang et al. 2008; Koontz et al., 2013). Yki is phosphorylated by Wts on three Serine residues, amongst which the most critical is Ser168 (Dong et al., 2007; Oh and Irvine, 2008; Zhang et al., 2008; Oh and Irvine, 2009).

Phosphorylation of Ser168 creates a binding site for 14-3-3 proteins. This negatively regulates Yki by keeping it localized in the cytoplasm preventing its transport to the nucleus (Dong et al., 2007; Oh and Irvine, 2008; Zhang et al., 2008). Fundamentally, one can think of the Hippo pathway as a constraint on Yki activity (reviewed in Oh and Irvine, 2010). *hpo* and *wts* mutants exhibit uncontrolled growth in multiple tissues due to excessive cell proliferation and reduced apoptosis as it does the overexpression of Yki (Udan et al., 2003; Huang et al., 2005) (Fig. 10).

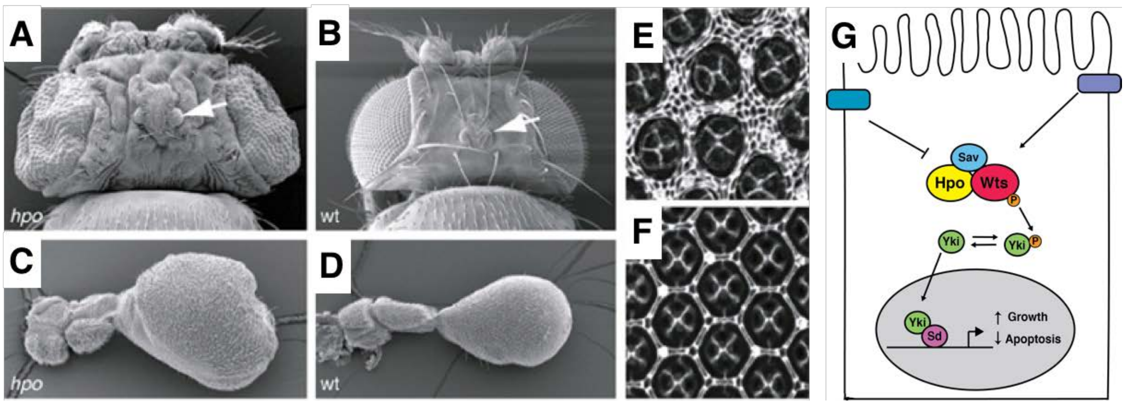

Fig. 10: The Hippo pathway in *Drosophila*. A-B) SEM images of the heads of flies mutant for *hpo* (A) and a *wt* (B). The mutant tissue is severely overgrown and folded. Ocelli (arrows), bristles and hairs differentiated normally. **C-D)** Equivalent images to A and B but for the halteres **E-F)** Mid-pupal retina stained with anti-Dlg antibodies to visualize cell outlines. *hpo* mutant mid-pupal retina shows excess inter-ommatidial cells (E) when compared with wt (F). **G)** Simplified schematic of the Hippo pathway. Multiple upstream inputs (blue and purple boxes) impinge positively (arrows) or negatively (blocked lines) into the Hpo/Sav/Wts core kinase cassette. The Hpo pathway controls tissue growth by regulating the subcellular localization of Yki, which when phosphorylated is cytoplasmic and unphosphorylated is nuclear. Yki associates with cognate transcription factors (Sd) to promote cell proliferation and inhibit apoptosis. Adapted from Udan et al., 2003 (A-to-F). Adapted from Parsons et al., 2014 (G).

A distinctive feature of Hippo signalling is the diverse and ever increasing number of inputs that can feed into the core kinase cassette. One of the main upstream regulators of Hpo/Wts is the apical protein Expanded (Ex) (Hamaratoglu et al., 2006). In addition to influencing Hippo activity, Ex binds directly to Yki tethering also to the cytoplasm, providing a potential alternate regulatory mechanism (Badouel et al., 2009; Oh et al., 2009).

Although The Hpo/Wts cascade is the main regulatory input in Yki (Meng et al., 2016), several lines of evidences have shown that Yki is also regulated by other extracellular and intracellular signals, as well as through complex cross talks with different signalling pathways (Piccolo et al., 2014; Hansen et al., 2015).

Interestingly, Fat has been linked to Hippo signalling. Fat influences the levels and localization of Hippo components, including Wts, Ex, and Yki (Bennett and Harvey, 2006;

Cho et al., 2006; Silva et al., 2006; Willecke et al., 2006; Tyler and Baker, 2007; Oh and Irvine, 2008) and phenocopies Hippo pathway mutants. Both lead to hypertrophy, up-regulating growth promoting factors such as Cyclin E and anti-apoptotic factors such as Diap1 in imaginal discs (Oh and Irvine, 2010). The influence of *ft* in the Hippo signalling is thought to be driven through *ex* (Bennett and Harvey, 2006; Silva et al., 2006; Willecke et al., 2006; Feng and Irvine, 2007) although their relationship needs to be clarified (Sharma and McNeill, 2013). Another way by which Ft can influence Hippo signalling is by its effects on *wts* via *dachs*. *ft* negatively regulates *d*, which in turn negatively regulates *wts*. This is supported by genetic epistasis studies placing *d* downstream of *ft* but upstream of *wts* (Oh and Irvine, 2010).

5. Ordered cell arrangement and planar polarity

In mature epithelia, individual cells of similar or distinct identities are packed together in quasi-two-dimensional arrays of varying complexity (Salbreux et al., 2012). This organization is of high functional relevance for tissue physiology.

The function of many epithelial tissues critically depends on the exact arrangement of their constituent cells. Sensory epithelia, like the vertebrate retina and inner ear, comprise an ordered array of photoreceptor or hair cells and supporting cells (McKenzie et al 2004, Wang et al., 2005) that must be precisely aligned to respond to mechanical perturbations caused by sound or motion (Roberts et al 1988). Indeed, the optical properties of vertebrate and invertebrate eyes depend on cellular arrangement. Small deviations in packing or aberrant spacing between photoreceptor cells within or between ommatidia would impinge proper photoreception. In the same way, the *Drosophila* wing is covered by an ordered array of trichomes, each constructed by a single wing epithelial cell. Trichomes are oriented distally and aligned in parallel to one another guiding the airflow over the surface of the wing during flight (Wootton 1992); regular hair spacing and orientation are clearly important for this function. In all these systems, well-ordered epithelia involve long-range planar polarity.

How epithelial cells adopt a regular arrangement and how such arrangements are iteratively achieved between siblings pose a fascinating biological problem. A related, yet poorly explored question is how such cell arrangements consistently align with the body axis. Cells not only align among each other to form a precise pattern but they due so in precise coordination to the body axis.

Epithelial populations tend to be more disordered in tissues undergoing cell intercalations or divisions (Zallen and Zallen, 2004; Gibson et al., 2006). Such tendency is characteristic of the morphogenetic movements of the early embryo. Later in development, as animals approach maturity, order tends to increase (Fig 11). In the *Drosophila* wing during pupal development, cells transit from a topologically disordered state to an ordered pattern of predominantly hexagonal cells aligned to the proximal-distal axis (Classen et al., 2005; Aigouy et al., 2010) (Fig. 11). Establishment of such ordered cellular array (in the wing) appears to be an active process that requires the coordinated action of PCP proteins, AJ components, and the vesicular trafficking machinery (Classen et al., 2005; Aigouy et al., 2010). Yet, mutations in Core PCP proteins do not completely block the ordering process (Classen et al, 2005), indicating that additional pathways must contribute to planar organization.

Remarkably, the packing arrangement does not seem to be determinant in order acquisition, as other arrangements are also characteristic of the mature epithelia. e.g. squared cells are the predominant topology in the zebrafish retina amongst other models (Santiago-Martinez et al., 2006; Chacon-Heszele et al., 2012; Salbreux et al., 2012) (Fig. 11). This suggests that the ordered arrangement *per se* is not intrinsically linked to the particular geometries a cell could acquired rather to the organized interactions of the cell to others.

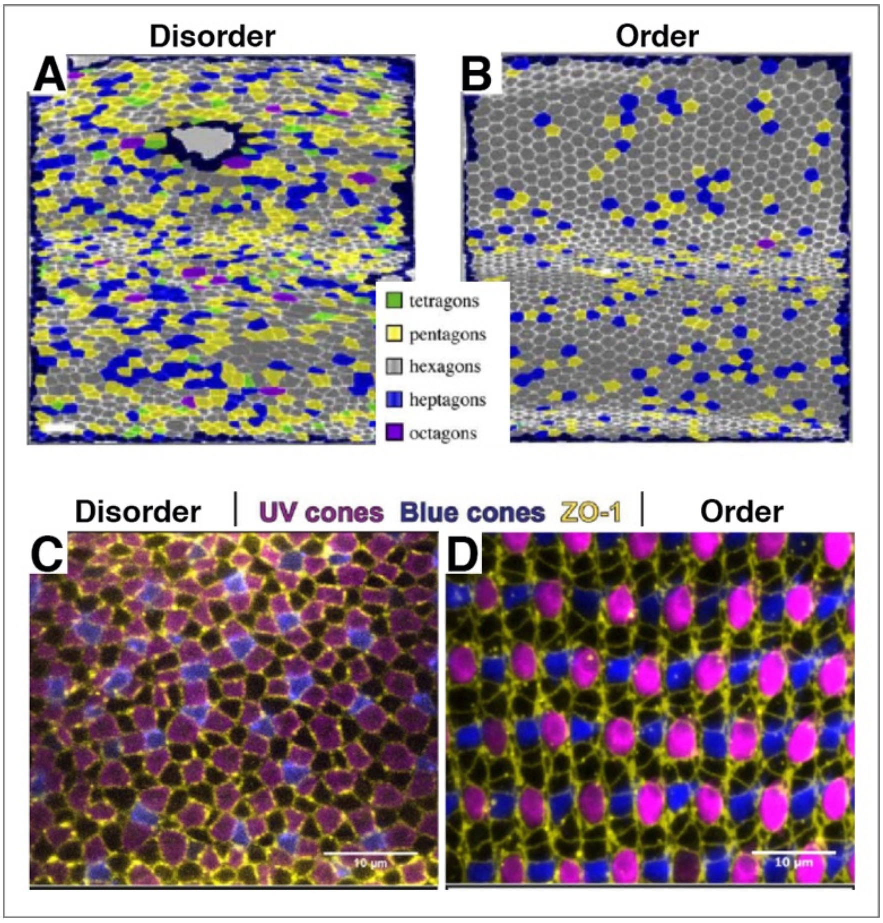

Fig. 11: **Changing in cell arrangements during development.** A-B) Ordering achievement amongst cells of identical fate. Image showing two steps of *Drosophila* wing pupal development showing increased order in the hexagonal packing characterizing the mature epithelium. A) early pupal wing cell shape geometries. B) Late-adult wing cell shape geometries. Cell outlines are marked with DE-Cadherin (grey) **C-D)** Tissue ordering by cells of different fate. Images showing two time points in the development of the zebrafish retina showing increased order toward a squared-like photoreceptors packing. The UV cone cells are magenta and the blue cone cells are blue. ZO-1 (Zonula Occludens 1) is a marker of the TJs in vertebrates that delineates apical cell outlines (yellow). Adapted from Classen et al., 2005 (A-B) and Salbreux et al., 2012 (B-C).

6. The abdominal epithelial monolayer as a model to study the orientation of cell alignment and planar polarity

The abdominal epidermis of *Drosophila* been defined as “the Antarctica of planar polarity research” (Strutt, 2009) as it has attracted very little attention. However, its unique mode of development, simple geometry and accessibility (Ninov and Martin-Blanco, 2007a) together with its completely uniform planar polarity (Struhl et al., 1997b; Lawrence et al., 2004) make this tissue particularly well suited for the dissection of planar polarity mechanisms through genetic analysis *in vivo*.

6.1 Morphogenesis of the adult abdominal epidermis: the imaginal histoblasts.

The fruit fly *Drosophila melanogaster* is a holometabolous insect undergoing complete metamorphosis (see Materials and Methods). Metamorphosis involves the full reshaping of the larva body plan (Robertson, 1936; Banbridge and Bownes, 1981). Most of the larval cells are removed and histolyzed while the adult body parts are shaped from groups of imaginal cells. The epidermal cells of the adult head, thorax and genitalia derive from sac-like structures called imaginal discs, whose growth and patterning initiate during larval stages and culminate half way through pupal development. The imaginal cells of the adult abdominal epidermis, however remain as an integral part of the epidermis and start growing and differentiate only after the initiation of pupariation.

The *Drosophila* abdomen consists of a chain of segments, each of which is divided into iterative anterior (A) and posterior (P) compartments. The adult abdominal epidermis of each segment develops from bilateral sets of diploid cells called abdominal histoblasts (Robertson, 1936), they are imaginal cells in intimate contact with large polyploid larval epithelial cells (LECs) (Madhavan and Schneiderman, 1977).

The histoblasts are segmentally specified during embryogenesis in stereotyped positions along the lateral side of each presumptive abdominal segment. There are four pairs of histoblast nests per segment: a pair of histoblast nest located ventro-laterally, the ventral nests, which specify the adult ventral pleura and sternite; two pairs of dorso-laterally located nests, anterior and posterior, from different compartments (Kornberg, 1981), which give rise to the tergite and the flexible inter-tergal membrane respectively; and two small spiracular nests located in between the dorsal and ventral nests, that contribute to the pleura connecting the dorsal and ventral epithelia (Madhavan and Schneiderman, 1977).

6.2 Histoblast growth and proliferation during larval and pre-pupa stages

Unlike the imaginal discs, histoblasts are arrested in the G2 phase of the cell cycle and do not proliferate during larval stages (Ninov et al., 2007 and 2009; Garcia-Bellido and Merriam, 1971; Guerra et al., 1972; Roseland and Schneiderman, 1979). Even though histoblasts appear to be refractory to mitotic stimuli (Kyisten and Saint, 1997), they accumulate Cyclin E (CycE, a G1 regulator protein) throughout larval stage (Fig. 12) (Ninov et al., 2009) while LECs increase in size by endo-replication of their nuclear content (Poodry, 1975; Pearson, 1974). Their diploid status is instead maintained from embryogenesis by *escargot* (*esg*) that suppresses the endo-replication of the DNA occurring in the larval cells (Whiteley et al., 1992; Hayashi et al., 1993; Fuse et al., 1994).

At the onset of metamorphosis (*i.e.* 0 h APF or pupariation), in response to the ecdysone pulse that trigger metamorphosis (Thummel, 2001), histoblasts start proliferating rapidly (Madhavan and Madhavan, 2004; Ninov et al., 2007) (Fig. 12). Both histological and *in vivo* analysis revealed that this initial increase in cell number is mediated by three rapid and synchronic cycles (around 2.5 h each) the last of which is occurring at about 8 h APF (Ninov et al., 2007; Madhavan and Madhavan, 1980; Roseland and Schneiderman, 1979; Guerra et al., 1973; Madhavan and Schneiderman, 1977). During this time histoblasts divide without inter-mitotic growth (*i.e.* bypass G1) in the absence of LECs extrusion reducing markedly in size and adopting a columnar/pseudo-stratified arrangement (Ninov et al., 2007; Roseland and Schneiderman, 1979; Madhavan and Madhavan, 1980).

Genetic analyses *in vivo* showed that the Ecdysone pulse at the onset of metamorphosis is required for the expression of the G2-M regulator String/cdc25 and thus the relief of histoblast G2 arrest (Ninov et al., 2007 and 2009).

6.3 Histoblast growth and expansion during pupation

A second Ecdysone pulse, approximately at 12 h APF, defines the transition from pupariation-to-pupation (*i.e.* the formation of the pupa) (Thummel, 2001) and it is concurrent with a decrease in histoblasts division speed, the onset of histoblast expansion and LECs removal by apoptosis (Ninov et al., 2007; Roseland and Schneiderman, 1979; Madhavan and Madhavan, 2004). By this time histoblasts experience an increase in cell cycle length (2.5-to-8 hours) once larval CycE is exhausted and inter-mitotic growth is restored (Fig. 12) (Ninov et al., 2007; Madhavan and Madhavan, 1980; Roseland and Schneiderman, 1979). Much later, histoblast proliferation slows down and decays at about 26-30 hours APF (Guerra et al., 1972; Garcia-Bellido and Merriam, 1971). This second phase of development is modulated by the EGFR and PI3K signaling, which lead to growth and cell cycle progression (Ninov et al., 2009; Madhavan and Madhavan, 1995). From 16 h APF, in synchrony with the decrease in the rate of the cell cycle, nests initiate expansion and invade the territories occupied by the LECs that become apoptotic (Ninov et al., 2007; Bischoff; Roseland and Schneiderman, 1979). By the onset of expansion (16 hours APF) histoblasts and LECs experiences dramatic changes in their behavior.

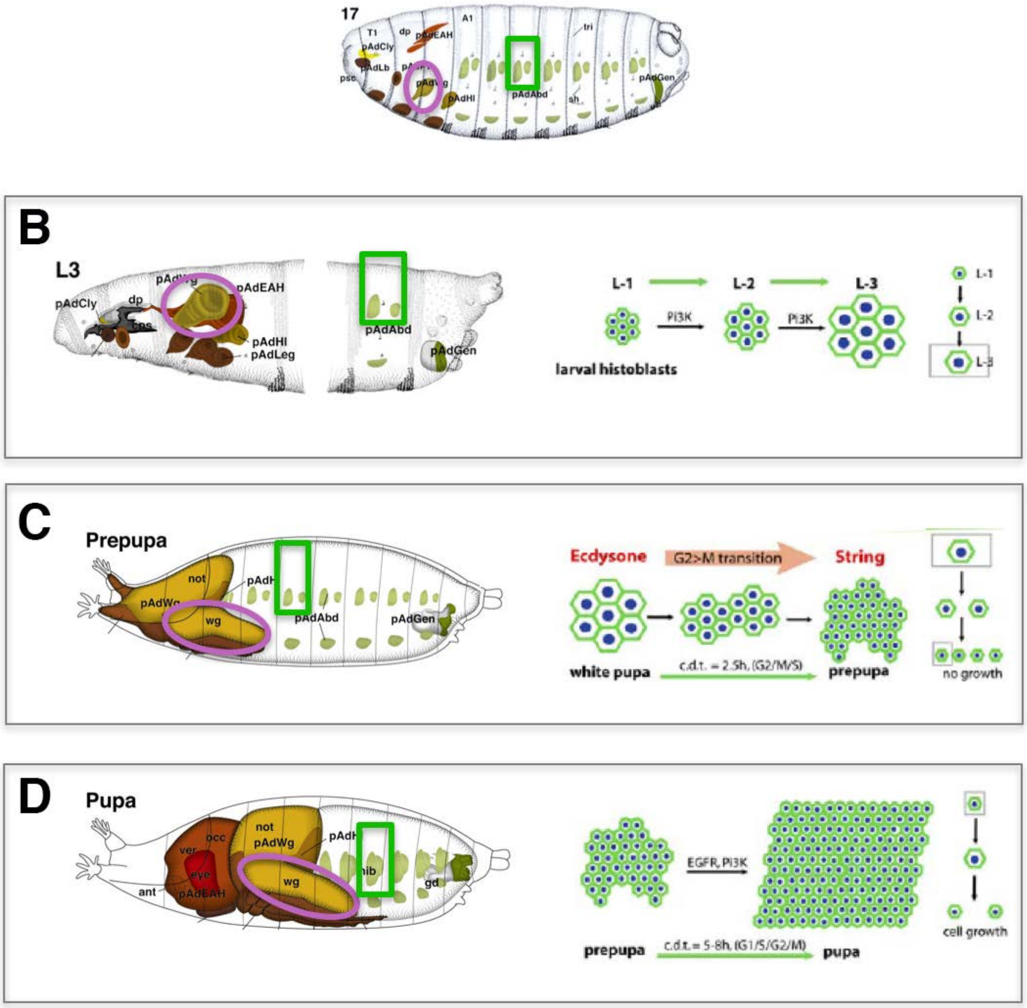
17
T1
dp
pAdEAH
A1
tri
pAdCly
pAdLb
pse
pAdHI
pAdAbd
sh
pAdGen
B
L3
pAdCly
dp
pAdEAH
pAdHI
pAdLeg
pAdAbd
pAdGen
L-1
L-2
L-3
PI3K
PI3K
larval histoblasts
L-1
L-2
L-3
C
Prepupa
not
pAdWg
wg
pAdAbd
pAdGen
Ecdysone
G2>M transition
String
white pupa
c.d.t. = 2.5h, (G2/M/S)
prepupa
no growth
D
Pupa
not
pAdWg
occ
ver
eye
ant
pAdEAH
wg
hb
gd
EGFR, PI3K
prepupa
c.d.t. = 5-8h, (G1/S/G2/M)
pupa
cell growth

Fig. 12: **Histoblasts growth behavior during *Drosophila* life cycle. Top:** Four histoblast nests are specified in each hemi-segment of the embryo: an anterior and posterior dorsal nest (Green box), a small spiracular nest and a ventral nest. The histoblasts nests are contiguous with the larval epidermis while the imaginal discs (pink oval marking the wing disc) invaginate and assume a sac-like structure. **B)** Left: During larval life histoblasts do not proliferate and are arrested in G2 while imaginal discs proliferate (pink oval). Right: Cartoon showing histoblast growth during larval stages. **C)** Left: At the onset of metamorphosis, a hormonal input mediated by ecdysone triggers pre-pupa formation. (Right) This hormonal input promotes cell-cycle progression without growth. Histoblasts undergo several fast synchronous G1-less divisions utilizing a stored pool of G1 regulators, including Cyclin E. During these divisions, histoblasts cleave into smaller cells, not undergoing interphase growth. **D)** Left: Pupation stage. The histoblasts start spreading and continue proliferating while the imaginal discs undergo terminal differentiation. Right) Division synchrony is lost, the cell cycle slows down with the restoration of a G1 phase, and histoblasts keep their size constant by growing between cycles. These late divisions are coupled to epithelial expansion and replacement of LECs. EGFR signaling triggered by the ligand Spitz is essential for progression of the cell cycle, and in the absence of EGFR signaling, histoblasts arrest in G2. Growth at this stage is mediated by insulin/PI3K signaling

Proliferating histoblasts change shapes by becoming increasingly flat, LECs undergo apoptosis by myosin II-dependent apical constriction and the basal lamina beneath the histoblast is progressively destroyed facilitating both histoblast spreading and the engulfment of the LECs by circulating macrophages (Ninov et al., 2007 and 2010).

All these events are accompanied by the preferential spreading of the nests in the dorsal-ventral (D/V) (Fig. 13) direction through cell intercalation based migration coupled with LECs delamination (Bischoff and Cseresnyes, 2009; Umetsu et al., 2014; Ninov et al., 2007).
All along this process the continuity between histoblasts and LECs is sustained. Histoblasts emit basal and apical actin-rich protrusions at the periphery of the nests (Ninov et al., 2007 and 2010) that facilitate nests expansion/spreading in response to *dpp* signaling (Ninov et al., 2010). From 22-24 hours APF the dorsal and ventral nests fuse with the spiracular nest and with nests from adjoining segments and their migratory behavior gradually change. As adjacent histoblasts from neighboring segments fuse proliferation slows down and cell movements are directed anteriorly (Fig. 13) (Bischoff and Cseresnyes, 2009). Through the expansion phase, cell divisions are not oriented towards any preferential axis and apoptosis is very scarce (Ninov et al., 2007; Bischoff and Cseresnyes, 2009; Guerra et al., 1972).

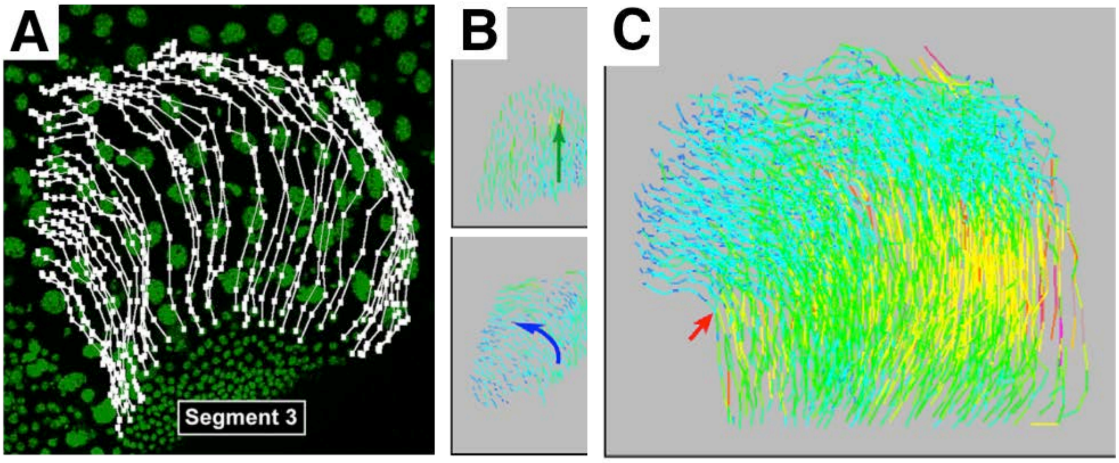

Fig. 13: **Histoblast oriented migration during pupation. A)** Tracking of histoblast nuclei (Green) showing their oriented migratory behavior (White dotted lines) between 25 and 40 hours APF. **B)** Representation of 2 different time points through nest expansion showing their trajectories color-coded according to their velocity (yellow-red: faster, green-blue: slower). Top: cells move straight towards the midline (Green arrow) during expansion (25-30 h APF). Bottom As they approach the midline (36-38 h APF), their movement is blocked by slowly delaminating LECs and they turn anteriorly (blue arrow). **C)** Cumulative plot of histoblasts trajectories during expansion close to confluence. More anteriorly positioned cells turn anteriorly earlier (red arrow). Adapted from Bischoff and Cseresnyes, 2009.

Around 34-38 hours APF, LECs delamination and nests expansion approach completion, proliferation stops completely and the bilaterally symmetric nests meet and fuse among each other at the dorsal and ventral midline (Garcia-Bellido and Merriam, 1971; Roseland and Schneiderman, 1979; Madhavan and Madhavan 1980; Bischoff and Cseresnyes, 2009), forming a confluent sheet that finally forms the mature epidermal monolayer of the abdomen.

6.4 Histoblast patterning and polarity during pupation

At the end of metamorphosis, the abdominal epidermis typically displays the patterning and planar polarity of the supporting epithelial cells (Casal et al., 2002; Struhl et al., 1997b). By 50 hours APF, the histoblasts begin to secrete the adult cuticle (Fristrom and Fristrom, 1993) with pigmentation becoming apparent around 70 hours APF (Madhavan and Madhavan, 1980). Pigmentation, bristles and trichome distribution within each segment field are not clonally determined but acquired in coordination with histoblasts proliferation and migration (Garcia-Bellido and Merriam, 1971; Shirras and Couso, 1996; Kopp et al., 1997; Fristrom and Fristrom, 1993) being patterned along the A/P and the D/V axis.

Each cell of the P compartment expresses the selector gene *engrailed* (*en*) (Morata and Lawrence, 1975; Kornberg *et al.,* 1985) which in turn activates the expression of *hedgehog* (*hh*). Hh diffuses in the A compartment (Lee *et al.,* 1992; Mohler and Vani, 1992; Tabata *et al.,* 1992) in a gradient, influencing its polarity (Struhl et al., 1997a and b; Kopp et al., 1997; Lawrence et al., 2002). The diffusion of the Hh into the A compartment leads to the activation of the receptor complex between Patched (Ptc) and Smoothened (Smo). This signal induces the expression of target genes such as *wingless* (*wg*) and *decapentaplegic* (*dpp*) (Struhl et al., 1997a and b; Chen and Struhl, 1996; Shirras and Couso, 1996). The patterning function of Hh is also mediated by the transcription factor Optomotor-blind (Omb) that is expressed in the posterior-most portion of the A compartment (Kopp and Duncan, 1997; Pflugfelder et al., 1992; Lawrence et al., 2002).

The morphogens Wg and Dpp specify the D/V patterning of each segment. *wg* and *dpp* have complementary expression domains; *wg* is expressed in the presumptive sternite and in the medio-lateral region of the tergite (Shirras and Couso, 1996), while *dpp* is expressed in the presumptive pleura and at the tergite dorsal midline (Kopp et al., 1999; Shirras and Couso, 1996). Wg, in concert with the EGFR signaling, promotes tergite and sternite fates at the expense of the pleura (Kopp et al., 1999; Shirras and Couso, 1996). Dpp promotes pleural identity and pigmentation at the dorsal midline by antagonizing Wg/EGFR activity (Kopp et al., 1999; Shirras and Couso, 1996).

Both tergites and sternites are decorated with multicellular bristles derived through asymmetric divisions from sensory organ precursors (SOP) (Fig. 14). SOPs subsequently generate a socket, a shaft, a neuron and a sheath cell (Gho et al., 1999). In the abdomen, SOPs divisions take place between 20 and 28 hours APF (Shirras and Couso, 1996; Fabre et al., 2008) even though the detailed temporal steps of the process are lacking.

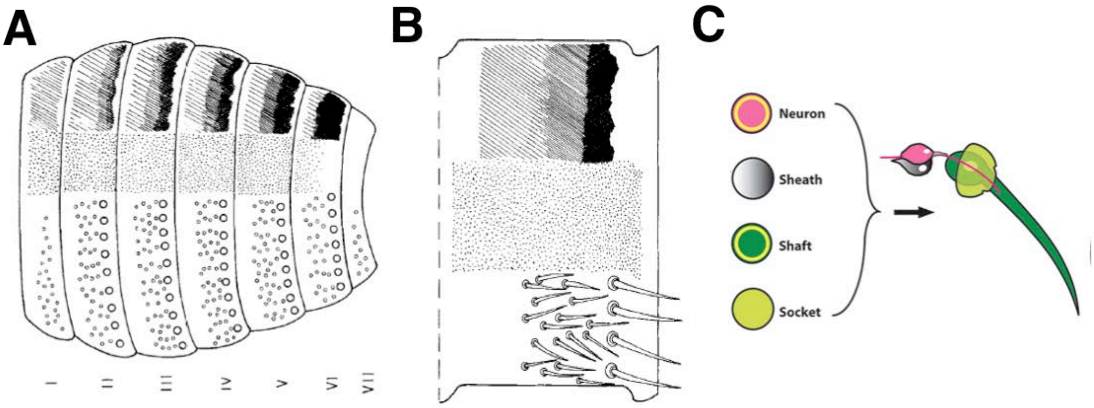

Fig. 14: **A-B)** Schematic representation of bristles, trichomes, and pigmentation on the dorsal female abdomen (A) and in a typical segments III tergite (B). Bristles, macrochaetae are indicated as big circles and microchaetae as small circles (Bottom). Trichomes are indicated as dots (centre). Different shades of grey indicate the pigmentation. **C)** Cartoon showing the four mature cells of the bristle lineage (left) and their arrangement in a microchaetae (right). Adapted from Garcia-Bellido and Merriam, 1971 (A-B); Maung and Jenny, 2011 (C).

In the adult fly, the planar polarity in the abdomen is manifested in the orientation of trichomes and multicellular bristles that uniformly point posterior (Casal et al., 2002; Struhl et al., 1997b; Kopp et al., 1997). In the tergite (Fig. 14), with the exception of the most anterior and posterior region of each segment, the entire field of the dorsal sclerotized epidermal cells is decorated by multiple tiny trichomes, uniformly oriented caudal-wards (Struhl et al., 1997b). Both the Core pathway and the Ds/Ft/Fj pathway are required for proper planar polarity in the abdomen (Casal et al., 2002 and 2006; Lawrence et al. 2004, Zeidler et al., 2000). Loss of Fmi/Stan, Fz or Stbm/Vang affect trichome polarities in most of the segment and fz and stbm mutant clones show consistent non-autonomous effect in trichome polarity in both compartments (Lawrence et al., 2004) (Fig 15).

Mutations in ds or ft cause extensive swirls in most of the A compartment and clone of cells mutant for these genes show directional non-autonomy that is largely the reverse to each others and of distinctive direction according to the compartment (Casal et al., 2002) (Fig. 15).

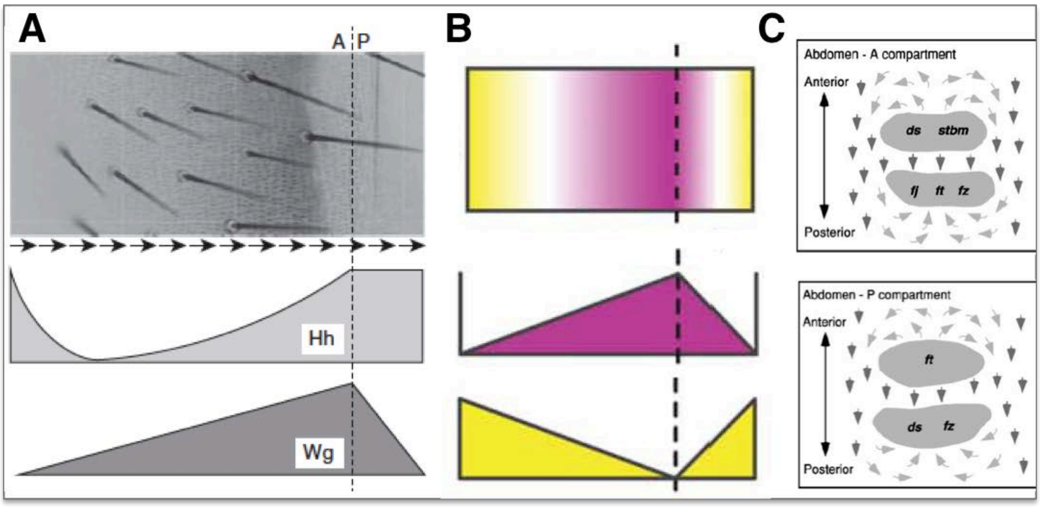

Fig. 15: **Patterning and planar polarity along the A/P axis of the segment in the abdominal epithelia. A)** Image (top) showing a single abdominal segment, anterior to the left, posterior to the right, with trichomes and bristles pointing posterior (bottom arrows). The A/P compartment boundary is marked with a dotted line. The diagrams below show gradients of factors, Hh and Wg, involved in patterning the A/P axis. **B)** Gradients of *ds* (magenta) and *fj* (yellow) along the AP axis of an adult segment. **C)** Non-autonomous activities of *fj*, *ds*, *ft*, *fz*, and *stbm* in the anterior (Top) and posterior (bottom) compartments. The position of loss of function clones for the genes indicated are shaded in grey (*wt* tissue is white). *wt* trichomes are shown in dark grey and non-autonomous disruptions of polarity are displayed in light grey. In the anterior compartment (left), *ds* and *stbm* clones cause swirls anterior to the clone while *fj*, *ft* and *fz* cause swirls posterior to the clone. In the posterior compartment (right), *ft* clones cause swirls anterior to the clone while *ds* and *fz* cause swirls posterior to the clone. Adapted from Strutt, 2009 (A); Thomas and Strutt, 2011 (B) and Strutt and Strutt, 2005 (C)

Animals double mutant in both pathways showed strong PCP phenotypes (Casal et al. 2006). In the absence of working Core pathway components such as Fz, Fmi or Stbm, cells containing different amounts of Ds or Ft can non-autonomously repolarize surrounding cells (Lawrence et al., 2004; Casal et al., 2006), providing evidence for a polarity mechanism that does not require Fz. Moreover, disruption of Fmi enhances the planar polarity defects in animals lacking Ds (Casal et al., 2006), indicating that Fmi function, at least partially, does not require Ds.

These studies point that the Ds/Ft/Fj signaling does not merely act as an input into the Core pathway but provides a distinct source of spatial information on its own in the establishment of PCP (Lawrence et al., 2007). The specific role/s of the Ds/Ft/Fj pathway on PCP and the cellular feature/s directly influenced by its activity are unknown.

Aims

Proper epithelial organization is essential for the physiology of the organisms. During development, order is achieved through precise changes in cell arrangements and polar organization.

Cell arrangements and planar polarity reach a fascinating precision when morphogenesis is accomplished.

The cellular behaviors underlying ordered cellular arrangements have been addressed in several contexts. However little is still known on the mechanisms governing the axial orientation underlying cell arrangement and planar polarity.

How a common orientation of cell arrangement is attained? How does cell arrangements influence planar polarity? Which factors produce the orderly acquisition of the orientation of cell alignments within an epithelium? What type of cellular interactions account for the uniform orientation of the cell arrangement in a uniaxial direction?

To tackle these questions, the following objectives have been designed:

1. To identify the axial characteristics of the mature cellular arrangement within the plane of the *Drosophila* abdominal epithelium and analyse the cellular dynamics leading to its attainment;

2. To assess the requirement of the Ds/Ft/Fj pathway in the attainment of axial order and planar polarity during the morphogenesis of the *Drosophila* abdominal epithelium.

Materials and Methods

1. *Drosophila* Husbandry and Stocks Maintenance

Fly stocks and crosses were kept at 25°C in plastic vials filled with standard culture medium. The dark/light cycle was also kept controlled (*i.e.* the flies experienced 10 hours of darkness every day). All mutant and transgenic flies used were maintained as stable stocks over balancer chromosomes (Lindsley and Zimm, 1992).

2. *In vivo* Imaging of Pupal Development

For live imaging, genetically encoded fluorescent probes, such as the Green Fluorescent Protein (GFP or its enhanced version EGFP) or derivatives were typically used for visualization of tissue morphology or for defining expression patterns. The transgenic fluorescence lines employed are listed in Table I.

2.1 Confocal Laser Scanning Microscopy (LSM) for Image and Time-lapse Acquisition

Transgenic pupae carrying fluorescence probes fused with proteins of interests (or responding to regulatory enhancers) or fixed preparations were imaged on an inverted Zeiss LSM 700 confocal microscope, with a Zeiss Plan-Neofluar 40X/1.3(NA) oil immersion objective lens at 0.5, 0.7 or 1X zoom at 25°C. Between 16 and 40 z-slices for each image were recorded, with a step size of 1 μm (voxel size of 0.31 x 0.31, 0.22 x 0.22 or 0.15 x 0.15 x 1 μm^3) for a total of 1024 x 1024 pixels (resolution of 3.199, 4.479 or of 6.398 pixel/μm). This image acquisition set-up was used both for single image or time-lapse captures, unless otherwise stated. In paired experiments (*e.g.* mutant condition versus its *wild-type* control), the same acquisition was consistently used to allow direct comparisons.

The time interval for each time-lapse recording was of 5 minutes. Such time resolution is suitable enough to follow relevant cellular details, such as divisions or rearrangements, with high fidelity.

To reduce bleaching and to minimize photo-toxicity, laser intensity was kept to a minimum and no averaging was taken. 95% of pupae hatched normally after image acquisition, indicating negligible tissue damage.

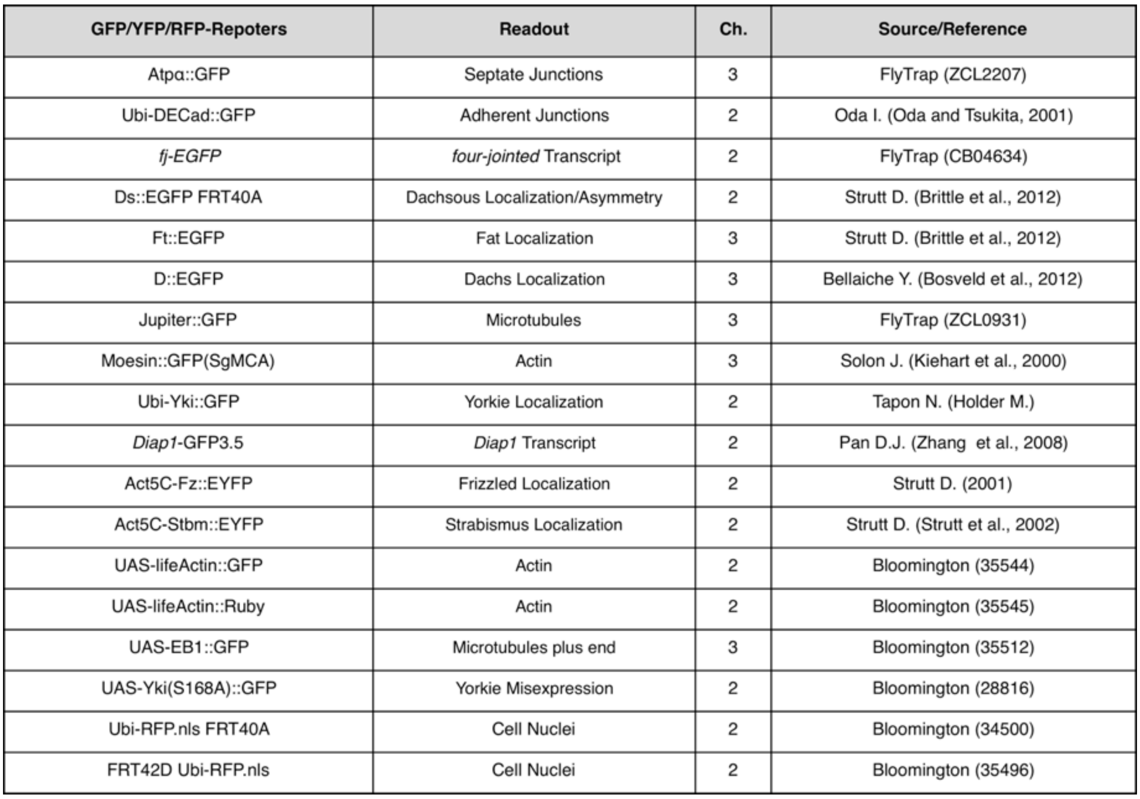

GFP/YFP/RFP-Repoters	Readout	Ch.	Source/Reference
Atpα::GFP	Septate Junctions	3	FlyTrap (ZCL2207)
Ubi-DECad::GFP	Adherent Junctions	2	Oda I. (Oda and Tsukita, 2001)
fj-EGFP	*four-jointed* Transcript	2	FlyTrap (CB04634)
Ds::EGFP FRT40A	Dachsous Localization/Asymmetry	2	Strutt D. (Brittle et al., 2012)
Ft::EGFP	Fat Localization	3	Strutt D. (Brittle et al., 2012)
D::EGFP	Dachs Localization	3	Bellaiche Y. (Bosveld et al., 2012)
Jupiter::GFP	Microtubules	3	FlyTrap (ZCL0931)
Moesin::GFP(SgMCA)	Actin	3	Solon J. (Kiehart et al., 2000)
Ubi-Yki::GFP	Yorkie Localization	2	Tapon N. (Holder M.)
Diap1-GFP3.5	*Diap1* Transcript	2	Pan D.J. (Zhang et al., 2008)
Act5C-Fz::EYFP	Frizzled Localization	2	Strutt D. (2001)
Act5C-Stbm::EYFP	Strabismus Localization	2	Strutt D. (Strutt et al., 2002)
UAS-lifeActin::GFP	Actin	2	Bloomington (35544)
UAS-lifeActin::Ruby	Actin	2	Bloomington (35545)
UAS-EB1::GFP	Microtubules plus end	3	Bloomington (35512)
UAS-Yki(S168A)::GFP	Yorkie Misexpression	2	Bloomington (28816)
Ubi-RFP.nls FRT40A	Cell Nuclei	2	Bloomington (34500)
FRT42D Ubi-RFP.nls	Cell Nuclei	2	Bloomington (35496)

Table I. List of transgenic lines tagged with Green, Yellow or Red Fluorescent Proteins (GFP, YFP and RFP) used for imaging.

2.2 Staging Pupae Before Imaging

Transgenic flies of the desired genotypes were cultured on standard medium at 25°C for 5 days (± 12 hours) after egg laying (AEL). Metamorphosis (Robertson 1936, Bodenstein 1950, Baindbrige and Bownes 1981) starts within the immobile confinement of the pupal case (a.k.a puparium or tanned LIII cuticle) approximately at 120 hours AEL - 0 hours after puparium formation (hours APF). In Fig. 1 transitions from pupariation to pupation (12 hours APF) and from pupation to eclosion (4-5 days) are indicated and staged according to Baindbridge and Bownes (1981). Pupation occurs at about 12 hours APF, when the imaginal discs are fully everted. The expansion of the histoblasts starts soon after the formation of the pupa (*i.e.* 16 hours APF). Wandering larvae or white pupae (0 hours APF) of the genotype of interest were transferred into fresh vials. In the following 10-12 hours of development, the pupae were ready to be dissected and mounted for live imaging.

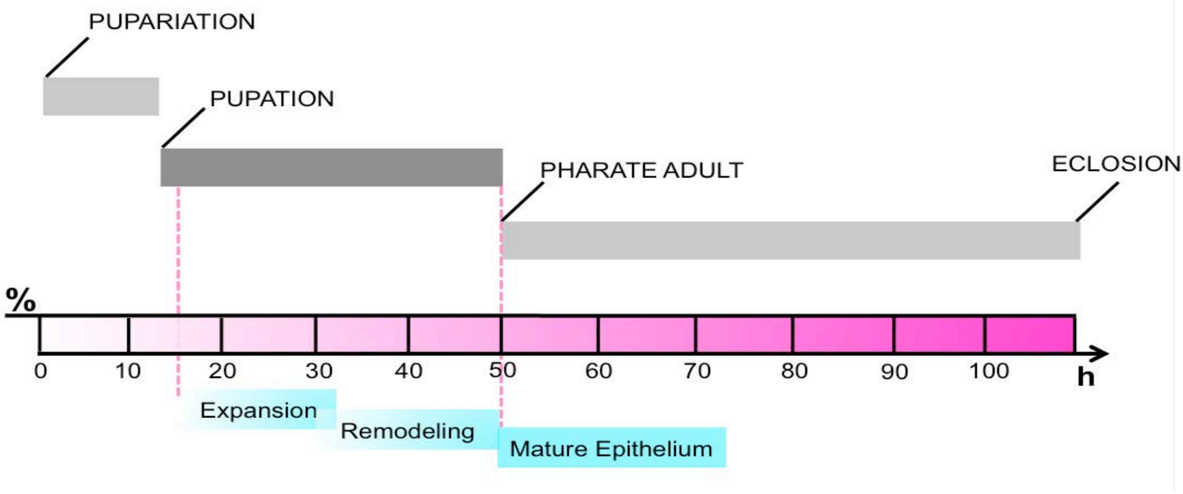

Fig. 16: Diagram of the Stages of Pupal Development. Pupal development can be broadly subdivided in three stages (gray rectangles). The correspondence between each stage and the hours/percentages of completed pupal development is shown in graded pink. Pupation starts half a day from the onset of pupariation (12 hours or % APF). Epithelial expansion and remodeling happens at pupation (16-to-50 hours or % APF). By the end of pupation the epithelial cells of the abdominal epithelium reach a stable configuration and do not move further. During the pharate adult stage (50 hours or % APF onward) the mature epithelial cells become pigmented and the differentiation pattern of the epithelium can be scored with standard stereomicroscope.

2.3. Preparing Pupae for Live Imaging During Pupation

After staging, the pupae were dissected and mounted following the protocol described in Fig. 2. Briefly, the pupa was deprived of the puparium (Fig. 17 A-D) and transferred to a Glass Bottom Microwell Dish (MatTek) (Fig. 17 E-H) containing a small drop of gas-permeable halocarbon oil (Voltaleff S10) to improve optics (Fig. 17 H-I). A piece of wetted tissue paper rolled at the edges of the dish maintained humidity and avoided dehydration of the pupa.

Compared to previous imaging protocols (Ninov and Martin-Blanco, 2007a), this procedure allows continuous live imaging for a longer period of pupal development. The removal of the whole pupal case allows more accessibility and favors orienting the pupae appropriately to record the region of interest. The development of the abdominal epidermis could be inspected from different angular perspectives.

2.4. Focusing on the AIII Segment

Both female and male pupae were employed for image collection. Adult female and male abdomens show size variations (females have slightly bigger abdomens than males) and dorsal differentiation patterns. However the third abdominal segments (AIII) are almost identical in terms of size, shape and patterning in between females and males. Therefore, this segment was used as a reference abdominal metamere and all images and time-lapses were acquired on the AIII segment, unless otherwise indicated.

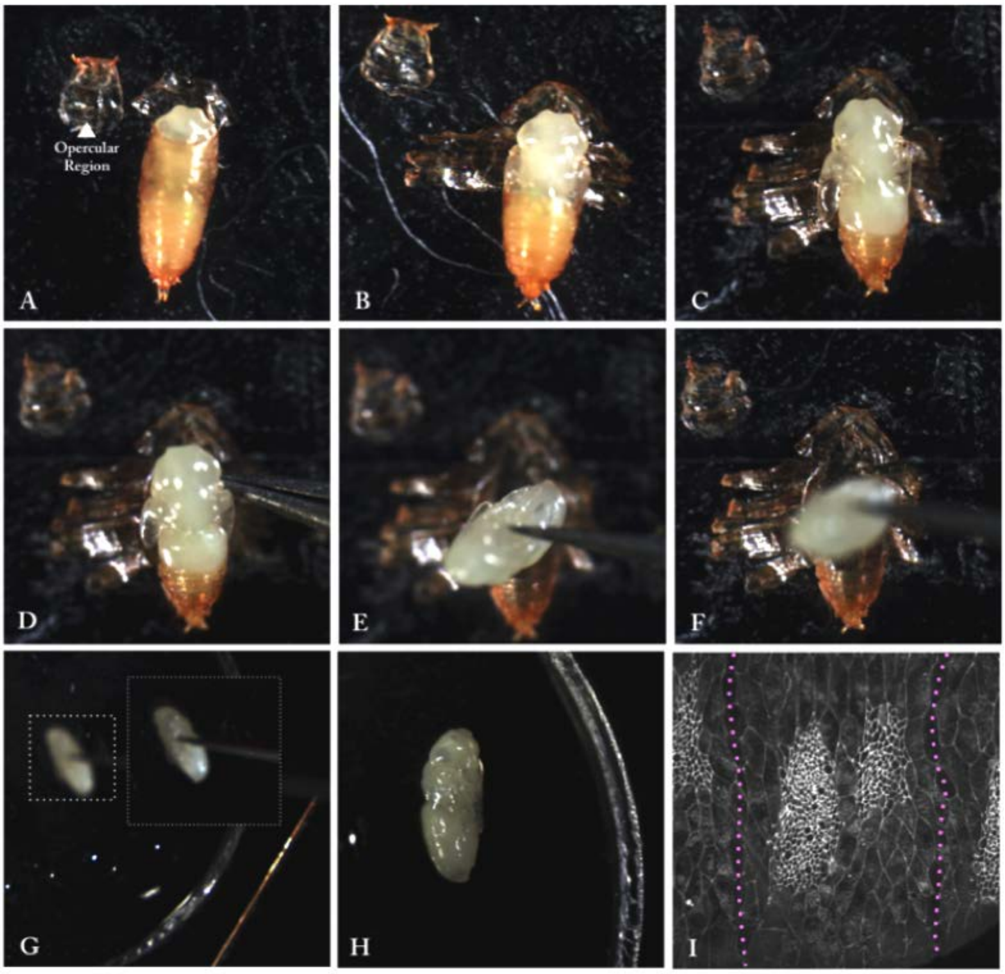

Fig. 17: Dissecting and Mounting Pupae for live Imaging. A) Staged pupae were immobilized on double-sided sticky tape on glass slides. The pupal case of each pupa was opened from the opercular region with surgical 5C Drummond forceps. **B-C)** The peeling of the whole pupal case was achieved by gradual tearing and folding to the sides, from the head to the abdomen. **D-F)** The pupa was gently taken from the ventral side with the tips of the forceps (**G**) and transferred to a MatTek plate over a minimal drop of 5S halocarbon oil. **H)** The pupa was then appropriately oriented (dorso-laterally, in this example). **I**) Image showing the tissue morphology (Atpα::GFP apical marker) of the dorsal histoblast nests of the AIII segment (with the pupa oriented as in **H**). The dynamic of the tissue can be visualized for several hours.

3. Immunohistochemistry of the Pupal Epidermis

To assess the transcriptional pattern of *dachsous (ds)* and *four-jointed (fj),* the ds^{2D60b} and fj^{P1} alleles (Clark et al., 1995; Brodsky and Steller, 1996) were employed. Both alleles contains a *lacZ* (*βgal*) sequence inserted in the proximity of the 5’ of an intron (*ds*) or of the 5’ un-translated region of the transcriptional unit (*fj*), resulting in the patterned transcription of *lacZ* reporters. Such patterns were detected by *βgal* immunocytochemistry employing the protocol described below.

3.1 Preparation of the Abdominal Tissue for Immunostaining

The pupal epidermis was dissected and isolated from internal organs in sterilized PBS (Phosphate Buffered Saline, 1X, pH 7.4) in a 3 x 3 glass multi-well plate. Whole pupae were bisected into two halves along the dorsal and ventral medial lines using surgical scissors and the anterior-most region, corresponding to the head and thorax, were cut out. Internal abdominal structures, such as the fat body, the gut or muscles were gently cleaned away by flushing with a pipette. The puparium was maintained to prevent the folding of the abdominal epidermis and the adherence of the tissue to the eppendorf tube surfaces. The tissue was then fixed with Paraformaldehyde (PFA, at 4% in PBS) at room temperature for 30 minutes without rocking to minimize cell loss. The PFA was then removed by multiple washes (up to three) with PBS. The epidermis was then permeabilized with a solution of PBS and Triton X-100 (PBT, at 0,3% Triton X-100 in PBS) at room temperature.

3.2. Staining and Mounting Protocol of Fixed Abdominal Epithelia

After permeabilization, the epidermis was incubated with a solution of PBT and Bovine Serum Albumin (PBT-BSA or PBTB, 1% BSA in PBT) for one hour at room temperature to block unspecific antibody absorption. Primary antibody against β-Galactosidase (anti-rabbit βGal, Cappel) was then diluted (1:1000 in PBTB) and incubated with the tissue at 4°C overnight with gentle rocking. The following day the primary antibody dilution was removed and the sample rinsed three times in PBTB to wash away non-specific or unbound primary antibody. The tissue was then incubated for 1 hour with PBTB at room temperature and, right after, with the secondary antibody (1:250 in PBTB, anti-rabbit FITC-conjugated, Molecular Probes) for 3 hours at room temperature with gentle rocking and in the dark to avoid photo bleaching. The sample was then rinsed in PBT (three times) to wash away the unbound secondary antibody. Before mounting, the Vectashield (Vector) mounting medium, supplied with DAPI (1:1000 in PBT) to label the cell nuclei, was added to the tissue and maintained with it for at least 30 minutes (the residual PBT undergoes phase separation, limiting the presence of residual water in the sample). The abdominal epidermis was mounted for imaging by placing some drops of Vectashield on a microscope slide and dragging the tissue into the medium using forceps. A cover slip was then placed on top of the sample, taking care to do not trap air bubbles. Clear nail polish was used to seal the edges of the cover slip to immobilize the preparation.

4. The Gal4/UAS Binary System

The Gal4/UAS binary system (Brand and Perrimon, 1993; Elliott and Brand, 2008) was employed to visualize, mis-express or down-regulate selected transgenes in specific domains of the abdominal epidermis. The Gal4/UAS system relies on two components: 1) the yeast transcriptional co-activator Gal4, genetically engineered to be expressed under specific regulatory elements, and 2) the Upstream Activation Sequences (UASs) to which the Gal4 protein specifically binds, placed upstream of protein coding or noncoding RNAs (*i.e.* RNAi). These two components are originally maintained in separated stocks, the “driver” and “responder” (Fig. 18). The elements of such bipartite system are brought together through a genetic cross, the progeny of which will express the UAS-transgene only in those cells or tissues in which the Gal4 is expressed. A list of the drivers and responders used is reported in Table II. Conditional expression of UAS-transgenes was performed at 25°C.

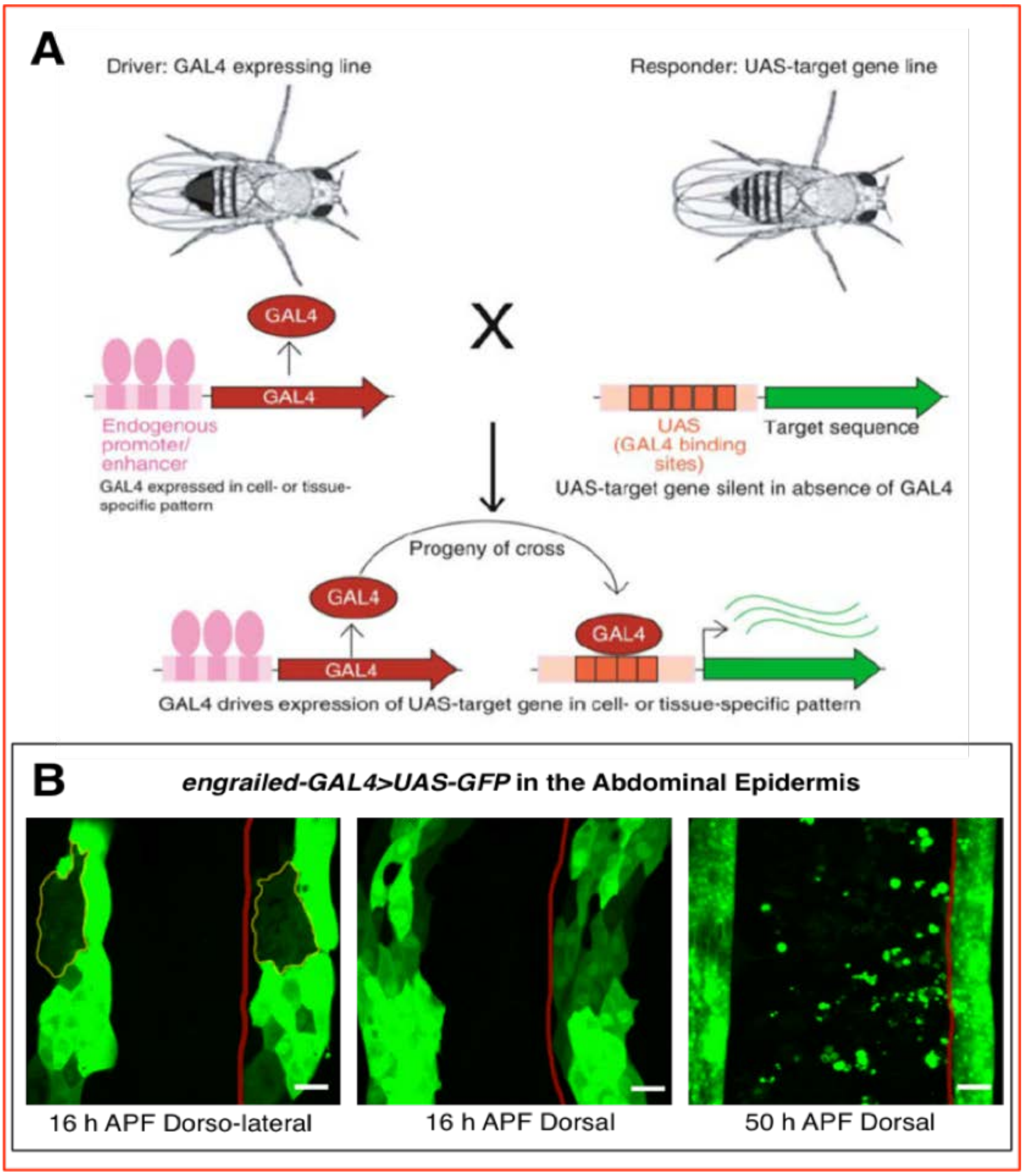
A
Driver: GAL4 expressing line
Responder: UAS-target gene line
GAL4
X
GAL4
Endogenous promoter/ enhancer
GAL4 expressed in cell- or tissue-specific pattern
UAS (GAL4 binding sites)
Target sequence
UAS-target gene silent in absence of GAL4
Progeny of cross
GAL4
GAL4
GAL4
GAL4 drives expression of UAS-target gene in cell- or tissue-specific pattern
B
engrailed-GAL4>UAS-GFP in the Abdominal Epidermis
16 h APF Dorso-lateral
16 h APF Dorsal
50 h APF Dorsal

Fig. 18 The Gal4/UAS Binary System for Target Gene Expression in the Abdominal Epithelium A) Schematic illustration of the Gal4/UAS strategy for transgene expression (from Elliott and Brand, 2008) **B)** Example showing how the *engrailed*-Gal4 transgenic driver can be used to target the expression of the responder UAS-GFP in the abdominal epithelium during pupation. *engrailed* (*en*) is expressed in the posterior (P) compartment, as en-Gal4 does. Note that *en* is originally expressed in both LECs and histoblasts (left panel). The red line marks the position of the A/P compartment boundary. Scale Bar is 22 μm. Anterior is to the left.

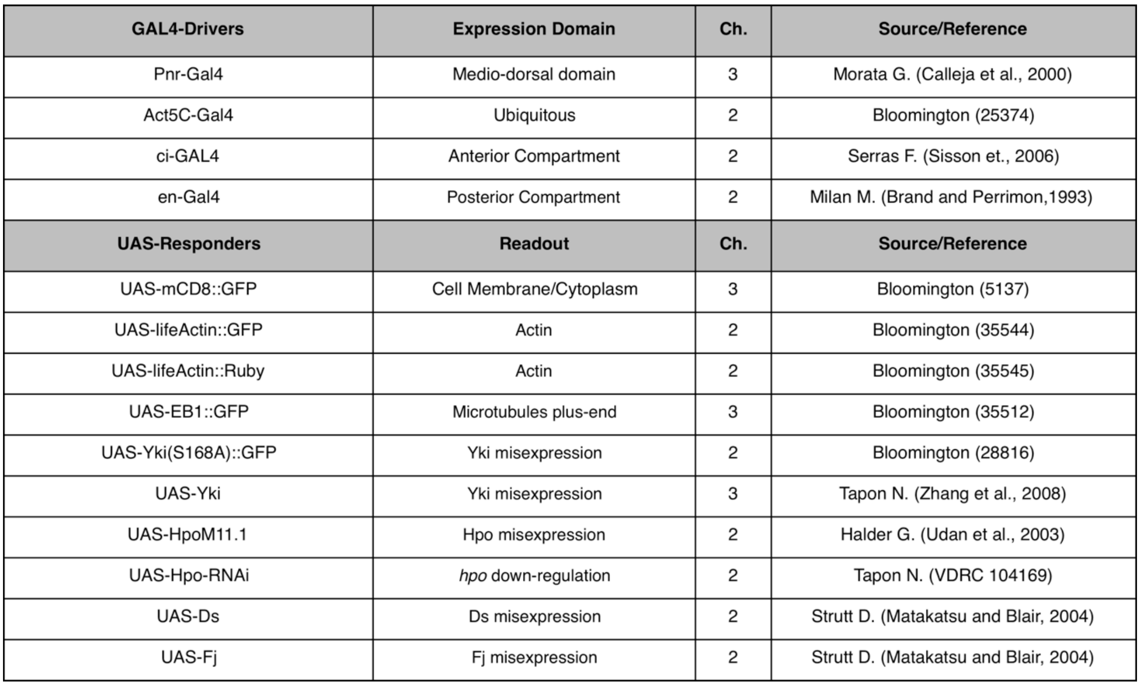

GAL4-Drivers	Expression Domain	Ch.	Source/Reference
Pnr-Gal4	Medio-dorsal domain	3	Morata G. (Calleja et al., 2000)
Act5C-Gal4	Ubiquitous	2	Bloomington (25374)
ci-GAL4	Anterior Compartment	2	Serras F. (Sisson et., 2006)
en-Gal4	Posterior Compartment	2	Milan M. (Brand and Perrimon,1993)
UAS-Responders	**Readout**	**Ch.**	**Source/Reference**
UAS-mCD8::GFP	Cell Membrane/Cytoplasm	3	Bloomington (5137)
UAS-lifeActin::GFP	Actin	2	Bloomington (35544)
UAS-lifeActin::Ruby	Actin	2	Bloomington (35545)
UAS-EB1::GFP	Microtubules plus-end	3	Bloomington (35512)
UAS-Yki(S168A)::GFP	Yki misexpression	2	Bloomington (28816)
UAS-Yki	Yki misexpression	3	Tapon N. (Zhang et al., 2008)
UAS-HpoM11.1	Hpo misexpression	2	Halder G. (Udan et al., 2003)
UAS-Hpo-RNAi	*hpo* down-regulation	2	Tapon N. (VDRC 104169)
UAS-Ds	Ds misexpression	2	Strutt D. (Matakatsu and Blair, 2004)
UAS-Fj	Fj misexpression	2	Strutt D. (Matakatsu and Blair, 2004)

Table II. List of Gal4 Drivers and UAS Responders used to visualize, mis-express or down-regulate the expression of selected transgenes in the abdominal epidermis.

5. Genetic Mosaics Induced by Site-Specific Mitotic Recombination

Mitotic recombination (Stern, 1934 and 1936) was used to induce genetic mosaics. In this work, three methods were used in the developing pupae: the FLP/FRT, the FLP-Out and the FLP-Out-Gal4. All these strategies rely on site-specific somatic recombination promoted by the yeast FLP/FRT system (Golic and Lindquist, 1989; Xu and Rubin, 1993; Ito et al., 1997; Struhl and Basler, 1993). The site-specific recombinase FLP (a.k.a. Flipase), expressed under the heat-shock-inducible promoter of the *hsp70* gene, specifically recognizes short DNA sequences called FRTs (FLP recombinase targets) and promotes recombination between them. Depending on the arrangement or location of the FRT sites, the recombination promoted by the FLP can lead to genomic exchanges (FLP/FRT), excisions (FLP-Out, FLP-Out-Gal4), or to inversions or integrations of DNA fragments.

5.1. The FLP/FRT Binary System for Gene Inactivation

FLP/FRT mutant clones (Xu and Rubin, 1993; Golic and Lindquist, 1989) in the histoblasts were generated by heat shock treatment of third-instar larvae in plastic vials placed in a water bath at 37°C for 1 hour. A schematic representation of the FLP/FRT mediated recombination is shown in Fig. 19.

The sensitive period for mitotic recombination is when cells are passing through the G2 phase of the cell cycle, because the cells have 4 chromatids per chromosome set (Fig. 19). Histoblasts are arrested in G2 during larval development, so they are sensitive at those stages. The histoblast will undergo several divisions from the onset of metamorphosis, so those in which recombination was successfully induced will form marked twin clones. The marked clones were scored from 16 hours APF onward by absence (mutant cells) or enhanced levels (*wt* twin-spot cells) of a fluorescent marker protein in an otherwise homogeneous marker background. Upon clone identification, living pupae were imaged at the desired stage. A list of the FRT/FLP strains used in this work is reported in Table III.

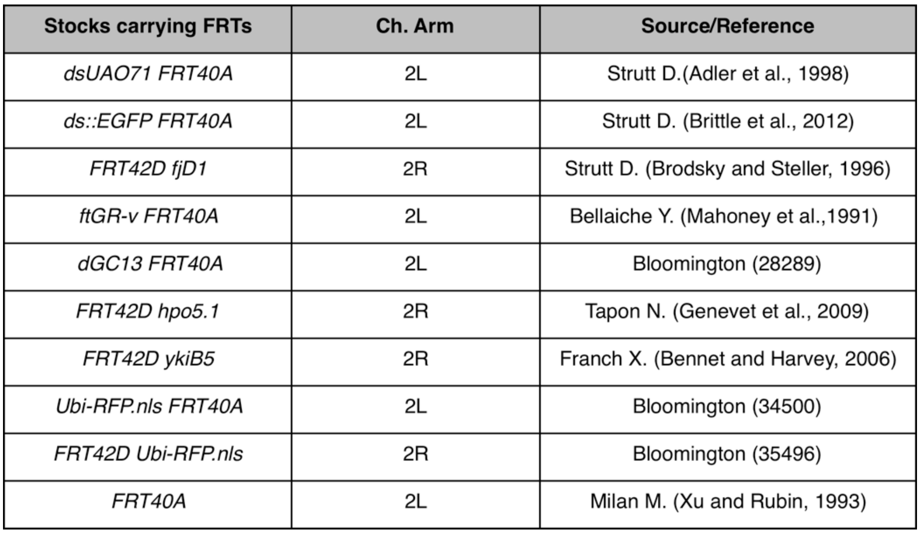

Stocks carrying FRTs	Ch. Arm	Source/Reference
dsUAO71 FRT40A	2L	Strutt D.(Adler et al., 1998)
ds::EGFP FRT40A	2L	Strutt D. (Brittle et al., 2012)
FRT42D fjD1	2R	Strutt D. (Brodsky and Steller, 1996)
ftGR-v FRT40A	2L	Bellaiche Y. (Mahoney et al.,1991)
dGC13 FRT40A	2L	Bloomington (28289)
FRT42D hpo5.1	2R	Tapon N. (Genevet et al., 2009)
FRT42D ykiB5	2R	Franch X. (Bennet and Harvey, 2006)
Ubi-RFP.nls FRT40A	2L	Bloomington (34500)
FRT42D Ubi-RFP.nls	2R	Bloomington (35496)
FRT40A	2L	Milan M. (Xu and Rubin, 1993)

Table III. List of FRTs-Containing genotypes used to generate mutant clones in the histoblasts by site-specific mitotic recombination. The *hs-FLP* transgene inserted on the first chromosome (X) was used to promote conditional somatic recombination in all cases.

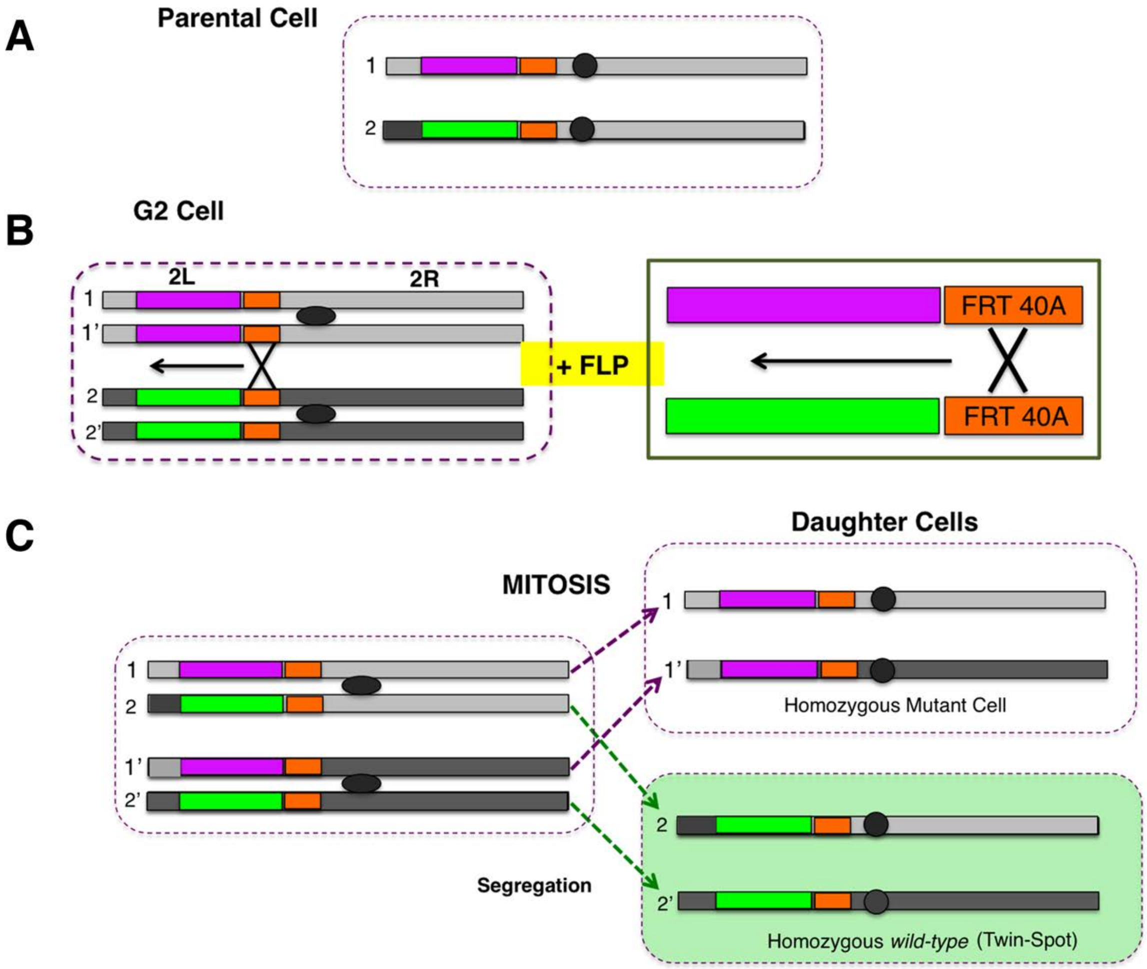

Fig. 19 Generation of Genetic Mosaics via FLP/FRT System. A) One chromosome arm harbors a mutant allele (magenta) and the homologous arm a marker gene (green). FRT sites (orange) lie at the same position between the mutant/marker region and the centromeres (grey ovals) **B)** Activation of the FLP recombinase by heat-shock will lead to recombination between the FRTs on homologous arms (sister chromatids are indicated as 1-1' or 2-2') in a cell paused in G2 phase of the cell cycle. Left: Magnification of the region undergoing genomic exchange (the region of the 2L arms distal to the FRT sites) **C)** Upon the polar segregation of rearranged regions (1-1' and 2-2'), two genetically different daughter cells from the parental one will be generated. One daughter cell is homozygous for the mutation and the entire chromosome arm distal to the site of recombination. This cell will be lacking the marker gene (negatively marked). The other daughter will be homozygous for the *wt* arm (given rise to the "twin-spot") and it will be expressing two copies of the marker gene. Note that the segregation of rearranged regions to opposite poles of the mitotic cell (*i.e.*1-2 and 1'-2') give heterozygous cells for both the mutation and the marker, leading to descendants phenotypically indistinguishable from the parental cell (*i.e.* heterozygous background).

5.2. FLP-Out to Assess aAsymmetric Localization of Proteins

The FLP-Out strategy (Strhul and Basler, 1993) was employed to assess asymmetric protein localization. The strategy is schematically illustrated in Fig. 20 and the transgenic lines used are reported in Table IV. This method allows the generation of positively marked clones of variables size. The possible protein localization asymmetries are measurable at the clone boundaries (Fig. 20).

Small FLP-Out clones were induced by heat shock treatment of third instar larvae in a water bath at 37°C for a period of 6-10 minutes.

Since the FLP-Out generates intra-chromatids recombination (*cis*), cell division (chromatids pairing in G2) is not a prerequisite to generate marked clones. However, cell divisions enlarge the marked area facilitating visualization. LECs are polythenic, implying a recombination frequency further greater than diploid imaginal cells; 6-10 minutes of heat-shocking were sufficient to positively mark about 70% of the LECs.

5.3 The FLP-Out-Gal4 Technique for Gene Modulation

FLP/FRT and Gal4/UAS systems can be combined to refine the temporal regulation of Gal4 (Ito et al., 1997; see Fig. 20 and Table IV). The FLP-Out-Gal4 system was employed to visualize, mis-express or down-regulate transgenes in the histoblasts by heat shock treatment of third-instar larvae in a water bath at 37°C for a period of 15 to 30 minutes.

As in the case of the FLP-Out, cell divisions were not a prerequisite to visualize the marked clones. However, cell divisions enlarge the labelled area, facilitating the scoring of the phenotypes.

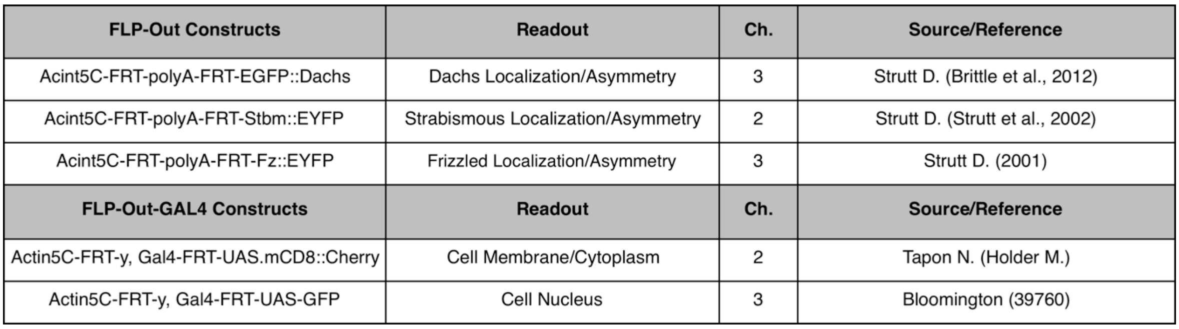

FLP-Out Constructs	Readout	Ch.	Source/Reference
Acint5C-FRT-polyA-FRT-EGFP::Dachs	Dachs Localization/Asymmetry	3	Strutt D. (Brittle et al., 2012)
Acint5C-FRT-polyA-FRT-Stbm::EYFP	Strabismous Localization/Asymmetry	2	Strutt D. (Strutt et al., 2002)
Acint5C-FRT-polyA-FRT-Fz::EYFP	Frizzled Localization/Asymmetry	3	Strutt D. (2001)
FLP-Out-GAL4 Constructs	**Readout**	**Ch.**	**Source/Reference**
Actin5C-FRT-y, Gal4-FRT-UAS.mCD8::Cherry	Cell Membrane/Cytoplasm	2	Tapon N. (Holder M.)
Actin5C-FRT-y, Gal4-FRT-UAS-GFP	Cell Nucleus	3	Bloomington (39760)

Table IV. List of FLP-Out based constructs used to assess protein asymmetry (FLP-Out) or to mis-express, down-regulate or visualize gene expression in marked clones. The *hs-FLP* transgene inserted on the first chromosome (X) was used to promote conditional somatic recombination in all cases (See the Results).

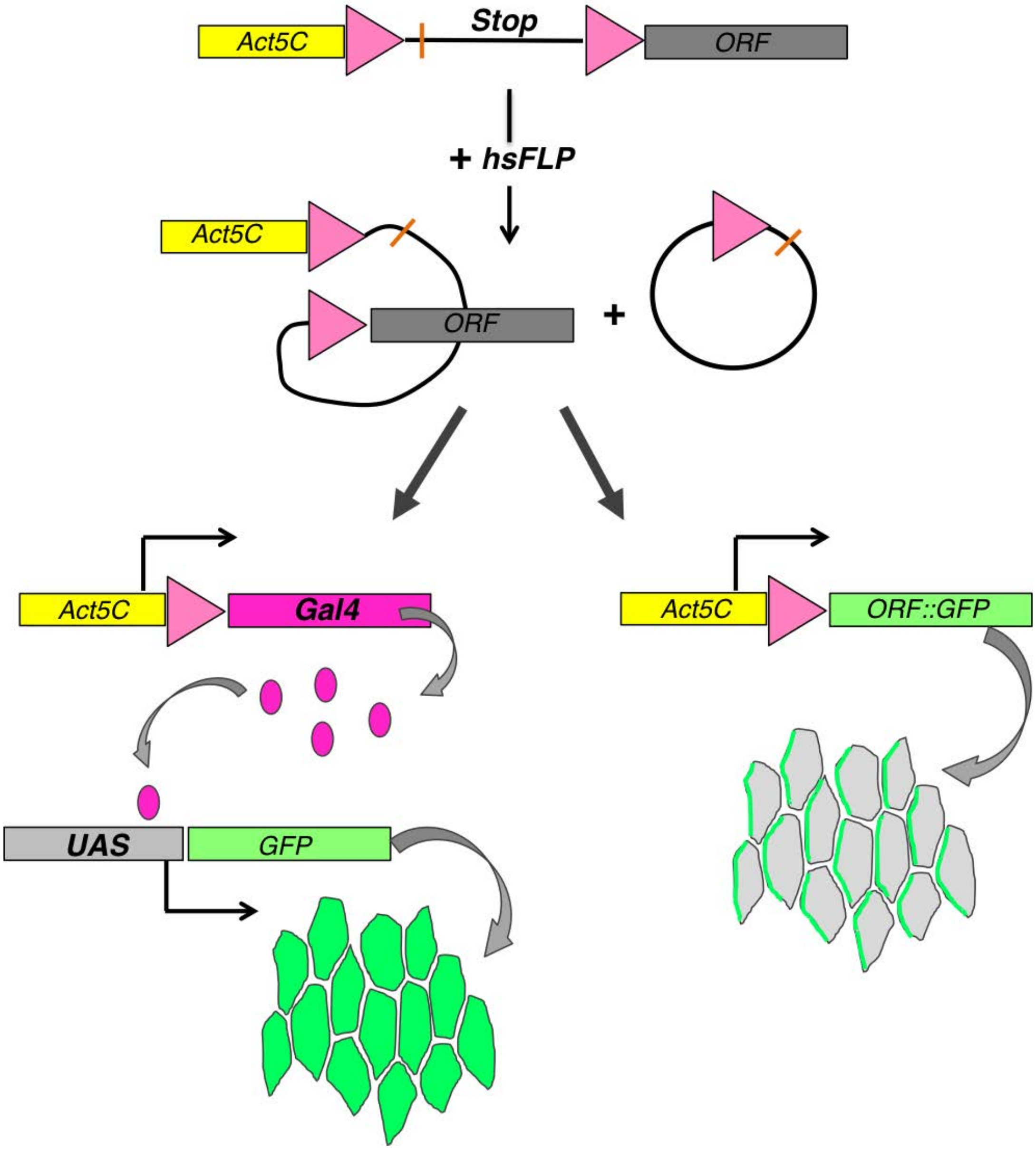

Fig. 20 Flp-Out and Flp-Out-Gal4 Strategies for Marked Clones. Upper panel) In the ground state the actin promoter (Act5C) will not transcribe the gene of interest (ORF) as an intervening "Stop" cassette is present in between these two elements. The Stop region contains a transcriptional terminator or poly A signal (orange bar) and eventually a marker to negatively mark the clone (*i.e.* commonly the gene *yellow*). The cassette is flanked by FRT sites (pink triangles) oriented in the same direction (directed repeats). Upon induction of FLP expression by heat-shock, the recombination between the two FRTs results in the elimination of the Stop cassette. This excision allows the promoter to direct the transcription of the coding sequence. The excised cassette is lost in subsequent cell divisions and asymmetric localization can be assessed at clone boundaries (right). Left) If the ORF encodes for Gal4, the activation of the FLP leads to the release of the cassette and thus to expression of the Gal4 protein (pink circles). The Gal4 will in turn activate the UAS-driven marker (GFP, in this case). The generated clones will be positively marked. Multiple UAS controlled transgenes can be activated simultaneously within the clone.

5.4. Mutant Alleles

The mutant alleles used are listed in Table V. All the alleles were used for the generation of mutant clones by FLP-FRT (see also Table III and Fig. 19). Some of the alleles of the same gene were combined in *trans* to generate hetero-allelic combinations. This strategy was used to circumvent the pupal lethality associated with strong mutant alleles of *ds*, *ft* and *hpo* genes. See the Results for examples of the hetero-allelic combinations used.

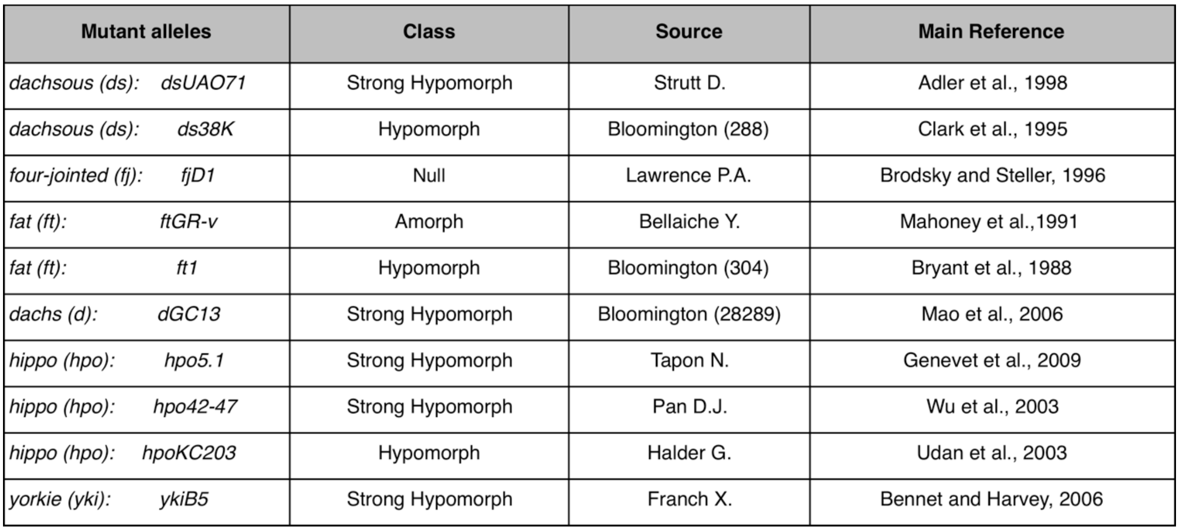

Mutant alleles	Class	Source	Main Reference
dachsous (ds): dsUAO71	Strong Hypomorph	Strutt D.	Adler et al., 1998
dachsous (ds): ds38K	Hypomorph	Bloomington (288)	Clark et al., 1995
four-jointed (fj): fjD1	Null	Lawrence P.A.	Brodsky and Steller, 1996
fat (ft): ftGR-v	Amorph	Bellaiche Y.	Mahoney et al.,1991
fat (ft): ft1	Hypomorph	Bloomington (304)	Bryant et al., 1988
dachs (d): dGC13	Strong Hypomorph	Bloomington (28289)	Mao et al., 2006
hippo (hpo): hpo5.1	Strong Hypomorph	Tapon N.	Genevet et al., 2009
hippo (hpo): hpo42-47	Strong Hypomorph	Pan D.J.	Wu et al., 2003
hippo (hpo): hpoKC203	Hypomorph	Halder G.	Udan et al., 2003
yorkie (yki): ykiB5	Strong Hypomorph	Franch X.	Bennet and Harvey, 2006

Table V. List of mutant alleles used. Examples of their use can be found in the Results.

6. Image Analysis

ImageJ (imagej.nih.gov/ij/) has been used to view and process all confocal images and time-lapses presented here. The Z-stack slices acquired to reconstruct the tissue were projected in 2D using the Maximum Intensity Projection (MIP) function of ImageJ, unless otherwise stated. To minimize the fluorescence noise given by the macrophages that patrol under the epidermis, the number of slices within the Z-stacks used to reconstruct the tissue in 2D was kept to a minimum.

6.1 Cell Orientation Dynamics from Cell Junction Outlines

The cell edges outlines were used to visualize and quantify the orientation of cell alignment within the plane of the epithelium relative to the A/P compartment boundary.

The A/P boundary was used as a reference to build a planar coordinate system in which its position and orientation was marking off the vertical axis (y-axis) of a Cartesian system of planar coordinates. Likewise, the horizontal axis (x-axis) related to the dorsal midline. Every cell or cell edge oriented parallel to the A/P boundary was considered as aligned to it. Orientations parallel to the dorsal midline were considered orthogonally aligned to the A/P boundary.

The OrientationJ software of ImageJ (Fonck et al., 2009 and Rezakhaniha et al., 2011) was used to visualize and quantify cellular orientations from 2D images. This plug-in is based on structure tensors, which are 2 x 2 symmetric matrix of eigenvalues derived from gradient and directional derivatives, commonly used in image processing to extract orientation features from input images (Jahne, 1997; Fonk et al., 2009; Puspoki et al., 2015). The structure tensor analysis computed with OrientationJ was employed with two purposes: 1) to color-code cell edge orientations relative to the A/P boundary over time (Cell edge orientation maps). 2) To quantify the magnitude of the local orientation and coherency between neighboring cells in region of interests (ROIs) (Locally averaged orientation maps). In Fig. 21 an example of the structure tensor analysis performed in histoblasts using OrientationJ is shown.

To quantify the local orientation (*i.e.* averaged orientation between neighboring cells) and to extract its orientation coherency, the territory occupied by the histoblasts was manually divided in small adjacent non-overlapping ROIs of uniform weight (64 x 64 pixels, which approximately correspond to 20 x 20 ⌠m). For each ROI, the software computed the predominant orientation (the direction of the largest eigenvector of the tensor matrix) and the coherency orientation of the cells within the ROI. The coherency is the ratio between the difference and the sum of the largest and smallest eigenvalues of the matrix. It describes the alignment of the cells with respect to the calculated predominant orientation. Coherency is bounded between 0 and 1, with values close to 1 indicating highly oriented cells and so uniformity in cell alignment with respect to the calculated dominant orientation. Values close to 0 indicate isotropic areas with low alignment degree.

The averaged numbers of cells locally oriented at certain angles relative to the A/P boundary in several pupae were reported in polar plots of axial values (16 bins distributed in 180°, ranging from +90°to -90°). The abundance of each resultant class was represented as proportional to the area of the class. Averaged values of coherency were reported in bar charts.

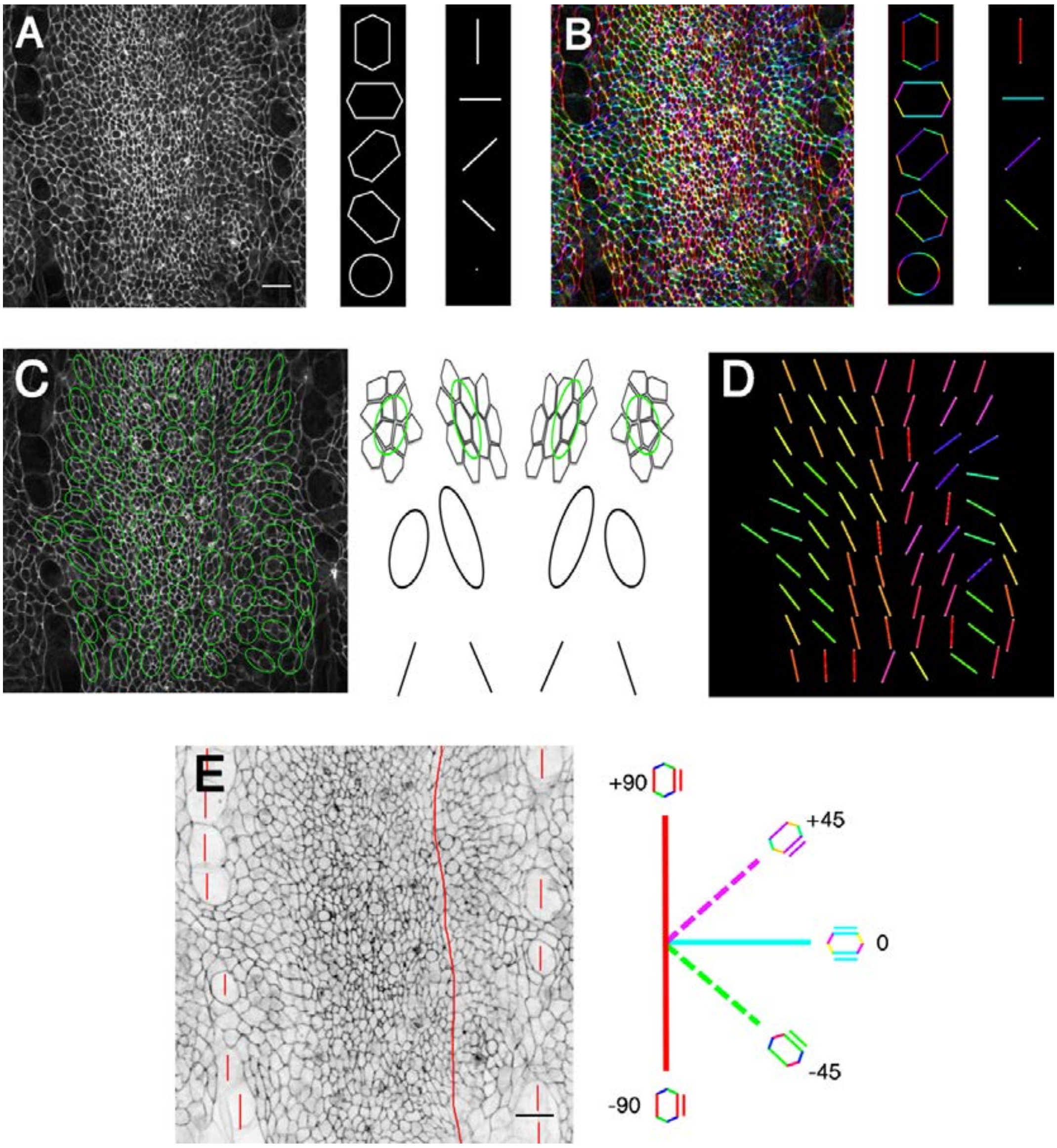

Fig. 21: Illustration of Cell Orientation Measurements. A) Left: input image showing histoblast morphologies outlined with the junctional marker Atpα::GFP. Right: different outline orientations for idealized cells (or their longest axis). A circle shows no preferred axis of orientation. **B)** Image as in A showing the orientations of the cell outlines after using OrientationJ filtering. The color-code takes the orientation angle as hue. **C)** Left: the image was divided in squared ROIs of uniform weight and the local orientation angle and magnitude (coherency) was calculated for each region. Right: illustration of the analysis outputs. The local angle and coherency of each ROI is visualized through ellipsoids. The ellipse longest axis represents the local preferred orientation and the ratio between its short and longest axis accounts for the magnitude or coherency of the orientations. **D)** A locally averaged orientation map was built by reporting the preferred local orientation of each ROI as a bar of uniform length. The colors highlight the orientation of each region. **E)** Inverted image as in A. Right: Colored compass of cell orientations aligned with the A/P boundaries. Anterior is to the left. Scale bar is 22 μm.

6.2. Composite Clone Diagrams

To represent the overall area, shape, orientation and position of the clones relative to their positions in the segmental field, the outline of individual clones were overlaid onto an idealized AIII hemi-segment using the location of its centroid employing the A/P boundary and the dorsal midline as reference points. Two independents clone diagrams were generated for each analyzed condition, one reporting the clone shapes at 26-28 hours APF and another reporting the clone shapes at 47-50 hours APF. The color-code employed was stochastically assigned (See also Sauret-Gueto et al., 2013).

6.3 Clonal analysis: 2D Geometrical and Shape Parameters from Clone Outlines

Geometrical and shape features were measured from Maximum Intensity Projections for images of the same magnification containing the clone(s) of interest in the segment. Clone areas were segmented with ImageJ by drawing their contours. From their outlines, geometrical and shape parameters were then calculated using ImageJ. The geometrical parameters included: the area, perimeter, aspect ratio (AR, a.k.a. length to width ratio) and the angle of orientation. The clone area was calculated as the sum of the pixels inside the clone boundary. The perimeter was calculated as the total boundary length of the clone. The AR was calculated as the ratio between the major and minor axes of the best-fit Legendre ellipse inscribed into the clone outline. The clone orientation was evaluated from the angle of the major axis of the clone relative to the A/P boundary. Four shape parameters were further evaluated. Shape parameters are non-dimensional ratios (Bounded values from 0 to 1) of the geometrical parameters described above. These dimensionless parameters represent the degree of deviation of the clones from ideal shapes such as a circle or a bounded convex hull. A shape factor equal to 1 usually represents an ideal case or maximum symmetry (and so, minimal complexity). This indicates that the measured shape is equal to the reference shape.

The shape parameters measured were: the Roundness, Roughness (Solidity and Convexity) and Circularity. These parameters were selected because of their sensitivity to specific aspect of clone morphology. Roundness, calculated as $4 \times [\text{area}]/\pi \times [\text{Major axis}]^2$, is a shape parameter that is just sensitive to the clone form. It is the inverse of the AR, revealing the elongation of the clone. Roughness describes the complexity of the clone form. For Roughness, two parameters were calculated: Solidity and Convexity. Solidity, calculated as Area/Convex Area, is sensitive to the area-based roughness of the clone morphology. Convexity, calculated as Convex Perimeter/Perimeter, is sensitive to the perimeter-based roughness of the clone morphology. Solidity and Convexity are normalized to the convex hull reference shape and are independent of the clone form. Circularity, calculated as 4π x [Area]/[Perimeter]^2, quantifies the similarity in outline of the form of the clone to the form of a circle and it is sensitive to the elongation of the clone form. Circularity is therefore sensitive to both form and roughness, since it measures the deviation of a particle from a circle, which can result from either changing particle elongation or increasing roughness.

The ratio for shape parameters (Circularity, Roundness, Solidity and Convexity) between the anterior and posterior edges of each clone was calculated by bisecting the clones' masks along their A/P axis. Shape parameters values were calculated independently for each hemi-clone. A simple ratio between the two values was determined. Values approaching 1 indicated no differences between the anterior and posterior edges, while values above 1 denote anterior higher values and below 1 posterior higher ones. For every parameter and ratios an independent red to green color-code LUT for increasing values was manually created.

6.4. Contact Angle and Contact Length Measurement

The angle between the cell edges aligned with the A/P boundary (A/P contact angle or α) was measured using ImageJ to assess the interfacial geometry between A/P oriented and parallel rows of cells in the mature epithelium. Similarly, the length of the two paired edges aligned between rows (A/P contact length or L) was also calculated. Both measurements were used to estimate adhesive distribution (differential adhesion) along the perimeter (Fagotto, 2014; Kafer et al., 2007; Hayashi and Carthew, 2004). The principle is schematically illustrated in Fig. 22 with hexagonal polygons. Regular hexagons are characterized by angles of 120° between paired edges, independently of the size of the polygon. Variations in one direction of this angle value will affect the form of the hexagon (Thomson, 1917) and, eventually, its orientation. The contact length is sensitive to both cell anisotropy and size.

21. Intensity Profiles Plots

To display and compare the expression profile levels of Ds, *fj* and Ft along the A/P axis at the selected stages, the averaged pixel intensity along the A/P axis of the tissue was plotted in 2D x-y graphs using the Plot Profile Option of ImageJ.

The averaged pixel intensity of Ds, *fj* or Ft within the histoblast territory was inspected by drawing rectangular selections covering the nests area at successive time points.

The resultant expression profiles were then over-imposed and their profiles normalized to the A/P boundary position.

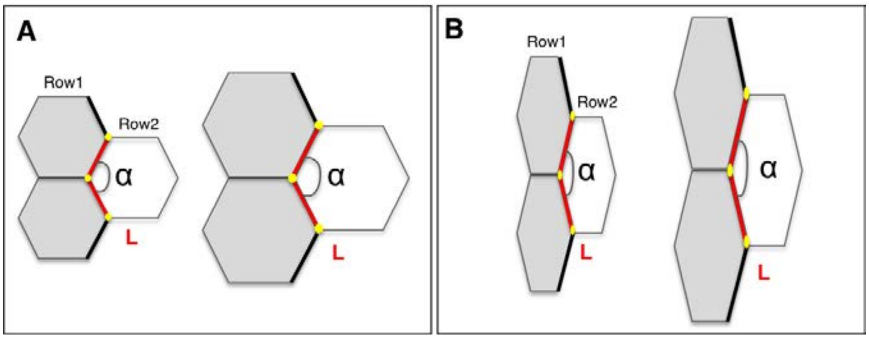

Fig. 22 Contact angle and length to estimate differential adhesion between cell rows A) Schematic illustration of the contact angle between rows composed by regular hexagons. Two adjacent rows are indicated by grey and white color. The A/P contact angle (α) and the contact length (red line) for one polygon are highlighted. Note that a simple variation in size does not affect α. **B)** Schematic illustration of the contact angle between rows composed by irregular hexagons. The A/P contact angle α will be larger than 120°. The contact length is sensitive to both cell shape and size. The contact angle is merely sensitive to cell shape (simple variations in cell size do not alter α either). See the Result section for more details.

7. Statistics

All graphs and statistics were performed with the PAST software (Hammer et al., 2001) unless otherwise indicated. Error bars in the graphs represent standard error of the mean (±SEM), and statistical significance of difference was determined using unpaired two-tailed Student’s t t-test for equal mean or the non-parametric Kolmogorov-Smirnov KS-test for equal distribution between the various measured genotypes or conditions.

Because axial data are appropriately described by directional statistics, the mean Rayleigh (R) vector, the circular mean (CM) and the angular deviation [AD, $\sqrt{2(1-R)}$] was calculated for each distribution of orientation. The statistical significance of differences between distributions was evaluated using the non-parametric Mardia-Watson-Wheeler W-test for equal distribution. In all cases the level of significance was set as: $p^* < 0.05$; $p^{**} < 0.01$; $p^{***} < 0.001$; $p^{****} < 0.0001$; NS, not significant $p > 0.05$ compared to control.

Results

Note for the Reader: In the course of this thesis I had considered the epithelial cells appearance as projected onto the plane. The following results are then presented from a merely two-dimensional or planar perspective.

"I call our world Flatland, not because we call it so, but to make its nature clear to you, my happy readers, who are privileged to live in Space. Imaging a vast sheet […] on which straight Lines, […], Squares, Pentagons, Hexagons, and other figures, instead of remaining in their place, move freely about, on or in the surface, but without the power of rising above or sinking below it, very much like shadows – only hard and with luminous edges – and you will then have a pretty correct notion of my country and countrymen"

Edwin A. Abbott, Flatland, Oxford University Press, 1884

Chapter I

Epithelial Morphogenesis and the Uniform Axial Orientation of Planar Cell Alignment (PCA) in the Mature Tissue

1.1 Long-term Live Imaging of the Abdominal Epithelial Morphogenesis during Pupation

To characterize the cell and tissue dynamics shaping the adult abdominal epithelium, long-term live imaging of the dorsal abdominal histoblasts was performed from the onset of tissue expansion until the acquisition of its final steady-state morphology. To faithfully image with high resolution, we outlined the cell junctions expressing a fusion protein, Atpα::GFP (Atpα localizes at the septate junctions), under its endogenous promoter. Further, to circumvent the ovoid shape of the pupa, we implemented two complementary imaging set ups. To follow up the initial epithelial expansion, the pupae were oriented dorso-laterally, while to image the last steps of expansion and to monitor contralateral nests fusion at the dorsal midline, the pupae were oriented dorsally. In both cases the analyses focused in the AIII segment (see also Materials and Methods).

The tissue expansion at the expense of the surrounding Larval Epidermal Cells (LECs) was followed from its onset. In The temporal progression of dorsolateral expansion within the plane of the AIII hemi-segment at 16, 20, 26 and 38 hours after puparium formation (hours APF) is shown in Fig. 23, Movie 1 and Movie 2. At the onset of expansion (16 hours APF) the anterior and posterior dorsal nests are physically separated by one row of intervening LECs (Fig. 23A and B). At 20 hours APF, the two nests already merged along the A/P compartment boundary and continue their expansion as a single group (Fig. 23A' and B') at the expense of the surrounding LECs that undergo basal delamination (Ninov et al., 2007). The differentiation of imaginal epithelial derivatives, such the external sensory organs (a.k.a. chaetae or bristles), initiates at this time.

At 26 hours APF the expanding nests fully occupy the territory bounded by the anterior and posterior inter-segmental larval cells (Fig. 23A'' and B'') and most of the bristles are already patterned. In the following 6-8 hours of development, histoblasts mitosis stop completely, their dorsal-ward expansion ceased and the last LECs disappear from the hemi-segment (Fig. 23A''' and B''') (Bischoff and Cseresnyés, 2009). During this time, the posterior-most two thirds of the P compartment folded down the epithelium, and only a very narrow band of the P compartment remained on the surface plane of the tissue (Fig. 23A''' and B'''). Between 16 and 30 hours APF proliferating histoblasts were migrating preferentially dorsal-ward while dividing (Fig. 23C and D) (see also Ninov et al., 2007b and Bischoff and Cseresnyes, 2009).

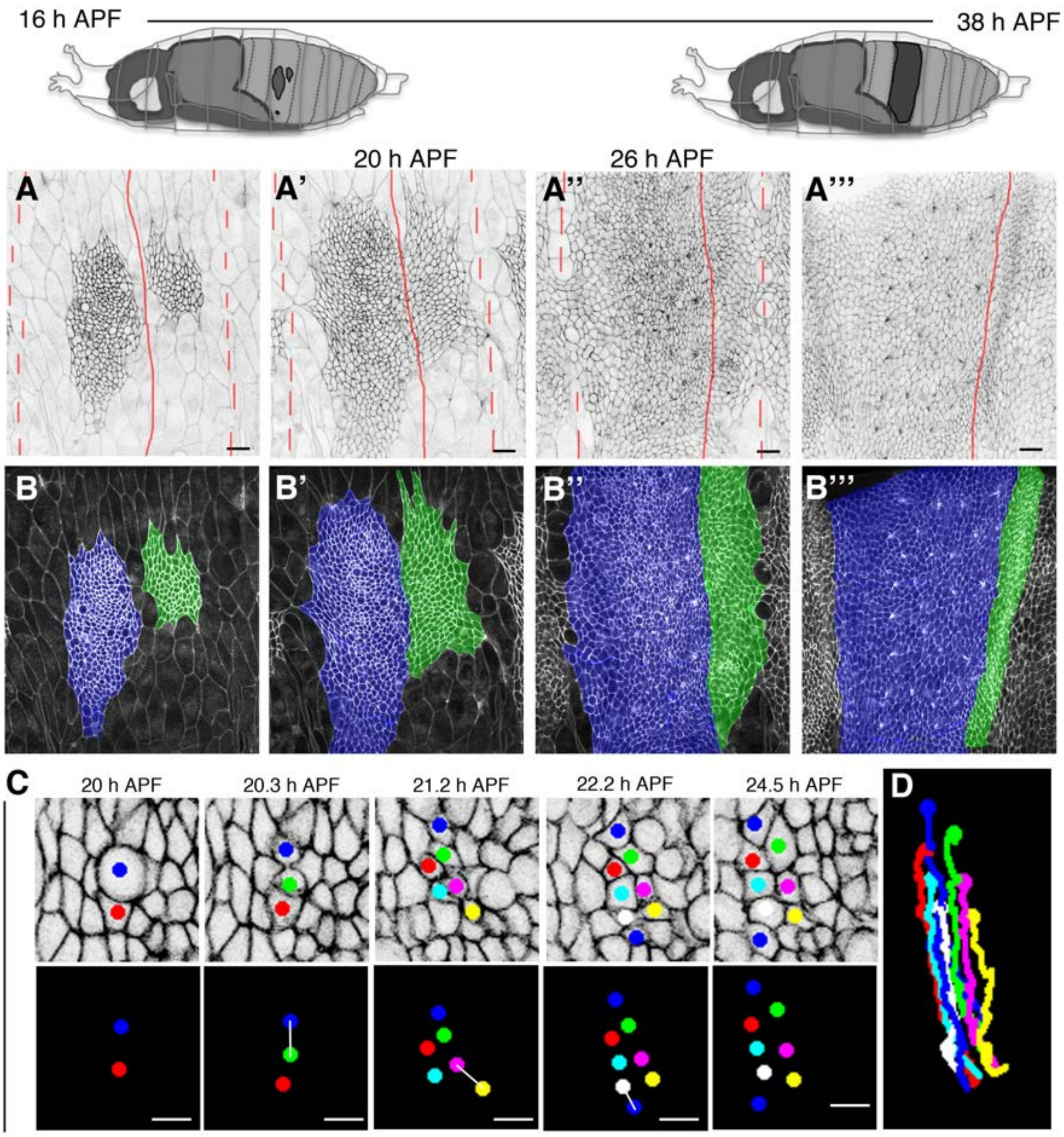

Fig. 23: Histoblast expansion and oriented movements in the AIII hemi-segment during pupation. Top: schematic view of the pupa and its orientation to image early histoblast expansion. The territory occupied by the nests is highlighted in dark grey. **A-A''')** Images showing cell outlines during expansion. The positions of the segmental boundaries are marked by red dashed lines (inter-segmental LECs, at the A/P and P/A segmental borders) or by red lines (A/P compartment boundary position). **B-B''')** Imaged as in A-A''', showing the anterior and posterior histoblast nests belonging to different compartments (color masked in blue – Anterior - and green - Posterior). Note that the P compartment narrows over-time. **C)** Tracking of dividing histoblasts and their relative movements between 20 and 25 hours APF in the A compartment. Daughter cells are linked with white lines (bottom panel). **D)** The displacement of the tracked cells highlights the dorsal-ward migration of the tissue (See also Bischoff and Cseresnyés, 2009). Anterior is to the left. Dorsal is up. Scale bar is 30 μm (A-A''' and B-B''') and 8 μm (C). Genotype was *Atpα::GFP*. See Movie 1 and Movie 2.

To report tissue remodeling, the temporal progression of the fusion at the dorsal midline within the plane of the expanding contralateral segment nests was reported at 34, 36, 38 and 47 hours APF (Fig. 24, Movie 3 and Movie 4).

Between 34 and 36 hours APF, the expanding contralateral nests progressively approach each other (Fig. 24A-A’) and by 38 hours APF, the presumptive segmental territory becomes fully occupied by histoblasts (Fig. 24A’’). By 47-50 % of pupariation (50 hours APF), the patterning of the bristles reached completion and cell movements arrest completely within the monolayer, indicating that the abdominal epithelium attains its final and stable configuration (Fig. 24A’’’). As histoblasts approached confluence (by 34 hours APF onwards) they were migrating preferentially anteriorly in absence of cell division (Fig. 24B and C) (see also Bischoff and Cseresnyes, 2009).

In summary, about 34 hours of development are required to shape and pattern the adult abdominal epithelium during pupation. The abdominal epithelial morphogenesis can be broadly divided into two phases. In the first phase, the imaginal tissue undergoes expansion by cell proliferation coupled to cell-by-cell LECs replacement. In the second phase, the imaginal tissue reaches confluence and cells readjust their final position in the absence of cell division. From now on, we will refer to the first phase as epithelial or tissue “Expansion” and to the second phase as epithelial or tissue “Remodeling”.

1.2 Proliferation and Intercalary Growth During Epithelial Expansion

From the onset of pupation until about 26-28 hours APF, the histoblast nests undergo expansion through cell proliferation and directional cell displacement at the expense of the pre-existing LECs (Fig. 23 Ninov et al., 2007; Bischoff and Cseresnyés, 2009). During histoblasts divisions, the nuclei move apically, leading to cell rounding and planar cleavage. At anaphase, the axes of division orient at variable angles with respect to the segmental borders and divisions orientations are not directionally biased at any time or position (Fig. 25A-B, Movie 5 and Garcia-Bellido and Merriam, 1971; Madhavan and Madhavan 1980; Bischoff and Cseresnyés, 2009). Interestingly, the absence of oriented mitosis was noticeable even before anaphase (Fig. 25C-E). *In vivo* visualization of mitotic spindles by expressing Jupiter::GFP (a microtubule-associated protein) revealed that in most cases the spindles rotate to align with the cells longest axes at anaphase (Fig. 25C-E and Movie 6). The rotational movements between prophase and anaphase do not follow stereotyped directions and encompass up to a 180° rotation (Fig. 25C’-E’).

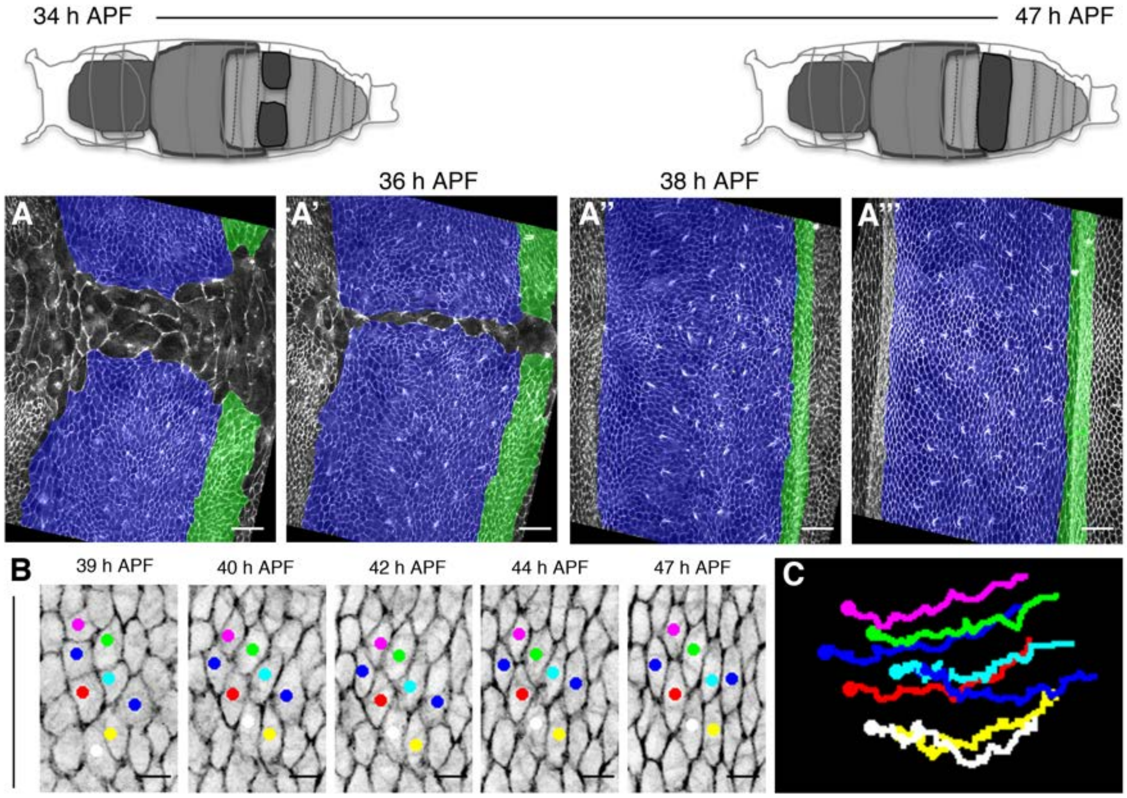

Fig. 24: Histoblast expansion and oriented movements in the AIII segment during pupation. Top: schematic view of the pupa and its orientation to image late histoblast expansion, fusion and confluence. The territory occupied by the nests is highlighted in dark grey. **A-A''')** Images showing cell outlines between 34 and 47 hours APF. The A/P boundary lies in between the two highlighted compartments (color masked in blue – Anterior – and green – Posterior). Note that the P compartment narrows over-time (see also Fig. 23B'''). The bright spots anterior to the rounded cells (bristle sockets) are the bristle shafts. **B)** Tracking of histoblasts movements at confluence (39-47 hours APF) in the A compartment. **C)** The displacement of the tracked cells describes their anterior-ward migration (See also Bischoff and Cseresnyés, 2009). Anterior is to the left. Scale bar is 30 μm (A-A''') and 5 μm (B). Genotype was *Atpα::GFP*. See text for details. See Movie 3 and Movie 4.

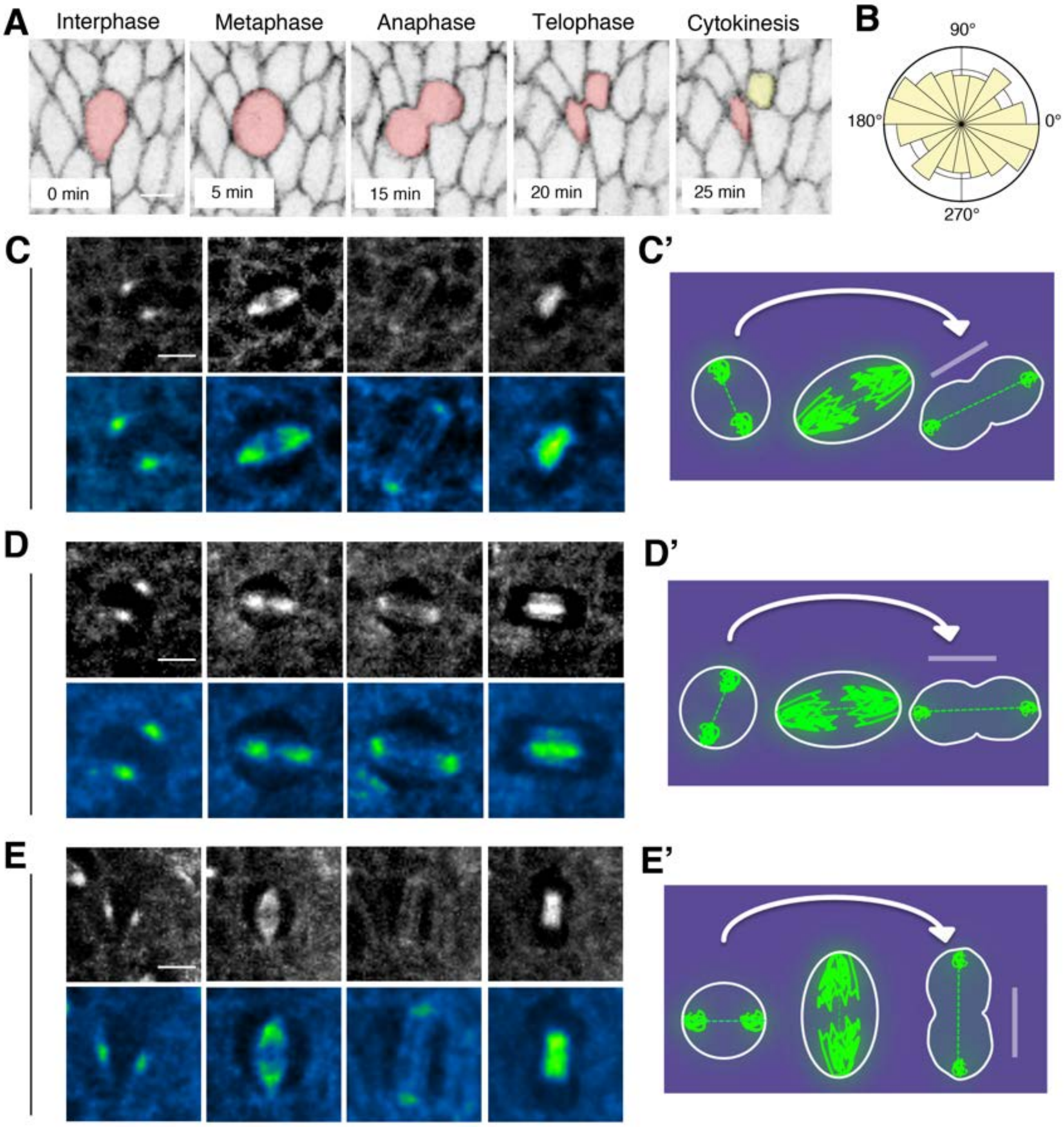

Fig. 25: Histoblasts divisions orient towards the cell longer axis during expansion. A) Dividing cell (red color masked) undergoing mitosis during tissue expansion. A full mitosis takes about 30 minutes. Note that the longer cell axis at anaphase correlates with the alignment of the daughter cells upon cytokinesis. **B)** Polar plot showing the orientation of cell division relative to the A/P boundaries (n=89 cells between 20 and 25 hours APF, A.D. ±78°, Bin size is 18°). A.D. is angular dispersion of the distribution. Note that the distribution is very dispersed. **C-E)** Examples showing mitotic spindle rotations prior to anaphase. Grey scale (Top) or Green-Fire-Blue LUT (bottom) for intensity (Green: high, Blue: low) are shown. **C'-E')** Cartoons illustrating spindle rotations before anaphase. In these examples clockwise rotations are shown; however counter-clockwise rotation were equally observed. Anterior is to the left, Dorsal is up. Scale bar is 5 μm. Genotype were *Atpα::GFP* (A) and *Jupiter::GFP* (C-E). See Movie 5 and Movie 6.

To study tissue growth patterning, marked clones were induced stochastically in the nests via the FLP/FRT technique (Xu and Rubin, 1993; and Materials and Methods). The growth of the clones was monitored to infer the cumulative effect of early migration and division on tissue growth at 26 hours APF.

We observed that the proliferative capacity of the tissue was fairly homogeneous throughout the nests; somatic recombination events were giving rise to growing clones of cells in any position within the anlage (Fig.26 A-G), so thus indicating a relatively uniform growth rate during expansion (see also Garcia-Bellido and Merriam, 1971; Guerra et al., 1973). Interestingly, the relative positions of sister-clones (twin spots) relative to each other were heterogeneous also reflecting the lack of a preferential orientation of the axis of divisions. Twin clones could lay either in tandem or in parallel arrangements within the A compartment (Fig. 26A-G).

Twin clones remained contiguous and the clone areas were not fragmented and very compact (Fig. 26A-G), indicating that despite extensive divisions and rearrangements and as previously reported (Garcia-Bellido and Merriam, 1971; Bischoff and Cserenyes, 2009; Umetsu et al., 2014), the contacts between sister-cells were maintained at short distance. Measurements of clones Aspect Ratio (AR, also known as length-to-width ratio) and angle of the longer axis (clone orientation) relative to the segmental boundaries indicate that at this stage most clones were elongated and oriented parallel to the anterior and posterior boundaries of the segment, (Fig. 26A-E). Just those clones abutting or closely apposed to the dorsal and ventral edges of the nests were more isodiametric in shape and often oriented perpendicularly to segmental boundaries (Fig. 26F-G). In summary, the growth of histoblasts during this period, up to 26 hours APF, is remarkably oriented (Fig. 26H). Further, the perimeter of the clones was irregular, showing numerous indentations (Fig. 26H and Lawrence et al., 1999 and display high shape complexity (Roughness, see also Materials and Methods). Complexity and elongation could be the cumulative result of short-range cell-to-cell intercalations and/or dorsal-ward directed migration (Bischoff and Cserenyes, 2009; Umetsu et al., 2014).

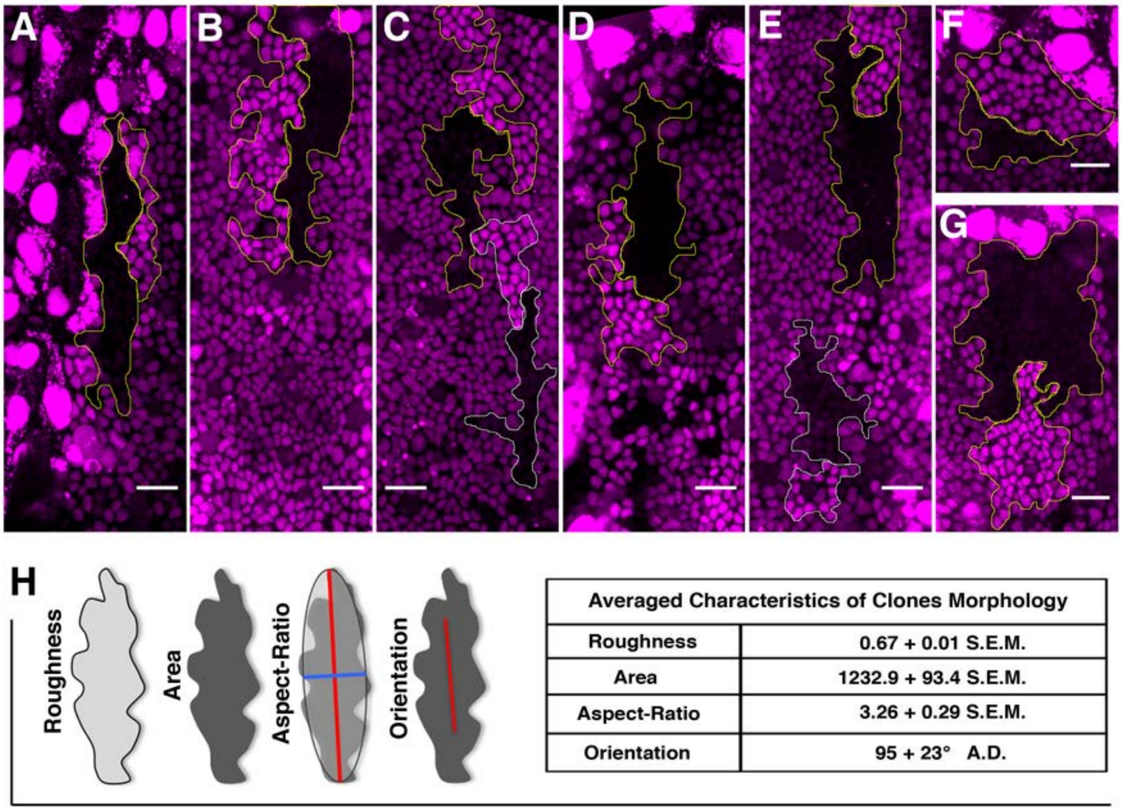

Averaged Characteristics of Clones Morphology	
Roughness	0.67 + 0.01 S.E.M.
Area	1232.9 + 93.4 S.E.M.
Aspect-Ratio	3.26 + 0.29 S.E.M.
Orientation	95 + 23° A.D.

Fig. 26: Tissue growth is preferentially oriented with the tissue axes during expansion. Clones of cells in the A compartment marked by the absence of RFP.nls (black) and their twin-spots (bright magenta) at 26 hours APF. **A)** Examples of clones at the anterior edge of the compartment. Note the elongated sister-clones laying parallel to each other. **B-D)** Examples of various clones located within the central region of the A compartment**.** Note that the clones are always elongated in parallel to the segmental boundaries. Twin clones arrange reciprocally in parallel (A) or in tandem (C, D). **E)** Example of a clone located at the posterior edge of the compartment. Note that it elongates in parallel to the segmental boundary. **F-G)** Examples of clones at the dorsal edge of the anterior nest. Note that the clones orient almost perpendicularly to the segmental boundaries (F) or are isodiametric (G). **H)** Left: Cartoons describing the parameters quantified from the clone outlines. Right: summary table reporting the average values for the indicated parameters (*n*=29). Anterior is to the left, Dorsal is up. Scale bar is 22 μm. Genotype was *hsflp1.22*;*FRT40A/FRT40A Ubi.RFP.nls*. See text and Materials and Methods for more details.

1.3 Cell-Cell Interactions Increase during Tissue Remodeling

By 26-28 hours APF the proliferative capacity of histoblasts decreases (Guerra et al., 1973; Santamaria and Garcia-Bellido, 1972; Garcia-Bellido and Merriam, 1971) and their migration upon confluence turn into an anterior direction (See Fig. 2C and Bischoff and Cseresnyés, 2009). To assess the impact of these events on tissue growth, geometrical (area, perimeter, AR and orientation) and shape parameters (roughness, roundness and circularity, see also Materials and Methods) were evaluated at the end of tissue remodeling (47 hours APF, Fig. 5A-B). At this time, the shape of the clones changed in two aspects (Fig. 27C-E), their area enlarged and their perimeter increased significantly (Fig. 27C).

Yet, their averaged elongation (AR, Roundness, Circularity) or orientation (Fig. 27C-D) and averaged shape complexity (Solidity, Convexity, Circularity) were unchanged (Fig. 27E). Thus, the directional changes in migration taking place in this time window did not have a measurable impact neither on the wiggly aspect of clone shape nor on its narrowing and orientation.

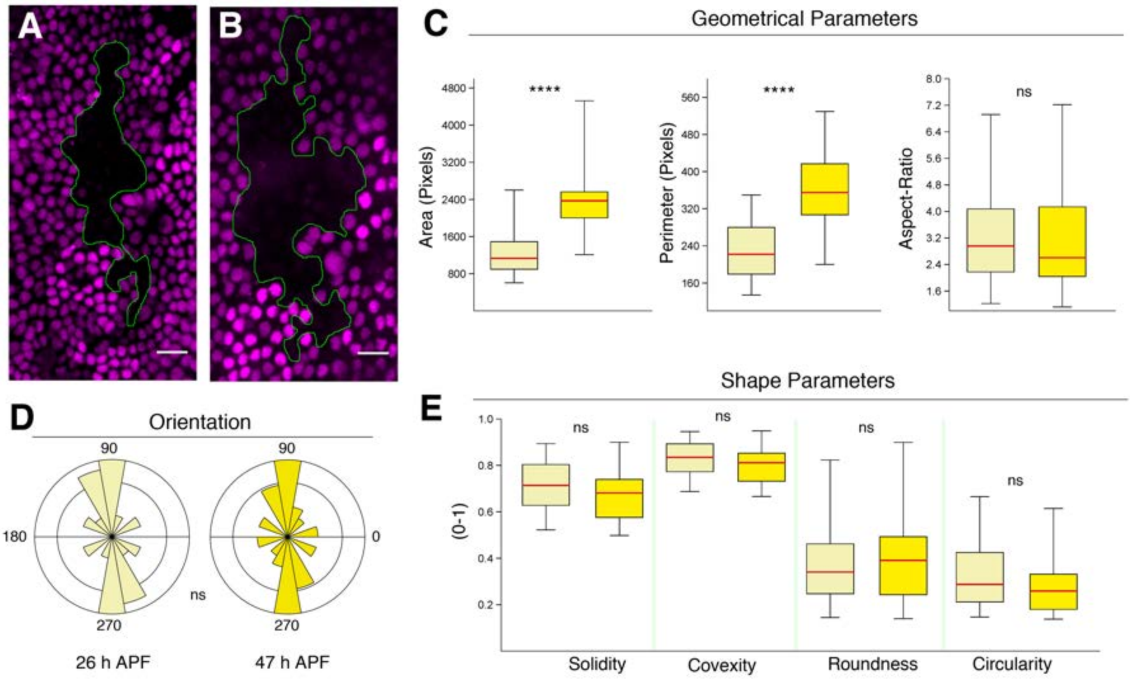

Fig. 27: Local tissue growth reveals increased cell-cell contacts during remodeling. A-B) Example of clone morphology at 26 (A) and 47 hours (B) APF. Note that the clones, marked by the absence of RFP.nls (black), show elongated and complex border morphology at both stages. **C)** Box and whisker plots for geometrical parameters at 26 (light yellow) and 47 hours APF (dark yellow). Note that the averaged area and the perimeter of the clones increase significantly in this time-window. **D)** Polar plots (Bin size 18°, abundance proportional to the area) representing the orientation of the clones. Note that the clones maintain their orientation during remodeling. **E)** Box and whisker plots for shape parameters at 26 (light yellow) and 47 hours APF (dark yellow). Note that roughness (solidity and convexity), roundness and circularity barely change. In all box plots, the 25-75% quartiles are drawn in a box. The median value is shown with a red horizontal line and whiskers extend to the minimum and maximum values of the distribution. Averaged values from clones collected at 26 (n= 29) and 47 hours APF (n=26) compared with the K-SM (C and E) or W-test (D). p<0.0001****, p>0.05 ns (not significant). Anterior is to the left, Dorsal is up. Scale bar is 16 μm. Genotype was *hsflp1.22*;*FRT40A/FRT40A Ubi.RFP.nls*. See text and Materials and Methods for details.

A proportionally higher change in perimeter than area indicated that, during remodeling, an extensive degree of contact between the clone and adjacent cells is built up. To evaluate cell contact rearrangements, junctional dynamics was monitored marking apical cell outlines with DE-Cadherin::GFP. This let to observe that during remodeling histoblasts changed their relative positions by intercalation (Fig. 28 and Movie 7; See also Fig. 24).

Neighboring cells moved in relation to each other at short distance, eventually leading to long-range cell arrangement in parallel rows (Fig. 28A-A’’ and B-B’’). Juxtaposed cells were either squeezing past each other or separated by intervening cells undergoing intercalation (Fig. 28A-A’’). Cells junctions often underwent shrinking and expansion by T1 transitions (Bertet et al., 2004). A full T1 transition generally took around 25-30 minutes (Fig. 28C-D and Movie 8). Remarkably, histoblasts undergoing T1 intercalations were just barely moving apart from each other as a result of their extreme anisotropic shape. They were markedly elongated, showing a compressed shape aligning in parallel to the A/P axis (Fig. 28C-D).

1.4 Cellular Arrangements and The Uniform Orientation of Planar Cell Alignment in the Mature Epithelium

As just shown, mid-way through pupal development (50 hours APF), the abdominal epithelium is fully shaped and almost completely differentiated. The cells composing each abdominal segment arrange in neat aligned rows uniformly oriented in parallel to the A/P compartment boundary (Fig. 29). This precise oriented arrangement was invariably detected across the entire segmental field, giving to the tissue its highly regular appearance. The ordered disposition of cells in iterative arrays was periodically interrupted by roundly shaped cells (Fig. 29A-D), which correspond to the bristle sockets. These were spaced almost uniformly within each segment (4-to-5 rows in the AIII segment) occupying the most posterior two thirds of the A compartment (Fig. 29A-C). Of note, however, neither the spaced bristles nor any variations in apical cell size or neighbor relationships (topology) disturbs the uniformity of cell alignments (Fig. 29D-D’’; see also Fig. 30). Thus, all histoblasts, with the exception of those of the bristle lineage, are similarly shaped within the plane of the tissue. Alongside the uniform elongation and orientation of histoblasts, the cell-cell contacts between rows were systematically larger than any other contact they make at steady state (Fig. 29E-H). This implies that the cell perimeter is not equally shared between adjoining cells, being maximized in parallel to the A/P boundary.

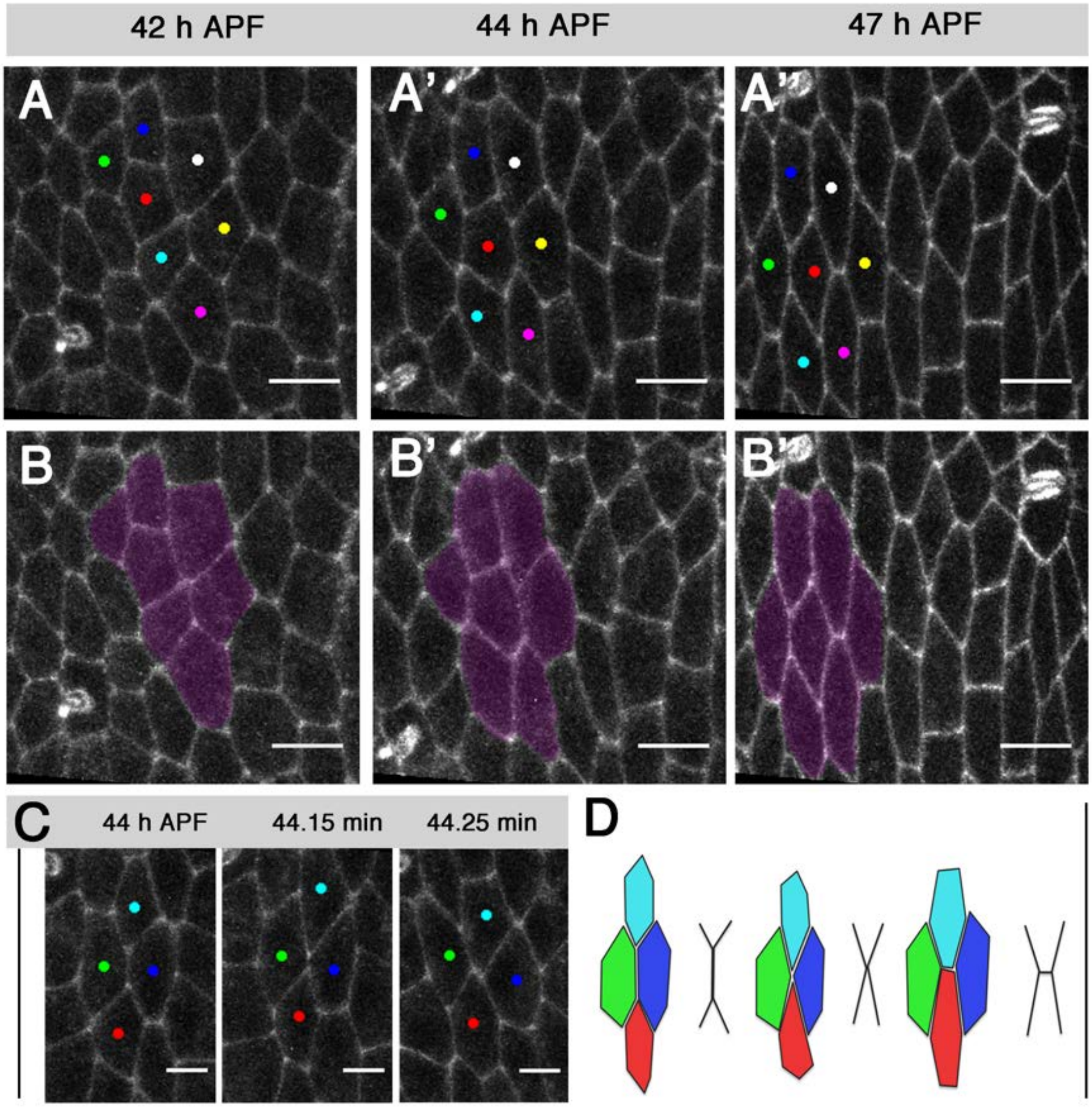

Fig. 28: Junctional dynamics during remodeling. A-A'') Images showing the tracking of seven cells between 42 and 47 hours APF. Note that most of the cells relocate in the plane over time without loosing or gaining new junctions (blue and white, green and red, cyan and magenta, or white and yellow cells squeeze past each others) while some of them slightly move apart (red and yellow, or white and cyan cells). By 47 hours APF no junctional exchanges occurs in the epithelium anymore. **B-B'')** The tracked region was masked in purple. Note that the tissue shifts anteriorly while cells progressively arrange in rows. **C)** Tracking of cells undergoing junctional remodeling through T1 transitions at 44 hours APF. **D)** Schematic diagram showing the steps characterizing a T1 transition as in C. Note that the cells have a remarkable anisotropic shape that does not change during remodeling. Anterior is to the left and posterior to the right (see also Fig. 29). Scale bar is 8 μm (A-A'' and B-B'') and 5 μm (C). Genotype was *ubi-DEcadherin::GFP*. See Movie 7 and Movie 8.

To evaluate histoblasts anysotropy in aligned arrays at steady state, we measured the internal angle between paired cell edges accross rows (A/P contact angle, α), together with the length of such oriented contacts (A/P contact length, L) (Fig. 29F-G). It has been suggested that the parameters α and L at steady state reflect differences in distribution of adhesive/contractile properties along cell perimeters (Hayashi and Carthew, 2004; Keifer et al., 2007).

Thus, if the adhesive/contractile properties of cells are equally distributed around a polygonal cell perimeter, the same angle value would be expected between paired edges independently on the size of the polygon (e.g. for a regular and planar hexagon all paired edges have a value of 120° indicating that the perimeter of the polygon has isodiametric properties (Fig. 29F, Thompson, 1917 and Materials and Methods). Unequal or differential distributions of adhesive/contractile properties at the cell periphery, however, will be reflected in deviations from this angular value (Fig. 29G). We found that, on average, the A/P aligned interfaces between histoblasts at steady state were oriented at 144° (± 11° A.D., n=232 angles) from each other, with an averaged contact length of 11 μm (± 0.11 SEM, n= 232 cells; Mean A.R. 2.3 ± 0.3 SEM n=356 cells).

Last, to investigate the spatial, temporal and angular dynamics driving the uniform orientation of cell arrangements, topographical maps displaying the angular orientation of individual cell edges relative to the tissue axes were built for both the expansion and remodeling periods. To do so, we employed the OrientationJ software (Rezakhaniha et al., 2011; Fonck et al., 2009; see also Materials and Methods). The reference axes correspond to the A/P compartment boundary (y-axis) and the dorsal midline (x-axis) on a standard Cartesian system of planar coordinates (Fig. 30). Any edge oriented in parallel to A/P boundary (±90°) was color-coded in red. Similarly, orthogonal orientations were color-coded in cyan. Any other angle in between (+90°, 0°, -90°) were color-coded with distinctive hues (*i.e.* +45°, magenta; -45° green; see Fig. 30, sections 1.5 and 1.6 and Materials and Methods). At steady state this methodology precisely recapitulate the uniform configuration of the anisotropic histoblasts in aligned rows parallel to the A/P compartment boundary (Fig. 30). From here onwards this tissue configuration will be refer as axial uniform orientation of "planar cell alignment” or PCA.

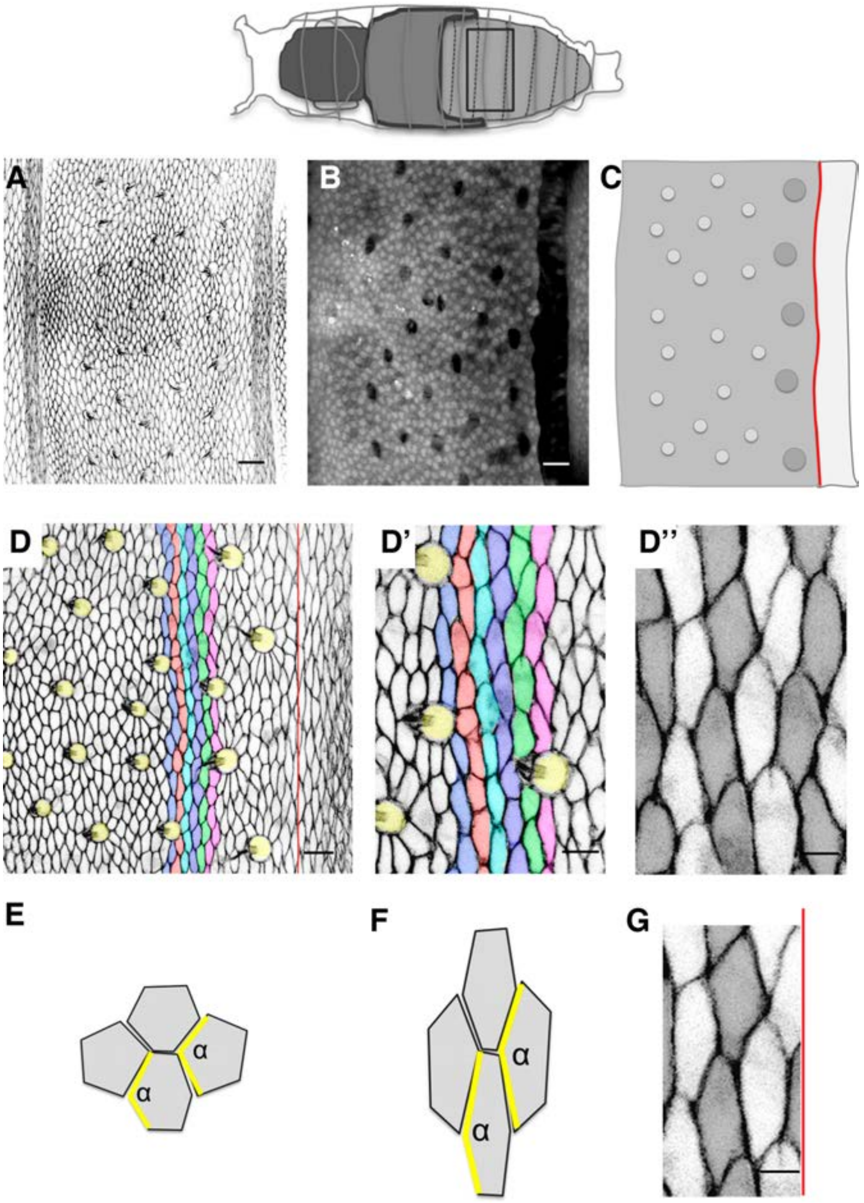

Fig. 29: Mature histoblasts are uniformly arranged in parallel rows across the A/P axis. Top: Schematic diagram of a pupa displaying the medio-dorsal region of the AIII segment. **A)** Uniform arrangement of cells in the mature epithelium (47-50 hours APF). The rounded cells correspond to the bristle sockets. **B)** Cells of the A compartment are marked by expressing GFP (grey) in the *ci* expression-domain with the Gal4/UAS system. Dark rounded cells correspond to bristle sockets. Note that the P compartment (unmarked) constitutes a very narrow band of few cells. **C)** Cartoon describing the mature dorsal epithelium of the AIII segment showing the pattern of the chaetae. Dark grey circles represent Macrochaetae (Mc) and light grey circles represent microchaetae (mc). Note that the Mcs lie close to the A/P boundary. **D)** Image highlighting the uniform arrangement of cells in rows (color masked in multiple hues) aligned parallel to the A/P boundary (Red line). Socket cells are masked in yellow. **D'-D'')** Magnifications highlighting the epithelial arrangements shown in D. Note that the periodic appearance of rounded sockets (D') does not perturb the arrangement in parallel rows. **E)** Cartoon representing cells approaching a regular polygonal geometry. The contact angle between the A/P oriented edges (yellow), as well as the other internal angles will approach 120° (regular hexagon) or 108° (regular pentagons) **F)** Cartoon representing anisotropic polygonal shapes such those of the histoblasts. The contact angle between the A/P oriented edges (yellow) is about 144° independently of the polygonal class and cell size. Other angles will consequently have values below 120°. **H)** Image showing the anisotropy of the histoblasts parallel to the A/P boundary (red line). Anterior is to the left. Scale bar is 22 µm (A-B), 16 µm (D), 10 (D') and 5 µm (D'', E and H) µm. Genotype were *Atpα::GFP* and *ci-Gal4>UAS-GFP*.

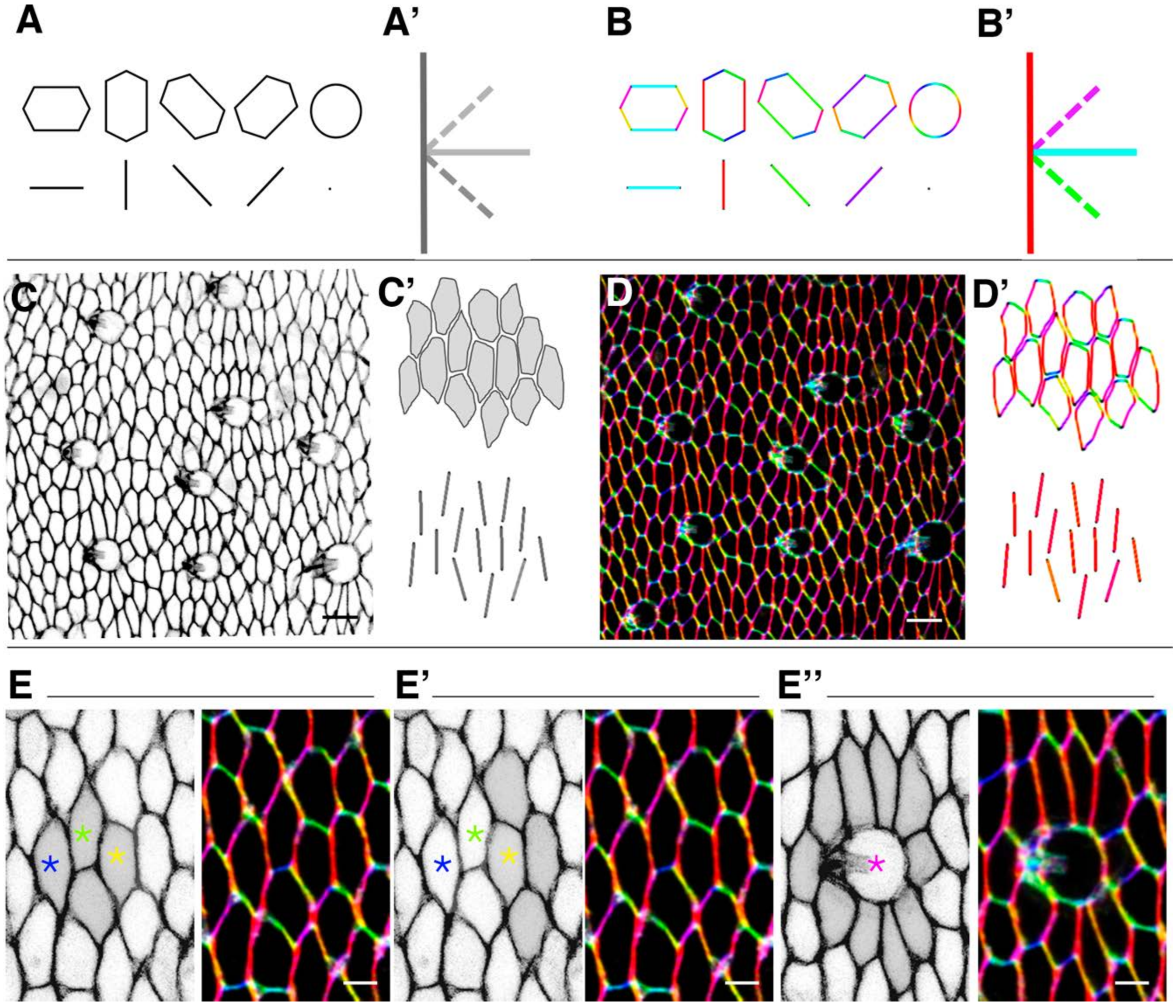

Fig. 30: The mature epithelium displays axial uniform orientation of planar cell alignment parallel to the A/P axis. A) Schematic representation of idealized cell outlines (hexagons) with different orientations. The bars below each polygon represent their orientation axis. A circle shows no preferred axis of orientation (point). The compass indicates the orientation axes. **B)** Same scheme as in A but with color-coded cell orientations relative to the tissue axes (compass) **C-C')** Abdominal cells outlines (C) and cartoons describing their shapes and their corresponding mean axis orientations (bars) (C'). **D-D')** Images and cartoons as in C-C' but color-coded as above. Note that the A/P oriented edges and means (bars) show the same color (reddish). **E-E'')** The oriented maximization of the cell contacts between rows is not influenced by variations in packing topology. E) Image showing a cell with 6 (green) or 7 (blue) neighbors (left) and their colored cell edge orientations (right). Note that the edges between A/P rows are always reddish in color. E') A cell with 5 neighbors (yellow) (left) and its colored edges orientations (right). E'') The presence of socket circular cells (left) only slightly perturbs the arrangement of the cells in parallel rows (right). Anterior is to the left. Scale bar is 12 μm (C, D) and 5 μm (E-E') μm. Genotype was *Atpα::GFP*. See text for details.

1.5 Axial Orientation of Planar Cell Alignment during Histoblast expansion and remodeling

In order to understand how the orientation of PCA is acquired and evolves, we monitored the topography of the orientation of cell outlines over-time. Two complementary analyses were employed: first, overall spatio-angular maps of cell outline orientations were generated. Second, the orientation of neighbors was locally averaged to highlight local patterns.

We focused first on the developmental window between the onset of expansion and the decay of proliferative activity of the tissue (16-to-26 hours APF) of histoblast expansion within the hemi-segment (Fig. 31A). Initially, at the onset of expansion phase, histoblasts are mostly anysotropic but do not organize in any particular orientation. In the A compartment, almost every cell orients in different directions while in the small P compartment predominantly orient parallel to the A/P boundary. As expansion evolves, some stereotyped local changes in orientation were observed, mainly in the A compartment, while in P, as the territory enlarges, some orientation differences can be distinguished amongst those cells not abutting the compartment boundary (Fig. 31B-B'', C-C'' and D-D''). Between 20 and 26 hours APF, the preferential A/P parallel orientation of cells close to the A/P boundary spread anteriorly to multiple cells within the compartment (Fig. 31B-B', C-C', D-D' and Movie 9). Thus, during expansion, a uniform axial orientation of PCA did not fully develop and regional or local patches of aligned cells were observed. The orientation of the cells was only locally concordant (between neighboring cells) and regionally organized (with some stereotyped variations across the A/P axis within the A compartment) by the end of expansion.

We then studied the developmental window of histoblasts remodeling (38 - 47 hours APF) within the A compartment and the accessible part or unfolded region of the P compartment (Fig. 32A). Notably, even though the cells were not yet uniformly oriented through the tissue as a whole, two main oriented patches, one anterior and one posterior were clearly visualized at 38 hours APF. Cells located in the anterior half of the A compartment oriented almost perpendicularly to the A/P boundary, while cells at the posterior half (as well as cells in contact to the anterior segmental border) of the A compartment and in the narrow P compartment aligned in parallel to the A/P boundary (Fig. 32B, C, D). Between 38 and 42 hours APF the histoblasts within the anterior half of the A compartment reoriented toward the A/P boundary in a process that occurred in a coordinate manner progressing from posterior to anterior (Fig. 32B-B', C-C', D-D' and Movie 10). In the following 5 hours, all histoblasts became uniformly oriented in parallel to the A/P boundary (Fig. 32B'-B'', C'-C'' and D'-D''), showing the uniaxial cell arrangement previously described (see also Figs. 29 and 30).

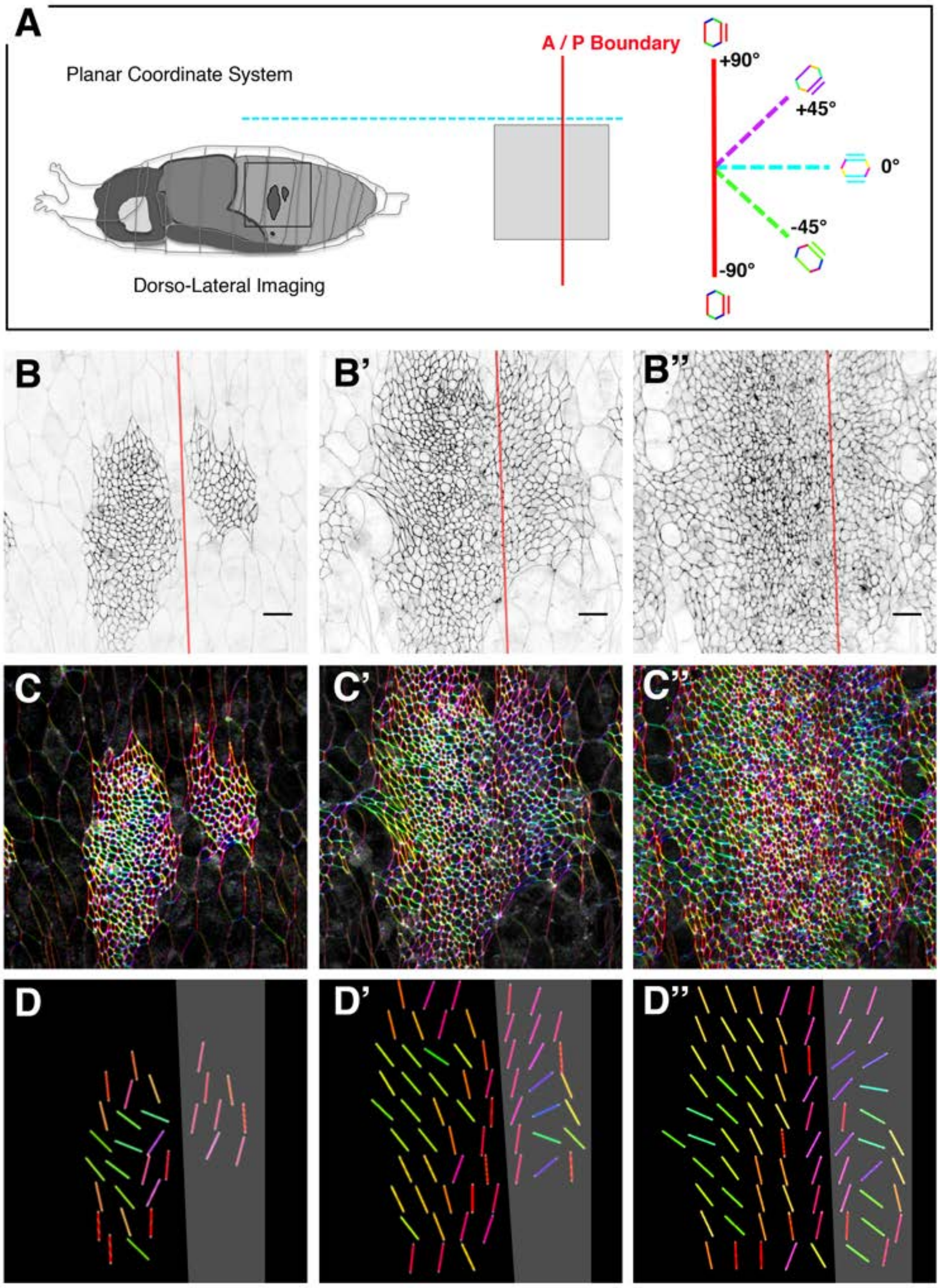

Fig. 31: Evolution of axial orientation of cell alignment during tissue expansion. A) Cartoon showing the orientation of the pupa (left) and the defined planar coordinate system (middle). The A/P boundary position (red line) and the dorsal midline (cyan dashed line) define the Cartesian plane. (Right) Axial compass showing the color-code employed for cell edges (polygons) or averaged orientation (bars). Red indicates cell orientations parallel to the A/P boundary, while cyan indicates orientations perpendicular to it. **B-B'')** Images showing cell outlines at 16 (B), 20 (B') and 26 hours (B'') APF. The position of the A/P boundary is indicated by red lines. **C-C'')** Cell edge orientations maps colored with OrientationJ. Note that cell edges orientations are not uniform relative to the A/P boundary. **D-D'')** Locally averaged maps showing heterogeneous cell edge orientations. The P compartment is masked in grey. Note that cells located in the proximity of the A/P boundary tend to be aligned to it. Anterior is to the left. Scale bar is 22 μm. Genotype was *Atpα::GFP*. See text and Materials and Methods for details. See Movie 9.

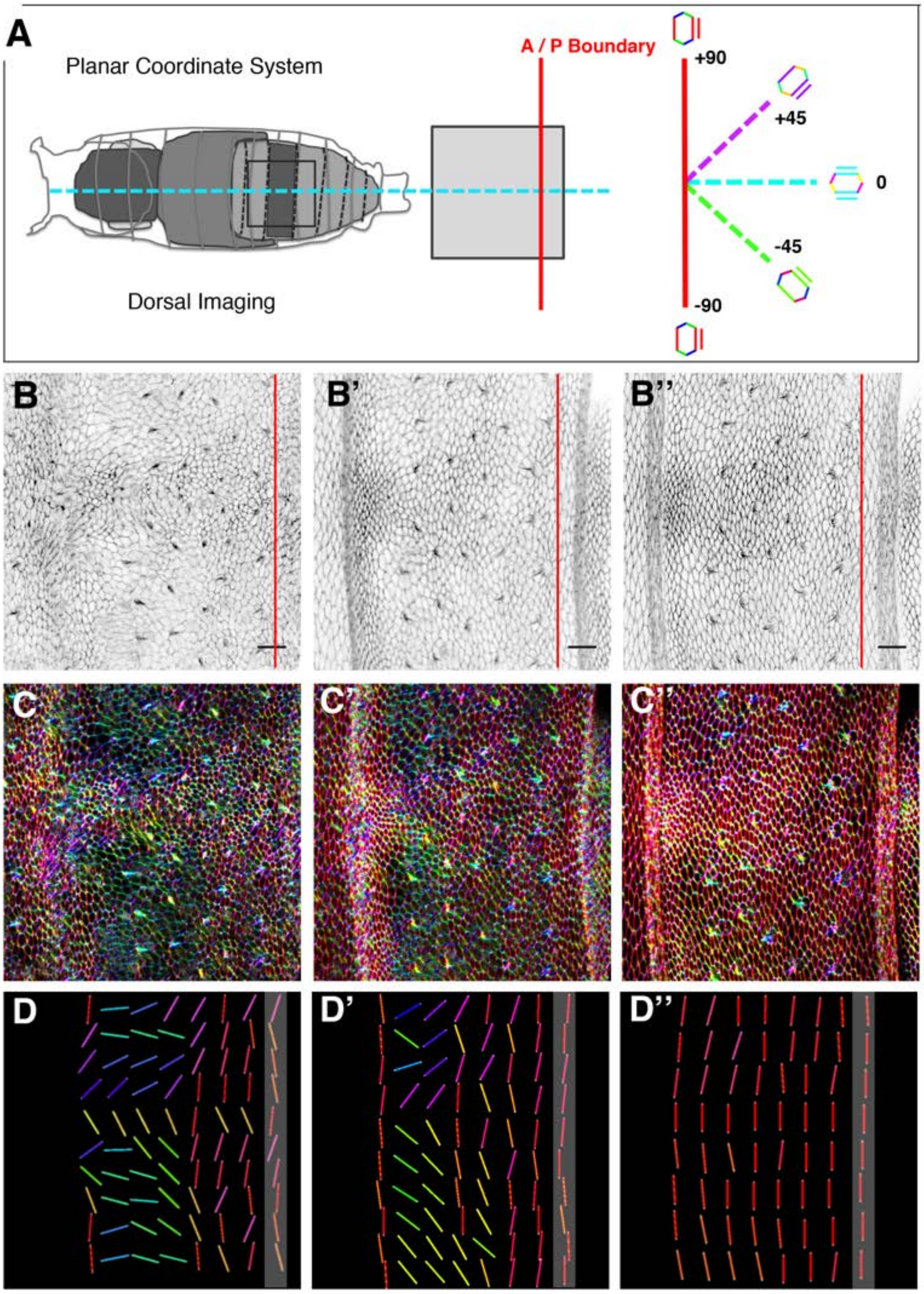

Fig. 32: Evolution of axial orientation of cell alignment during tissue remodeling. A) Cartoon showing the orientation of the pupa (left) and the defined planar coordinate system (middle). The A/P boundary position (red line) and the dorsal midline (Cyan dashed line) define the Cartesian plane. (Right) Axial compass showing the color-code employed for cell edges (polygons) or averaged orientations (bars). Red indicates cell orientations parallel to the A/P boundary, while cyan indicates orientations perpendicular to it. **B-B'')** Images showing cell outlines at 38 (B), 42 (B') and 47 hours (B'') APF. The position of the A/P boundary is indicated by red lines. **C-C'')** Cell edge orientations maps colored with OrientationJ. Note that over time, cells orient parallel to the A/P boundary progressing from posterior to anterior. **D-D'')** Locally averaged maps highlighting the posterior-to-anterior cell re-orientation during remodeling. The P compartment is masked in grey. Anterior is to the left. Scale bar is 22 μm. Genotype was *Atpα::GFP*. See text and Materials and Methods for details. See Movie 10.

To further characterize the overall dynamics of the process, the orientation of cell alignment with the A/P boundary and the evolution of cell alignment between neighboring cells during morphogenesis were quantified at the onset and completion of expansion and remodeling (Fig. 33A to C’). This quantification (Fig. 33D and E) confirmed that before remodeling, cells locally aligned to each other with disperse orientations and did not achieve an overall parallel alignment to the A/P boundary. During remodeling, however, cells reoriented their axis and by 47 hours APF uniformly aligned both with the A/P boundary and with each other. Uniformity in cell orientation was accompanied by a sharp increase in mutual alignment.

Taken together these data indicated that the attainment of a uniform oriented PCA in parallel to the A/P axis is an emerging phenomenon with a long time-scale dynamics. The above analyses showed that the attainment of a uniform orientation of cells follows a stereotyped pattern. The axial orientation of PCA evolves along morphogenesis through a temporally controlled topographical progression intimately linked to the body axes.

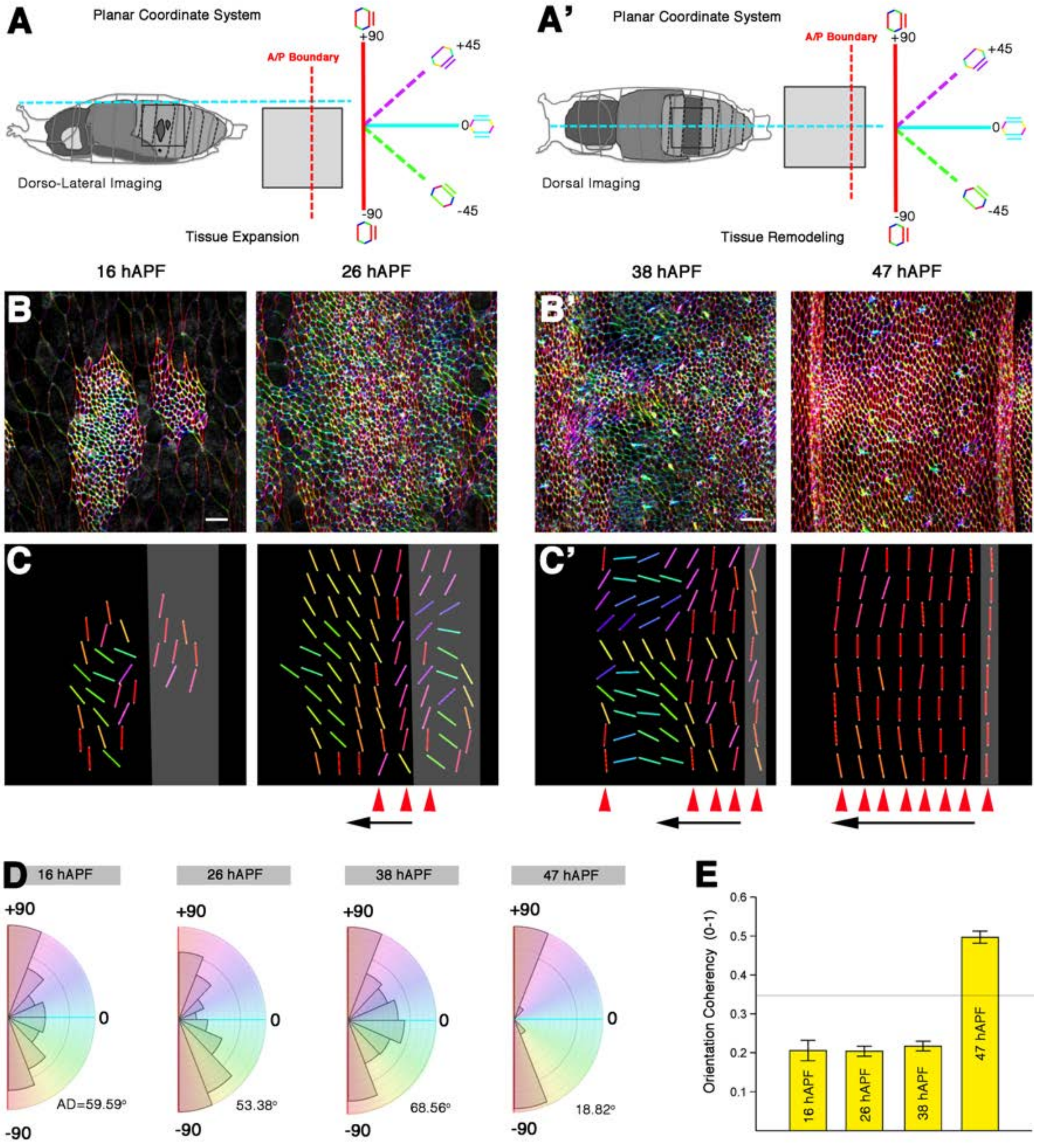

Fig.33: Axial orientation of PCA is patterned along the A/P axis. A-A') Cartoon showing a dorso-lateral (A) or a dorsal view of a pupa (A') and the defined planar coordinate system. The A/P boundary position (red line) and the dorsal midline (Cyan dashed line) define the Cartesian axes of planar coordinates. The axial compass shows the color-code employed for cell edges (polygons) or averaged orientations (bars). Red indicates cell orientations parallel to the A/P boundary, while cyan indicates orientations perpendicular to it. **B-B')** Cell edge orientations colored with OrientationJ at expansion (B) and remodeling (B'). **C-C')** Locally averaged orientations maps showing the pattern of oriented PCA at expansion (C) and remodeling (C'). Red arrowheads indicate the extension of the aligned regions. Black arrows indicate the direction of propagation. The P compartment is masked in grey. **D)** Polar plots displaying the distribution of orientations relative to the A/P boundary. Bin size is 16°. Abundance is proportional to the area. **E)** Quantification of mutual alignment (Orientation Coherency) between neighboring cells. Values below 0.35 represents low mutual alignment, greater values indicate coherent alignment along the mean orientation. Error bars represent SEM n=80 (16 hours APF), 225 (26 hours APF), 240 (38 hours APF) and 192 (47 hours APF) ROIs in 6 pupae. Anterior is to the left. Scale bar is 22 μm. Genotype was *Atpα::GFP*. See text and Materials and Methods for details.

1.6 The Uniform Orientation of PCA and Planar Cell Polarity (PCP) in the Abdominal Epidermis

In *Drosophila* each mature epithelial cell displays a precise array of cytoskeletal protrusions that invariably point posteriorly (Struhl et al., 1997). The consistent orientation of these subcellular structures in the adult fly reflects the distinctive planar polarity of the abdominal epithelium. Both hairs (a.k.a. trichomes) and bristles (a.k.a. chaetae) are actin- and microtubule-rich cell structures that arise from the apical cell surface (Turner and Adler, 1996). While trichomes are non-sensory apical protrusions elaborated by single epithelial cells, bristles are sensory protrusions produced by shaft cells of Sensory Organ Precursor (SOP) clusters (Fristrom and Fristrom, 1993).

To assess the relationship between the planar polarization of mature epithelial structures (PCP) and the acquisition of uniformity in the orientation of histoblasts, the timing and behavior of planar polarity was analyzed by *in vivo* imaging. Fluorescent microtubules or actin cytoskeletal markers were monitored soon after histoblast confluence (40 hours APF, Fig. 34 and Movie 11 and Movie 12). By this time both microtubules (Fig. 34A-B) and actin microfilaments (Fig. 34C-D) rapidly extended posteriorly from bristles shafts. This posterior-ward directed elongation of bristles was almost completed in around 10 hours (Fig. 34-A-C). Actin-rich trichomes growing posteriorly were instead detected late during remodeling when bristle outgrowth was half-way accomplished (Fig. 34B-D). To characterize the implementation of PCP, the dynamic outgrowth of the trichomes was studied in detail (Fig. 35). Neither microtubules nor their growing tips (*e.g.* +ends) were showing an obvious polarized behavior prior to 43 hours APF (Fig. 35A-B and Movie 13). Similarly, actin was uniformly distributed through the cell perimeters until about 43 hours APF (Fig. 35C-D). By 45 hours APF, however, histoblasts started accumulating actin microfilaments and, to a lesser extent, microtubules, at the posterior side of each cell (Fig. 35A-D), and soon after, the posteriorly accumulated actin/microtubule network gave rise to multiple trichomes stumps. On average, each cell produced around 5 trichomes (Fig. 35E-F and Movie 14). The elongation of these structures was almost completed at about 50 hours APF. Therefore, the whole trichome growth occurred in 5-6 hours and at the very end of tissue remodeling.

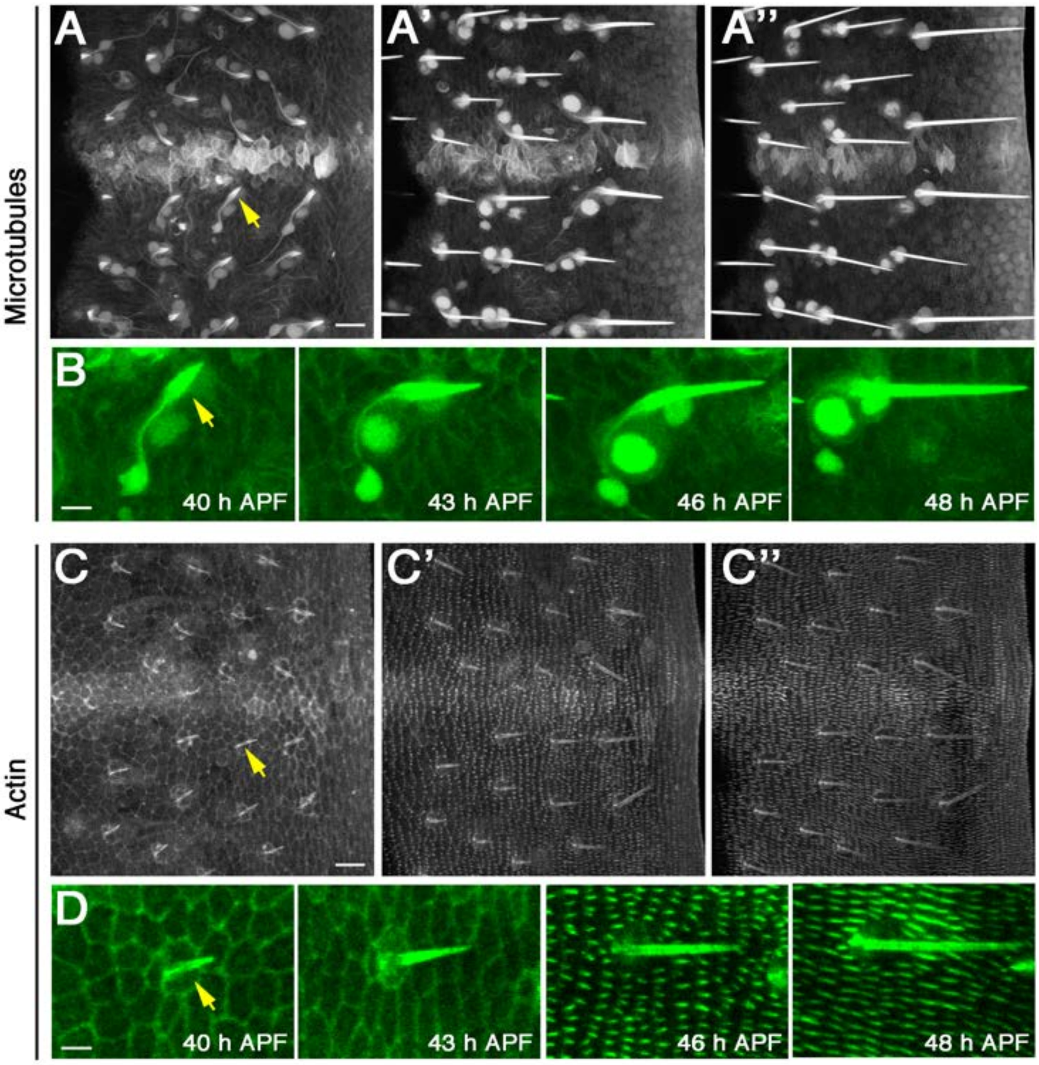
Microtubules
A
A'
A''
B
40 h APF
43 h APF
46 h APF
48 h APF
Actin
C
C'
C''
D
40 h APF
43 h APF
46 h APF
48 h APF

Fig. 34: The oriented eversion of bristles precedes the oriented eversion of trichomes. A) From about 40 hours APF (A), the bristle shafts extend oriented microtubules (yellow arrow). Between 46 (A') and 50 hours APF (A'') the microtubules emanating from the shafts grow posteriorly. **B)** Close-up of the bristle (microchaetae) outgrowth, indicated by a yellow arrow in A. **C)** From about 40 hours APF (C) the bristle shafts extend oriented actin microfilaments (yellow arrow). Between 46 (A') and 50 hours APF (A'') the actin microfilaments grow posteriorly. **D)** Close-up of bristles (microchaetae) outgrowth (yellow arrow in C). Anterior is to the left and posterior to the right. Scale bar is 22 μm (A-A'' and C-C'') and 5 μm (B and D). Genotype were *Jupiter::GFP* (A-A'' and B) and *Moesin::GFP* (C-C'' and D). See Movie 11 and Movie 12.

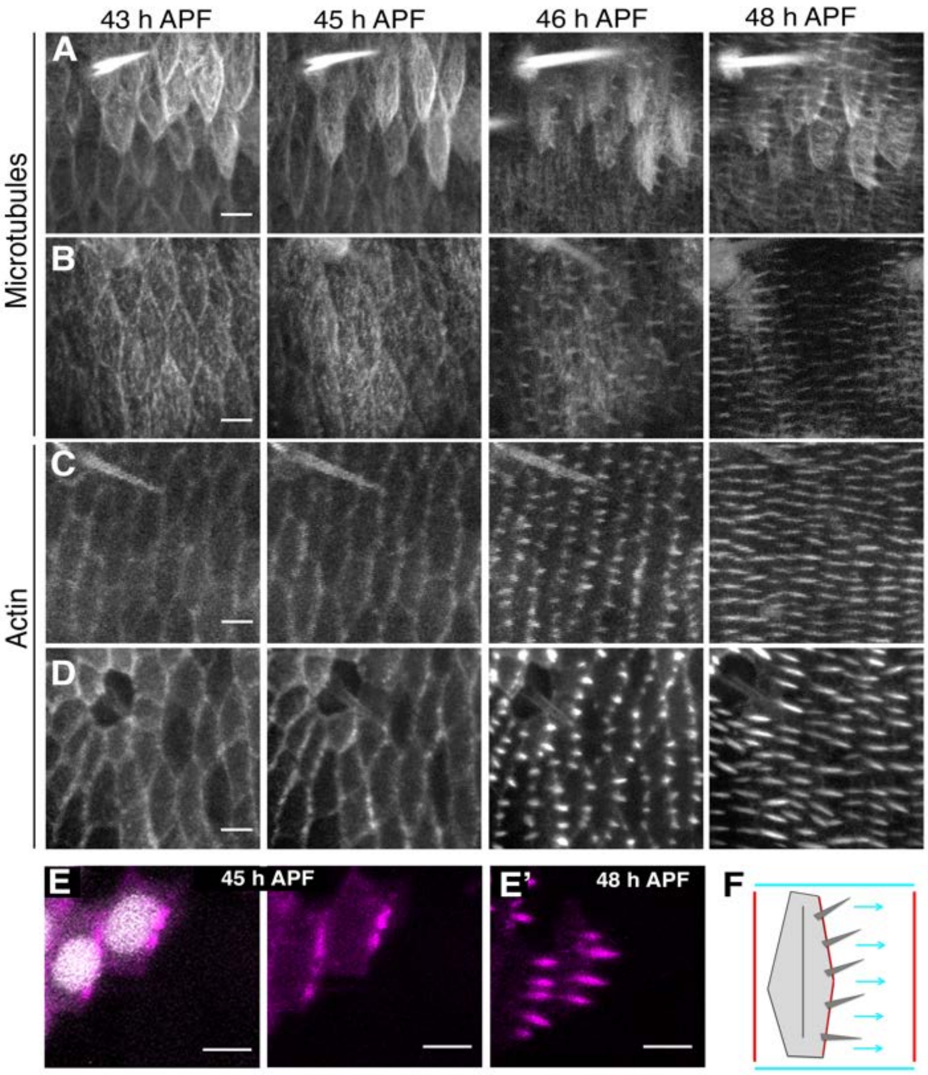

Fig. 35: Oriented trichome outgrowth initiates upon attainment of uniform cell alignment. A-B) Dynamics of microtubules (A) and their plus ends (B) during remodeling. **C-D)** Dynamics of actin microfilaments visualized with moesin (C) or life-actin (D) markers. Note that the polarized behavior of the cytoskeleton is visible from 45 hours APF onward**. E-E')** Close-up of two cells showing the accumulation of actin (magenta) at the posterior edges of a marked clone of cells (grey). From the posterior accumulation up to five hairs grow posteriorly within the next few hours (E'). **F)** Cartoon showing the relation between PCA and PCP in a single cell. The genotypes were *Jupiter::GFP* (A), *Act5C-Gal4>UAS.EB1::GFP* (B), *Moesin::GFP* (C), *Act5C-Gal4>UAS.lifeactGFP* (D) and *hsflp1.22;Act5C>>Gal4,UAS.GFP/UAS.lifeactRuby* (E-E'). See Movie 13 and Movie 14.

Although the axial uniform orientation of PCA largely preceded PCP in the abdomen, their geometrical/spatial references were the same and the quantified angular features of each of them resulted fully correlative at steady state (Fig. 36A-B). Both kinds of orientation were uniform across the segment field although trichomes arranged totally perpendicular to the A/P boundary while the axial orientation of PCA was fully parallel to it (Fig. 36A'-B' and C).

In summary, both trichomes and bristles oriented within the plane of the epithelium as soon as they formed. Bristle eversion initiated during the remodeling phase and preceded the eversion of non-sensory trichomes. Notably, trichome outgrowth initiated with the attainment of stable tissue arrangement and its orientation was uniformly orthogonal to the orientation of the alignment of the anisotropic histoblasts.

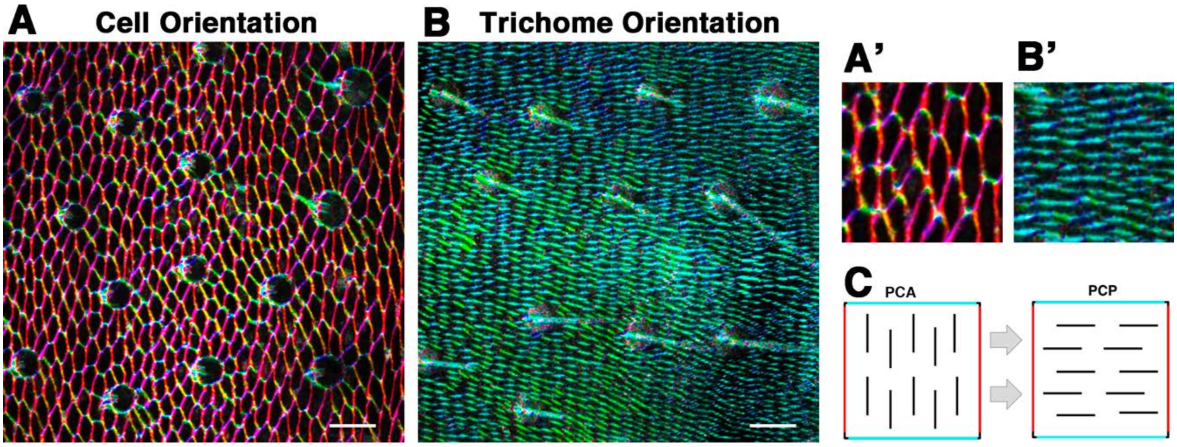

Fig. 36: Orientation of PCA and PCP are uniformly orthogonal. **A)** Colored cell edge orientations showing uniform orientation of PCA across the medio-dorsal region of the A compartment at about 50 hours APF. Cells are uniformly shaped and oriented in parallel to the A/P axis. **B)** Colored cell protrusion orientations showing uniform orientation of planar cell polarity (PCP) across the medio-dorsal region of the A compartment as in A. The PCP is manifested in the orientation of the trichomes, uniformly perpendicular to the A/P axis. **A'-B')** Close-up views from A and B to highlight the orthogonal relation between PCA (A') and PCP (B'). **C)** Cartoon describing the orthogonal relation between PCA (left) and PCP (right). Anterior is to the left. Scale bar is 16 μm. Genotype were *Atpα::GFP* and *Moesin::GFP*. See text for details.

Synopsis

The abdominal epithelial cells reach their steady state planar arrangement within about 34 hours of pupation. During this time, the epithelial morphogenesis can be broadly divided into expansion and remodeling phases. During expansion, histoblasts divide randomly relative to the tissue axis while migrating dorsally. During remodeling, histoblasts adjust their final position within the plane while migrating anteriorly. During both phases tissue growth is oriented dorsal-ward and cell-cell contact interactions progressively increase parallel to the A/P boundary. When cell movements arrest, a stable arrangement of the cells within the plane of the segmental field is attained. Cell arrangements at steady state displayed a striking axial bias along the A/P axis leading to the uniform orientation of planar cell alignment (PCA). This uniformity is achieved in a precise spatial and temporally controlled manner. The histoblasts “transit” first through local stereotyped intermediate orientation patterns. Then, they reach their final orientation parallel to the A/P axis first in cells abutting the A/P boundary and sweeping anteriorly, aligning among themselves, in a wave-like manner. The axial uniformity in the orientation of cell alignment (PCA) is reflected on the uniform orientation of planar polarity (PCP). Every cell produces oriented trichomes whose outgrowth is uniformly orthogonal to the axial orientation of cell alignments.

Chapter II

The PCP Signalling and the Axial Orientation of PCA

2.1 Dachsous is Expressed in Opposing Gradients along the A/P Axis

The Dachsous/Fat/Four-jointed (Ds/Ft/Fj) signalling relies on the interaction of two cadherins, Ds and Ft, and on the Golgi-kinase Fj that modulates the strength and stability of Ds-Ft heterodimeric interactions across cell interfaces (Strutt and Strutt, 2002; Ma et al., 2003; Matakatsu and Blair, 2004; Brittle et al., 2010 and 2012; Ambegaonkar et al., 2012; Simon et al., 2010; Clark et al., 1995; Ishikawa et al., 2008; Hale et al., 2015). Although the expression pattern of the components of this cascade during pupation remains barely explored, it is known that this pathway is required to provide polarity guidance in the plane of the abdominal epithelium for the control of trichome polarity (Casal et al., 2002 and 2006). *ds*, at late pupal stages (*i.e.* over 70% of pupation), is expressed in a transcriptional gradient along the A/P axis throughout the A compartment in abdominal segments (Casal et al., 2002). However, it was unknown how this graded expression developed. Analyzing early *ds* expression with a specific enhancer trap transgene, we found that, its transcription was graded along the A/P axis since the onset of expansion (Fig. 37A-A’’ and B). In this sense, it was equivalent to other imaginal tissues such as the wing disc (Fig. 37C-C’’).

To gain insights on the dynamic of Ds expression, we further employed an endogenous GFP-tagged Ds protein reporter (Ds::EGFP, Brittle et al., 2012) and performed a time course analysis of Ds localization. We found that Ds was recruited to the membrane and was accumulated in gradients with opposite slopes in the A and P compartments with a maxima at the A/P compartment boundary (Fig. 38A-B and Movie 15). Remarkably, these gradients were maintained all throughout expansion and remodeling (Fig. 38C-D and Movie 15) with their steepness progressively decaying with time. This dynamic was further appreciated by graphically plotting the level of expression along the A/P axis at successive time points (Fig. 38D).

To determine whether Ds show any preferential subcellular localization, we generated stochastically positioned mitotic clones in a Ds::EGFP background (Brittle et al., 2012). This strategy allowed the assessment of Ds localization at the edges of unmarked patches *in vivo*. We found that Ds was asymmetrically localized at the apical cell perimeter, accumulating anteriorly in the A compartment and posteriorly in the P compartment since early stages of morphogenesis (Fig. 39A). These asymmetries were invariably detected at any point along the A/P axis, irrespectively of the level of Ds expression, thereby indicating that Ds subcellular polarization opposes the slope of its own gradient. The tendency of Ds to asymmetrically localize at the cell interfaces oriented with the A/P boundary was maintained and became even more appreciable at the end of remodeling (Fig. 39B).

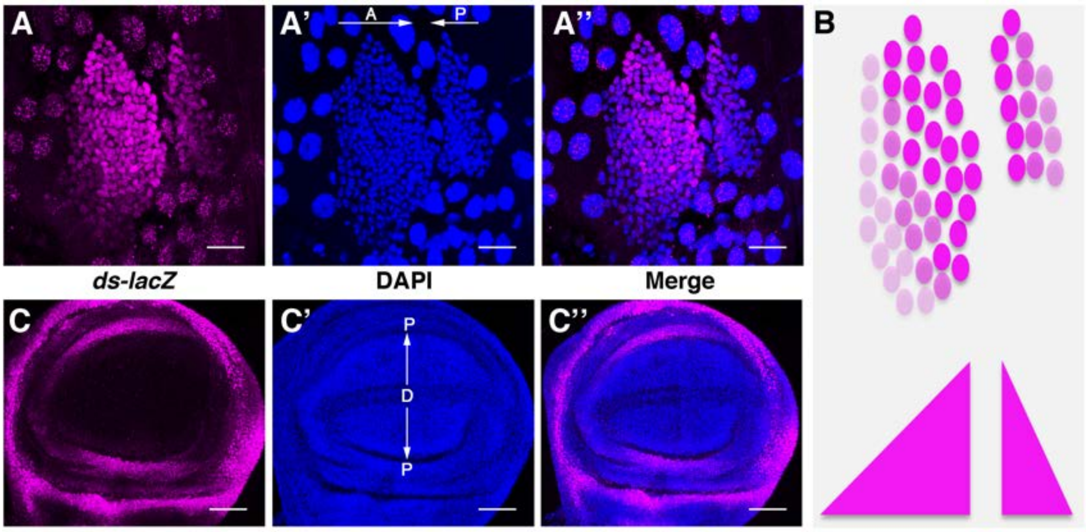

Fig. 37: *dachsous* is expressed in a transcriptional gradient early in development. A-A'') Expression pattern of *dachsous* (*ds*) in dorsal nests at 16 hours APF. **A)** *ds* expression levels (magenta) are graded along the A/P axis and throughout the nests. *ds* is also expressed in the LECs. A') DAPI staining (Blue) reveals homogeneous DNA nuclear content in the A and P compartments. Arrows indicate the direction toward which *ds* levels increase (see A). A'') *ds* (magenta) and DAPI (blue) merge. **B)** Schematic representation of the levels of *ds* within the dorsal nests. *ds* transcriptional levels increase toward the posterior of the A nest and decreases toward the posterior of the P nest. **C-C'')** Expression pattern of *ds* in a LIII wing disc. The pouch and hinge regions of the disc are shown. *ds* (magenta) is strongly expressed in the proximal region of the pouch and in the hinge and at lower levels distally The proximo-distal (P/D) axis is indicated in C' and the arrows point to the direction to which *ds* levels increase. Genotype was ds^{2D60b}*-lacZ/+*. Scale bar is 22 μm. Anterior is to the left. Dorsal is up.

Ds was expressed asymmetrically at different levels in cell contacts and graded throughout the A/P axis (Fig. 40A-A') clustering in punctated structures (dotted clusters or punctae) around the apical perimeter of individual cells (Fig. 40A-A' and B). These junctional punctae were mobile but yet preferentially accumulating at the A/P oriented cell edges (Fig. 40B and Movie 16).

In summary, Ds was expressed in opposing gradients along the A/P axis of the segment throughout development. These gradient slopes become shallow over time. Ds accumulated in punctae along the apical cell perimeter and asymmetrically localized at cell edges in correlation to its tissue-wide expression differences. The tissue-wide A/P asymmetry of Ds, as well as the Ds asymmetry along A/P oriented cell edges preceded the uniform orientation of planar cell alignment (PCA) parallel to the A/P.

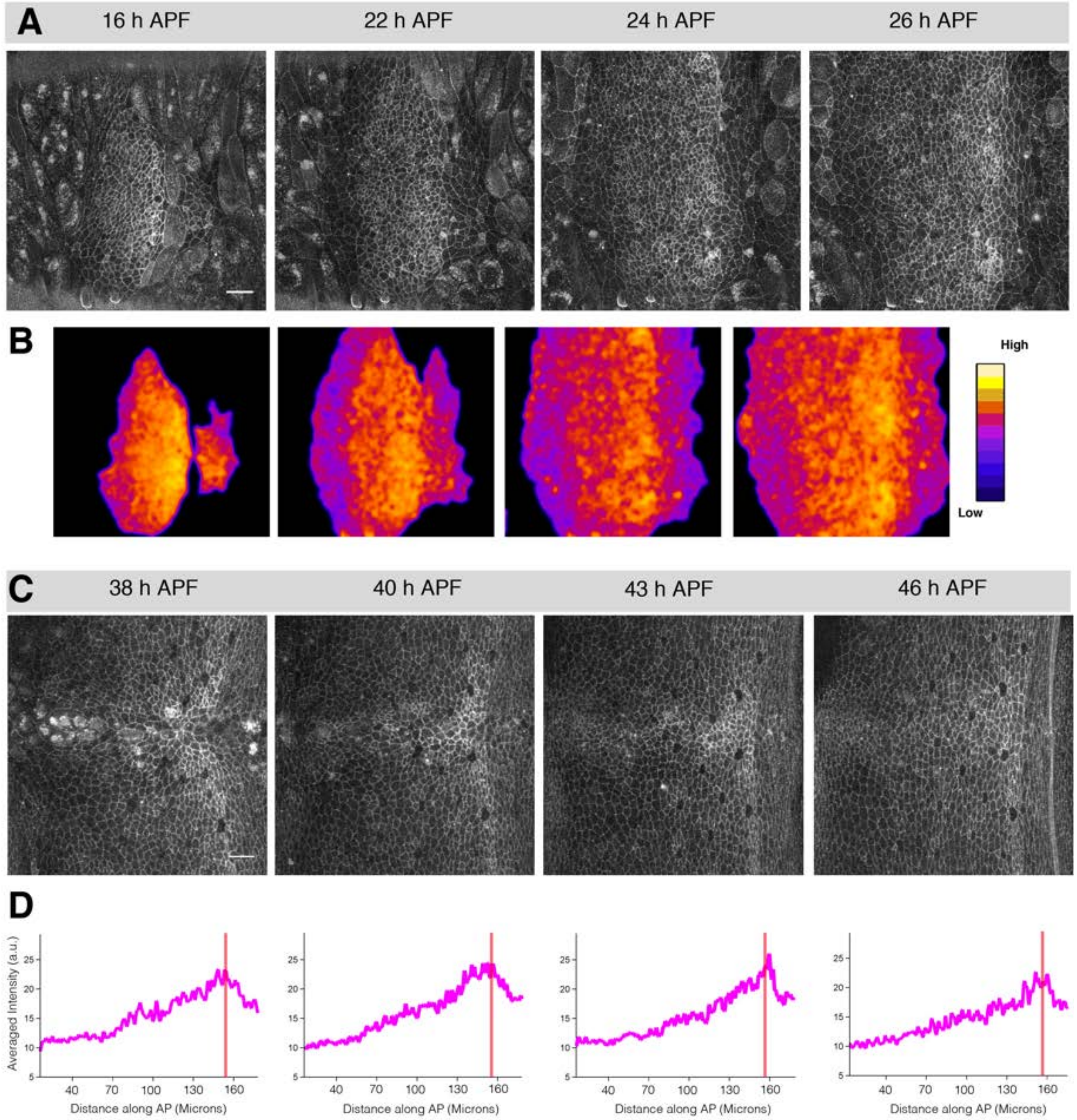
A
16 h APF
22 h APF
24 h APF
26 h APF
B
High
Low
C
38 h APF
40 h APF
43 h APF
46 h APF
D
Averaged Intensity (a.u.)
5
10
15
20
25
40
70
100
130
160
Distance along AP (Microns)

Fig. 38: Dachsous is recruited to the membrane and expressed in a gradient along the A/P Axis. A) Expression pattern of Ds during expansion. Ds is recruited to the membrane and expressed in a gradient along the A/P axis from the onset of expansion. **B)** Heat maps of Ds levels in the expanding nests (Fire-LUT Filter for intensity). Note that the Ds gradient orientation is maintained all throughout expansion. **C)** Expression pattern of Ds during remodeling. **D)** Plots reporting the expression levels of Ds (magenta) along the A/P axis of the segment field at 38, 40, 43 and 46 hours APF. The A/P boundary position is marked with red lines. Note that the Ds gradient maintains the same orientation all the time. Genotype was *Ds::EGFP*. Scale bar is 22 µm. Anterior is to the left. See Movie 15.

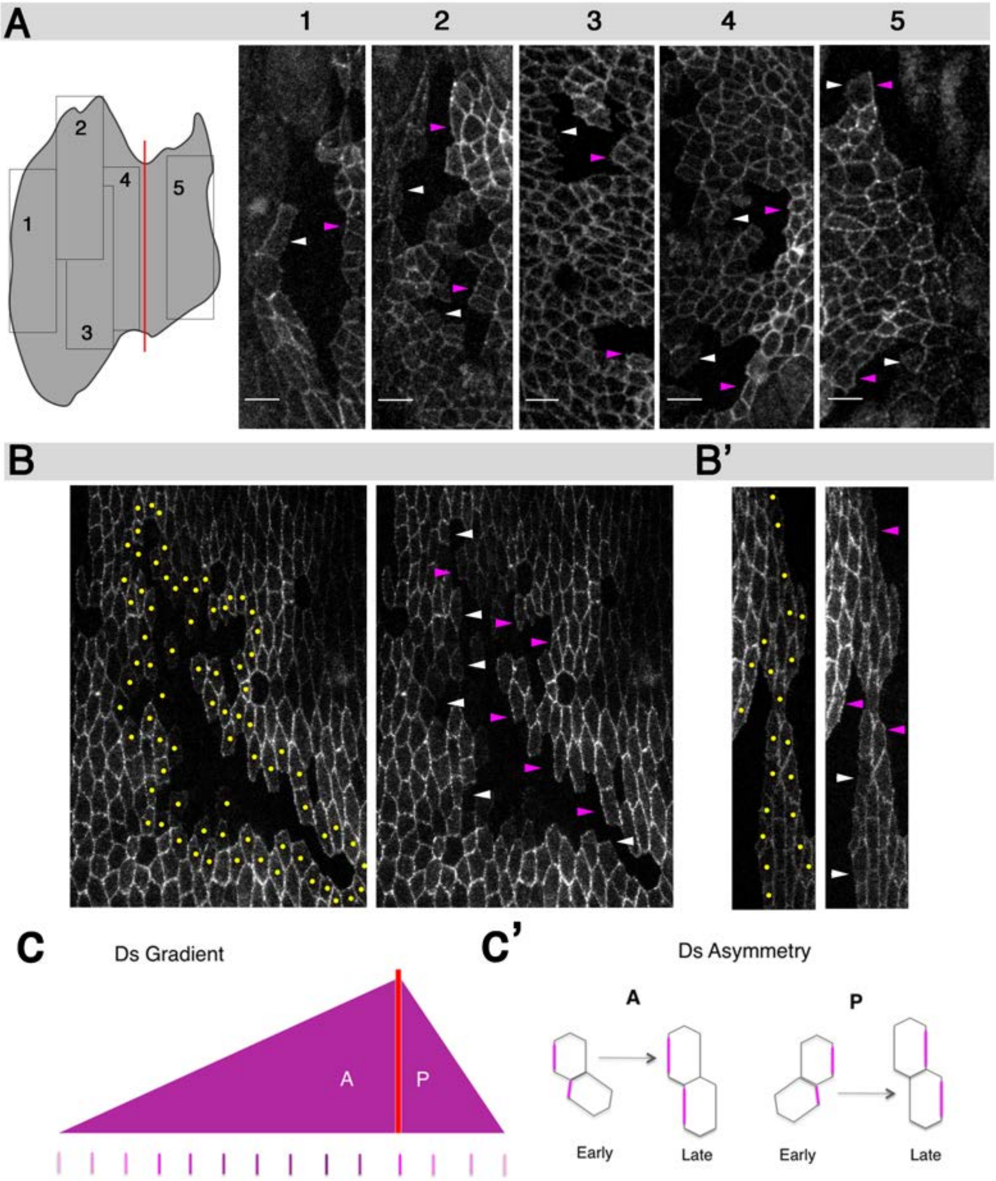

Fig. 39: Dachsous is asymmetrically enriched at A/P oriented cell interfaces. A) Ds asymmetry at expansion. (Left) Cartoon illustrating fused histoblast nests at 18-20 hours APF subdivided in 5 regions along the A/P axis. Regions 1-4 correspond to different anterior-to-posterior domains within the A compartment and region 5 is within the P compartment. (Right) Images of Ds::EGFP-less clones in the indicated regions. Ds::EGFP is enriched at anterior cell edges in the A compartment and in posterior cell edges in the P compartment. Magenta arrowheads point to Ds enriched cell edges and white arrowheads point to Ds low expressing cell edges. **B-B')** Ds asymmetry at remodeling. 46 hours APF clones of cells lacking Ds::EGFP. (Left) The boundary of the clones is marked with yellow dots. (Right) Magenta arrowheads point to Ds enriched cell edges and white arrowheads point to Ds low expressing cell edges. **C)** Cartoon representing the Ds gradient slope along the A/P axis and the graded Ds levels across cell interfaces (bars). **C')** Cartoon od the Ds asymmetry during expansion and remodeling stages. Note that Ds was found enriched in A/P oriented edges irrespectively of cell orientation. Scale bar is 16 μm. Anterior is to the left. Genotype was *hsflp1.22;Ds::EGFP FRT40A/FRT40A*.

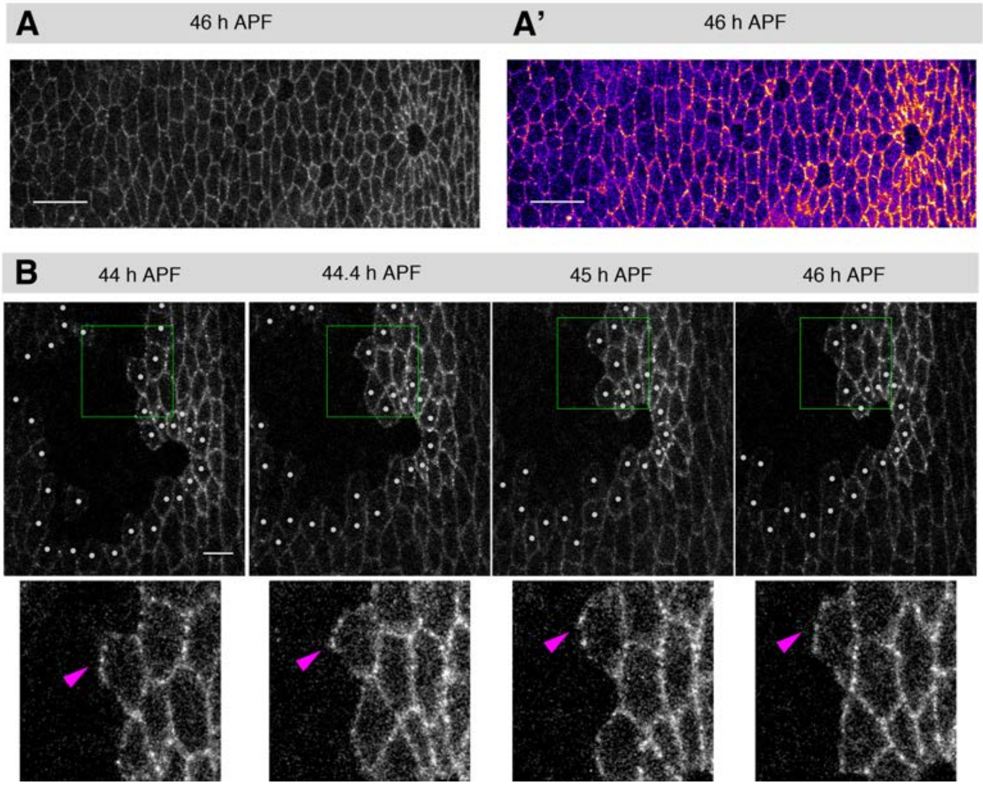

Fig. 40: Ds localizes within motile junctional punctae. A-A’) Expression gradient of Ds at steady state. A) Ds levels visualized in grey scale. A’) Heat map of Ds levels (Fire-LUT Filter for intensity). Blue indicates low and yellow indicates high levels of Ds expression. **B)** Images showing patches of Ds::EGFP expression abutting unmarked clones. Note that Ds localizes in junctional punctae that preferentially move in A/P oriented cell edges (purple arrowheads). Scale bar is 16 μm. Anterior is to the left. Genotype were *Ds::EGFP* (A and A’) and *hsflp1.22;Ds::EGFP FRT40A/FRT40A* (B). See Movie 16.

2.2 Four-jointed Opposite Gradients Dynamics during Expansion and Remodeling

Similarly to *ds*, the expression pattern of *fj* has been only assessed at late pupal stages (*i.e.* over 70% of pupation, Zeidler et al., 2000; Casal et al., 2002). It has been shown that *fj* is expressed in a transcriptional gradient across the A/P axis in each adult abdominal segment opposing to that of *ds*. As for *ds*, it was unknown how *fj* graded expression developed. Analyzing early *fj* expression with a specific enhancer trap transgene, we found that, *fj* transcription was graded along the A/P axis since the onset of expansion (Fig. 41A’-A’’). Remarkably, high levels of expression were also detected in the dorsal-most regions of both the anterior and the posterior dorsal nests (Fig. 41B). Thus, despite being differentially expressed in the imaginal histoblasts as in the imaginal discs, *fj* gradient was not strictly uniaxial within the nests (Fig. 41C-C’’).

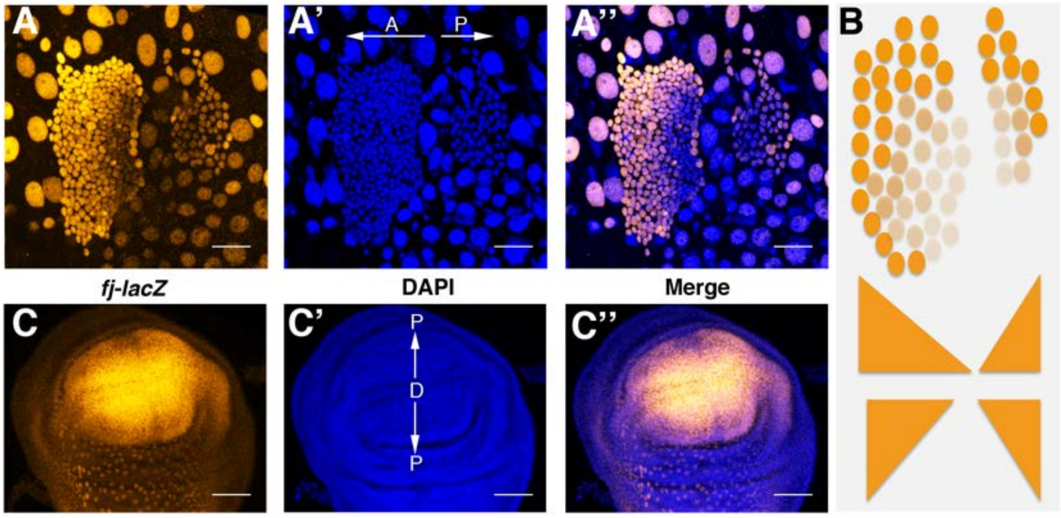

Fig. 41: *four-jointed* is expressed in a gradient early in Development. A-A'') Expression pattern of *four-jointed* (*fj*) in dorsal nests 16 hours APF. **A)** *fj* expression levels (orange) are graded along the A/P axis and throughout the nests. *fj* is also expressed in the LECs. A') DAPI staining (Blue) reveals homogeneous DNA nuclear content in A and P compartments. Arrows indicate the direction toward which *fj* levels increase (see A) A'') *fj* (magenta) and DAPI (blue) merge. **B)** Schematic representation of the levels of *fj* within the dorsal nests. *fj* transcriptional levels increase toward the posterior of the A nest and decreases toward the posterior of the P nest. *fj* levels are higher in the dorsal edges of both nests. **C-C'')** Expression pattern of *fj* in a LIII wing disc. The pouch and hinge regions of the disc are shown. *fj* (magenta) is expressed more strongly in the distal region of the pouch. The P/D axis is indicated in C' were the arrows point to the direction towards *ds* levels increase. Genotype was *fj*^{P1}*-lacZ/+*. Scale bar is 22 μm. Anterior is to the left.

A time course analysis employing a GFP marked *fj* enhancer trap reporter (*fj-EGFP*) further revealed that, during expansion, *fj* was expressed in opposite gradients whose slopes decreased toward the posterior of the A compartment and increased toward the posterior of the P compartment (Fig. 42A-B and Movie 17). Besides, *fj* transcript levels were also elevated in the dorsal-most part of the segment territory (toward the dorsal midline) in both compartments (Fig. 42A-B). As histoblasts approach confluence, the *fj* gradient progressively evolves towards uniaxial opposite gradients along the A/P axis, although during early remodeling dorsal *fj* levels are still slightly elevated (Fig. 42C-D and Movie 17).

Summarizing, *fj* expression evolves during the expansion and remodeling stages from a dual graded pattern (A/P and D/V) toward a uniaxial A/P gradient with opposite slopes in A and P compartments.

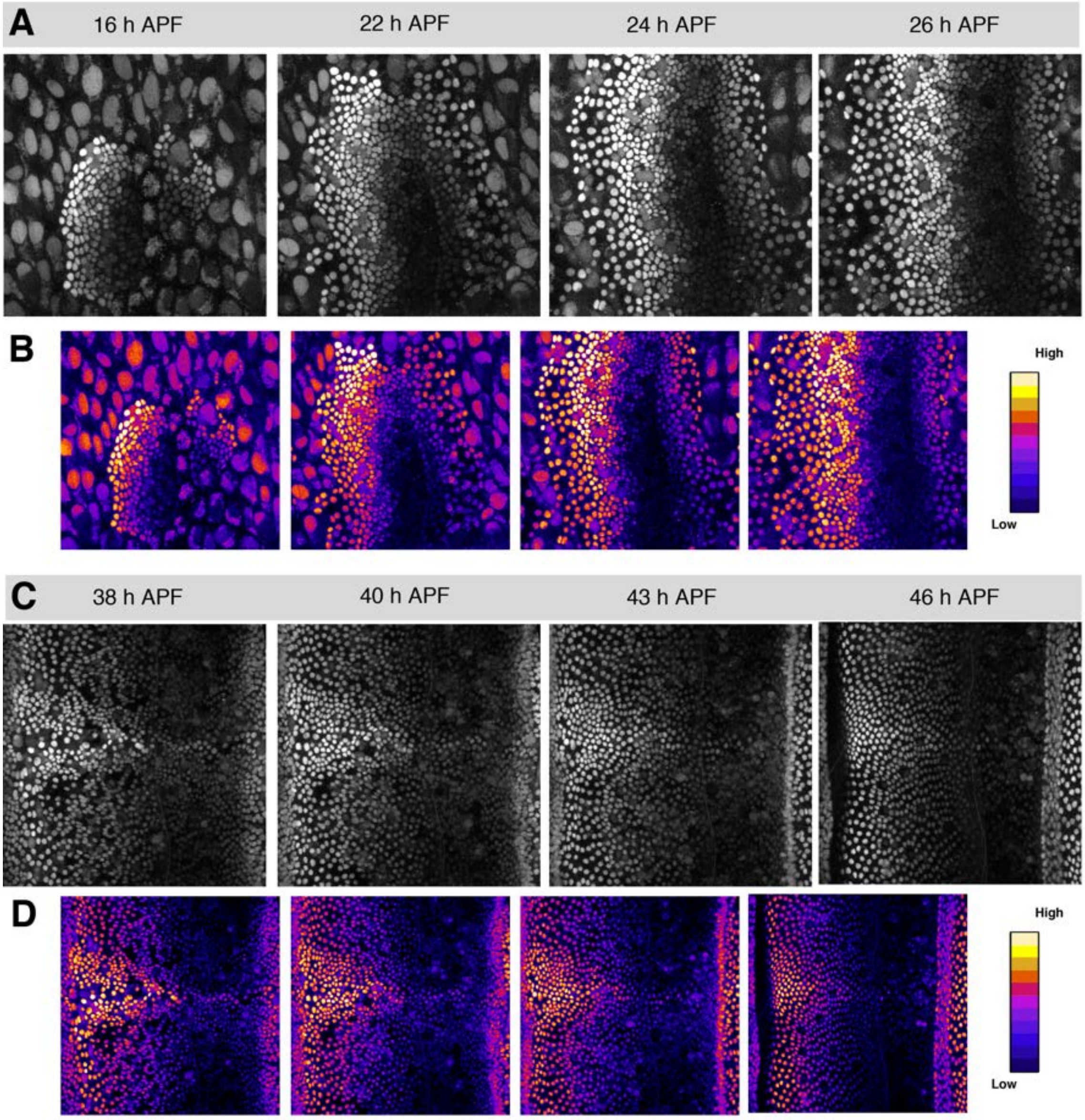

Fig. 42: *four-jointed* gradient evolution during expansion and remodeling. A) Expression pattern of *fj* during expansion. **B)** Heat maps of fj levels in the expanding nests (Fire-LUT Filter for intensity). *fj* levels are distributed in a gradient along the A/P axis from the onset of remodeling. Note also that levels of *fj* are higher dorsally through expansion. **C)** Expression pattern of *fj* during remodeling. **D)** Heat maps of *fj* levels in the expanding nests (Fire-LUT Filter for intensity). *fj* levels are distributed in a gradient along the A/P axis from the onset of remodeling. Genotype was *fj-EGFP*. Scale bar is 22 μm. Anterior is to the left. See text for details. See Movie 17.

2.3 The Emerging Axial Gradient of Fat

The expression pattern of Ft was not previously reported in the abdomen, neither in terms of its transcription nor in terms of its localization. To uncover its expression pattern dynamics, we made use of an endogenous Ft reporter fused with GFP (Ft::EGFP, Brittle et al., 2012) enabling *in vivo* imaging of Ft localization.

We found that Ft was expressed heterogeneously during expansion (Fig. 43A-B and Movie 18). Ft highest expression in the A compartment was observed in the center and dorsal parts, while in the P compartment Ft levels were quite uniform (Fig. 43A-B). This pattern was maintained for most of the expansion phase. Strikingly, from 30 hours APF, Ft expression evolved progressively towards a graded distribution with a maxima at the anterior edge of the A compartment with the same slope as *fj* (Fig. 43C-D and Movie 18). The Ft gradient was initially present at the most posterior part of the compartment eventually propagating anteriorly. As observed for Ds, the Ft gradient got shallow with time (Fig. 43D). At the end of morphogenesis it fully opposed the Ds gradient.

In summary, Ft expression was more dynamics than those of *fj* and Ds. A Ft gradient of expression along A/P establishing first in the center-posterior regions of the A compartment emerges by the end of expansion.

2.4 Reciprocal Cross-Regulation of Ds, Ft and Fj

-Ds, Ft and Fj Expression Profile Dynamics

As just showed, the expression patterns of Ds, Ft and *fj* are dynamic during the abdominal epithelial morphogenesis. They all are expressed in the histoblasts from the onset of expansion but follow distinct pattern changes in a precise spatio temporal manner.

It has been extensively documented that Ds, Ft and Fj regulate each other's activities (Casal et al., 2002; Yang et al., 2002; Rawls et al., 2002; Matakatsu and Blair, 2004; Simon et al., 2004; Rogulja et al., 2008; Willecke et al., 2008; Sopko et al., 2009; Hale et al., 2015). Ds negatively influences Ft localization (Matakatsu and Blair, 2004; Ma et al., 2003; Strut and Strutt, 2002; Yang et al., 2002) and Fj modulates Ds-Ft heterodimeric affinity phosphorylating both Ds and Ft (Brittle et al., 2010; Simon et al., 2010; Ishikawa et al., 2008; Hale et al., 2015).

In this scenario, the dynamic changes in the pattern of Ft along the A/P axis of the tissue during histoblasts development might be a consequence of the concerted actions of Ds and Fj. Ds was expressed in an axial gradient (Fig. 44A-A') throughout development, while Ft and, to a lesser extent, *fj* expression patterns changed over time (Fig. 44B-B' and C-C').

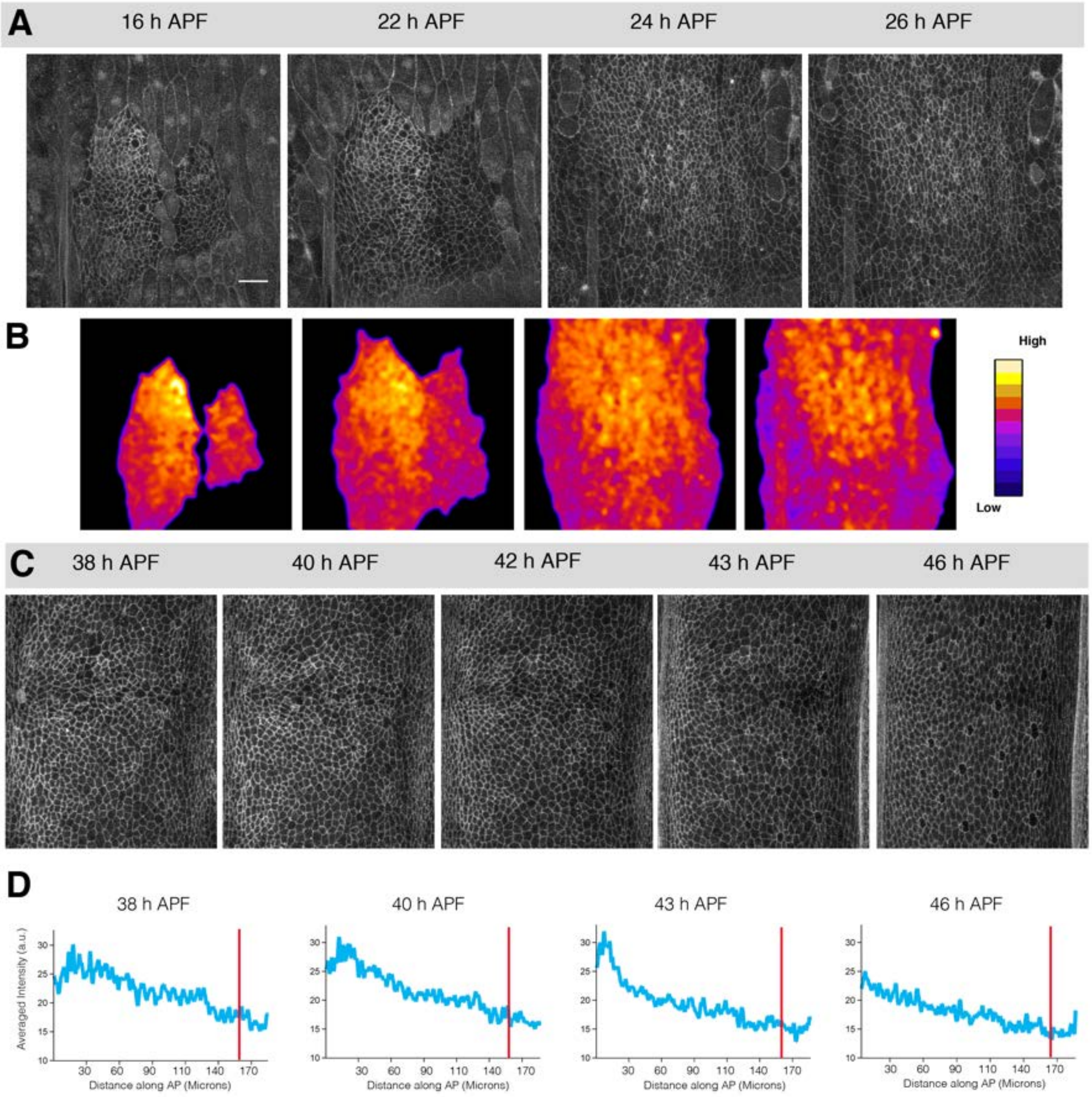
A
16 h APF
22 h APF
24 h APF
26 h APF
B
High
Low
C
38 h APF
40 h APF
42 h APF
43 h APF
46 h APF
D
38 h APF
40 h APF
43 h APF
46 h APF
Averaged Intensity (a.u.)
10
15
20
25
30
30
60
90
110
140
170
Distance along AP (Microns)

Fig. 43: An axial gradient of Fat forms over-time along the A/P axis. A) Expression pattern of Ft during expansion. Ft levels are not graded along the A/P axis during expansion, being stronger at the centre-dorsal region of the A compartment (See also Fig. 44). **B)** Heat maps of Ft levels in the expanding nests (Fire-LUT Filter for intensities). **C)** Expression pattern of Ft during remodeling. Ft levels are graded along most of the A/P axis. **D)** Plots reporting the expression levels of Ft (Cyan) throughout the A/P axis. The A/P boundary position is marked with red lines. Note that the pattern of Ft becomes expressed in a gradient along A/P, with maxima at the A/P segmental boundary (like *fj*). By 43-44 hours APF Ft gradient expand to the entire segment and opposes that of Ds. Genotype was *Ft::EGFP*. Scale bar is 22 μm. Anterior is to the left. See Movie 18.

Comparing the axial profiles of the three genes products along the A/P axis (Fig. 44D-G) uncovered stereotyped events with potential functional significances regulated in a precise spatio temporal fashion. First, Ft expression, which initially was very heterogeneous presenting maximum levels midway along the A/P axis within the A compartment, progressively develops into an anterior-to-posterior gradient by gradually displacing its maximum towards more anterior positions. In such way the Ft expression profile evolves to mimic the *fj* gradient, opposing the gradient of Ds all over the compartment field. Second, at the end of the expansion period and at the most posterior section of the A compartment in proximity to the A/P boundary, Ft expression decays posteriorly in a gradient from its maxima at the central section of the compartment. In this posterior domain at this precise time, Ft and fj gradients slopes correlate and oppose that of the Ds gradient. Third, this composite configuration spreads anteriorly over time throughout the remodeling period to cover the full compartment (Fig. 44G). Fourth, at the end of the process, the Ft and Ds gradients show similar steepness reaching an overall balance along the A/P axis.

Remarkably, both the maturation timing and the spatial dynamics of tissue-wide Ds, Ft and *fj* gradients evolution precisely match that of the orientation of PCA along the A/P axis (See Chapter I and Discussion). This spatiotemporal correlation suggests that the Ds/Ft/Fj signalling might play a role in the attainment of the uniform axial orientation of PCA.

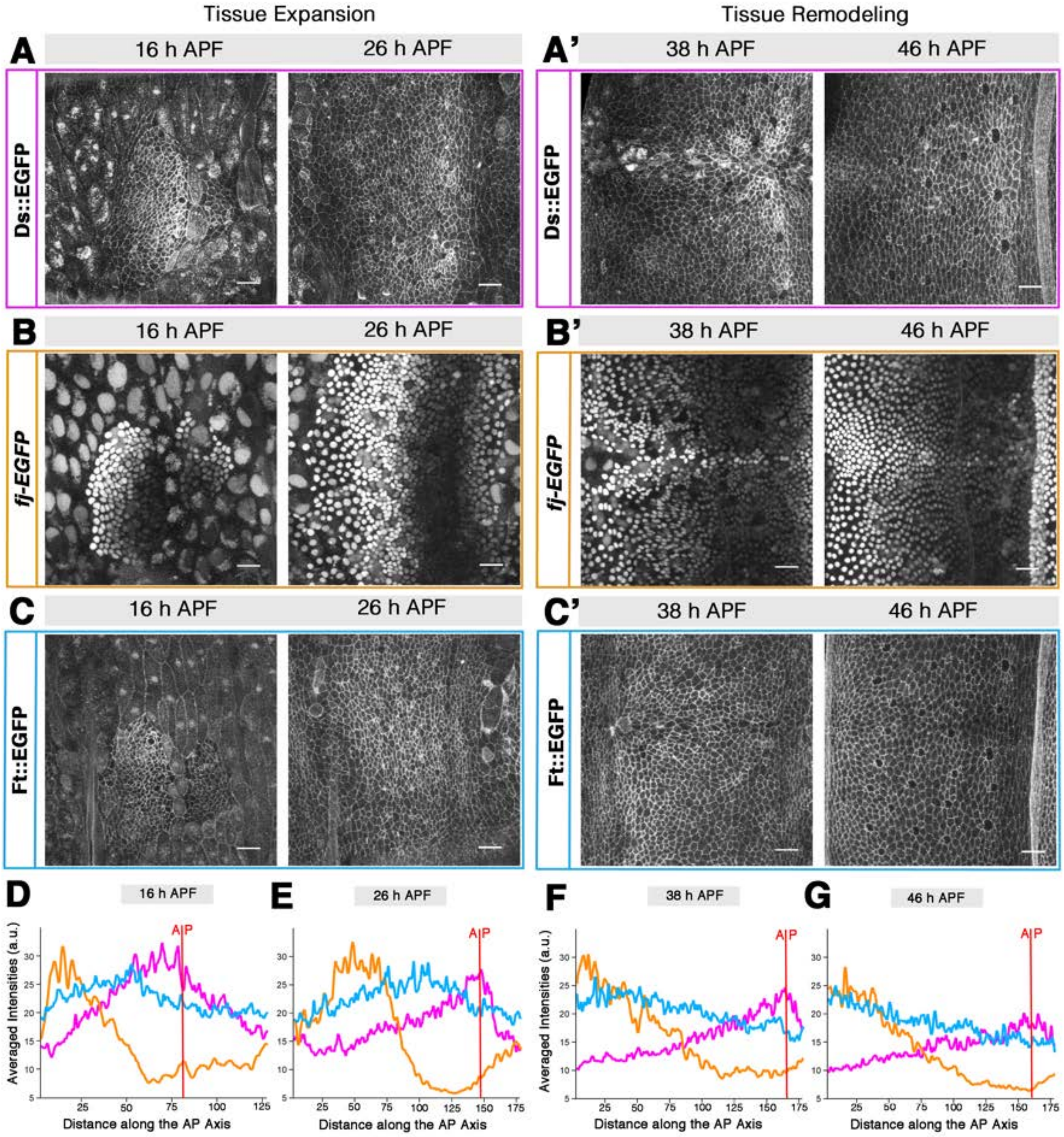
Tissue Expansion
Tissue Remodeling
A
16 h APF
26 h APF
A'
38 h APF
46 h APF
Ds::EGFP
B
B'
fj-EGFP
C
C'
Ft::EGFP
D
E
F
G
A|P
Averaged Intensities (a.u.)
Distance along the AP Axis

Fig. 44: Expression Pattern Dynamics of the Ft-Ds-Fj Pathway during Morphogenesis. A-A') Expression pattern of Ds at the indicated times during expansion (A) and remodeling (A'). Ds is expressed in a gradient throughout development, with maximum levels at the A/P boundary (See also magenta profiles in D-to-G). **B-B')** Expression pattern of *fj* at expansion (B) and remodeling (B'). *fj* is expressed in a gradient along the A/P axis that largely oppose that of Ds. Further, *fj* is expressed at higher levels dorsally. During remodeling this pattern evolves toward a uniaxial A/P gradient (See also orange profiles in D-to-G). **(C-C')** Expression pattern of Ft at expansion (C) and remodeling (C'). Ft is heterogeneously expressed during expansion, while it is expressed in a gradient opposing that of Ds at remodeling (D) (See also Cyan profiles in D-to-G). **D** and **E**) Colored plots representing the combined expression profiles of Ds (magenta), *fj* (orange) and Ft (cyan) at 16 and 26 hours APF. Normalized averaged intensities across the A/P axis are in arbitrary units. **F** and **G**) Colored plots representing the combined expression profiles of Ds (magenta), *fj* (orange) and Ft (cyan) at 38 and 46 hours APF. Normalized averaged intensities across the A/P axis are in arbitrary units. Genotypes were *Ds::EGFP* (A) and *Ft::EGFP* (B) and *fj-EGFP* (C). Anterior is to the left. Scale Bar is 22 μm. See text for details.

At steady state, Ds and Ft opposing expression profiles appears to enforce a tissue-wide equilibrium along the A/P axis (Fig. 45A-D). The expression data presented above, together with the known genetic and functional interactions between the pathway components, may suggest that Ds, Ft and Fj will be influencing each other localization/activity along the A/P axis in the abdominal epithelium and over the developmental time of pupation. The three pathway components could constitute a minimal regulatory network, a Ds/Ft/Fj Triad (Fig. 45E).

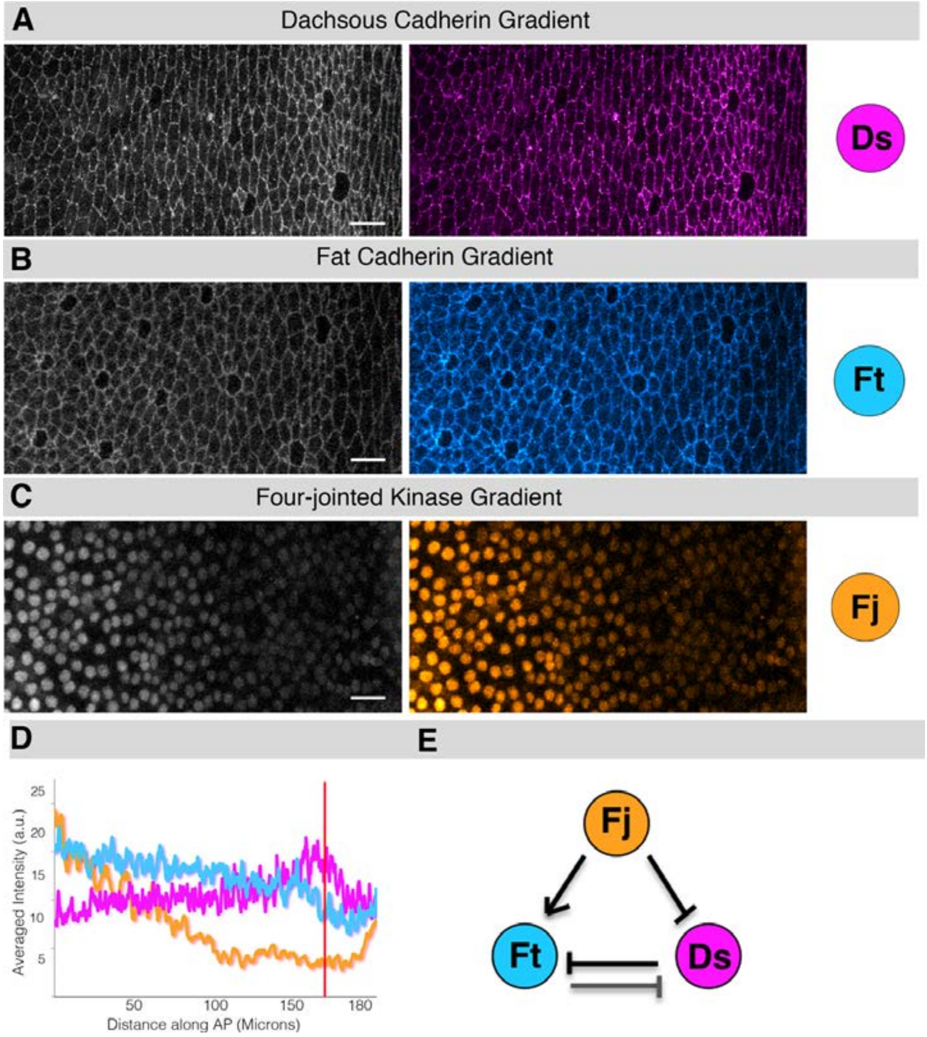
A
Dachsous Cadherin Gradient
Ds
B
Fat Cadherin Gradient
Ft
C
Four-jointed Kinase Gradient
Fj
D
E
Averaged Intensity (a.u.)
25
20
15
10
5
50
100
150
180
Distance along AP (Microns)
Fj
Ft
Ds

Fig. 45: Ds and Ft gradients are balanced in the mature epithelium. A) Ds gradient in a section of the AIII segment at steady state. Ds levels in grey scale (left) and magenta (right). **B)** Ft gradient as in A. Ft levels in grey scale (left) and cyan (right). **C)** *fj* gradient as in A. *fj* levels in grey scale (left) and orange (right). **D)** Over-imposed expression profiles of Ds (magenta), Ft (Cyan) and *fj* (Orange) along the A/P axis of the AIII segment. The position of the A/P boundary is marked by a red line. **E)** Proposed Ds/Ft/Fj signalling network ('Triad'). The colored circles represent the nodes of the network, color-coded as in A, B and C. The network links indicate the regulatory inputs between the nodes. Genotypes were *Ds::EGFP* (A) and *Ft::EGFP* (B) and *fj-EGFP* (C). Anterior is to the left. Scale is 12 μm.

-Dachs Asymmetry as a Ds and Ft Heterodymeric Interaction Readout

The axial modulation of Ds, Ft and *fj* expression strongly suggests that the activity of the pathway should be axially asymmetrical. Indeed, the subcellular anterior and posterior localization of Ds (depending on the compartment) at the apical perimeter of histoblasts (Figs. 39 and 40) supports this scenario. To directly evaluate the activity of the pathway, we resorted on the subcellular localization of Dachs (D). D is a downstream target of the pathway, which polarizes in response to the asymmetric interaction of Ds and Ft across cell interfaces (Cho and Irvine, 2004; Mao et al., 2006; Brittle et al., 2012; Ambegaonkar et al., 2012; Bosveld et al 2012; Carvajal-Gonzalez and Mlodzik, 2014; Bosveld et al., 2016). The cortical association of this atypical myosin is stabilized by Ds and inhibited by Ft.

D expression pattern was monitored *in vivo* using a GFP-tagged transgene driving D expression under its endogenous promoter (Bosveld et al., 2012). D was expressed apically at the onset of expansion and primarily enriched along A/P oriented cell boundaries (Fig. 46 and Movie 19). This asymmetry was very evident at the posterior-central region of the A compartment. In this region, D displayed “polarity lines” (Bosveld et al., 2012) that tend to be oriented in parallel to the A/P boundary. These polarity lines persisted throughout nest fusion and the end of expansion, propagating anterior-ward in the A compartment (Fig. 46 and Movie 19).

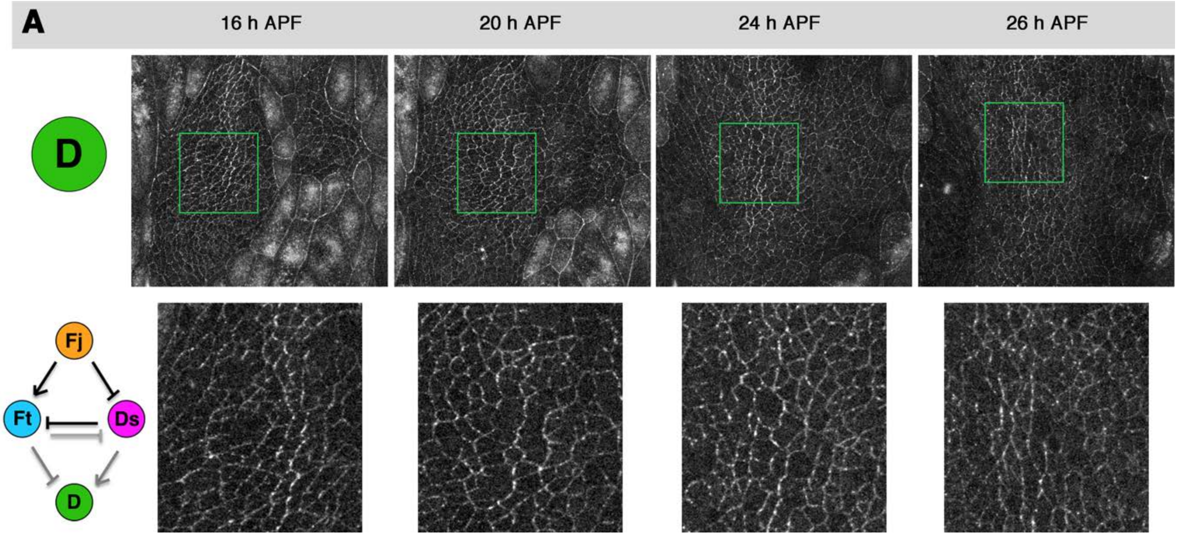

Fig. 46: D “polarity-lines” are early detected in the center-posterior front of the A compartment. A) Top: expression pattern of D at the indicated times during expansion. D is apically localized in histoblasts and LECs. D is strongly expressed within the center-posterior section of the A compartment (green boxes) throughout expansion. Bottom: Cartoon pointing to the regulatory inputs of the Triad onto D (Left). Magnification of the green boxes showed in A. D is either clustered or in punctae along apical cell outlines. Note that D polarity lines slightly spread anteriorly throughout expansion. Genotype was *D::GFP*. Anterior is to the left. See text for details. See also Chapter III. See Movie 19.

As endogenous D levels weaken over-time (by 28-30 hours APF), it was not possible to follow up their evolution throughout remodeling.

To define the subcellular localization of D, we generated Flp-Out clones expressing D by employing a EGFP::Dachs fusion protein whose expression was driven by the actin promoter (Act5C) (Brittle et al., 2012 and Materials and Methods). Any asymmetry of the localization of D was assessed at the boundary of the induced clones.

We found that D was already asymmetrically localized along the A/P axis of the nests from 16 hours APF (Fig. 47A-to-B’’’ and Movie 20). D also primarily enriched at anterior and posterior oriented cell interfaces within the A and P compartments respectively, therefore presenting the same axial asymmetry observed for Ds (Fig. 39 and 40). Remarkably, at early stages D anterior subcellular localization was more robust in the posterior-most region of the A compartment, while in anterior-most regions some cells showed a slightly dorsal bias or even no asymmetry (Fig. 47A-to-B’’’). Remarkably, this anterior region is where the steady combinatorial arrangement of Ds, Ft and *fj* was reached last. As morphogenesis progressed, D became enriched anteriorly all throughout the A compartment (Fig. 47C-C’’). Thus, D asymmetry orientation broadly followed the vector imposed by the Ds gradient, indicating that this may prefigure the directional activity of the pathway.

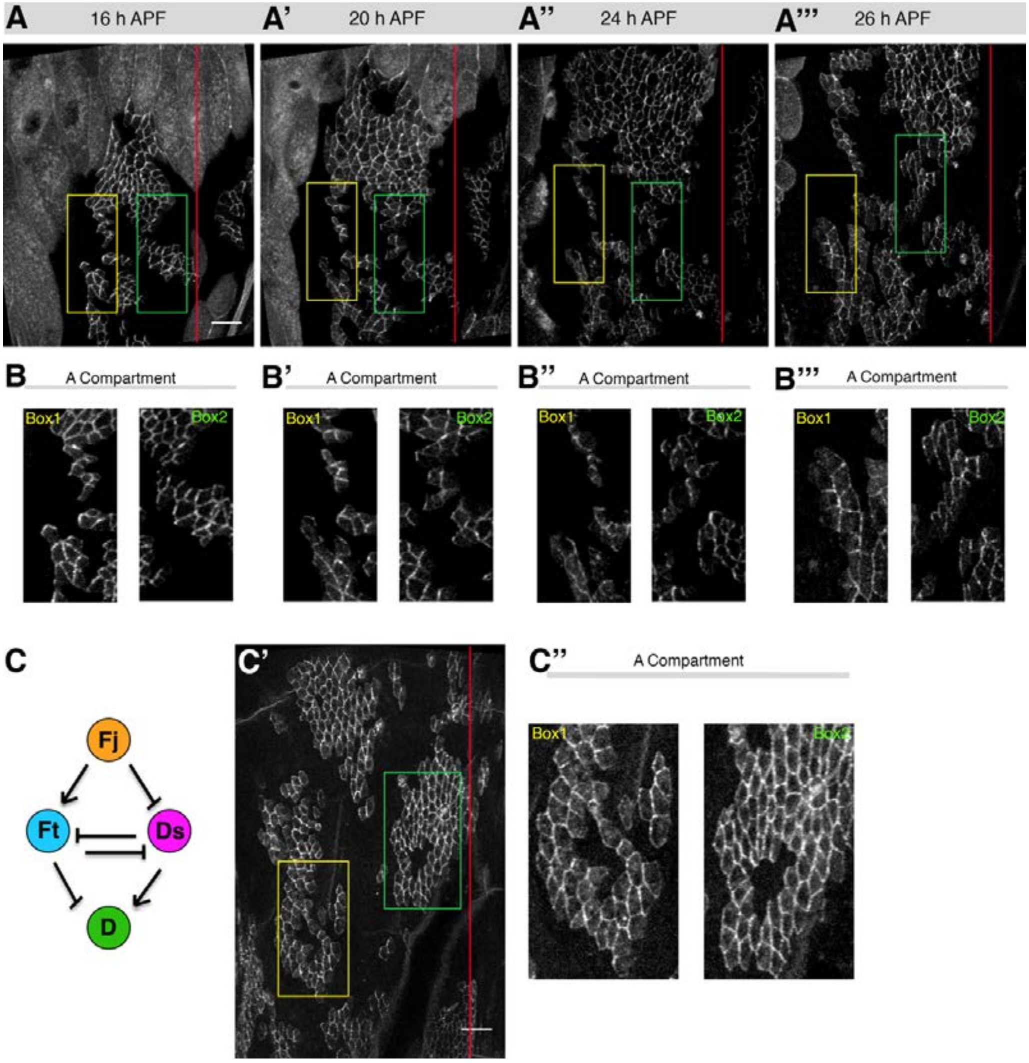
A
16 h APF
A'
20 h APF
A''
24 h APF
A'''
26 h APF
B
A Compartment
B'
A Compartment
B''
A Compartment
B'''
A Compartment
Box1
Box2
C
Fj
Ft
Ds
D
C'
C''
A Compartment
Box1
Box2

Fig. 47: D subcellular localization respect to A/P axial cues. A-A''') Evolution of D asymmetry during expansion. The position of the A/P boundary is marked by red lines. Note that from the onset of expansion D is preferentially enriched anteriorly in the A compartment. In the P compartment D asymmetry is reversed (A-A''). **B-B''')** Close-up of the boxed regions shown in A-A'''. The yellow boxes (1) indicate the localization of D in the anterior region of the A compartment. The green boxes (2) point to D localization in more posterior regions of the A compartment. Note that in the anterior most region of the A compartment, D is not asymmetrically localized. **C)** Cartoon pointing to the regulatory inputs of the Triad onto D. **C')** D subcellular localization at 46 hours APF in the AIII hemi-segment. The A/P boundary position is marked by a red line. **C'')** Close-up of the boxed regions shown in C' at the time in which Ds and Ft gradient are at steady-state Anterior is to the left. Scale bar is 16 µm. Genotype was *hsflp1.22; Act5C>>EGFP::d/+*. See text for details. See also Chapter III. See Movie 20.

2.5 Strabismus Expression Pattern and its Late Asymmetry During Morphogenesis

The analyses of the Ds/Ft/Fj expression patterns during expansion and remodeling strongly suggest that this pathway provides guidance for the orientation of PCA. We then checked whether the Core PCP signalling could potentially influence PCA dynamic.

While the Ds/Ft/Fj and the Core pathway independently control planar polarity in the abdominal epidermis (Lawrence et al., 2004; Casal et al., 2006), as in the case of the Ds/Ft/Fj pathway, the expression pattern of the Core pathway components has not been previously analyzed. To monitor its dynamics, we focused on two key components, namely Strabismus (Stbm, a.k.a. Vang) and Frizzled (Fz). Both are trans-membrane proteins that in multiple epithelial tissue contexts segregate at opposite edges of the same cells, thereby coupling polarized signals.

We first employed a Stbm::EYFP transgene driven by the actin (Act5C) promoter, which mimics the endogenous Stbm pattern and rescues polarity defects in *stbm* mutant animals (Strutt, 2001; Strutt and Strutt 2002 and 2007). From 16 to 26-28 hours APF, Stbm was both localized at the apical cell junctions and diffused within the apical surface of all cells. Overall, no obvious asymmetry was detected during these stages (Fig. 48A-A''' and Movie 21). One possibility was that early Stbm asymmetry was too weak to be detectable at tissue level. To define its subcellular localization more precisely, we induced clones of cells by Flp-Out (Materials and Methods). However, no obvious signs of axial asymmetry were detected at clone boundaries (Fig. 48B-B'''and Movie 22). Except in few scattered cells, Stbm was evenly localized all over the periphery of the clones (Fig. 48B-B''' and Movie 22). The absence of early polarization in Stbm localization indicated that was unlikely that the Core pathway influence PCA dynamics during expansion.

From 26-28 hours APF and during remodeling, the localization pattern of Stbm started showing some signs of asymmetries (Fig. 49 and Movie 23). By 40-42 hours APF a certain number of histoblasts display asymmetrical Stbm localization although these asymmetries were not oriented in any consistent direction (Fig. 49A-A'' and B-B''). Notably, just before trichome eversion (44-45 hours APF), Stbm became localized and axially polarized to the anterior edges of every cell irrespectively of the compartment, in both A and P (Fig. 49A'''-B''' and C-C''').

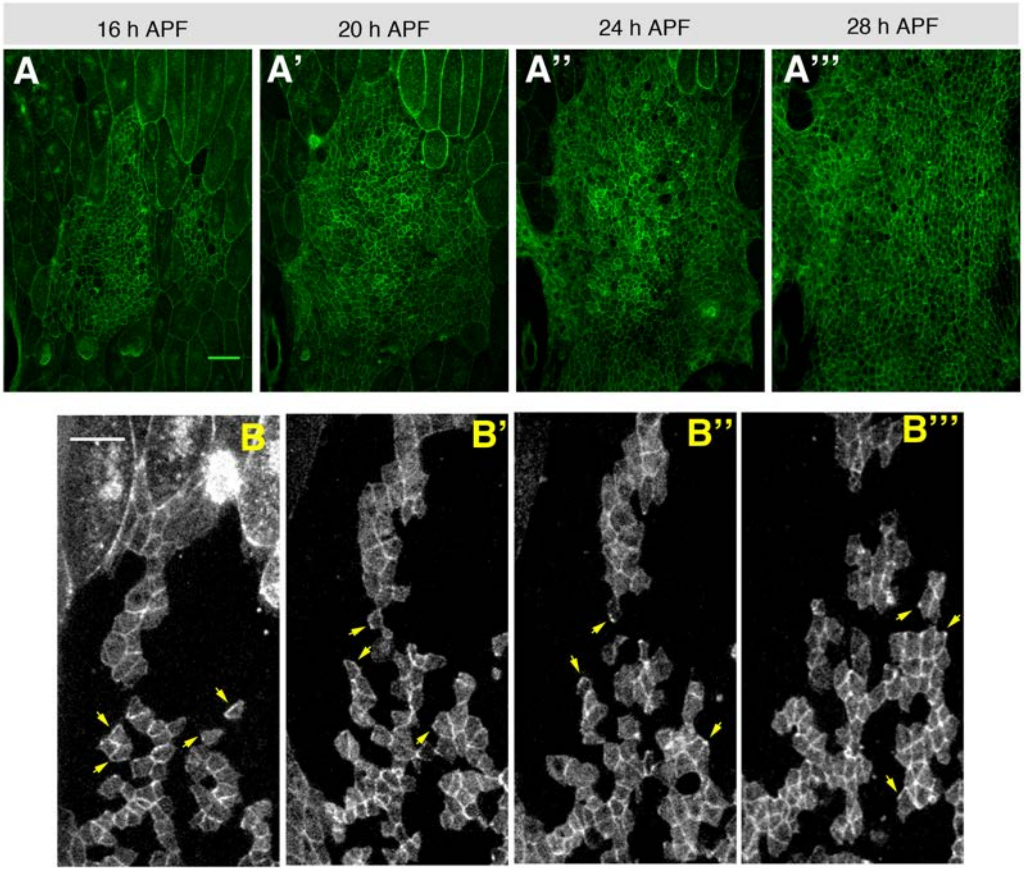

Fig. 48: Stbm asymmetry is either scattered or non-axial during expansion. A-A’’’) Expression pattern of Stbm (Green) during expansion. **B-B’’’)** Visualization of Stbm polarization at 16, 20,24 and 28 hours APF. Yellow arrows point to Stbm expression. Note that asymmetries were scattered and not aligned to any preferential axis. Genotypes were *Act5C-Stbm::EYFP* (A-A’’’) and *hsflp1.22;; Act5C>>Stbm::EYFP/+* (B-B’’’). Anterior is to the left. See text for details. Scale is 20 µm (A-A’’’) and 16 µm (B-B’’’). See Movie 21 and Movie 22.

The mutually exclusive Stbm and Fz subcellular localization reported in other epithelial derivatives (Strutt et al., 2002; Bastock et al., 2003; Tree et al., 2002) also held in the abdominal epithelium. Fz at the time of trichome eversion (44-45 hours APF) localized at the posterior edge of each cell irrespectively of the compartment (Fig. 49D-D’’’), so thus opposing Stbm asymmetry.

Taken together, these data indicate that the orientation of PCA precedes Stbm/Fz-Core polarization, suggesting that the Core components are unlikely influencing the establishment of the axial orientation of PCA.

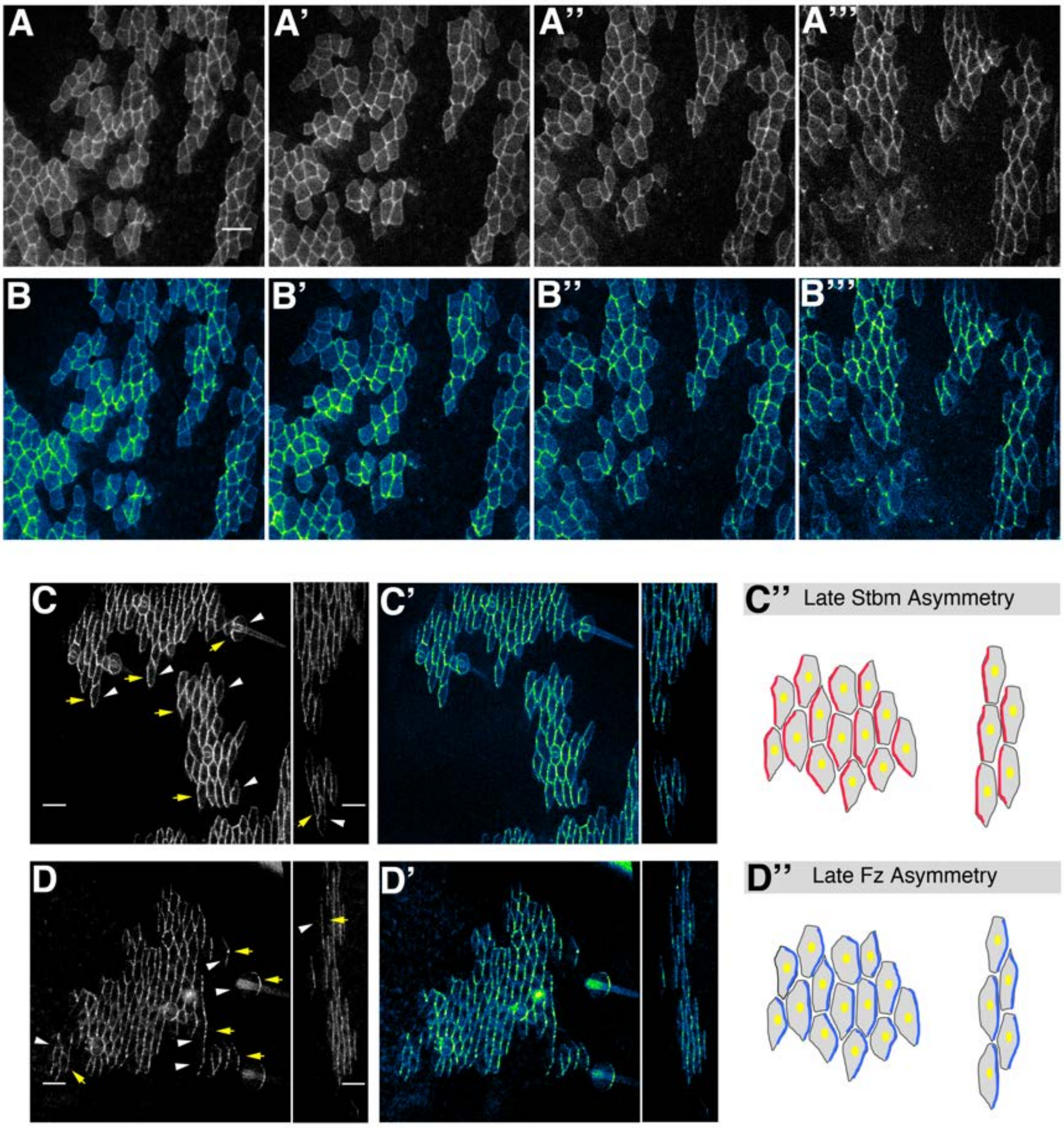

Fig. 49: Stbm asymmetry becomes uniaxial shortly before trichome eversion and opposes Fz polarity. A-A’’’) Images showing the dynamic evolution of Stbm localization within the A compartment at 40, 42, 43 and 44 hours APF in clones of cells expressing Stbm::EYFP. **B-B’’’)** Images as in A-A’’’ but after applying the Green-Blue-FireLUT for intensities. Green indicates high and blue indicates low intensity. **C)** Clone of cells in the A (Left) and P (right) compartment at 45 hours APF expressing Stbm::EYFP. Yellow arrows point to Stbm-enriched edges. White arrowheads point to low Stbm signal. **C’)** Images as C but after applying the Green-Blue-FireLUT for intensities. **C’’)** Cartoon describing the asymmetry of Stbm in mature epithelial cells within the A (left) or P (right) compartment. Note the anterior polarization of Stbm in both compartments. **D)** Clone of cells in the A (Left) and P (right) compartment at 45 hours APF expressing Fz::EYFP. Yellow arrows point to Fz-enriched cell interfaces. White arrowheads indicate low detection of Fz. **D’)** Images as in D but after applying the Green-Blue-FireLUT for intensities. **D’’)** Cartoon describing the asymmetry of Fz in mature epithelial cells within the A (left) or P (right) compartment. Note the posterior polarization of Fz in both compartments. Genotypes were *hsflp1.22;; Act5C>>Stbm::EYFP/+* (A-to-C’) and *hsflp1.22; Act5C>>Fz::EYFP/+* (D-D’). Anterior is to the left. See text for details. Scale is 16 µm (A-to-B’’’) and 12 µm (C-C’ and D-D’).See Movie 23.

Synopsis

The pattern of expression of the Ds/Ft/Fj pathway in the abdominal epidermis is very dynamic yet biased along the A/P axis from early stages reaching a stable axial organization along the A/P axis at morphogenesis completion. The steps followed to reach this configuration appear to correlate with the spatiotemporal evolution of the axial orientation of PCA over developmental times. Further, the Ds-Ft interaction across cells (highlighted by the preferential subcellular localization of Ds-D) orient parallel to the A/P axis from early developmental stages, following the orientation of the Ds membrane-bound gradient. The tendency of cells to orient in parallel to the A/P axis in the A compartment gradually propagates across the entire segmental field from the posterior-most regions, as also the axial orientation of PCA does. This temporal and spatial correlation suggests that the Ds-Ft heterodimeric interactions may actually be involved in the axial progression of the orientation of PCA toward its uniform arrangement.

The expression of key members of the Core pathway becomes polarized along the A/P axis shortly before trichome eversions and once the axial bias underlying orientation of PCA has been established.

Chapter III

The Ds/Ft/Fj pathway is required to coordinate the axial uniform orientation of PCA

3.1 The Uniform Orientation of PCA is Lost in *ds* Pupae

In order to explore if the Ds/Ft/Fj pathway influences the uniform orientation of PCA, we analyzed cells and tissue organization in different allelic combinations of the distinct components of the pathway.

Strong *ds* alleles lead to larval lethality preventing the analysis of *ds* in the pupal histoblasts. Viable *ds* pupae were raised by combining two strong hypomorphic alleles; ds^{UAO71} and ds^{38K} (see Materials and Methods) were then studied. This hetero-allelic combination gave place to slightly dysmorphic pharates and escapers, whose abdomens were barely shorter and broader than their heterozygous siblings (Fig. 50A-F). In this condition, the abdominal segments were slightly shorter than in *wt* (Fig. 50G-I). The orientation of PCA, on the contrary, was dramatically altered. At 50% of pupariation, histoblasts were arranged in multiple local patterns without uniform orientation and at steady state a “patchwork” of divergently oriented cells was observed (Fig. 50L-L’ and M-M’). Remarkably, these modifications in cell arrangements were not accompanied by patterning defects. The number and position of bristles were fairly normal in the A compartment (Fig. 50M-M’).

To assess how the progression in the orientation of PCA was affected in *ds* pupae, cell orientations relative to the A/P boundary and mutual cell alignments were monitored at 16, 26, 38, and 47 hours APF (Fig. 51, Movie 24 and Movie 25 ; see also Chapter I and Materials and Methods). As for *wt*, until 26 hours APF, cell orientation was neither uniformly aligned with the A/P boundary nor cells were arranged locally in a preferential common orientation (Fig. 51A-C and D-E). Cells immediately in contact with the A/P boundary were the only ones orienting parallel to it. Of note, the dorsal-ward displacement of the nests coupled to LECs occurred normally (Ninov et al, 2007; Bischoff and Cseresnyes, 2009), indicating that Ds was not involved in modulating histoblast migration or LECs delamination.

During tissue remodeling defects in the orientation of PCA were very evident (Fig. 51A’-C’). As observed at the end of expansion, the only cells orienting parallel to the A/P axis were those contacting the A/P compartment boundaries or those located within the narrow P compartment (Fig. 51B’-C’). The anterior-ward spreading of the orientation of PCA taking place between 38 and 47 hours APF did not occur. The orientation of histoblasts followed very different directions and the proportion of those aligning with the A/P boundary was drastically reduced (Fig. 51D). Further, coherency became also affected and the mutual histoblasts oriented alignment was very low (Fig. 51E). In consequence, at 47 hours APF, the steady state configuration of the tissue was dramatically different than in the *wt* (Fig. 51A'-C'; see also Chapter I). Thus, Ds was required for the progression of the orientation of PCA towards axial uniformity.

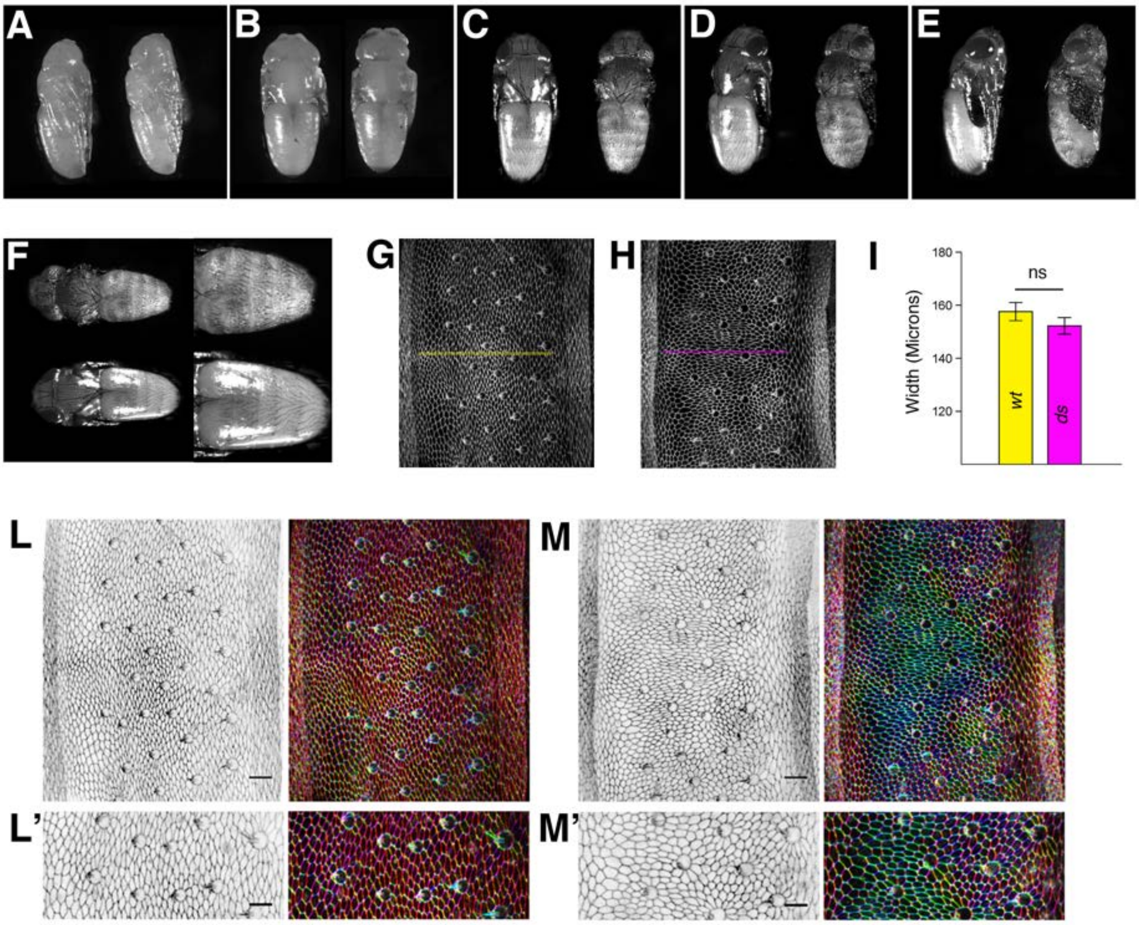

Fig. 50: At steady-state epithelial cell outlines reveal loss of uniform orientation of PCA in *ds* pupae. A-B) Lateral (A) and dorsal (B) view of *wt* (left) and *ds* (right) pupae at the end of pupation (47-50 hours APF). **C-E)** Dorsal (C), dorso-lateral (D) and lateral (E) view of *wt* (left) and *ds* (right) pupae at late pharate stage (about 80 hours APF). Note that the abdominal region is slightly shorter in *ds* and that the head, thorax and wings are enlarged. **F)** Magnification of the abdominal region showed in C. **G-H)** Images showing a dorsal view of the AIII segment of a *wt* (G) and a *ds* (H) pupa at 50 hours APF. The width of the A compartment in the *wt* segment is marked with a yellow line (G) and in the *ds* segment is marked with a magenta line along the dorsal midline (H). **I)** Bar-charts reporting the averaged A compartment widths of *wt* and *ds* pupae. n=12 (*wt*) and 10 (*ds*) AIII segment widths. Error bars are SEM; Two-tailed unpaired t-test for significance of difference was applied; ns $p>0.05$ not significant. **L-M)** The *wt* tissue is characterized by uniform orientation of PCA at steady state (L), while in the *ds* tissue coexist multiple PCA orientations (M). **L'-M'**) Close up of the A compartment of *wt* (L') or *ds* (M'). Anterior is to the top (A-E) or to the left (F-to-M'). Genotype were *Atp*α*::GFP* and *ds*^{UAO71}/*ds*^{38K}*; Atp::GFP/+*. Scale bar is 22 μm (G-H, L-M) and 16 μm (L'-M'). See text for details.

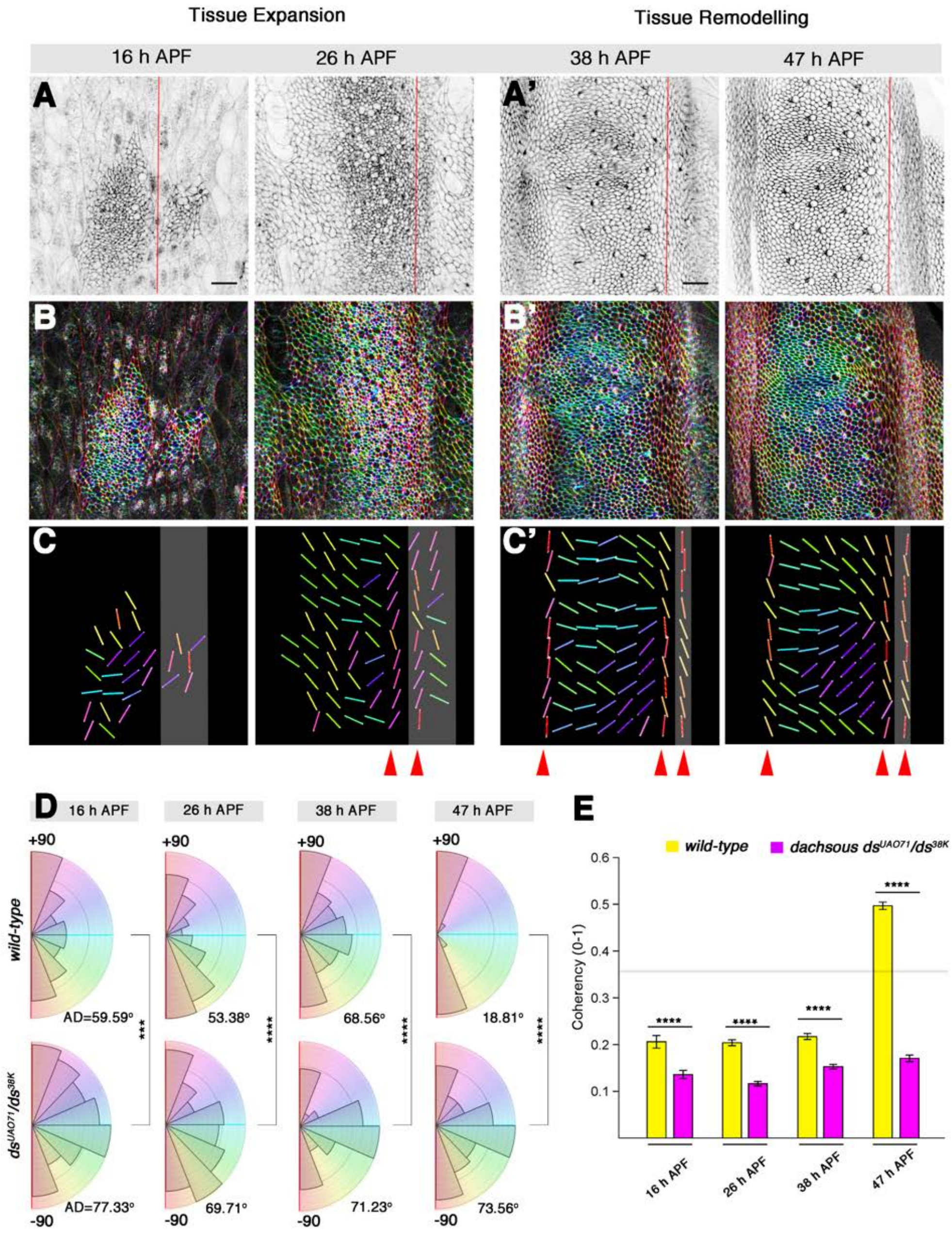
Tissue Expansion
Tissue Remodelling
16 h APF
26 h APF
38 h APF
47 h APF
A
A'
B
B'
C
C'
D
16 h APF
26 h APF
38 h APF
47 h APF
+90
-90
wild-type
dsUAO71/ds38K
AD=59.59°
53.38°
68.56°
18.81°
AD=77.33°
69.71°
71.23°
73.56°
***
****
****
****
E
wild-type
dachsous dsUAO71/ds38K
Coherency (0-1)
0.6
0.5
0.4
0.3
0.2
0.1
****
****
****
****
16 h APF
26 h APF
38 h APF
47 h APF

Fig. 51: The uniform attainment and axial progression of the orientation of PCA is severely impaired in *ds*. A-A') Cell outlines in *ds* pupae during expansion (A) and remodeling (A'). The position of the A/P boundary is marked with red lines. **B-B')** Color-coded angular cell edge orientations during expansion (B) and remodeling (B'). **C-C')** Locally averaged orientations during expansion (C) and remodeling (C') highlighting topographic changes in orientation relative to the A/P boundary. Averaged orientations between neighboring cells are visualized by colored bars. The P compartment is masked in grey. Note the impairment of the P to A progression of the orientation of PCA (red arrowheads). **D)** Polar plots reporting the angular distribution of cell orientations relative to the A/P boundary. Abundances are proportional to areas. Bin size is 16°. AD indicates angular dispersion (in degrees) of each distribution. The W-test for significance was applied. Each distribution was significantly different of controls, ***p<0.001 or ****p<<0.0001; **(E)** Quantification of cell-cell alignment coherency along the mean orientation. The bar charts report mean values of alignment coherency in *wt* and *ds* pupae over time. Values below 0.35 indicate misalignment. Error bars indicate SEM. The K-S test for significance of difference was applied. Significance level ****p<0.001 between columns linked by bars. For D and E n=76, 214 ROIs in 3 *ds* pupae for expansion and n=240, 205 ROIs in 3 *ds* pupae for remodeling were employed. Anterior is to the left. Genotype was ds^{UAO71}/ds^{38K}; $Atp\alpha$::*GFP*/+. Scale bar is 22 μm. See Movie 24 and Movie 25.

3.2 Local Orientation of PCA in *fat* and *four-jointed*

To study the contribution of Ft in the progression of the orientation of PCA, *ft* pupae were generated by hetero-allelic combination of ft^{GRV} and ft^{1} alleles (See Materials and Methods). The segmental size of these pupae resembled that of *ds*, indicating absence of overgrowth (Matakatsu and Blair 2006; Casal et al., 2002). We analyzed the spatial and temporal dynamics of the orientation of PCA in these pupae (Fig. 52) and found that, as in *ds*, the progression towards uniformity was abolished. Cells orientation was neither uniformly aligned parallel to the A/P boundary nor between neighboring cells (Fig. 52A-C and D-E; See also Chapter I). Cells immediately in contact with the A/P boundary were the only ones orienting in parallel to it. Nests movements occurred normally indicating that Ft, as Ds, was not involved in modulating histoblast migration or LECs delamination.

During tissue remodeling, again, defects in the orientation of PCA were obvious (Fig. 52A'-C'). Histoblasts oriented parallel to the A/P axis were only present close to the A/P compartment boundaries or within the P compartment, and the anterior-ward spreading of the cells orientation did not occur properly (Fig. 52B'-C'). As in *ds*, the orientation of histoblasts followed very different directions, the proportion of those aligning with the A/P boundary was reduced, and the coherency and mutual oriented alignment amongst histoblasts was very low (Fig. 52D-E). Thus, Ft, as Ds, is required for the progression of the orientation of PCA towards axial uniformity.

We next performed equivalent analyses to investigate the contribution of Fj to the progression of the orientation of PCA. *fj* null (fj^{D1}/fj^{D1}) pupae previously shown to have slightly short abdominal segments (Zeidler et al., 2000) were analyzed (Fig. 53). In contrast to *ds* or *ft*, *fj* pupae did not display substantial changes in the axial dynamics of the orientation of PCA during expansion (Fig. 53A-D), although by 26 hours APF the local coherency in cell alignment was already reduced (Fig. 53E). During remodeling, defects were more obvious and the anterior-ward spreading of the orientation of PCA and mutual cell alignments were reduced (Fig. 53A'-C' and D-E). At remodeling completion, the alterations in the uniformity of the orientation of PCA in *fj* pupae were much milder than those observed for *ds* or *ft*. The most dramatic effects were restricted to the anterior-most region of the A compartment and closed to the midline (Fig. 53C').

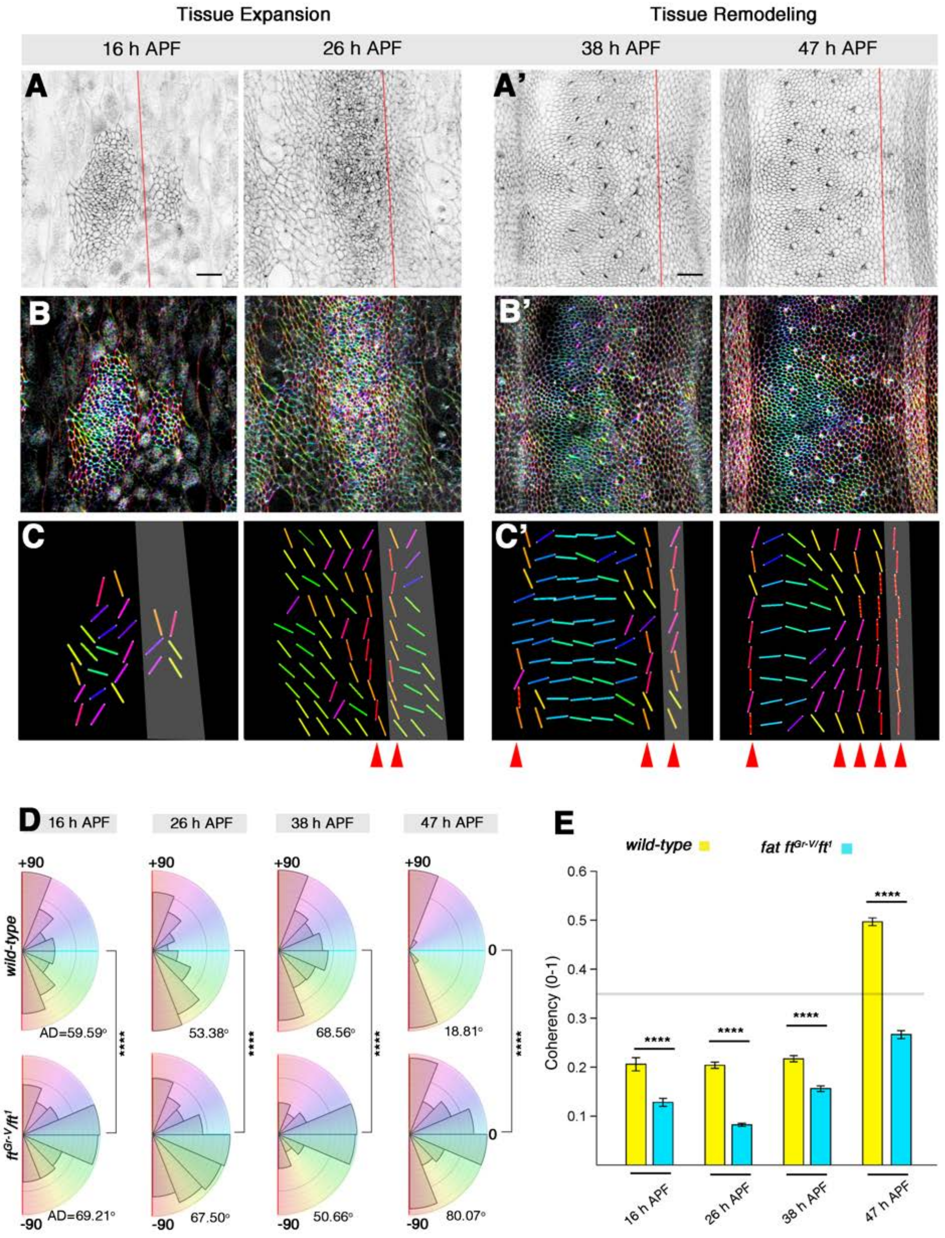
Tissue Expansion
Tissue Remodeling
16 h APF
26 h APF
38 h APF
47 h APF
A
A'
B
B'
C
C'
D
16 h APF
26 h APF
38 h APF
47 h APF
+90
0
-90
wild-type
ft^Gr-V/ft^1
AD=59.59°
53.38°
68.56°
18.81°
AD=69.21°
67.50°
50.66°
80.07°
****
E
wild-type
fat ft^Gr-V/ft^1
Coherency (0-1)
0.6
0.5
0.4
0.3
0.2
0.1
****
16 h APF
26 h APF
38 h APF
47 h APF

Fig. 52: The uniform attainment and axial progression of the orientation of PCA is severely impaired in *fat*. A-A') Cell outline morphologies in *ft* during expansion (A) and remodeling (A'). The position of the A/P boundary is marked with red lines. **B-B')** Color-coded angular orientations of cell junctions during expansion (B) and remodeling (B'). **C-C')** Local averaged orientations between neighbors (bars) during expansion (C) and remodeling (C'). The P compartment is masked in grey. Note that the P to A progression of the orientation of PCA is impaired (red arrowheads). **D)** Polar plots of the angular distribution of cell orientations relative to the A/P boundary at the indicated times. Abundances are proportional to the areas. Bin size is 16°. The angular deviation, AD, in degrees is reported to the right of each plot. Each distribution was significantly different from control, ***p<0.001 or ****p<<0.0001; the W-test for significance was applied. **(E)** Quantification of cell-cell alignment coherency along the mean orientation. The bar charts report the mean values of the cell-cell alignment coherency in *wt* and *fat* pupae. Values below 0.35 indicate misalignment. Error bars indicate SEM. Significance level ****p<0.001 between columns linked by bars. The K-S test was applied. n=76, 223 ROIs in 3 *ft* pupae for expansion and n=240, 224 ROIs in 3 *ft* pupae for remodeling were used to calculate mean orientation and alignment coherency. Anterior is to the left. Genotype was $ft^{GR\text{-}v}/ft^{1}$; $Atp\alpha$::*GFP*/ +. Scale bar is 22 μm.

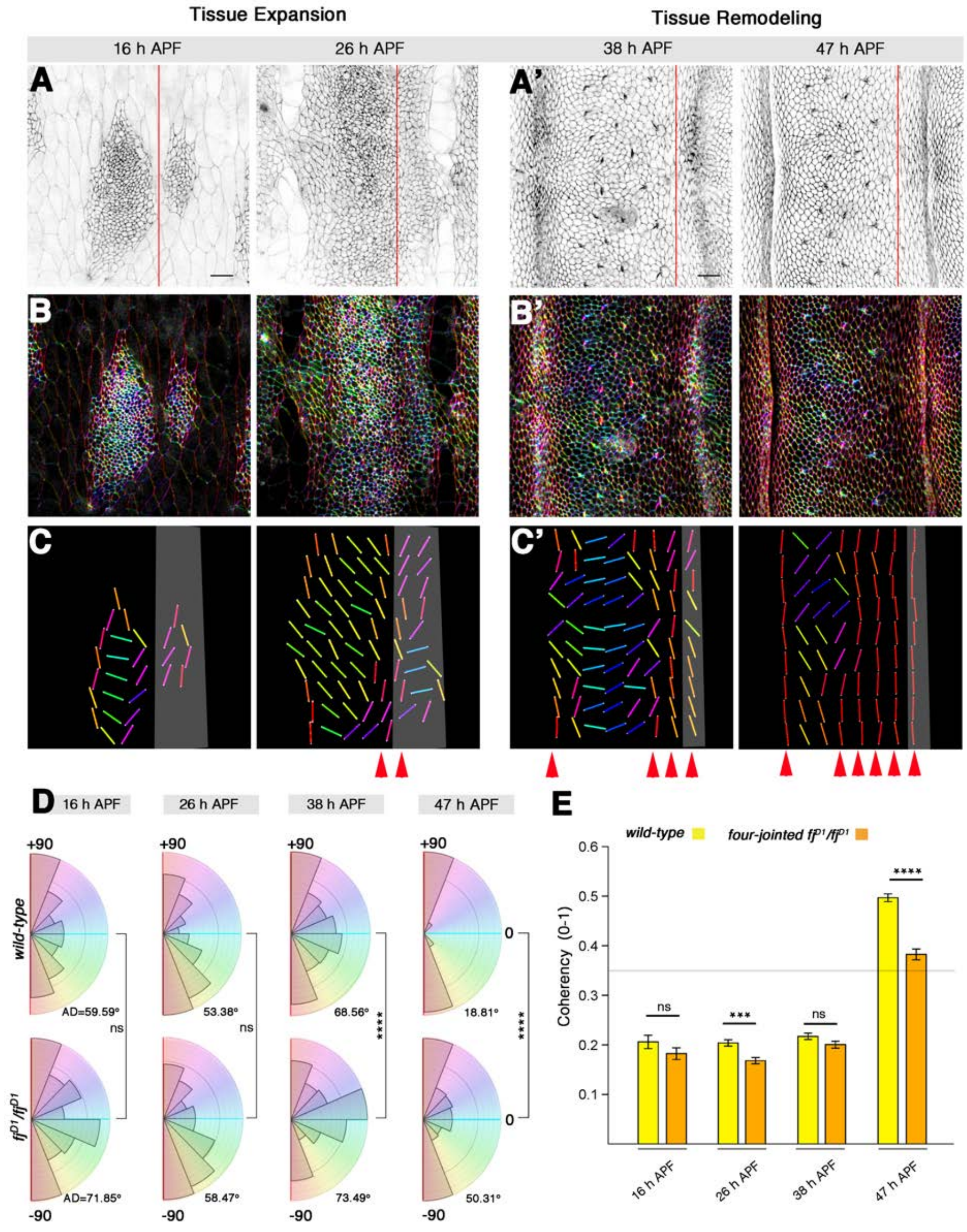

Fig. 53: The Uniform Attainment and Axial Progression of the Orientation of PCA is disturbed in *four-jointed*. A-A') Cell outline morphologies in *fj* pupae during expansion (A) and remodeling (A'). The position of the A/P boundary is marked with red lines. **B-B')** Color-coded maps of the angular orientations of cell junctions during expansion (B) and remodeling (B'). **C-C')** Locally averaged orientations between neighboring cells (bars) during expansion (C) and remodeling (C'). The P compartment is masked in grey. Note that the P to A progression of the orientation of PCA is impaired (red arrowheads). **D)** Polar plots of the angular distribution of cell orientations relative to the A/P boundary at the indicated times. Abundances are proportional to the areas. Bin size is 16°. AD indicates angular dispersion in degrees. The W-test for significance was applied between distributions. ****p<0.0001; p>0.05 ns (not significant) **(E)** The bar charts report the mean values of cell-cell alignment coherency in *wt* and *fj* pupae between 16 and 47 hours APF. Values below 0.35 indicate misalignment. Error bars indicate SEM The KS-test for significance was applied. Significance level, ****p<0.0001; ***p<0.001 or p>0.05 ns (not significant) between columns. n=75, 213 ROIs in 3 *fj* pupae for expansion and n=230, 216 ROIs in 3 *fj* pupae for remodeling were used to calculate mean orientation and alignment coherency. Anterior is to the left. Genotype was fj^{D1}/fj^{D1}; *Atpα::GFP/+*. Scale bar is 22 μm.

In summary, the analyses described above indicate that the perturbation of the Ds/Ft/Fj pathway activity disrupts the dynamics of the axial orientation of PCA and prevents the uniform arrangement of histoblats along the A/P axis. The three components are all required for the attainment of cells uniform orientation and the fidelity of its progression.

3.3 Perturbations of the Ds/Ft/Fj Signaling Affect the Uniform Orientation of PCA and Reduce Cell Shape Anisotropy.

To test whether tissue wide perturbations of the Ds/Ft/Fj signaling had an impact into cell shape anisotropy, we measured cell elongation evaluating the aspect-ratio (AR), the roundness and circularity from cell outlines, together with the orientation of the cell longest axis in steady state *ds, ft* and *fj* epithelia (Fig. 54). Mutant cells for any pathway components showed reduced cell shape anisotropy (Fig. 54A-D and H-I) and randomized cell orientation (Fig. 54L, see also Figs. 51 to 53). Thus, alterations in the functional configuration of the Ds/Ft/Fj network, just by altering the balanced levels of the cadherins Ds or Ft or the stability of their interactions through Fj affects both cell shapes and their orientations.

We further analyzed this functional equilibrium by overexpressing Ds or Fj uniformly and monitoring cell shapes and orientations. Either excessive Ds or Fj affected both cell elongation and the PCA orientation (Fig. 32E-F and H-L). We found that abolishing or enhancing Fj expression have similar net effects on both cell elongation and PCA orientation (Fig. 54D, F and H-L). Reducing Ds activity has a stronger impact in both these cellular features with respect to loss or enhanced Fj activity (Fig. 54B, D, F and H-L). We found that high Ds levels randomize PCA orientation although less strongly compared to *ds* mutants. In contrast, high Ds levels reduce cell elongation more strongly than *ds* mutant, having cells more isometric shapes (Fig. 54B, E and H-L). Strikingly, excessive Ds levels and reduced Ft activity levels (*ft* pupae) have the same net effect on cell shape anisotropy reduction, but not in the orientation of PCA. The orientation of PCA is more strongly affected in *ft* mutants (Fig. 54C,E and H-L), suggesting that the levels of Ds and Ft affect cell shape anisotropy while their activities modulate the orientation of PCA.

Cell anysotropy was reduced in all mutant conditions, strongly in *ft* and mildly in *ds* and *fj*. Elongation was also diminished after overexpressing Ds [strongly (at the level of *ft* loss of function)] or Fj [mildly (at the level of *ds* and *fj*)]. Regarding the uniform orientation of PCA, *ft* again displayed the strongest phenotype, also *ds* loss of function was also very strong while *fj* show very weak defects. Overexpressions of Ds and Fj, on the other hand, gave very mild phenotypes almost comparable to *fj* loss of function.

We also tested if reduced cell size had an impact on cells anisotropy and/or the orientation of PCA. We genetically accelerated the cell cycle by overexpressing simultaneously String and Cyclin E in clones (Fig. 54F) and no effects were found. We observed an autonomous reduction in cell size but cell shapes and orientations were almost identical to *wt* (Fig. 54H-L), suggesting that the defects observed in *ds/ft/fj* mutants like the reduced cell shape anisotropy and the failure in the orientation of PCA cannot be assigned to differences in growth rates.

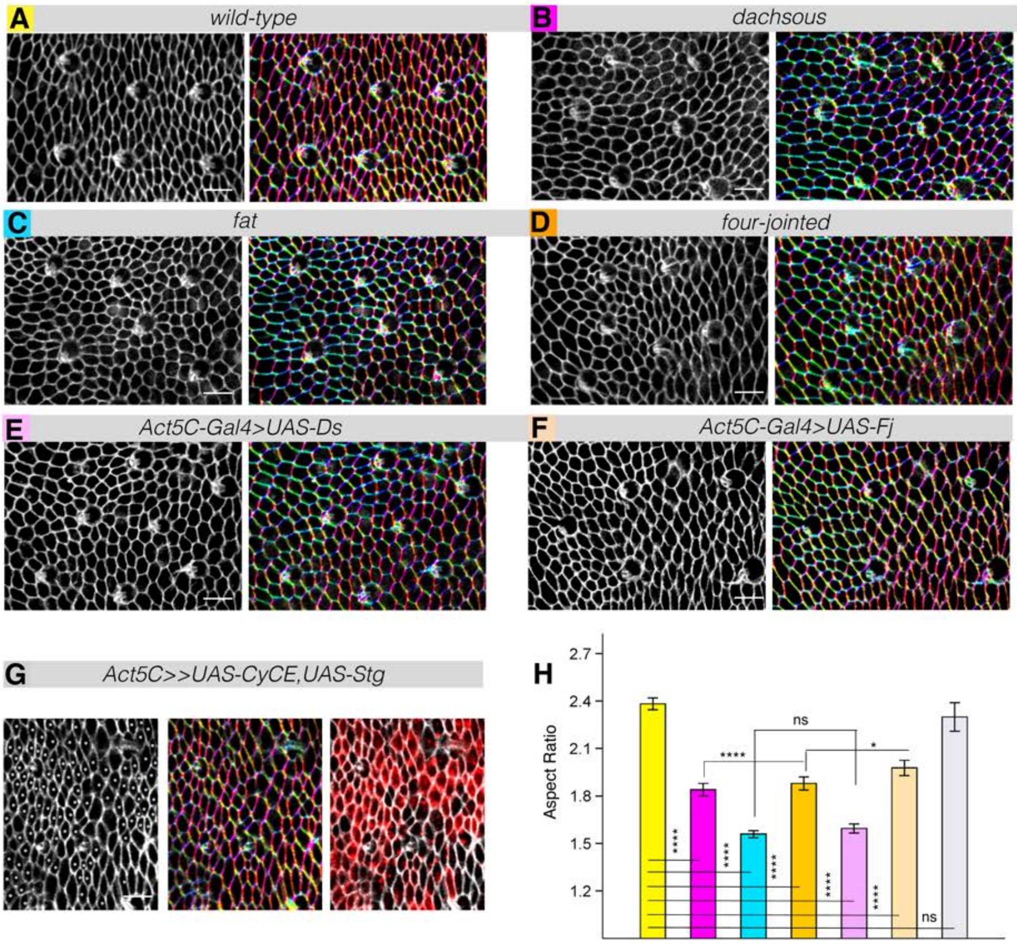
A
wild-type
B
dachsous
C
fat
D
four-jointed
E
Act5C-Gal4>UAS-Ds
F
Act5C-Gal4>UAS-Fj
G
Act5C>>UAS-CyCE,UAS-Stg
H
2.7
2.4
2.1
1.8
1.5
1.2
Aspect Ratio
ns
****
*
****
****
****
****
****
ns

I

	wild-type	*dsUAO71/ds38k*	*ftGR-v/ft1*	*fjD1/fjD1*	*Act5C-Gal4>UAS-Ds*	*Act5C-Gal4>UAS-Fj*	*Act5C>>UAS-CycE,UAS-Stg*
n. of cells	956	955	991	629	660	745	200
Area/Perimeter	1.13±0.2	1.26±0.2	1.30±0.2	1.32±0.2	1.43±0.15	1.27±0.18	1.01±0.22
Aspect Ratio	2.39±0.59	1.84±0.62	1.56±0.36	1.87±0.52	1.59±0.37	1.97±0.67	2.29±0.64
Roundness	0.44±0.11	0.59±0.16	0.67±0.13	0.57±0.15	0.65±0.14	0.55±0.16	0.47±0.14
Circularity	0.61±0.09	0.72±0.09	0.76±0.06	0.69±0.09	0.71±0.06	0.66±0.1	0.61±0.1

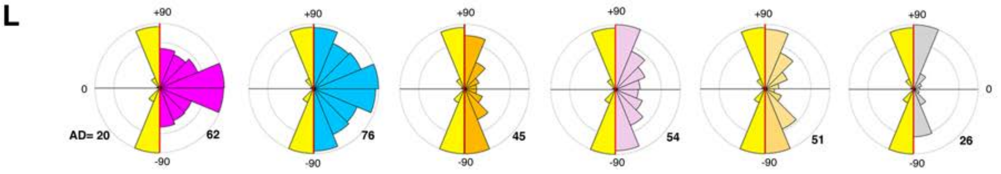

Fig. 54: Perturbations of the Ds/Ft/Fj signaling affect orientation of PCA and reduce A/P cell anisotropy.) **(**The legend of Fig. 54 is written in the next page)

Fig. 54: Perturbations of the Ds/Ft/Fj signaling affect orientation of PCA and reduce A/P cell anisotropy. A-G) Cell outlines (left) and colored edge orientations (right) within the A compartment of the AIII segment at steady state for *wt* (A), *ds* (B), *ft* (C), *fj* (D), UAS-*Ds* (E), UAS-*Fj* (F) and UAS-Stg/UAS-CycE (G). **H)** The bar charts report the averaged AR values for each case. Yellow bar indicates *wt*; while magenta, cyan and orange bars point to *ds, ft* and *fj* respectively. UAS-Ds, -Fj and –CycE-Stg bars are colored in light magenta, orange and grey respectively. Error Bars indicate S.D.; The KS-test for significance was applied. Significance level, ****$p<0.0001$; *$p<0.05$ or $p>0.05$ ns (not significant). **I)** Summary table reporting the averaged values (± S.D.) of the parameters used to evaluate cell shape anisotropy. **L)** Polar plots of the orientation of the cell axis relative to the A/P boundary for each condition. The *wt* distribution of cell orientation is shown on the left hemi-circle in all cases (yellow). Bin size is 16°. The angular dispersion (AD) of each distribution is reported below each plot. Genotypes were *Atpα::GFP/+* (A) *ds*^{UAO71}/*ds*^{38K}*; Atpα::GFP/+* (B), *ft*$^{GR-v}$/*ft*^{1}*; Atpα::GFP/ +* (C) *fj*^{D1}/*fj*^{D1}*; Atpα::GFP/+* (D), *Act5C-Gal4/UAS-Ds: Atpα::GFP/+* (E), *Act5C-Gal4/UAS-Fj: Atpα::GFP/+* (F) and *hsflp1.22;Act5C>>UAS-CD8.mCherry; UAS-CycE, UAS-Stg* (G). Anterior is to the left. Scale bar is 16 μm.

3.3 Fat expression and Dachs Localization Respond to Perturbations in the Ds/Ft/Fj Signaling

To explore if cells shape anisotropy and the orientation of PCA were a result of the axial activity of the Ds/Ft/Fj pathway (See also Chapter II), we analyzed both, the attainment of the Ft gradient over time and the subcellular localization of D in response to loss of function conditions for *ds* and *fj*.

-Ft Gradient in ds and fj Pupae

The analysis of Ft in *ds* pupae showed that its expression pattern was strongly affected (Fig. 55A-A’ and B-B’). Ft expression remained higher within most of the A compartment and the maturation of an axial Ft gradient was abolished (Fig. 55B-B’). The anterior sector of the A compartment, which fails to acquire a graded expression of Ft by anterior-ward spreading, precisely matched the domain in which the orientation of PCA was affected (Fig. 55A’’-B’’). Fj also participates in the patterning of Ft, and Ft expression was affected in pupae lacking *fj* (Fig. 55A-A’ and C-C’). Ft was expressed gradually in most of the A compartment of *fj* but it arrived to a plateau at the anterior-most region and its gradient never reached completion (Fig. 55C-C’). Again, in this precise domain the PCA failed to orient along the A/P axis (Fig. 55C’’). In summary, both Ds and Fj are required to shape the Ft gradient, what it seems to be directly related with the sectorial defects in the orientation of PCA observed in *ds* and *fj* pupae.

-D in ft and ds Pupae

The lack of progression in the profile of Ft expression on *ds* and *fj* mutants suggests that in these conditions the balance between Ds and Ft and hence, the pathway activity will be compromised all around the field. Further, the spatial and temporal correlation of the defects observed in the orientation of PCA with the abnormal evolution of Ft expression points to the possibility that functional Ds and Ft heteromeric interaction may be directing the orientation of PCA. To explore this possibility, we monitored the subcellular localization of D as readout of the activity of the pathway (see also Chapter II) in *ft* and *ds* pupae. The endogenous enrichment of D on apical clusters and spots in A/P oriented cell interfaces (polar lines) observed in *wt* conditions was lost upon reducing Ft activity (Fig. 56A-B, Movie 26 and Movie 27; See also Chapter II). D remained clustered in randomized locations across the apical cell perimeter of *ft* mutants (Fig. 56A-B). Moreover, the dynamic changes in D localization at the apical membrane also failed (Fig. 56B), indicating that Ds and Fj in the absence of Ft are unable to generate functional axial information.

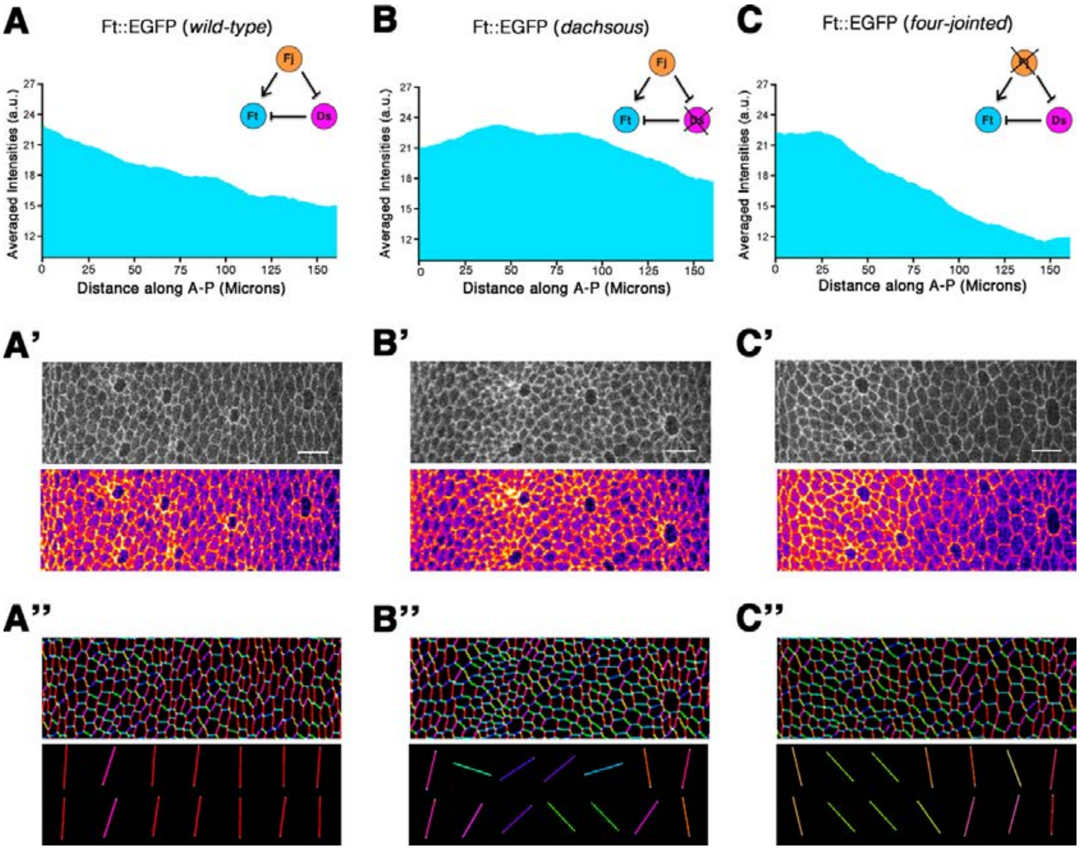

Fig. 55: Ds and Fj are required to shape the gradient of Ft. A-C) Plot profile of Ft::EGFP expression levels throughout the A compartment of a AIII segment at 46 hours APF for *wt* (A), *ds* (B) and *fj* (C). The triads point to the regulatory inputs of Ds and Fj on Ft. **A'-C')** Grey (top) and Fire-LUT scale (bottom) imag**es** showing Ft expression as above. Yellow indicates high and pink-violet low Ft expression. **A''-C'')** Cell edge orientations (Top) or locally averaged orientations (bottom) from A'-C' (segmented images). Red indicates A/P biased orientations. Genotypes were Ft::EGFP/+ (A-A''), ds^{UAO71}/ds^{38K}; *Ft::EGFP/+* (B-B'') and fj^{D1}/fj^{D1}; *Ft::EGFP/+* (C-C''). Anterior is to the left. Scale bar is 16 µm.

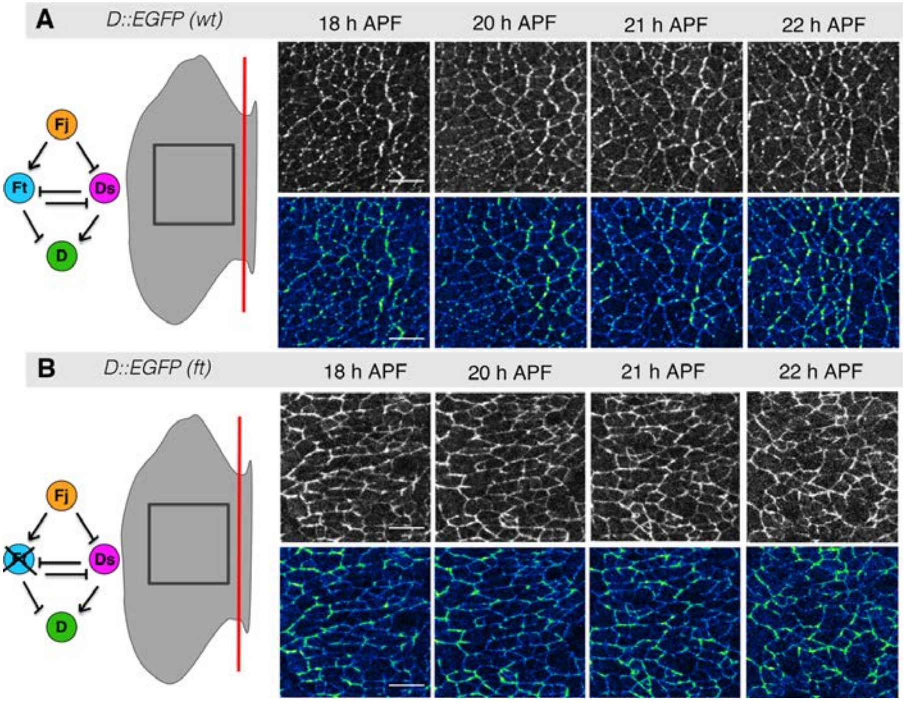

Fig. 56: The tendency of D to localize parallel to the A/P axis is lost in *ft* mutants. A) (Left) Cartoon describing the territory of the A compartment (box) in which the expression of D has been monitored. The position of the A/P boundary is drawn in red. (Right) Dynamic localization of D. Note that D localizes in strong clusters along the apical cell perimeter and tends to accumulate parallel to the A/P axis. **B)** (Left) Equivalent cartoon to A for *ft* pupae. (Right) Dynamic localization of D. Note that D does not localize parallel to the A/P boundary. Anterior is to the left. Scale bar is 12 μm. Genotype were *D::GFP/+*, $ft^{GR\text{-}v}/ft^{1}$; *D::GFP/+*. See Movie 26 and Movie 27.

The defects observed for D localization in *ft* pupae also held in the absence of *ds*. Expressing EGFP::D in clones in *ds* pupae showed that the tendency of D to localize at anteriorly oriented edges was lost (Fig. 57A-B, Movie 28 and Movie 29). D localization was randomized, despite some residual asymmetries that did not follow any preferential orientation.

In summary, the absence of either Ds or Ft was sufficient to abolish their axially polarized signaling (D subcellular localization), possibly as a result of their altered expression balance that will influence their heterodimeric interaction.

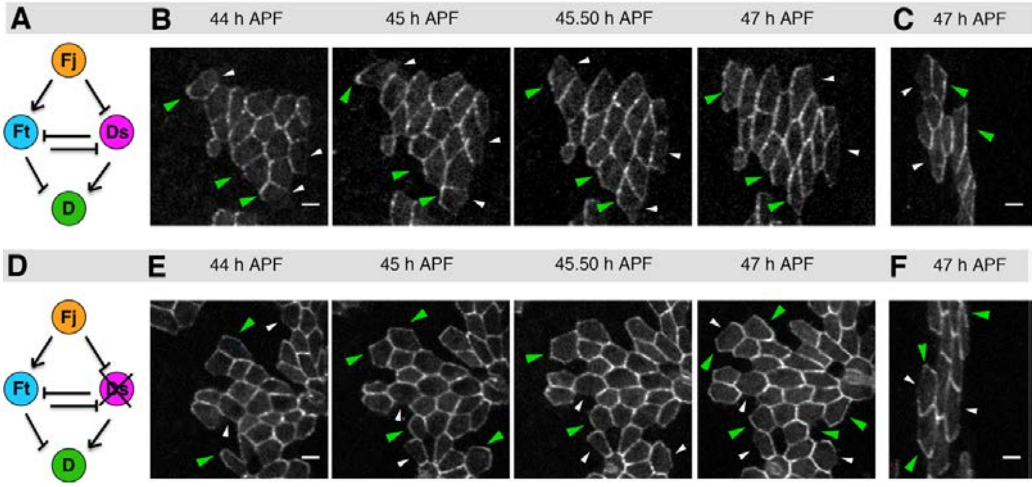

Fig. 57: Perturbed Ds activity abolishes Ds-Ft axial interaction along A/P cell interfaces. A) Cartoon describing the regulatory inputs of the Triad onto D. **B)** Images showing the localization of D during remodeling in clones of cells expressing EGFP:D in the A compartment in a *wt* background. **C)** Image showing the localization of D at the end of remodeling in the P compartment. **D)** Cartoon describing the regulatory inputs of the Triad onto D when Ds is perturbed. **E)** Images showing the localization of D during remodeling in clones of cells expressing EGFP:D in the A compartment in a *ds* background. **F)** Image showing the localization of D at the end of remodeling in the P compartment. Note that D asymmetry is either lost or randomized in the absence of *ds*. Green arrowheads indicate D-enriched cell edges and white arrowheads indicate cell edges with low D in all panels. Genotypes were hsflp1.22;Act5C>>EGFP::D/+ (A-A'') and hsflp1.22;ds^{UAO71}/ds^{38K}; Act5C>>EGFP::D /+ (B-B''). Anterior is to the left. Scale bar is 5 µm. See Movie 28 and Movie 29.

3.4 Loss of the axial uniform orientation of PCA causes the swirling of trichomes in *ds* and *ft* mutants

ds, *ft* and *fj* mutants display planar cell polarity (PCP) phenotypes in the adult abdominal epithelium consisting in extensive swirls of trichomes that have been extensively studied (see Introduction). The mechanisms behind such PCP phenotypes, however, are still poorly understood (Zhu, 2009).

As described (see Chapter I), in *wt* animals the axial uniform orientation of PCA is orthogonal to the planar polarization of trichomes at steady state. If the orientation of PCA would be a guidance cue for the establishment of PCP in trichomes, we would expect correlative effects on trichomes swirling in perturbed Ds/Ft/Fj conditions. We found that trichomes in *ds*, *ft* and *fj* mutants at 50 % of pupariation (steady-state) did not uniformly orient perpendicular to the A/P segmental boundaries as in *wt* (Fig. 58A), but displayed multiple orientations in a characteristic spatial manner (Fig. 58B-D). Trichome orientations were patchy (locally arranged) across almost all the A compartment in *ds* (Fig. 58B) and, to a lesser extent, in *ft* mutants (Fig. 58C). In *fj*, instead, trichome orientations were just affected at the anterior-most cells of the A compartment (Fig. 58D). Remarkably, these stereotyped local defects in trichomes polarity closely mimic those observed for the orientation of PCA in the same mutants.

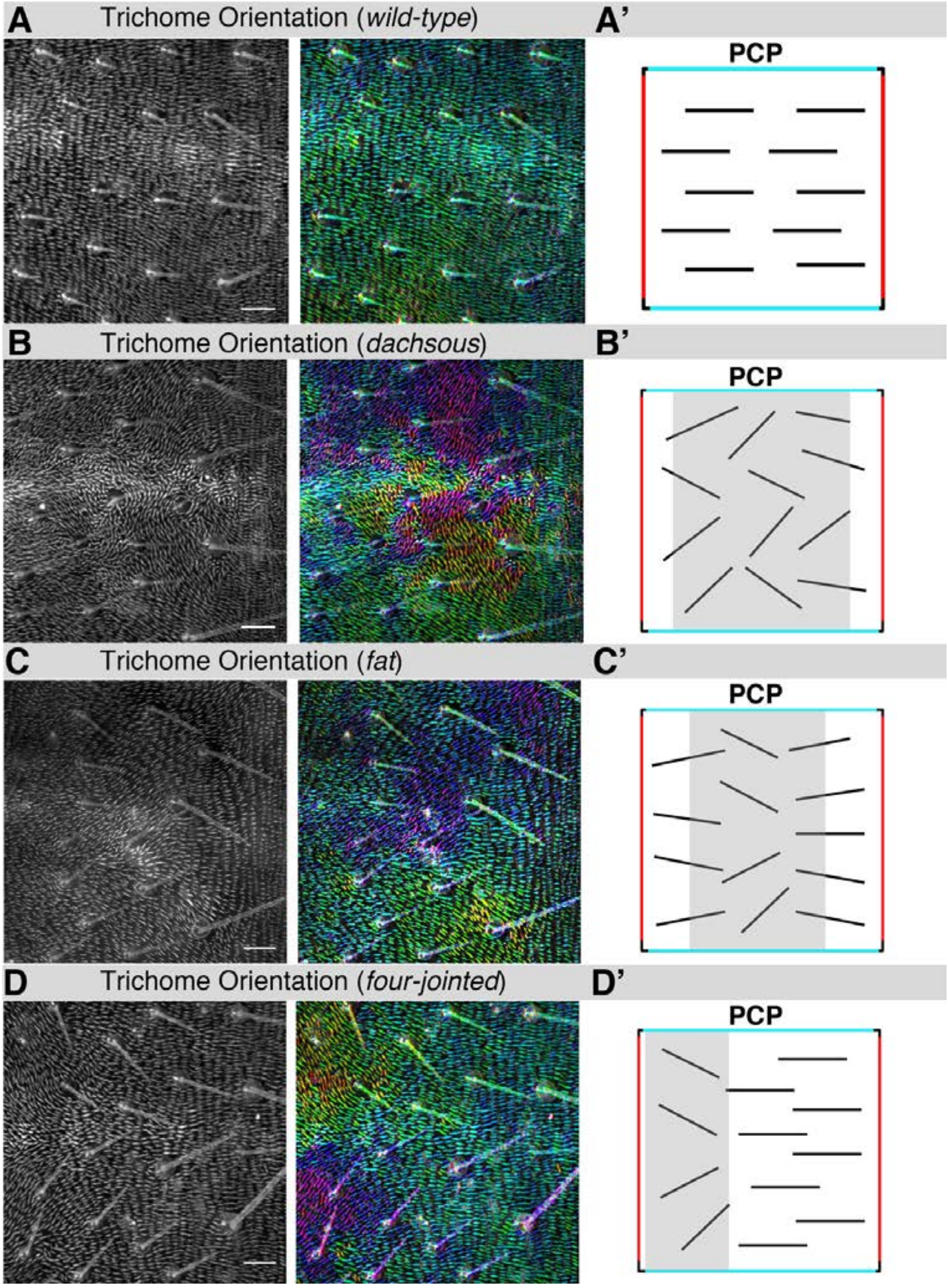
A
Trichome Orientation (*wild-type*)
A'
PCP
B
Trichome Orientation (*dachsous*)
B'
PCP
C
Trichome Orientation (*fat*)
C'
PCP
D
Trichome Orientation (*four-jointed*)
D'
PCP

Fig. 58: Trichome orientations in the mature epithelium of *ds/ft/fj* pupae A) Uniform PCP at steady state in the medio-dorsal region of the AIII segment in a *wt* pupa. Image showing trichome orientations in grey scale (Left) or after employing color-code filtering with OrientationJ (right). **A')** Cartoon describing PCP orientation (black lines) in the *wt* segmental field (square). Red lines indicates A/P boundaries. Note that all trichomes are oriented perpendicular to the A/P boundary (cyan). **B-B')** Equivalent panels to A-A' for *ds* mutants. **C-C')** Equivalent panels to A-A' for *ft* mutants. **D-D')** Equivalent panels to A-A' for *fj*. Anterior is to the left. Scale bar is 16 μm. Genotype were *Moesin::GFP/+*; ds^{UAO71}/ds^{38k}; *Moesin::GFP/+*; f^{GRv}/ft^{1}; *Moesin::GFP/+*; fj^{D1}/fj^{D1}; *Moesin::GFP/+*.

This local coupling (orthogonal relationship between the orientation of PCA and PCP) became evident when we compared the orientation of cell outlines and trichomes orientation in equivalent segmental regions of *ds* mutants (Fig. 59A-D). The non-uniformly aligned cells still retained autonomous planar cell polarity (Fig. 59A'-D' and E-F).

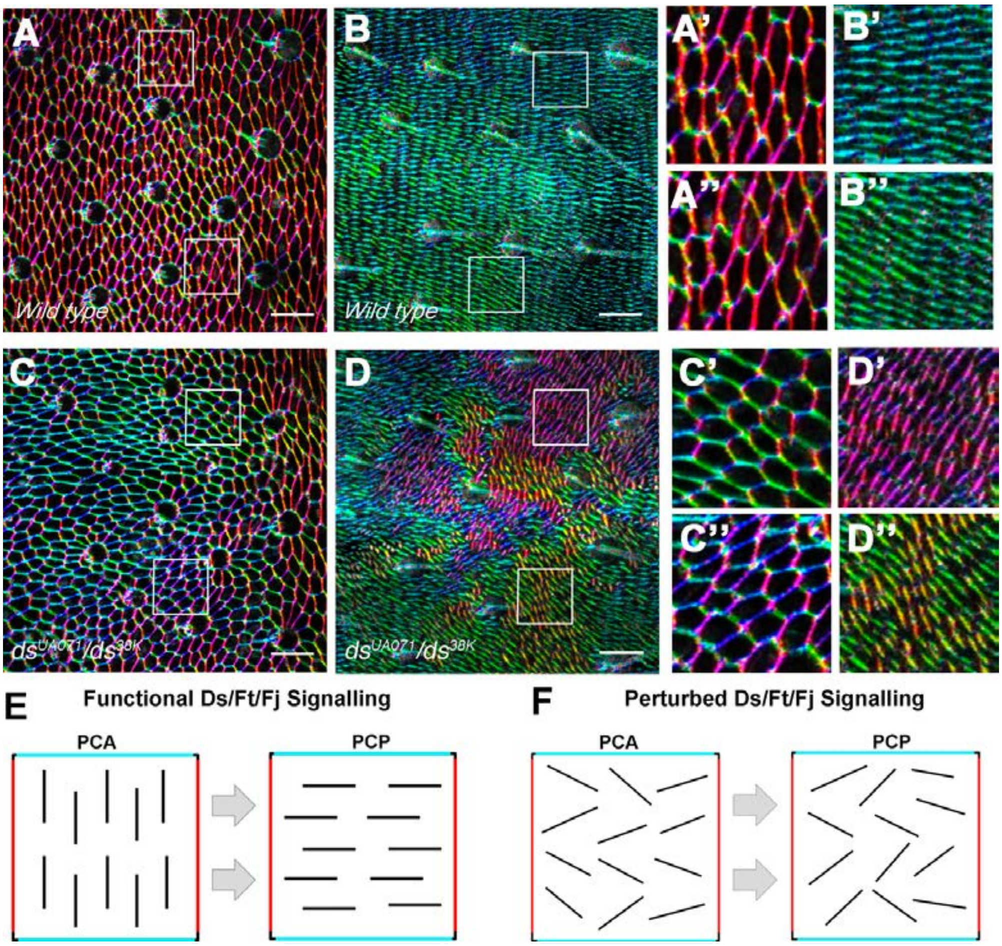

Fig. 59: Orientation of PCA and PCP are orthogonally related at local level in *ds* mutants. A-B) Uniform orientation of PCA and PCP at steady state in the medio-dorsal region of the A compartment. **A)** Colored orientation of cell outlines at 50 hours APF. Red color indicates cell orientation parallel to the A/P boundaries of the segment. **B)** Colored orientation of the trichomes at 50 hours APF. Cyan color indicates trichome orientation perpendicular to the A/P boundaries. **A'-B'** and **A''-B'')** Close up of the boxed region in A and B respectively. Note the orthogonal relationship between the orientation of PCA and PCP at any point of the tissue (uniform). **C-D)** Patchy orientation of PCA and PCP at steady state in *ds* mutants. **C'-D'** and **C''-D'')** Close up of the boxed region in C and D respectively. **E)** Cartoon showing the orientation of PCA (left) and PCP (right) relative to the tissue axes. Red indicates the A/P segmental boundaries while cyan indicates the D/V axis. Note that PCA and PCP are uniformly orthogonally oriented to each other. **F)** Cartoon of the orientation of PCA (left) and PCP (right) in ds mutants. Note that the orthogonal relationship between orientation of PCA and PCP is locally sustained. Anterior is to the left. Scale bar is 12 μm. Genotype were *Moesin::GFP/+*, *ds*^{UAO71}/*ds*^{38k}; *Moesin::GFP/+*.

Last, we explored if PCP spatiotemporal dynamics could be affected upon interference in Ds/Ft/Fj signaling, which could be eventually influencing its correlation to PCA orientation. Remarkably, we found that in the vast majority of *ds* cells, the trichomes outgrowth always initiated at the cell periphery at equivalent developmental times as for *wt*, and that their overall growth dynamics occurs at normal speed (Fig. 60A-B, Movie 30 and Movie 31). Thus, even if cells are oriented in disparate directions and misaligned relative to the A/P boundary, the elongation of the trichomes was still consistently perpendicular to the long axis of the cells as in the *wt* (Fig. 60A'-B').

In summary, the orthogonal relationship between the cell orientation axis and the axis of cell polarity is maintained at local level. The swirling polarity of trichomes pattern is fully autonomous and a direct consequence of the locally aberrant orientation of PCA, which is associated to the *ds* and *ft* mutant conditions.

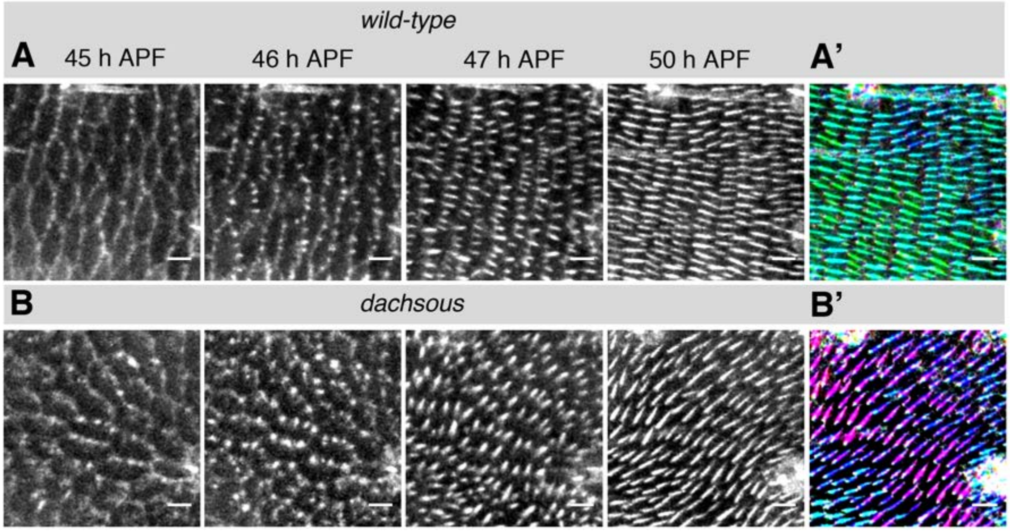

Fig. 60: *ds* mutants largely retain autonomous Planar Cell Polarity (PCP). A-A') Trichome outgrowths in *wt* cells between 45 and 50 hours APF. A) The cells accumulate actin on their posterior edges that rapidly elongates perpendicular to the A/P boundaries of the segment with a polarity vector orthogonal to the cells longest axis. A') Colored trichome polarity showing the orthogonal orientation of PCP relative to that of the PCA. **B-B')** Trichome outgrowths in *ds* cells between 45 and 50 hours APF. B) Cells accumulate actin that rapidly elongates orthogonally to the cell longest axis as in *wt*. B') Colored trichome polarity showing the orientation of PCP orthogonal to the local cell alignment. Scale bar is 5 μm. Anterior is to the left. Genotype were *Moesin::GFP/+*, *ds*^{UAO71}/*ds*^{38k}; *Moesin::GFP/+*. See text for details. See Movie 30 and Movie 31.

Synopsis

The axial rearrangements characterizing the orientation of PCA in the *wt* tissue are disrupted in *ds/ft/fj* mutant pupae. Tissue-wide interferences in *ds*, *ft* and *fj* show that these genes are not only required to provide fidelity to the progression of the orientation of PCA, but also that they are essential for the attainment of the uniform pattern of cell orientation. Failing to achieve uniformity leads to pharate adults displaying cells arranged in locally oriented patches The loss of the axial uniform orientation of PCA in these mutants is accompanied by an overall reduction in mutual cell alignment and in cell shape anisotropy.

These defects appear to be caused by the compromised cross-regulation of Ds, Ft and Fj implementing the development of the A/P linked Fat expression gradient, and potentially, efficient heteromeric interactions between Ds and Ft, which as a readout affect the asymmetrical localization of Dachs.

The primary role of the Ds/Ft/Fj signaling is to axially coordinate the orientation of cell alignment (PCA) in parallel to the A/P axis. The polarity (PCP) phenotypes of *ds*, *ft* and *fj* are just a direct consequence of their defects in the orientation of PCA. PCP itself is fully autonomously functional.

Chapter IV

The Ds/Ft/Fj Signaling Coordinates PCA by Oriented Cell-Cell Contact Adhesiveness

4.1 *ds, ft,* and *fj* Clones of Cells Minimize the Contacts with *wt* Cells when Juxtaposed Genetically

The axial uniform orientation of PCA is achieved through the progressive alignment of intercellular contacts in response to the activity of the Ds/Ft/Fj pathway. To bring light to the contribution of the pathway components regulating the cellular behaviors associated to this process we generated loss of function clones for each component of the pathway, including *dachs,* in an otherwise *wild-type* background. Clones with strongly reduced (ds^{UAO71}, $ft^{Gr\text{-}V}$) or abolished (fj^{D1}, d^{GC13}) activities were analyzed to infer clonal behavior and to extract geometrical, growth and shape parameters during expansion (Figs. 61-62 and Movie 32) and remodeling (Fig. 63).

As expansion progresses, mutant and control clones reached similar elongated shapes (Fig. 61A-E). However, the highly irregular perimeter of *wt* clones was smoothed (Fig. 61B-D), with the exception of the clones depleted of *d* (Fig. 61E). The smoothed shapes of *ds, ft* and *fj* clones indicated that the cells lacking these genes bear some sort of incompatibility with the *wt* cells in the surroundings.

We then performed a quantitative analysis of the morphological changes associated to clones. To gain quantitative insights on these changes, multiple clones for *ds*, *fj* and *ft* were staged. Similarly, *wt* clones were generated and collected as a morphological reference control. The silhouettes from clones collected at the end of expansion (26-28 hours APF) and remodeling (47-50 hours APF) were overlaid onto an idealized AIII hemi-segment territory (see Materials and Methods), generating composite diagrams reporting the position, shape and orientation of the clones within the A compartment (Figs. 62 and 63).

By the end of expansion, the *ds*, *ft* and *fj* clones, as the *wt* ones, were, in general, longitudinally elongated although isodiametrical clones could be found at the compartment dorsal edge (Fig. 62A-D; see also Fig. 65 and Chapter I). Also, the clone borders were smoother in mutants, particularly in *ft.* To evaluate these morphological differences we quantified multiple geometrical and shape parameters (See Summary Table VI). The geometrical parameters employed were the clone surface area, the perimeter, the aspect ratio (AR) and the orientation relative to the A/P boundary of the clone longest axis. Together, these parameters provided information on clonal growth (Fig. 62). Four shape parameters describing different aspects of the clone morphology were also measured. Roundness, which evaluates the elongation of the clone form; Solidity and Convexity describing the complexity of the surface area (*i.e.* Roughness); and Circularity informing on cumulative changes in clone form and roughness (See also Materials and Methods).

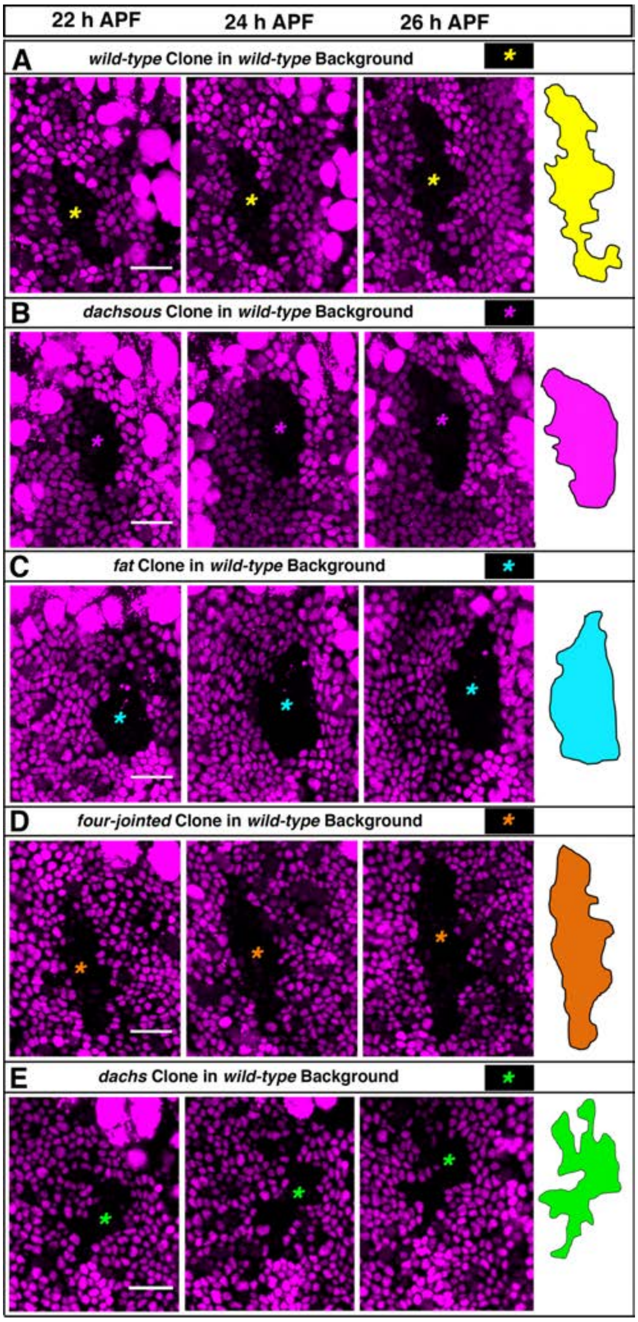
22 h APF
24 h APF
26 h APF
A
wild-type Clone in *wild-type* Background
B
dachsous Clone in *wild-type* Background
C
fat Clone in *wild-type* Background
D
four-jointed Clone in *wild-type* Background
E
dachs Clone in *wild-type* Background

Fig. 61: *ds, ft and fj* but not *d* mutant cells minimize their contacts with *wt* cell during expansion. A-E) Changes in clone morphology of *wt* (A), *ds* (B), *ft* (C), *fj* (D) and *d* (E) mutant clones in an otherwise *wt* background at the centre of the A compartment at 22, 24 and 26 hours APF. The mutant areas are marked by the absence of *Ubi-RFP.nls* expression (black). Cartoons on the right outline the clones at 26 hours APF color-coded for each genotype (*wt*, yellow; *ds*, magenta; *ft*, cyan; *fj*, orange; *d*, green). Note that the *wt* (A) and *d* (E) clones present numerous indentations while *ds, ft* and *fj* clones (B-D) have smoother outlines. Genotypes were *hsflp1.22; Ubi-RFP.nls FRT40A/FRT40A* (A,); *hsflp1.22;* ds^{UAO71} *FRT40A/FRT40A Ubi-RFP.nls* (B); *hsflp1.22;* ft^{Gr-V} *FRT40A/FRT40A Ubi-RFP.nls* (C); *hsflp1.22; FRT42D* fj^{D1}*/ Ubi-RFP.nls FRT42D* (D); *hsflp1.22;* d^{GC13} *FRT40A/FRT40A Ubi-RFP.nls* (E). Anterior is to the left. Dorsal is up. Scale bar is 16 μm. See Movie 32.

From these quantitative parameters could be inferred that neither intercalary growth nor growth orientation were affected at any mutant clone within the A compartment (Fig. 62 and Summary Table I; see also Fig. 65). The areas of mutant clones were only modestly enlarged, while the perimeter of *ds* and *ft* clones showed a mild reduction in length. Clones anisotropy was essentially preserved (AR and Roundness). On the other hand, mutant clones tend to minimize their contact with *wt* cells and clone roughness (Solidity and Convexity) and, consequently, Circularity, were affected. *ds* and *ft* clones show a reduction of indentations along their clone borders when compared to *wt*.

We performed an equivalent clonal analysis at the end of remodelling at steady state (47-50 hours APF) (Fig. 63 and Summary Table II; see also Fig. 66). At this stage, mutant clone areas were slightly enlarged, except for *ft* whose surface area was significantly larger. Similarly, clones anisotropy (AR and Roundness) was affected in *ft* but not in *ds* or *fj* clones (Fig. 63A and C). Both roughness (Solidity and Convexity) and length of the border (Perimeter) were also significantly reduced (Fig. 63B and D). Remarkably, while enlargement of *wt* clones was accompanied by lengthening of borders (see also Chapter I), the increase in *ds*, *ft* and *fj* clones areas was not followed by increments in their perimeter length, indicating that the cell-cell contacts between *ds/ft/fj* and *wt* cells tend to minimize. Indeed, changes in Circularity, as found, can possibly be ascribed, no to the form of the clones themselves but to the smoothness of the clones surface (see Summary Table VII).

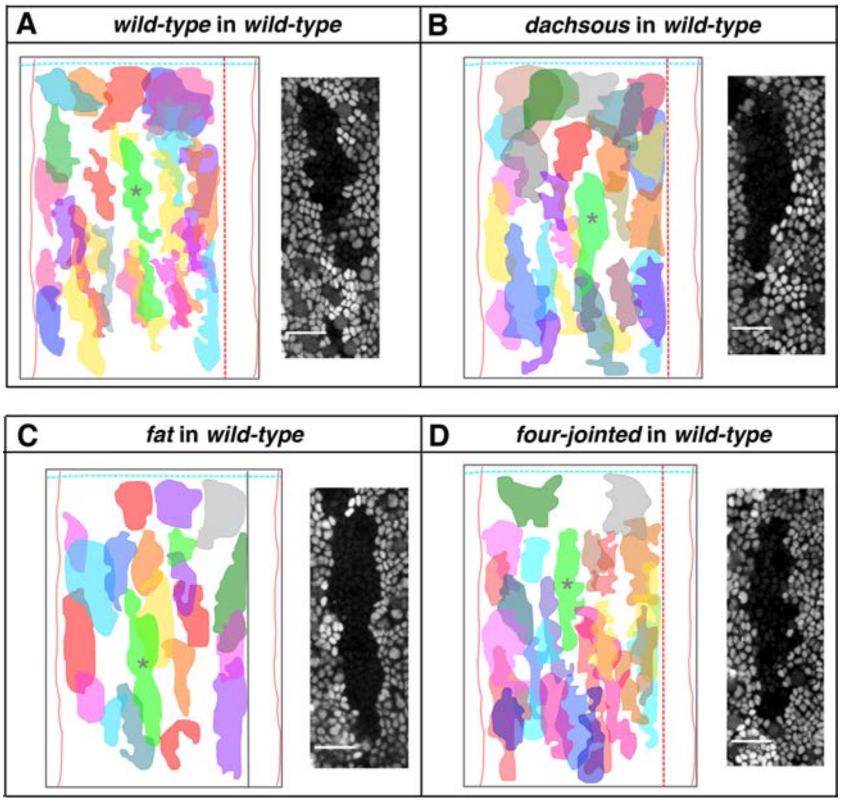

Fig. 62: Clones of *ds, ft or fj* do not affect the pattern of growth during expansion. A-D) Composite diagram showing the position, shape and orientation of *wt* (A), *ds* (B), *ft* (C) or *fj* (D) clones within the A compartment of the AIII hemi-segment induced before pupation and collected at 26-28 hours APF. A representative example is shown on the right of each panel (grey asterisk on the diagram). All collected clones were identified by the absence of Ubi-RFP.nls and imaged from living pupae. Clones are colored stochastically (see also Sauret-Gueto et al., 2013). Genotypes were *hsflp1.22; Ubi-RFP.nls FRT40A/FRT40A* (A); *hsflp1.22; ds^{UAO71} FRT40A/FRT40A Ubi-RFP.nls* (B); *hsflp1.22; ft^{Gr-V} FRT40A/FRT40A Ubi-RFP.nls* (C); *hsflp1.22; FRT42D fj^{D1}/ Ubi-RFP.nls FRT42D* (D). Anterior is to the left. Dorsal is up. Scale bar is 16 µm. See Summary Table I and Fig. 64 for quantifications. See also Materials and Methods and text for details.

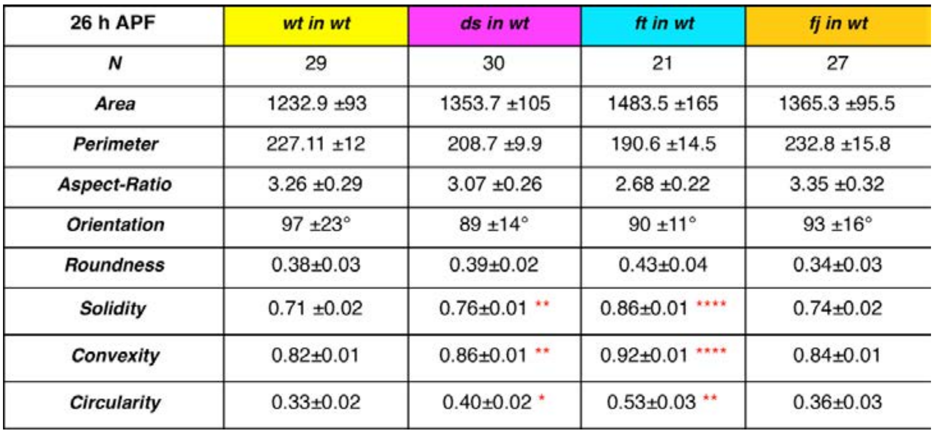

26 h APF	*wt in wt*	*ds in wt*	*ft in wt*	*fj in wt*
N	29	30	21	27
Area	1232.9 ±93	1353.7 ±105	1483.5 ±165	1365.3 ±95.5
Perimeter	227.11 ±12	208.7 ±9.9	190.6 ±14.5	232.8 ±15.8
Aspect-Ratio	3.26 ±0.29	3.07 ±0.26	2.68 ±0.22	3.35 ±0.32
Orientation	97 ±23°	89 ±14°	90 ±11°	93 ±16°
Roundness	0.38±0.03	0.39±0.02	0.43±0.04	0.34±0.03
Solidity	0.71 ±0.02	0.76±0.01 **	0.86±0.01 ****	0.74±0.02
Convexity	0.82±0.01	0.86±0.01 **	0.92±0.01 ****	0.84±0.01
Circularity	0.33±0.02	0.40±0.02 *	0.53±0.03 **	0.36±0.03

Summary Table VI: Averaged values (± SEM or AD) of geometrical and shape parameters extracted from the clone outlines for each conditions at 26 hours APF. Red asterisks mark statistic significant differences relative to *wt*. *P< 0.05; **P< 0.01; ***P< 0.001; ****P< 0.0001. No significant P >0.05 (not shown). See text and Materials and Methods for details.

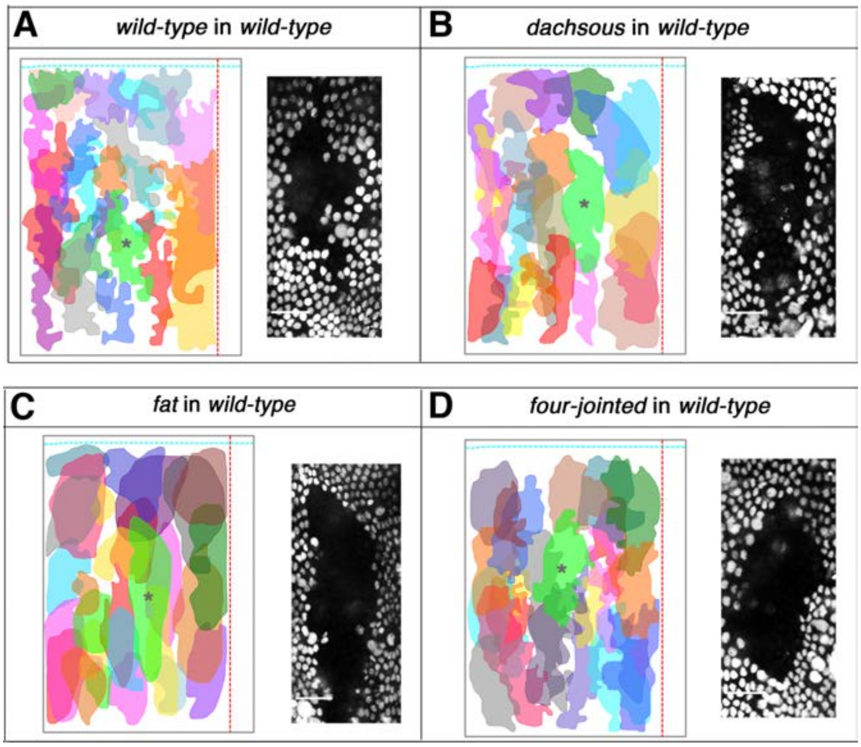

Fig. 63: Clones of *ds, ft or fj* affect clone shape complexity at steady state. A-D) Composite diagram showing the position, shape and orientation of *wt* (A), *ds* (B), *ft* (C) or *fj* (D) clones within the A compartment of the AIII hemi-segment induced before pupation and collected at 47-50 hours APF. A representative example is shown on the right of each panel (grey asterisk on the diagram). All collected clones were identified by the absence of Ubi-RFP.nls and imaged from living pupae. Clones are colored stochastically (see also Sauret-Gueto et al., 2013). Genotypes were *hsflp1.22; Ubi-RFP.nls FRT40A/FRT40A* (A); *hsflp1.22; ds*^{UAO71} *FRT40A/FRT40A Ubi-RFP.nls* (B); *hsflp1.22; ft*$^{Gr-V}$ *FRT40A/FRT40A Ubi-RFP.nls* (C); *hsflp1.22; FRT42D fj*^{D1}*/ Ubi-RFP.nls FRT42D* (D). Anterior is to the left. Dorsal is up. Scale bar is 16 µm. See Summary Table II and Fig. 64 for quantifications. See also Materials and Methods and text for details.

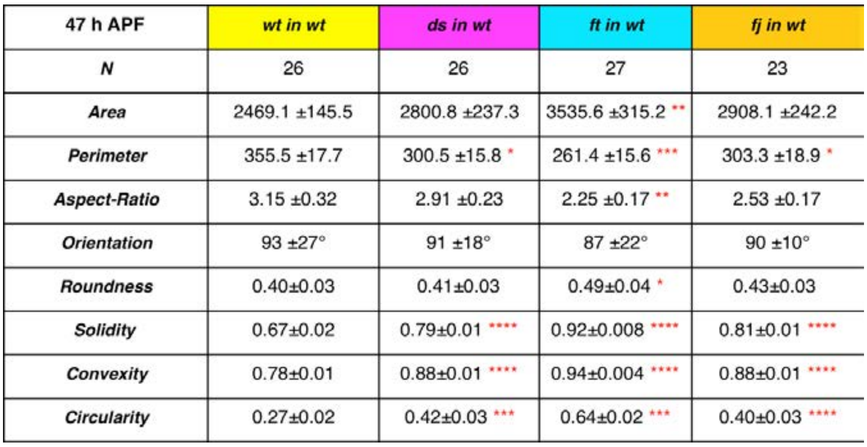

47 h APF	*wt in wt*	*ds in wt*	*ft in wt*	*fj in wt*
N	26	26	27	23
Area	2469.1 ±145.5	2800.8 ±237.3	3535.6 ±315.2 **	2908.1 ±242.2
Perimeter	355.5 ±17.7	300.5 ±15.8 *	261.4 ±15.6 ***	303.3 ±18.9 *
Aspect-Ratio	3.15 ±0.32	2.91 ±0.23	2.25 ±0.17 **	2.53 ±0.17
Orientation	93 ±27°	91 ±18°	87 ±22°	90 ±10°
Roundness	0.40±0.03	0.41±0.03	0.49±0.04 *	0.43±0.03
Solidity	0.67±0.02	0.79±0.01 ****	0.92±0.008 ****	0.81±0.01 ****
Convexity	0.78±0.01	0.88±0.01 ****	0.94±0.004 ****	0.88±0.01 ****
Circularity	0.27±0.02	0.42±0.03 ***	0.64±0.02 ***	0.40±0.03 ****

Summary Table VII: Averaged values (± SEM or AD.) of the geometrical and shape parameters extracted from the clone outlines for each conditions at 47 hours APF. Red asterisks mark statistic significant differences relative to *wt*. *P< 0.05; **P< 0.01; ***P< 0.001; ****P< 0.0001. Not significant P >0.05 (not shown). See text and Materials and Methods for details.

Altogether, these analyses indicate that sharp local differences in the activity of the pathway at clones edges affect the way cells contact each other increasing the complexity of the clones perimeters rather than affecting their form (Fig. 64). Mutant cells for *ds*, *ft* and *fj* prefer to contact cells with similar surface properties (*i.e.* cells within the clone) than those surrounding them.

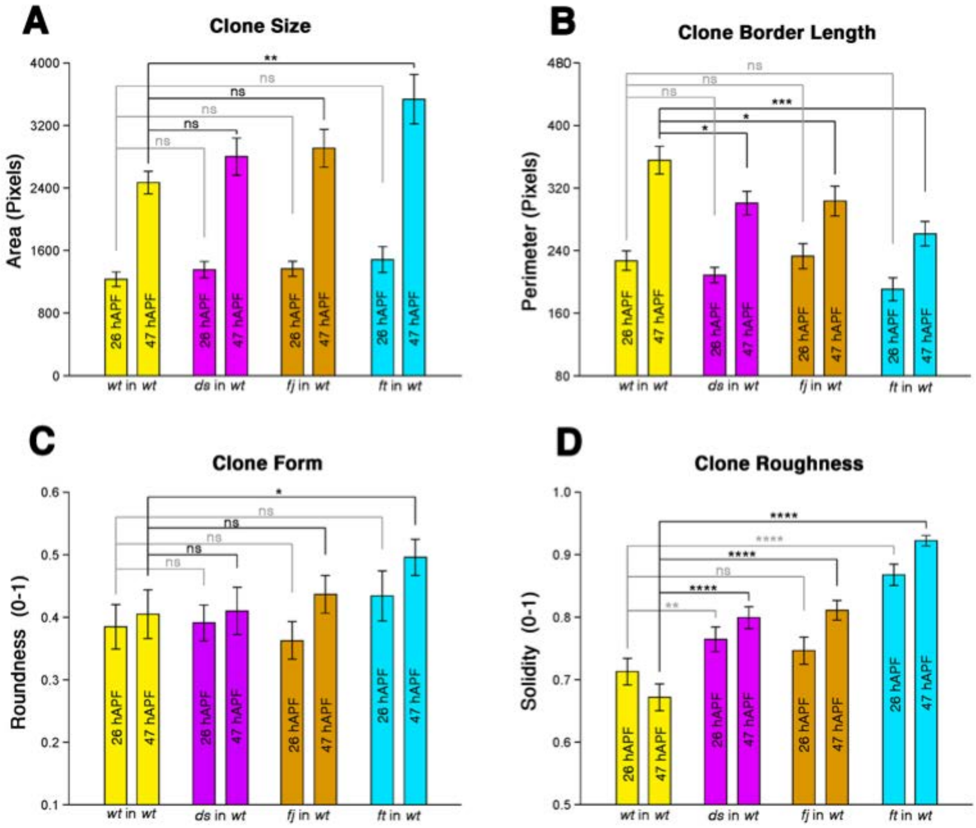

Fig. 64: Local differences in Ds/Ft/Fj activity affect clones shape complexity. Averaged values (± SEM or AD) of geometrical and shape parameters at 26 and 47 hours APF. KS-test for significance was applied. *P< 0.05; **P< 0.01; ***P< 0.001; ****P< 0.0001. No significant (ns) P >0.05. Genotypes were *hsflp1.22; Ubi-RFP.nls FRT40A/FRT40A* (*wt*); *hsflp1.22; ds*^{UAO71} *FRT40A/FRT40A Ubi-RFP.nls* (*ds*); *hsflp1.22; ft*$^{Gr-V}$ *FRT40A/FRT40A Ubi-RFP.nls* (*ft*); *hsflp1.22; FRT42D fj*^{D1}*/ Ubi-RFP.nls FRT42D* (*fj*).

4.2 The Directional Activity of Ds Influences Cell-Cell Interactions Throughout the A Compartment

The cumulative data on clone behavior pointed that, on average, mutant cells for *ds*, *ft* and *fj* progressively minimize their contact with surrounding *wt* cells. Also, they indicated that the contacts (Solidity) in between *ds* or *ft* and *wt* cells was strongly reduced from the very early phases of expansion, To analyze if the histoblasts behave uniformly all throughout the A compartment field or if sectorial differences were present, we evaluated the geometrical and shape parameters just described of individual *wt* clones at 26-28 and 47-50 hours APF at different positions within the A compartment (Fig. 65A-to-F, H-to-J and L). We found that, during expansion the *wt* clones showed low roundness, being elongated in a D/V direction (except for those located close to the dorsal edge, see also Chapter I). They were also extremely rough from the beginning, with roughness increasing overtime (Fig. 65I and L). We also compared differences in clone form and roughness along the A/P axis of the clones (Fig. 65G and K) and found that in terms of solidity *wt* clones showed a non-random directional bias progressively acquired over time. Most anterior clones exhibited posterior roughness and anterior smoothness, while those located at the posterior displayed the opposite at steady state.

We then performed equivalent analyses in *ds*, *ft* and *fj* clones in *wt* backgrounds (Fig. 66). We found that mutant clones areas were just slightly larger than controls, except for *ft* whose clones sizes were somehow heterogeneous (big and small clones were detected all throughout the segment). In the mutant clones were also observed an increase on the smoothness of the borders along with a reduction in perimeter. These effects pointed to a reduction of cell-cell interactions between the cells inside and outside of the clones indicating that the major alterations in the morphology of mutant clones were the result of the tuning of cell-cell contacts at the clone borders (Fig. 66). The reduction in clone shape complexity further indicated some sort of conflict between surface properties of mutant and surrounding *wt* cells. In this context, we found that the smoothness of borders was directionally biased depending on the mutated gene. While the surface of *ft* clones smoothed up all around their perimeter, *ds* clones smoothness was more prominent at their posterior edges, while for clones lacking *fj* this behavior was reversed (Fig. 66). Notably, and in close correlation with the distinct topographical influence of *ds* and *fj* in the long-range orientation of the tissue and in Ft gradient formation, *ds* clones asymmetric smoothness was observed anywhere within the A compartment. Moreover, the overall smoothness of *ft* clones throughout the A compartment suggest that Ft behaves autonomously.

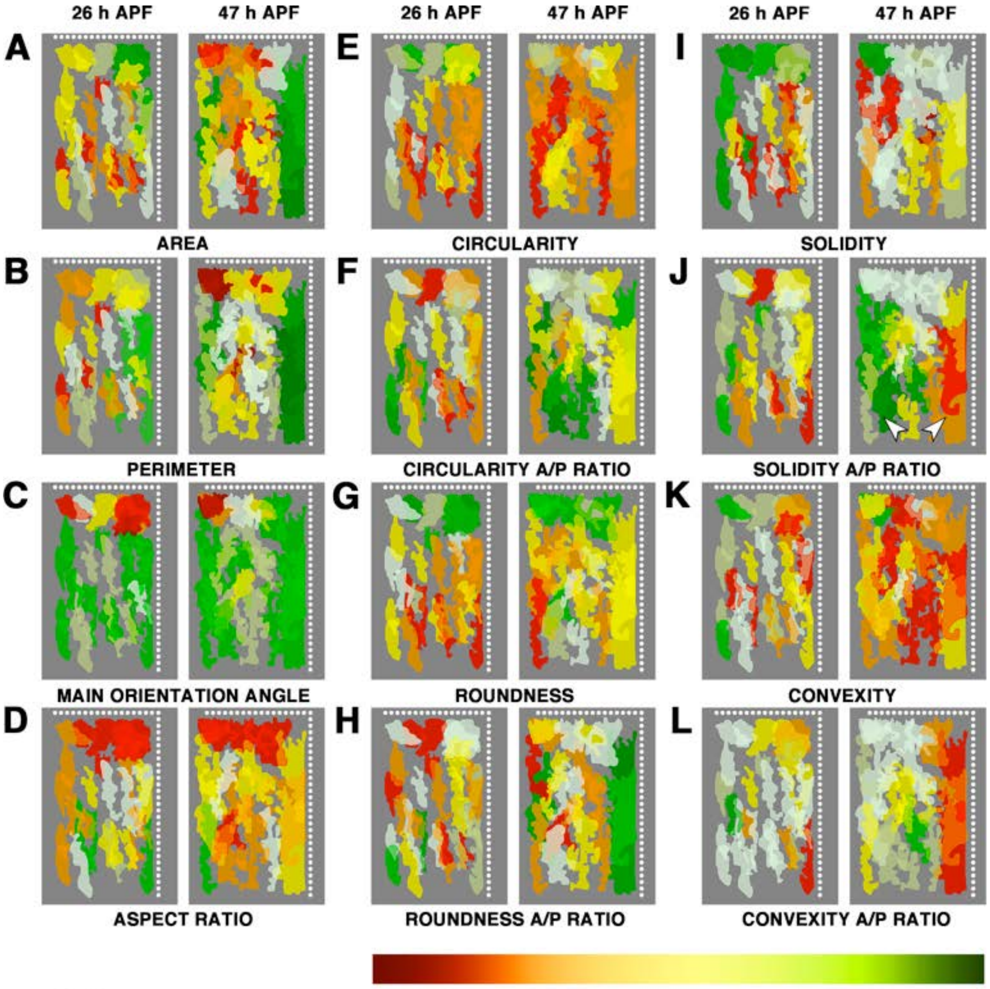

AREA	1000	50000
PERIMETER	300	1500
MAIN ORIENTATION ANGLE	90°	0°
ASPECT RATIO	1	10
CIRCULARITY	0	1
CIRCULARITY A/P RATIO	0	3
ROUNDNESS	0	1
ROUNDNESS A/P RATIO	0	3
SOLIDITY	0	1
SOLIDITY A/P RATIO	0	3
CONVEXITY	0	1
CONVEXITY A/P RATIO	0	3

Fig. 65: Geometrical and shape parameters from individual *wt* clones in *wt* background at 26-28 and 47-50 hours APF. Cumulative topographic plots displaying the positions and shapes of individual clones in an idealized A compartment (dorsal and posterior edges are represented by dotted white lines) at 26 and 47 hours APF. Individual clones were color-coded according to a graded Green-Red LUTs. The different maximum and minimum values for each analyzed parameter are stated at the bottom legend (see also Materials and Methods). For some parameters (Circularity, Roundness, Solidity and Convexity), values were calculated for the anterior and posterior bisected halves of each clone and their ratio was color-coded for each clone as above. **A)** Area. **B)** Perimeter. **C)** Orientation angle. **D)** Aspect Ratio. **E)** Circularity. **F)** Circularity A/P Ratio. **G)** Roundness. **H)** Roundness A/P Ratio. **I)** Solidity. **J)** Solidity A/P Ratio. **K)** Convexity. **L)** Convexity A/P Ratio. The bias in Solidity A/P Ratio at different positions in the compartment is highlighted (arrowheads). Anterior is to the left. Genotypes was *hsflp1.22; Ubi-RFP.nls FRT40A/FRT40A.*

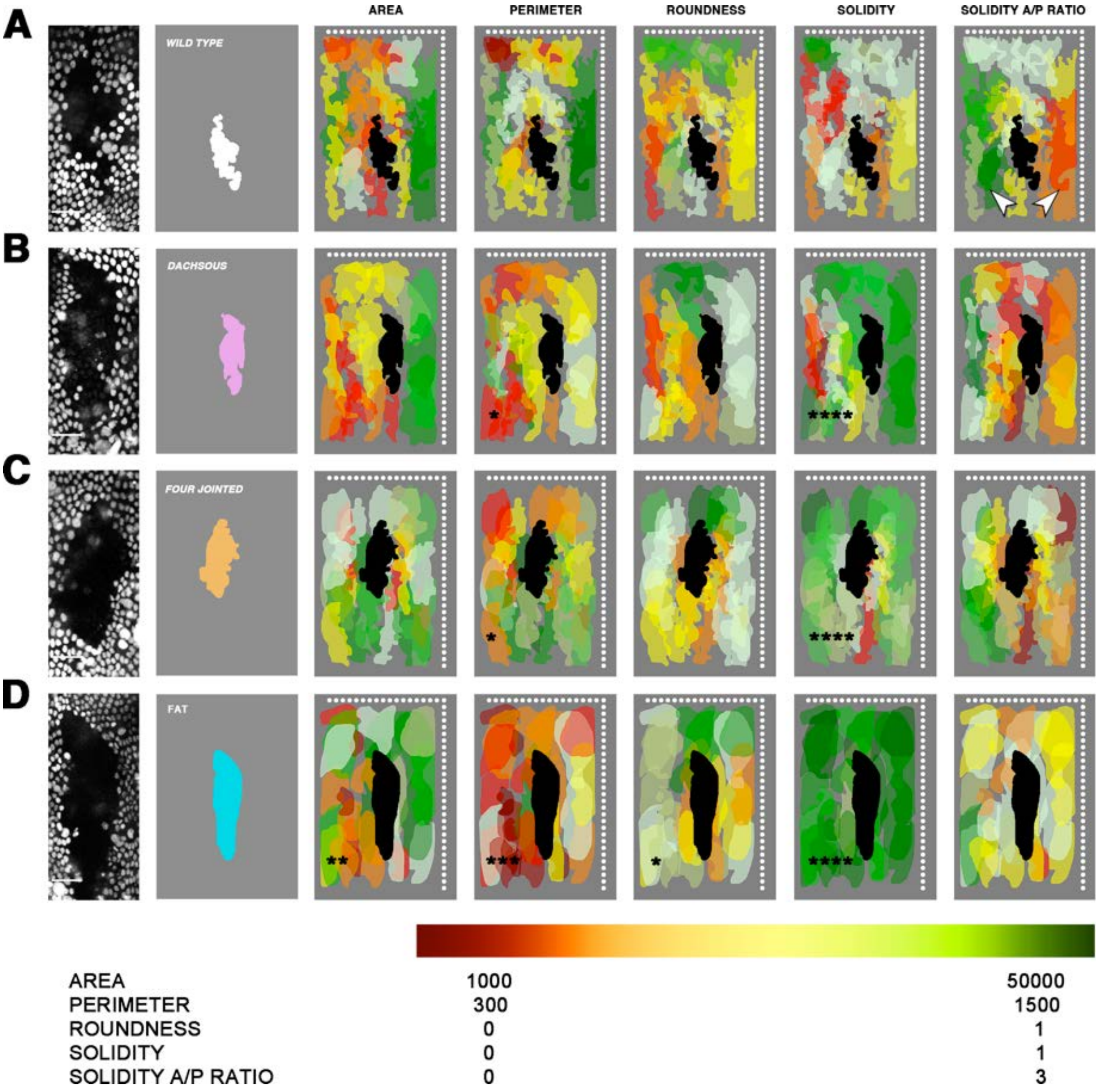

Fig. 66: Geometrical and shape parameters from individual mutant clones in *wt* background at 26-28 and 47-50 hours APF. A) From left to right: Representative single clone of *wt* cells in a *wt* background (absence of *RFP.nls* expression); Mask corresponding to this representative clone (white) positioned within the anterior compartment; Cumulative topographic map displaying the shapes and positions of individual *wt* clones (n=26-the representative clone is shown in dark grey) at the steady state (47-50 hours APF) within the A compartment (dorsal and posterior edges are represented by dotted white lines). The values for geometrical (Area and Perimeter) and shape (Roundness and Solidity) parameters are represented by different colors according to a graded Green-Red LUT in sequential illustrations, from left to right (see also Materials and Methods). At the far right panel, the ratio of solidity between the anterior and posterior bisected halves of individual clones is also displayed and arrowheads point to the different solidity axial bias between *wt* clones at anterior and posterior positions within the compartment. The different maximum and minimum values for each analyzed parameter in the graded Green-Red LUTs are stated at the bottom legend (see also Materials and Methods). **B)** Equivalent panels as in A but for *ds*^{UAO71} clones (magenta) (n=26). **C)** Equivalent panels as in A but for *fj*^{D1} clones (orange) (n=23). **D)**. Equivalent panels as in A but for *ft*$^{Gr\text{-}V}$ clones (cyan) (n=27). Significant differences were evaluated by K-S test. Black asterisks indicate significance levels for the averaged parameters values for each genotype vs. *wt* control clones (p*< 0.05, p** < 0.01, p*** < 0.001 or p**** < 0.0001; see also Table II). Anterior is to the left. Genotypes were *hsflp1.22; Ubi-RFP.nls FRT40A/FRT40A*; *hsflp1.22; ds*^{UAO71} *FRT40A/FRT40A Ubi-RFP.nls*; *hsflp1.22; ft*$^{Gr\text{-}V}$ *FRT40A/FRT40A Ubi-RFP.nls*; *hsflp1.22; FRT42D fj*^{D1}*/ Ubi-RFP.nls FRT42D*.

In summary, border smoothing (contact minimization) showed a directional bias in *ds* or *fj* (Fig. 67). Mutant areas lacking *ds* showed more pronounced smoothing in the posterior side of the clone than on the anterior side (Fig. 67B), while the directional smoothing of *fj* clones was the opposite although such effect was restricted to antero-central regions. Instead, *ft* clones were smooth all around irrespectively on the clone location (Fig. 67C).

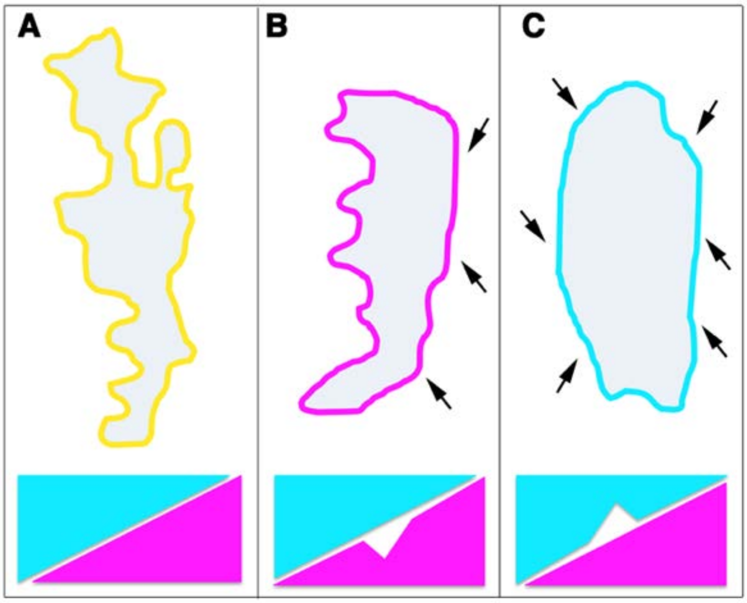

Fig. 67: *ds* but not *ft* clones show directional changes in clone border complexity. Clones outlines for *wt* **(A)**, *ds* **(B)** or *ft* **(C)** extracted from the diagrams in Fig.63 and Fig.66. *wt* clones display numerous indentations at their edges (A). The complementary gradients of Ds (magenta) and Ft (cyan) at steady-state are drawn at the bottom. *ds* clones show a smaller number of indentations particularly on their posterior sides (arrows) (B), The local reduction in Ds is shown below as a notch in the magenta gradient. *ft* clones show no indentations all around (arrows) (C). The local reduction in Ft is shown below as a notch in the cyan gradient. Anterior is to the left.

4.3 Differential Adhesiveness Drives the Axial Orientation of Cells

The reduced cell shape anisotropy observed in loss of function conditions for the Ds/Ft/Fj pathway and the minimization of contacts between mutant cells and *wt* ones upon local perturbations suggest that a potential function for the pathway could be to modulate differential adhesion between cell interfaces.

To investigate whether mutant clones behavior was directed by differential adhesive properties, we analyzed cells shape geometries (contact angle (α) and contact length (L) between A/P oriented interfaces) within, outside and at the boundary of clones lacking *ds*, *fj* or *ft* at steady-state (Fig. 68).

ds, *fj* and *ft* mutant cells showed autonomous reduction of both α and L compared to cells located outside the clones (Fig. 68B-to-G). Such reduction in anisotropy was stronger in *ds* and *ft* mutant cells than in *fj* cells. Mutant cells were more isodiametric than *wt* ones (Fig. 68H) as also observed in whole mutants (Chapter III). The changing of the shape was accompanied by shortening of the length of the contact and the change in the contact angle between A/P aligned interfaces (Fig. 68E-G and E'-G'). Notably, despite the different adhesion properties, both mutant and *wt* cell types kept in contact and neither gaps nor sorting-out behaviors were ever observed. The epithelium retains continuity and keeps being a monolayer.

The interfaces of mutant cell abutting the surrounding territories did not necessarily behave in the same way as those between the cells of the clone or those *wt* cells in surrounding territories. By distinguishing and analyzing the posterior or anterior sides of *ds/ft/fj* clones (namely, A-Border and P-Border) was possible to determine the potential relationships between the characteristics of the cell contacts at the interfaces between mutant and *wt* cells, and the sense of each gene graded expression (see Chapter II). We found that α contact angles at the posterior side of *ds* mutant clones were similar to those between *wt* cells (Fig. 68E- E', P-Border). Quite the opposite, the anisotropy (α) of anterior *ds* cells abutting *wt* ones was similar to the *ds* cells within the clone (Fig. 68E- E', A-Border). L Contact lengths follow the same trend. This indicated that cell-cell contacts at the A-Border were similar to those within the clone and quite different at the P-Border, were the clones were smoother. For *fj*, α contact angles were similar *to wt* contacts at both sides (Fig. 68F). L contact lengths, however, were different for those *fj* cells abutting *wt* cells at the anterior border of the clone (equivalent to *wt*) than for those at the posterior side, which were similar to those within the clone (Fig. 68F'). Last, for *ft*, as for *fj*, α contact angles were similar at both sides and to those between *wt* cells (Fig. 68F). Quite the opposite, overall, L was reduced all around *ft* clones (Fig. 68G').

Importantly, besides their variable cell shape geometries, along the smooth borders, mutant cells for *ds* and *ft* always oriented parallel to the clone boundaries and such behavior was largely independent on clone size (Fig. 69). Altogether, these data indicate that the cell anisotropy, alignment and orientation at the boundary of mutant cells can be in part rescued via short-range communication if at the right positions within the field.

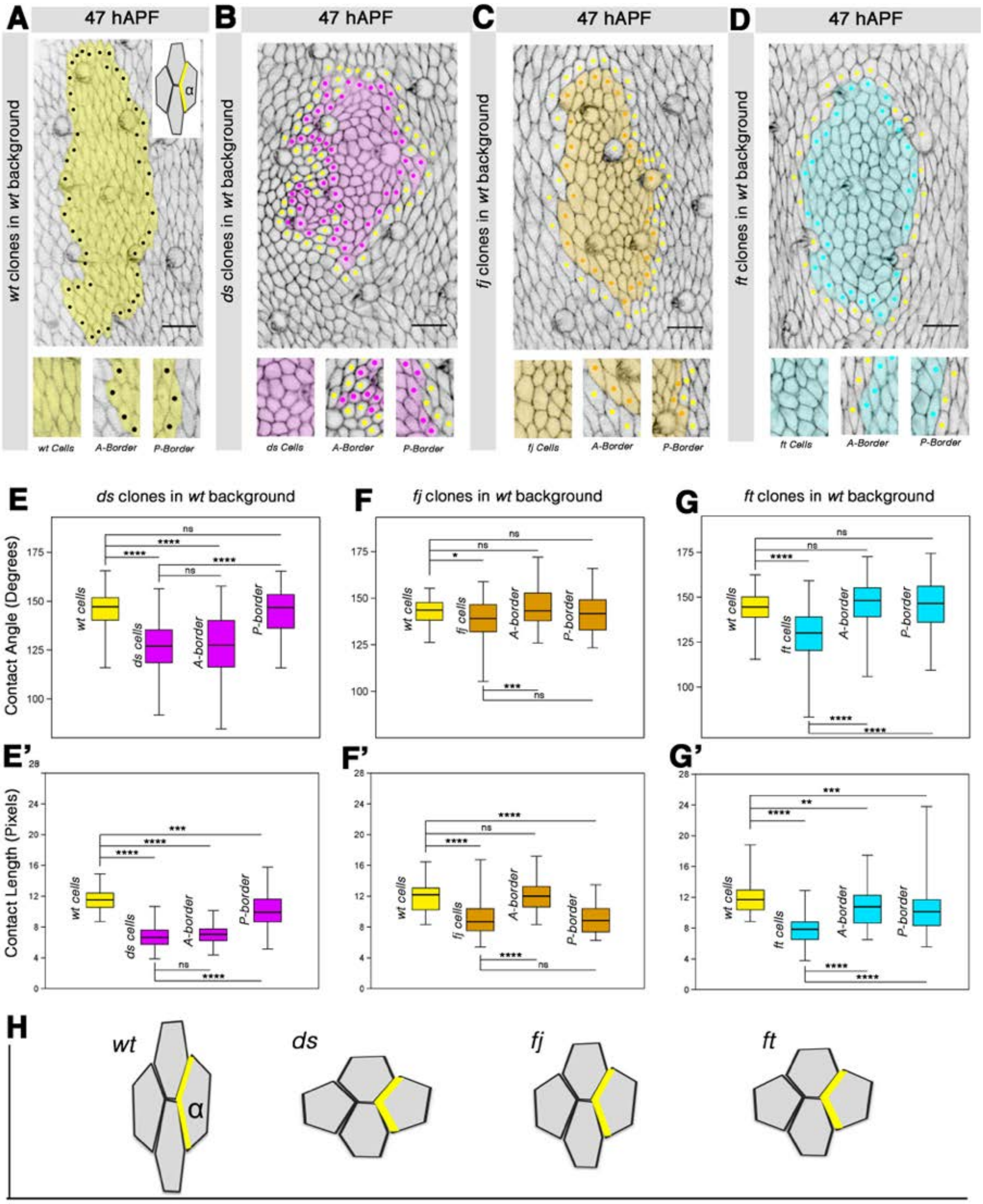

Fig. 68: Ds/Ft/Fj signaling modulates PCA through differential cell-cell adhesiveness.

(The legend of Fig. 68 is written in the next page).

Fig. 68: Ds/Ft/Fj signaling modulates PCA through differential cell-cell adhesiveness. A) Top: Cell shape morphology of a *wt* clone in otherwise *wt* background at steady-state. The most external row of cells of the clone (color masked in yellow) is marked with black dots. The inset diagram (top right) shows the contact angle (α) and length (L) estimations (see Material and Methods). Bottom: close-up of cell outlines at the indicate locations. Note that cell shapes are similar outside or within the clone. **B)** Top: Cell shape morphology of a *ds* clone. The most external row of cells of the clone (color masked in magenta) is marked with magenta dots, while the first row of *wt* cells is marked by yellow dots. Bottom: close-up of cell outlines at the indicate locations. Note the altered shapes of the cells anteriorly and within the clone. **C)** Top: Cell shape morphology of a *fj* clone. The most external row of cells of the clone (color masked in orange) is marked with orange dots, while the first row of *wt* cells is marked by yellow dots. Bottom: close-up of cell outlines at the indicate locations. Note the mildly altered shapes of the cells posteriorly and within the clone with reduced size. **D)** Top: Cell shape morphology of a *ft* clone. The most external row of cells of the clone (color masked in cyan) is marked with cyan dots, while the first row of *wt* cells is marked by yellow dots. Bottom: close-up of cell outlines at the indicate locations. Note the altered shapes of the cells anteriorly and within the clone. **E-G** and **E'-G')** Box and whiskers plots showing the range of contact angles (E-G) and contact lengths (E'-G') for each condition. The box size indicates the range of angles in the middle of each of the distribution. The 75 and 25 % quartiles are the top and the bottom of the box, The red lines indicate the median value. Whiskers outside the box extend to the minimum and maximum distance obtained in each distribution of values. Two-sample unpaired two-tailed student t-test for significance was applied. $p^{*} < 0.05$, $p^{**} < 0.01$, $p^{***} < 0.001$ or $p^{****} < 0.0001$. *ns* $p > 0.05$ not significant. **H)** Cartoons showing changes in cell shapes in the different mutant clones. Note that *ds* and *ft* are more isodiametric then *fj* and *wt* cells, indicating loss of asymmetric Ds-Ft heterodimeric interaction (see text for details). For E-G and E'-G' α and L were measured for the first row of mutant cells facing the anterior side of the clone (A-Border), the first row of mutant cells facing the posterior side of the clone (P-border), inside the mutant territory (*ds*, *fj* and *ft* cells) and *wt* cells located outside the clone. For E-E'. n=75 *wt*, 132 *ds*, 69 *ds* A-Border and 53 *ds* P-Border contact angles and contact lengths were measured in 5 clones; For F-F'. n=45 *wt*, 94 *fj*, 69 *fj* A-Border and 53 *fj* P-Border contact angles and contact lengths were measured in 4 clones; For G-G'. n=108 *wt*, 191 *ft* 62 *ft* A-Border and 74 *ft* P-Border contact angles and contact lengths were measured in 7 clones located within the center of the A compartment. Anterior is to the left. Scale bar is 14 µm. Genotypes were *hsflp1.22; Ubi-RFP.nls FRT40A/FRT40A; Atpα::GFP/+* (A); *hsflp1.22;* ds^{UAO71} *FRT40A/FRT40A Ubi-RFP.nls; Atpα::GFP/+* (B); *hsflp1.22; FRT42D* fj^{D1}*/ Ubi-RFP.nls FRT42D; Atpα::GFP/+* (C); *hsflp1.22;* $ft^{Gr\text{-}V}$ *FRT40A/FRT40A Ubi-RFP.nls; Atpα::GFP/+* (D).

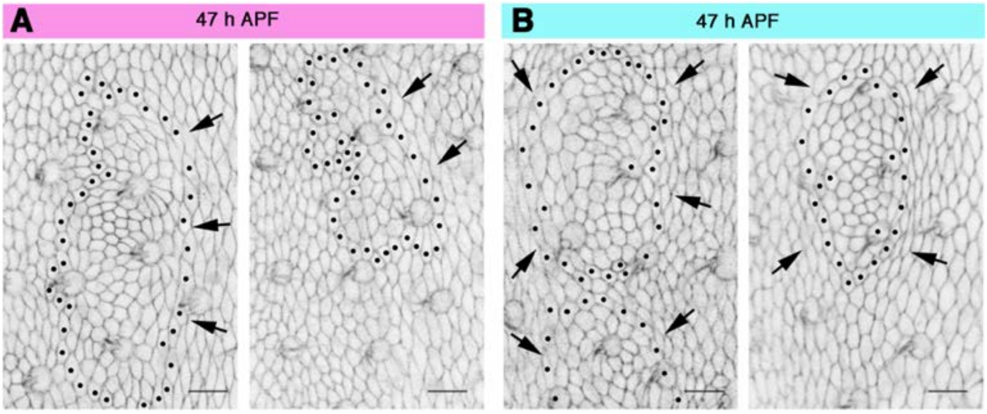

Fig. 69: *ds* and *ft* clones morphology are not dependent on clone size. A) *ds* clones of different sizes within the A compartment at steady state. Clone borders are marked with black dots. Black arrows point to the smoother side of *ds* clones. Note that *ds* cells tend to be more isodiametric than *wt* cells. Note also that mutant cells abutting the *wt* cells at the posterior are of similar shape to those in the background. **B)** *ft* clones of different size within the A compartment at steady state. Clone borders (black dots) are smooth all around (black arrows). Mutant cells tend to be more isodiametric than *wt* cells. Note that mutant cells abutting *wt* cells have similar shape to those in the background. Anterior is to the left. Scale bar is 14 µm. Genotypes were *hsflp1.22;* ds^{UAO71} *FRT40A/FRT40A Ubi-RFP.nls; Atpα::GFP/+* (A); *hsflp1.22;* $ft^{Gr\text{-}V}$ *FRT40A/FRT40A Ubi-RFP.nls; Atpα::GFP/+* (B).

4.4 Ds/Ft/Fj Activity Autonomous and Non-Autonomous Effects

-Ds from wt Cells Directionally Influence Ft Levels around ds Mutant Clones

Cell shape changes and PCA were lost in clones lacking *ds*. However, these outcomes were non-autonomously rescued in the most posterior cells of the mutant area. To test whether the directional non-autonomous cell morphology rescue at the clones borders was accompanied by changes in the pathway activity, we studied the localization of Ft (Ft::EGFP; Brittle et al., 2012) within and around *ds* clones. We found that Ft::EGFP levels were overall enhanced within *ds* clones, except for those *ds* cells abutting *wt* cells at the posterior side of the clone (Fig. 70). Here, mutant cells showed reduced levels of Ft to an equivalent level to that of the *wt* cells surrounding the posterior side where it also becomes downregulated. These behaviors within and around *ds* clones support the axial directional role of Ds in regulating Ft expression and the orientation of PCA. These local interferences recapitulate the alterations observed upon tissue-wide perturbation of the pathway in loss of function conditions (see Chapter II).

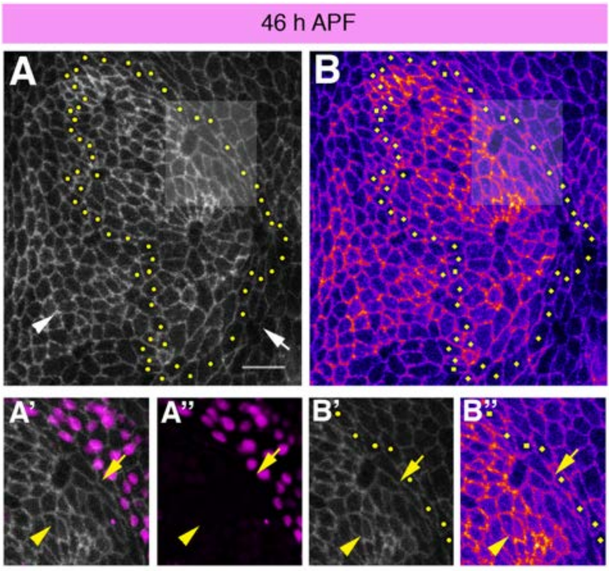

Fig. 70: Ft::EGFP is reduced on the posterior side of *ds* mutant clones. **A)** Localization of Ft in *ds* mutant clones at 46 hours APF. The first row of *wt* cells abutting the mutant area is marked by yellow dots. Yellow arrowheads point to high levels of Ft::EGFP inside the clone. Yellow arrows point to reduced levels of Ft::EGFP inside the clone. Note that this domain extends up to three rows of cells. **A'-A'')** Magnifications of the region boxed in A. Yellow arrows point to reduced Ft levels while yellow arrowheads point to elevated levels. **B)** Heat map of the clone in A (Fire-LUT filter). Yellow-pink colors indicate high intensity, magenta-blue colors indicate low intensity. **B'-B'')** magnification of the same region showed in A'-A''. Yellow arrows point to reduced Ft levels while yellow arrowheads point to elevated levels. Note that the level of Ft are similar to those in *wt* cells up to two rows within the clone. Anterior is to the left. Genotype was *hsflp1.22; ds*^{UAO71} *FRT40A/FRT40A Ubi-RFP.nls; Ft::GFP/+*.

-Ds-Ft Heterodimeric Interactions Are Rescued at the Periphery of ft Clones

Clones lacking *ft* displayed a non-directional rescue of cell shape and alignment all around the clone border. To explore if this rescue correlates with the restoration of functional Ft heterodimeric interaction with Ds at clone borders we monitored the localization of D at the cell surface (See Chapter III). D expression (D::GFP, endogenous reporter; Bosveld et al., 2012) was markedly increased within *ft* clones at steady-state (Fig. 71), although its subcellular localization within the clone was, despite sustaining some residual asymmetry, stochastically oriented, as we also observed in *ft* mutant pupae (Chapter III). Such behavior was independent on clone size or position throughout the A compartment (Fig. 71). On the contrary, D at the cells at the edge of *ft* clones was asymmetrically localized and aligned perpendicular to the A/P axis all around the clones (Fig. 71 and Fig. 72). The restoration of D asymmetry and thus of Ds/Ft/Fj activity in mutant cells associates to shape and alignment rescue at the clone border.

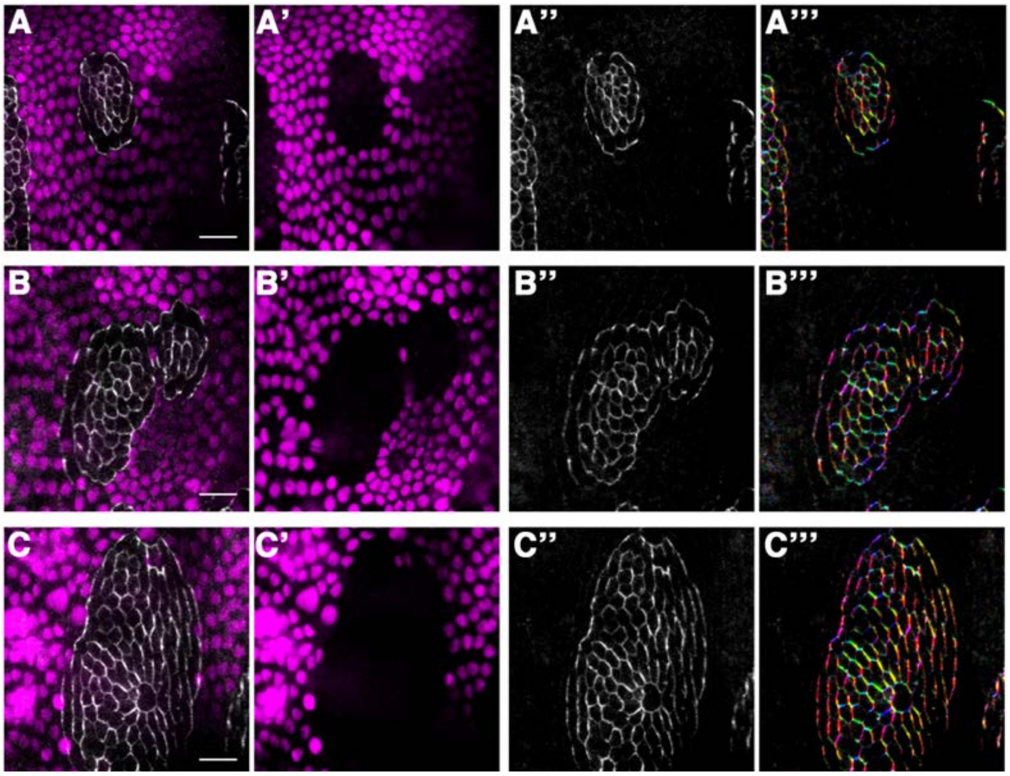

Fig. 71: D levels are enhanced autonomously in *ft* clones. A-A''') Example showing D:GFP localization and levels in a small *ft* clone. The mutant area is marked by the absence of RFP.nls expression (magenta, A and A'). D::GFP localization is showed in grey scale (A and A'') or in colored cell edge orientations (A'''; Reddish colors indicate edges aligned in parallel to the A/P axis). **B-B''')** As in A but a larger clone. **C-C''')** As in A and B but a much larger clone. Anterior is to the left. Scale bar is 14 μm. Genotype was *hsflp1.22;* $ft^{Gr\text{-}V}$ *FRT40A/FRT40A Ubi-RFP.nls; D::GFP/+*. See text for details.

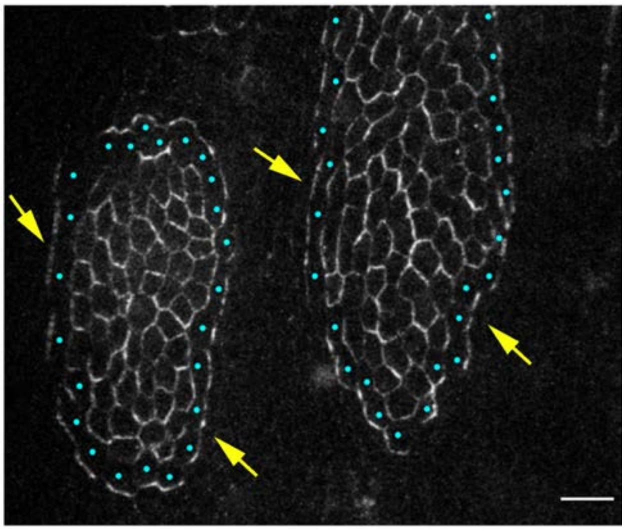

Fig. 72: D asymmetry is rescued around *ft* clones. Image showing D::GFP localization and levels in two *ft* mutant clones. The mutant cells contacting the *wt* surroundings are marked by cyan dots. D levels are very high in all mutant cells. D::GFP within the clone are not polarized or uneven. D is asymmetrically localized around the clone borders (yellow arrows). Anterior is to the left. Scale bar is 12 μm. Genotype was *hsflp1.22; ft*$^{Gr\text{-}V}$ *FRT40A/FRT40A Ubi-RFP.nls; D::GFP/+*.

4.5 *ds* and *ft* Clones Differentially Influence the Orientation of Trichome Polarity

It was reported that *ds* and *ft* clones respectively non-autonomously influence *wt* trichome polarity orientation at the anterior or posterior side within the A compartment in the abdominal epithelia (Casal et al., 2002). However, we found that *ds* but not *ft* directionally affect the axial orientation of PCA in clones (see above). To reconcile this difference, we re-examined the pattern of trichome orientations within and outside *ds* (Fig. 73) and *ft* (Fig. 74) clones at pharate stage. We observed non-autonomous effects in the orientation of trichomes at the anterior side of *ds* mutant clones at any position within the A compartment and in clones of any size (Fig. 73), in line with previous findings (Casal et al., 2002). In the clone's posterior edge the trichome polarity orientation was instead unaltered (Fig. 73 and Casal et al., 2002). A different scenario was observed when trichome polarity orientation was monitored within and outside *ft* mutant clones. Overall, PCP was generally randomized (less dramatically than within *ds* clones) although at the anterior side of the clones the trichome polarity orientation was unaltered (Fig. 74 and Casal et al., 2002). However, we did not observe any non-autonomous effect in trichome polarity orientation at the posterior side of *ft* clones (Fig. 74). If, occasionally, some perturbation in trichome orientations were seen in *wt* cells abutting the clones, such alterations did not spread along the border (Fig. 74) as observed at the anterior front of *ds* clones.

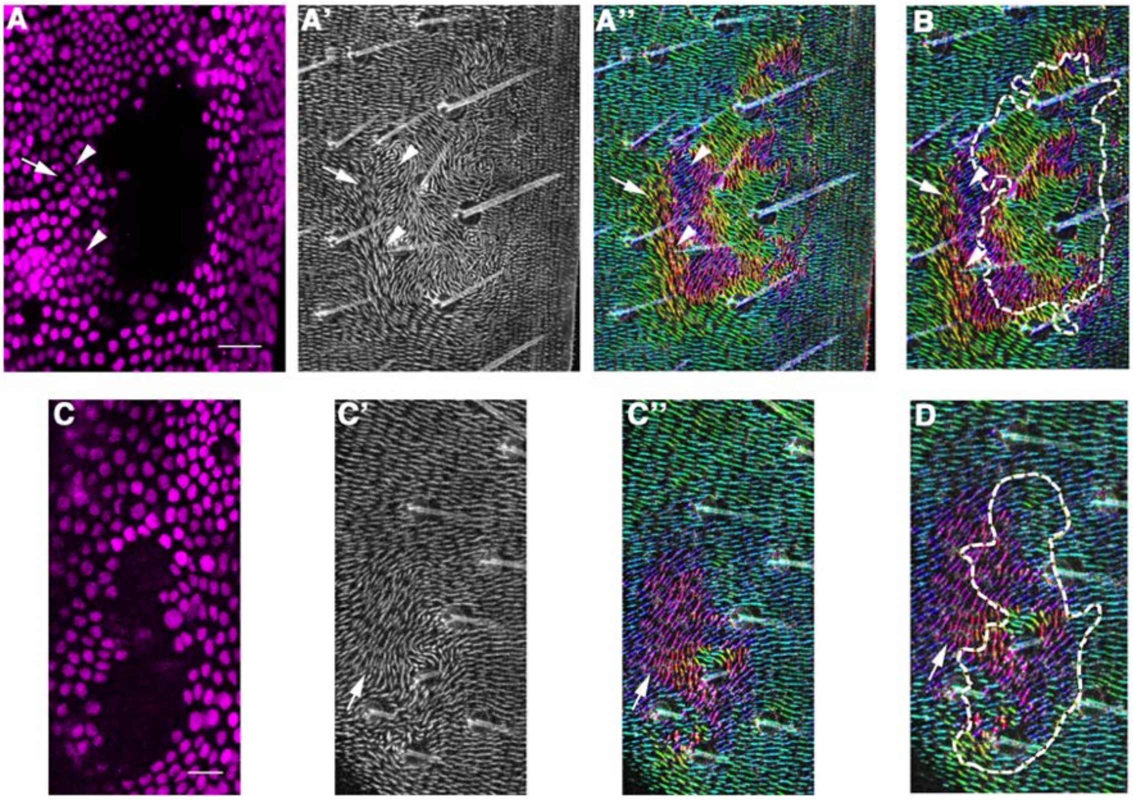

Fig.73: The orientation of trichomes is perturbed anteriorly and within *ds* clones. A-A’’) Image showing trichomes polarity in and around a large ds clone at the posterior of the A compartment. The clone is marked by the absence of *RFP.nls* (black, A). The white arrow and arrowheads point to the aberrant trichomes orientation outside the clone (non-autonomy) in grey in A’ or upon color-coding with Orientation-J (A’’’). Cyan indicates *wt* orientation. **B)** Magnification from A’’’. The mutant region is outlined with a white dashed line. The white arrow and arrowheads indicate the anterior non-autonomy of the *ds* clone.–Note that the trichome polarity is swirled within the clone. **C-C’’’)** Image showing trichomes polarity in and around a large *ds* clone at the anterior of the A compartment. The clone is marked by the absence of *RFP.nls* (black, C). The white arrow point to non-autonomy effects in grey in C’ or upon color-coding with Orientation-J (C’’’). Cyan color indicates *wt* orientation. Note that the trichomes swirl within the clone and are unperturbed at the posterior **(D)**. Anterior is to the left and posterior is to the right. Scale bar is 15 μm (A-A’’’) and 12 μm (C-C’’’). Genotype was *hsflp1.22; ds*^{UAO71} *FRT40A/FRT40A Ubi-RFP.nls;Moesin::GFP*.

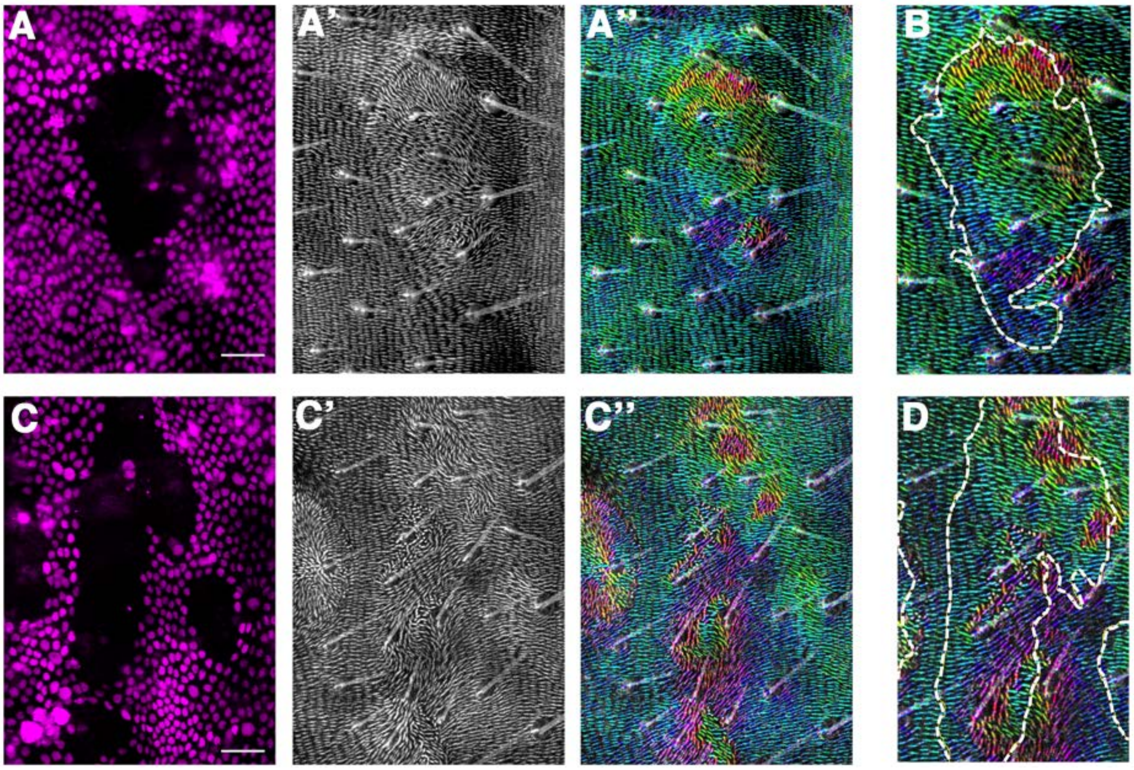

Fig. 74: Trichome polarity is perturbed but not uniformly rescued posteriorly to *ft* clones. A-A'') Images showing trichome polarity in and around a large *ft* clone close to the posterior of the A compartment and the dorsal midline. The clone is marked by the absence of RFP.nls (magenta, A). Trichome orientation in grey (A') or after color coding with Orientation-J (A''). Cyan color indicates *wt* orientation. **B)** Magnification of the clone shown in A''. The mutant region is outlined with a white dashed line. Note the aberrant trichome polarity restricted at the posterior of the clone to two small regions. Note that trichomes swirl within the clone. **C-C'')** Images showing trichome polarity within and outside multiple *ft* clones at the anterior and central region of the A compartment. The mutant clones are marked by the absence of RFP.nls (magenta, B). Trichome orientation in grey (B') or after color coding with Orientation-J (C''). Cyan color indicates *wt* trichome orientation. **D)** Magnification of the clone shown in C''. The mutant regions are outlined with white dashed line. Note that the trichomes swirl within the clone but are perturbed in small regions of the posterior clone side. Anterior is to the left and posterior is to the right. Scale bar is 15 μm. Genotype was *hsflp1.22; ft*$^{GR-v}$ *FRT40A/FRT40A Ubi-RFP.nls;Moesin::GFP*.

Synopsis

The juxtaposition of cells expressing different Ds and Ft levels influence cell-cell alignment in parallel to the A/P axis. The net effect of the local changes in pathway components was the minimization of contacts with surrounding tissues. Clones reduce their perimeter, smoothing their surface. Contact minimization was more pronounced upon Ft and Ds signaling perturbation than in Fj, implying that the two cadherins must co-exist to ensure contact maximization and PCA in parallel to the A/P axis. Yet, Ds, but not Ft, was able to directionally restore cell-cell alignments orientation. An oriented Ds-Ft heterodimeric interaction following directionally the Ds gradient appears to be necessary and sufficient to coordinate the axial uniform orientation of PCA.

Chapter V

Hippo Signaling and the Control of Growth through Yki Activity in the *Drosophila* Abdominal Epidermis

This section originates in a shared project focusing on the control of growth through the Hippo and Yki activities in the *Drosophila* abdominal epidermis with the laboratory of Dr Nicolas Tapon at the Francis Crick Institute in London working together with Miss Anna Ainslie and Dr John Robert Davis.

An axial uniform orientation of PCA is achieved under the genetic control of the Ds/Ft/Fj pathway during the extensive growth of the abdominal histoblasts. An important issue is whether differences in growth rates influence this global planar organization of the abdominal epithelia.

The conserved Hippo pathway is required for growth control in all imaginal discs (Halder and Johnson, 2011; Huang et al., 2005; Tapon et al., 2002) but the role/s that this cascade may have in the control of growth in histoblasts have not been characterized yet. Understanding how Hippo signalling is regulated in time and space may inform not only on how the abdominal epithelia sense its size, but also on how size sensing may be coupled with tissue planar organization.

5.1 Yki Expression Pattern during Tissue Expansion and Remodeling

To analyse the subcellular localisation of Yki during the morphogenesis of the abdominal epidermis *in vivo*, we employed a Yki::GFP reporter expressed under the control of an *Ubiquitin-p63E (Ubi-yki::GFP)* promoter (M. Holder, Tapon's Lab, unpublished). During expansion (16-26 hours APF), Yki expression levels were generally weak and uniform throughout the tissue (Fig. 75 and Movie 33). Yki was principally localized in the cytoplasm of both histoblasts and LECs from the onset of expansion (Fig. 75-A' and B-B'). In some histoblasts, Yki was more diffuse apically (Fig. 75A'-A' and B-B') probably pointing to dividing cells (although the expression of Yki was too low to ensure this possibility). In line with Yki expression in growing imaginal discs, Yki was not clearly detected into the histoblast nuclei during its proliferative period (see Fig.45 and Oh and Irvine, 2008; Dong et al., 2007). As expansion progressed and the proliferative activity of the histoblasts decreased, Yki cytoplasmic localization became more prevalent and Yki was less frequently diffusely found apically (Fig. 75A''-A''' and B''-B''').

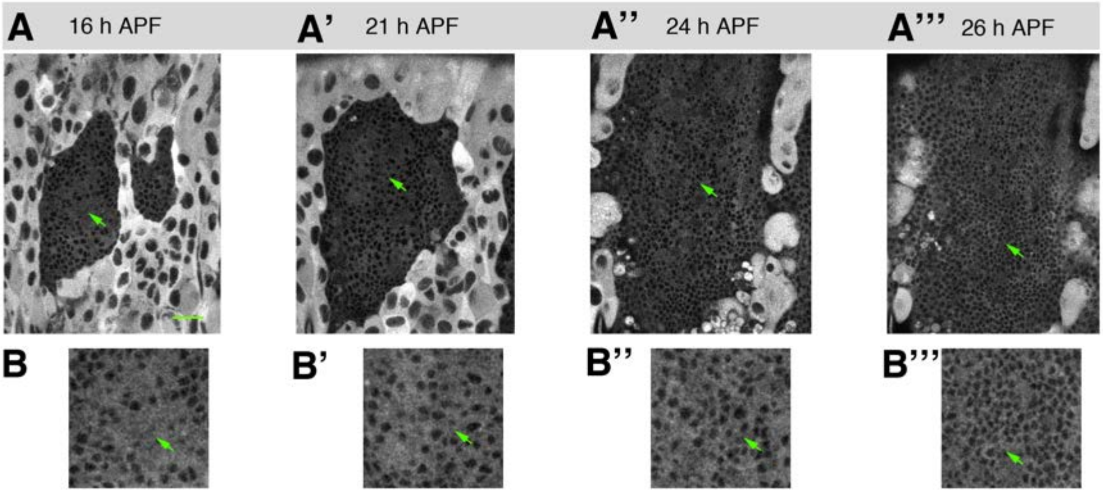

Fig. 75: Yki Localization during Tissue Expansion. A-A’’’) Temporal evolution of Ubi-Yki::GFP localization during expansion. **B-B’’)** Close-up of the regions indicated by green arrows in A-A’’’. Yki is cytoplasmic and apically diffuse (B-B’). Note that Yki cytoplasmic localization spreads over time (B’’-B’’’). Scale bar is 25 μm (A-A’’’). Anterior is to the left. Genotypes was *Ubi-yki::GFP*. See text for details. See Movie 33.

During tissue remodelling, no changes were found in Yki expression, which keeps been low and cytoplasmic. However, upon confluence (38 hours APF onward) some individual histoblasts markedly accumulated higher levels of Yki (Fig. 76 and Movie 34). This cells distributed in a precise periodically repeated pattern through the A compartment, resembling the bristle pattern. Indeed, they corresponded to the cells anteriorly positioned respect to the socket cells of bristles (identified by their characteristic rounded shape and larger size) (Fig. 76A-D).

Between 40 and 46 hours APF, the histoblasts expressing high levels of Yki further increased such expression reaching stable intensity at morphogenesis completion (Fig. 76A-D). These observations suggested a potential role of Yki in the Sensory Organ Precursor (SOP) lineage.

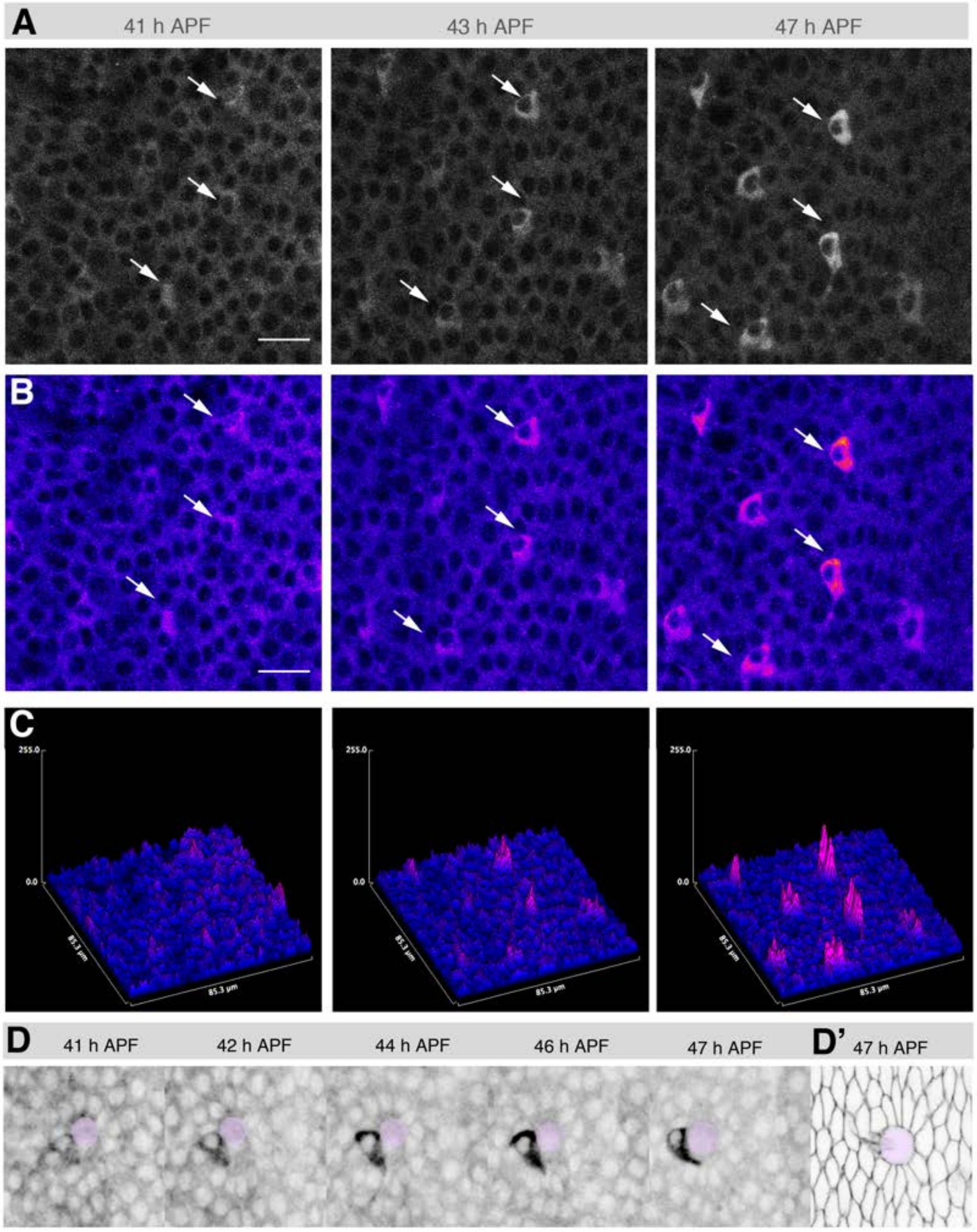

Fig. 76: Yki accumulates in cells anterior to the socket cells during remodelling. A) Progressive enhancement of Yki expression levels during remodelling. Some cells (white arrows) of the A compartment show increased levels of Yki in their cytoplasm **B)** Images as in A through a Fire-LUT filter. Blue indicates low and Pink indicates high expression. **C)** Surface plots of the regions shown in B. Note that the intensity of Yki increases over time (Pink). **D)** Progression in the accumulation of Yki around a Macrochaeta. The socket cell body is masked with a light violet circle. A cell located anteriorly to the socket retains more Yki on its cytoplasm (dark grey). D') Cell outline morphologies of the epithelial cells surrounding a socket cell (light violet). A small portion of the shaft positions anteriorly to the socket. Anterior is to the left. Genotypes were *Ubi-yki::GFP* (A to D), and *Atpα::GFP* (D'). Scale bar is 12 µm (A and B) and 5 µm (D and D'). See Movie 34.

5.2 *diap1* Expression Pattern during Tissue Expansion and Remodeling

To monitor the transcriptional activity of Yki we used a well-characterized Yki transcriptional target, the apoptosis inhibitor gene *diap1/thread* (*Drosophila* Inhibitor of Apoptosis 1 or D-

IAP1) (Gulev et al., 2008; Wu et al., 2008; Zhang et al., 2008). Specifically, we employed a reporter expressing GFP under the control of a *diap1* Yki-dependent enhancer (*diap1-GFP*$^{3.5}$, Zhang et al., 2008). We observed that *diap1* expression was highly dynamic and stereotyped during histoblast expansion (Fig. 77 and Movie 35). *diap1* levels were not uniform at the onset of expansion and cells within the A compartment expressed lower levels when compared to those at the nests edges (specially at the ventral and dorsal edges) (Fig. 77A, B and C). Conversely, all cells of the P compartment expressed *diap1* uniformly and at higher levels than in A (Fig. 77A, B and C). *diap1* was also expressed in the LECs at very high levels. Upon fusion of the dorsal nests, the pattern of *diap1* was sustained (Fig. 77A'-A'', B'-B'' and C'-C''). Interestingly, *expanded* (*ex*), another Yki target, was expressed in a similar pattern at comparable stages (John Robert Davis, personal communication). From 22-26 hours APF, Yki expression pattern was generally maintained with some notable exceptions. First, SOPs, which become specified at this time, down-regulate *diap1-GFP* (Fig. 77A''', B''' and C'''); second, Yki expression increased in the very central region of the A compartment (Fig. 75A''', B''' and C'''); and third, the histoblasts positioned at the periphery of the A compartment now express more *diap1-GFP* than neighbouring cells (Fig. 77A''', B''' and C'''). Upon confluence and during remodelling, *diap1* differences in expression became less pronounced, giving rise to a fairly homogenous pattern. At this time, the histoblasts located anteriorly to socket cells (at an equivalent position of those retaining more Yki in their cytoplasm at comparable stages) expressed up to three-folds more *diap1* than their immediate neighbours (Fig. 78A-C and Movie 36, see also Fig. 79).

The position and shape of the cells strongly expressing Yki in their cytoplasm suggest they might correspond to the sensory organ shaft cells. The identity of the cells expressing high *diap1-GFP* levels were, however, more difficult to assess as only the nuclei were marked with this reporter. Nevertheless, the apical position of these nuclei suggests that *diap1-GFP* levels are enhanced in one of the external cells of the lineage, the shaft or the socket.

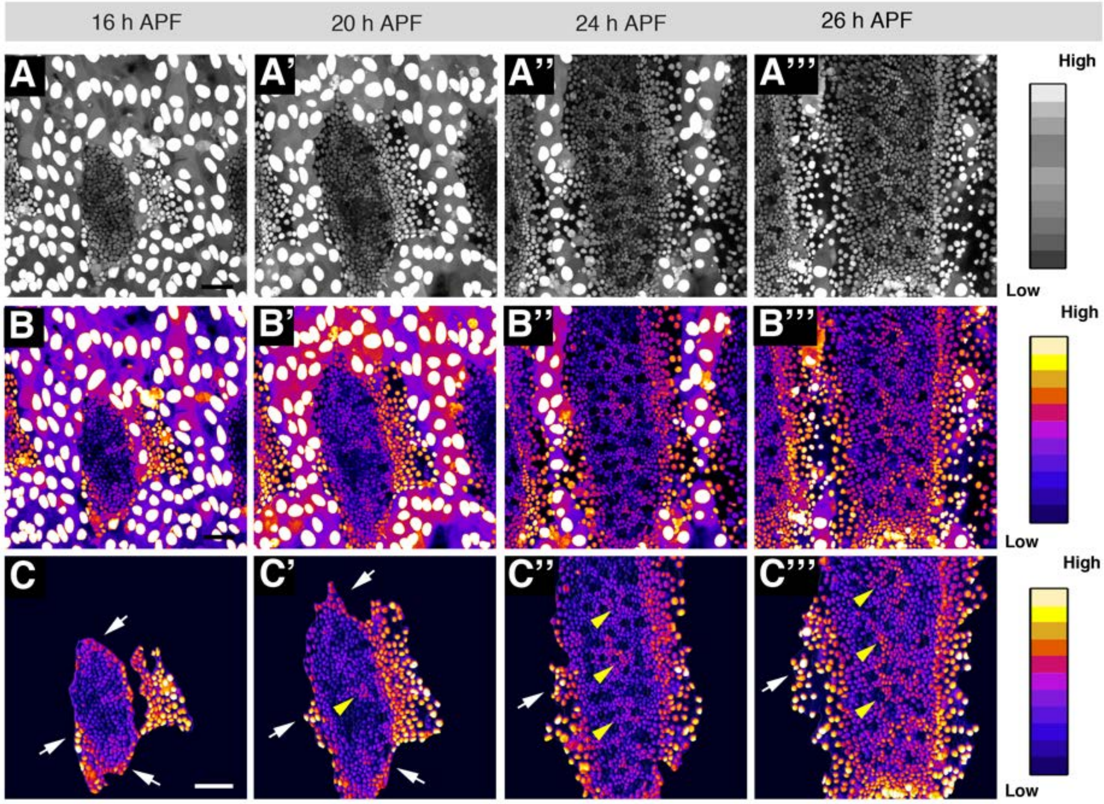

Fig. 77: The *diap1-GFP* pattern is highly dynamic during tissue expansion. A-A’’’) Expression pattern dynamics of a *diap1-GFP* reporter during expansion. *diap1* is dynamically expressed at different levels through the anlage over time. The inset on the right shows the intensity levels in grey. **B-B’’)** Images as in A applying a Fire-LUT filter. The inset on the right shows the intensity levels. **C-C’’’)** Images as in B showing the pattern of *diap1* within the imaginal tissue only. White arrows point to high *diap1* at the edges of the A compartment. Yellow arrowheads point to *diap1* within the A Compartment. The colour scale for intensity is shown on the right panel. Genotype was *diap1-EGFP*$^{3.5}$. Scale bar is 30 μm (A to B’’’) and 25 μm (C-C’’’). Anterior is to the left. See Movie 35.

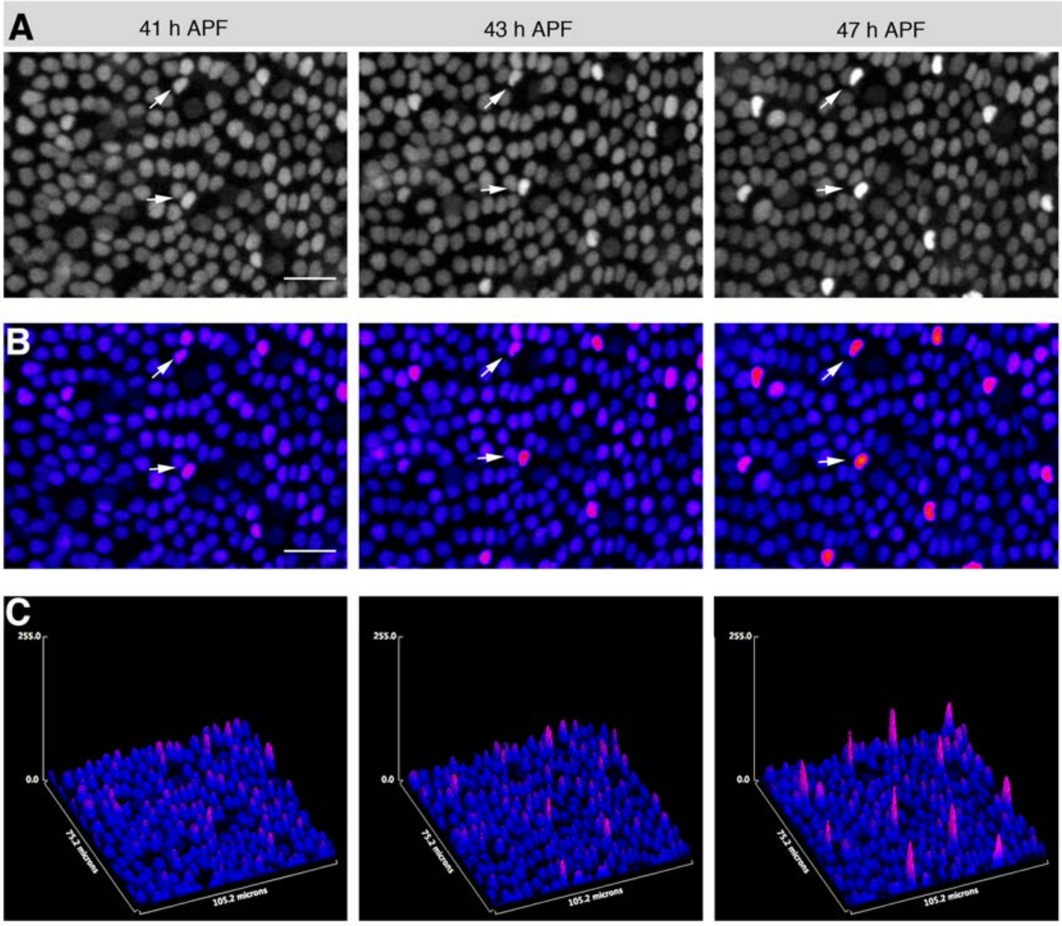

Fig. 78: *diap1-GFP* levels increased in cells anterior to the SOP cluster during Remodelling. A) Progressive increase in *diap1-GFP* expression levels during remodelling. Some cells of the A compartment show increased expression levels of *diap1* (white arrows). **B)** Same images as in A after applying the Fire-LUT filter. Blue points to low and Pink points to high intensity. **C)** Surface plots of the regions in B. Note that the intensity levels of *diap1* increase over-time (Pink). Scale bar is 16 μm. Anterior is to the left. Genotype was *diap1-EGFP*$^{3.5}$. See Movie 36.

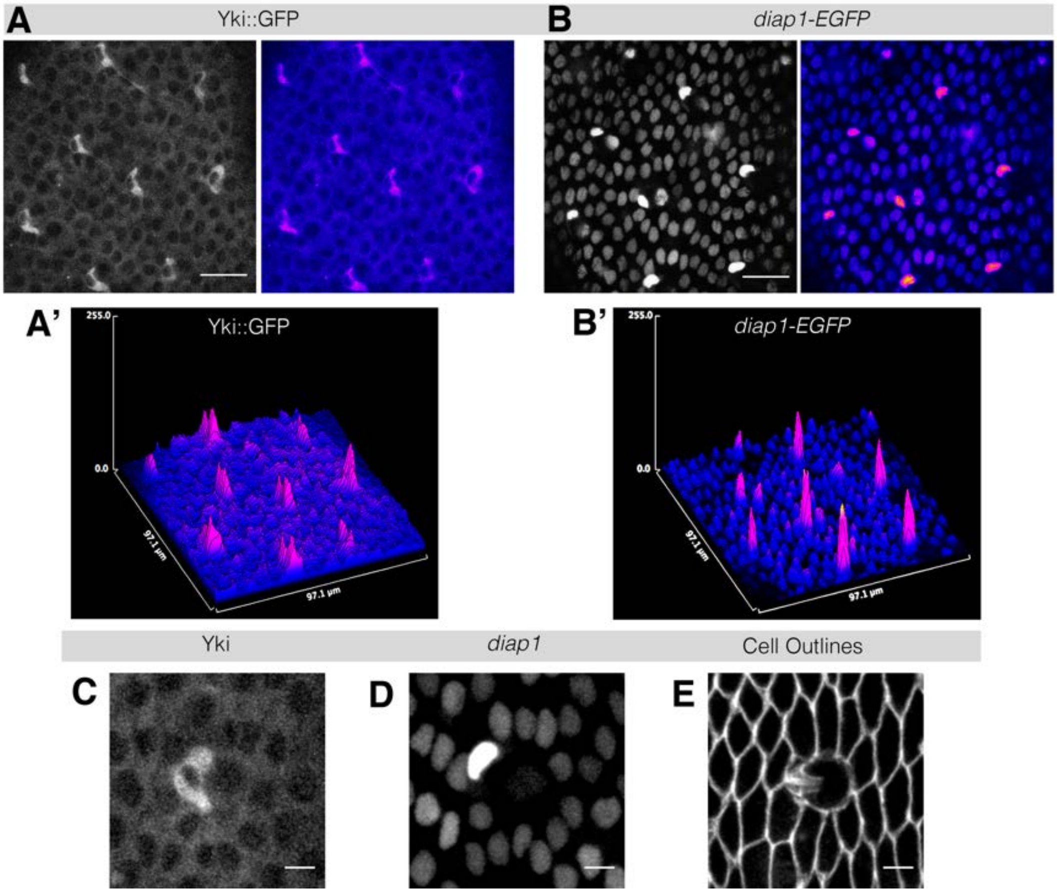

Fig. 79: Yki and *diap1-GFP* levels increased in cells anterior to each Socket Cell. A-B) Expression pattern of Yki (A) and *diap1-GFP* (B) in the A compartment at 47 hours APF. Grey scale (left) and Fire-LUT filtered (right) levels of expression are shown. Blue indicates low and pink high levels of expression. **A'-B')** Surface plot of the images showed in A and B highlighting the spatial similarity of Yki and *diap1-GFP* patterns at steady state. **C-E)** High magnification images showing the increased cytoplasmic expression of Yki (C) or nuclear expression of *diap1-GFP* (D) anterior to the socket. Genotypes were *Ubi-Yki::GFP* (A, A' and C), *diap1-EGFP*$^{3.5}$ (B, B' and D) and *Atp*α*::GFP* (E). Scale bar is 12 µm (A and B) and 5 µm (C, D and E). Anterior is to the left. See text for details.

5.3 *hippo* and the Upstream Control of Yki in the Abdominal Epithelium

-Perturbation in Yki Activity Affects Apoptosis during Morphogenesis

Inactivation of *yki* in clones in imaginal discs affects growth and survival autonomously (Huang et al., 2005). We explored whether clones of cells mutant for *yki* behave similarly in the histoblasts and found that growth was indeed affected. Clones became progressively fragmented and irregularly shaped (Fig. 80), while twin-spot areas were not noticeable enlarged, suggesting that the *wt* cells were not undergoing non-autonomous compensatory proliferation.

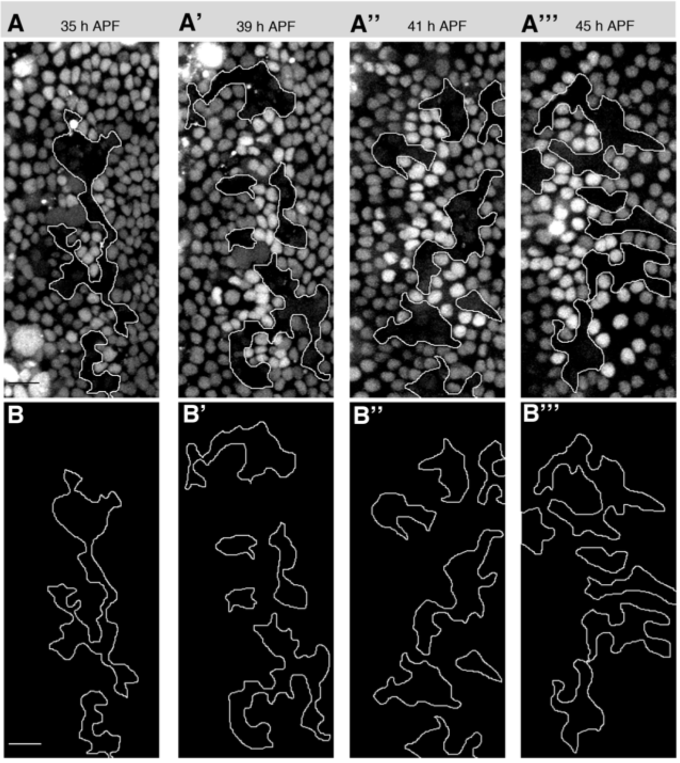

Fig. 80: ***yki*** **loss of function clones become fragmented over-time. A-A''')** Example showing the behaviour of *yki* cells in an otherwise *wt* background within the A compartment. The *yki* patches are marked by the absence of *RFP.nls* (black areas outlined by white lines). Note that the mutant areas undergo dynamic fragmentation over-time. **B-B''')** Outlined mutant areas.. Genotype was *hsflp1.22; FRT42D* yki^{B5}*/Ubi-RFP.nls FRT42D*. Scale bar is 16 μm. Anterior is to the left.

Increasing Yki expression in clones by Flp-Out-Gal4 somatic recombination (See Materials and Methods), however, had an impact on the surrounding *wt* territory. Mutant patches showed rounded and smoothed shapes and the territories in contact with Yki clones were occasionally abnormally domed (Fig. 81 and Movie 37). Yet, Yki ectopic overexpression in histoblasts did not lead to any overgrowth with this clonal strategy, while it has been extensively documented that it promotes excessive growth and reduces apoptosis in the imaginal discs, mimicking the *hpo* and *wts* mutant phenotypes (Huang et al., 2005). The LECs ectopically expressing Yki were not extruded or underwent apoptosis, thus preventing the expansion of histoblasts (Fig. 81) leading to lethality during pupation.

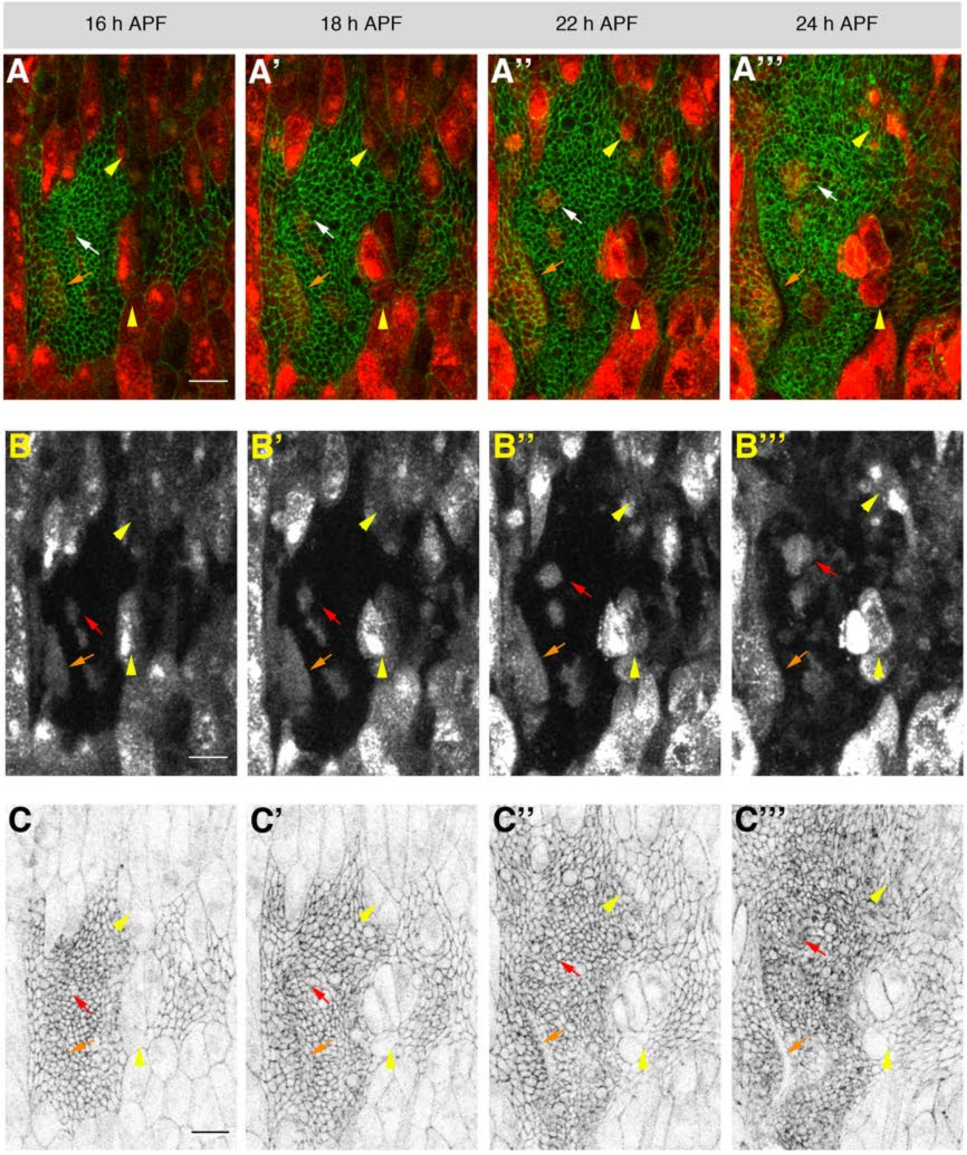

Fig. 81: Flp-out-Gal4 UAS-Yki expression prevents LECs apoptosis. A-A''') Images showing cell outline morphologies (green) and Yki overexpression (red) after heat-shock promoted *cis*-recombination (see also Materials and Methods). Note that almost all LECs underwent recombination. **B-B''')** Images showing UAS-Yki expressing clones of different sizes that simultaneously express CD8-Cherry (grey scale, red and orange arrows). **C-C''')** Inverted grey LUT images showing cell outline morphologies in a AIII segment in which Flp-out-Gal4 somatic recombination has been induced to promote the ectopic activity of Yki. The LECs expressing UAS-yki do not apoptose (yellow arrowheads). White (A-A''') or red (B-B''' and C-C''') arrows point to the round shape of a small clone. Orange arrows indicate the tissue folding adjacent to a large clone. The genotype was *hsflp1.22; Act5C>>Gal4, UAS-CD8Cherry/UAS-yki;Atp*α*::GFP/+*. Scale bar is 22 μm. Anterior is to the left. See text for details. See Movie 37.

To circumvent this problem and study the effect that the excess of expression of Yki could have in the histoblasts, we mis-expressed Yki in the *pannier* (*pnr*) domain (Calleja et al., 2000) with the Gal4/UAS binary system. This domain encompasses the whole medial region of the animal (Fig. 82A), allowing comparisons between the thoracic and the abdominal imaginal populations. We found that, while in the thorax Yki overexpression led to overgrowths, in the abdomen it was causing necrosis and clefts of different magnitude (Fig. 82A-C). This occurred both for the ectopic expression of *yki* or its constitutively active form Yki^{S168A} (Fig. 82B and C). Strikingly, while the overexpression of the Yki negative regulator Hpo in the thorax promoted apoptosis and led to undergrowth (Udan et al., 2003), its expression in the abdomen blocked LECs delamination as Yki overexpression did (Fig. 82D). This open the possibility that, in the abdomen, Yki function would not relate to *hpo* (and possibly *wts*) as it does in the imaginal discs.

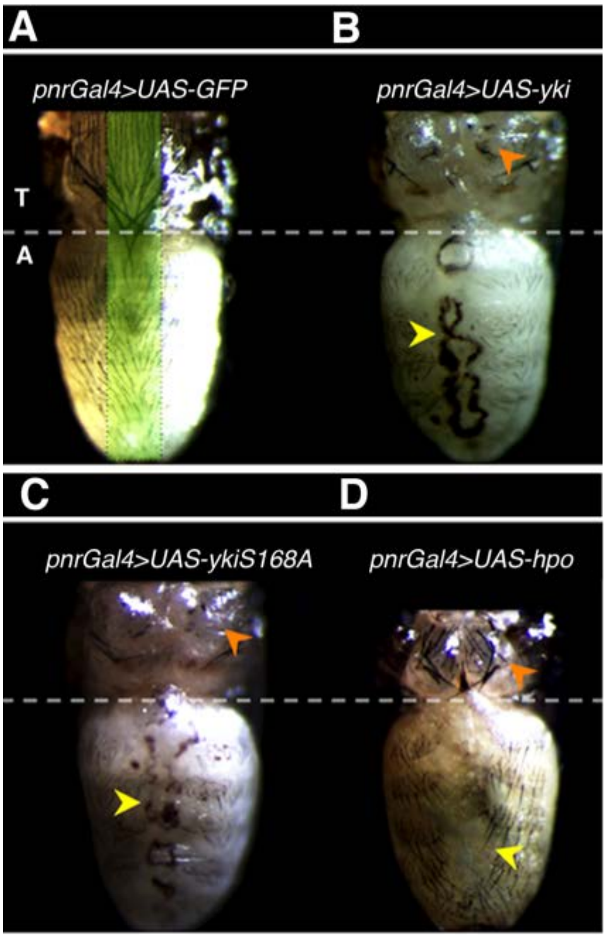

Fig. 82: Ectopic Yki and Hpo expression cause clefts in the abdominal epidermis. A) *wt* pharate (>80 hours APF) in which the domain of expression of *pnr* is highlighted (green masked rectangle at the medio-dorsal region of the thorax and the abdomen). **B)** Pharate in which ectopic Yki has been expressed in the *pnr* domain. Orange arrowhead indicates overgrowth in the thoracic region. Yellow arrowhead points to necrotic areas surrounding persistent LECs in the abdomen (cleft). **C)** Pharate in which a constitutive active form of Yki has been expressed in the *pnr* domain. Orange arrowhead indicates overgrowth in the thoracic region. Yellow arrowhead indicates necrotic areas surrounding persisting LECs in the abdomen (cleft). **D)** Pharate in which Hpo has been expressed in the *pnr* domain. Orange arrowhead indicates size reduction of the thoracic region. Yellow arrowhead indicates the extensive cleft caused by LECs persistence. Anterior is to the top and posterior to the bottom. T= Thorax; A=Abdomen. Genotypes were *pnr-Gal4/UAS-GFP* (A); *pnr-Gal4/UAS-yki* (B); *pnr-Gal4/UAS-yki::GFP(S168A)* (C) and *pnr-Gal4/UAS-hpo* (D).

-hpo Perturbations Do Not Phenocopy Yki Over-Expression in the Abdominal Epithelium

Strong reduction or inactivation of *hpo* or *wts* in imaginal discs increased cell proliferation (*i.e.* cell cycle speed) and reduced apoptosis, phenocopying Yki overexpression (Huang et al., 2005). To test if *hpo* would display equivalent phenotypes to those observed after overexpressing Yki, we down-regulated its expression in clones by Flp-Out-Gal4 inducing a UAS-hpoRNAi. Surprisingly, *hpo* clones were indistinguishable from control clones (Fig. 81A-A' and B-B'). Further, *hpo* down-regulation did not affect LECs delamination as it was observed after Yki overexpression. Equivalent clones for an *hpo* null allele (*hpo5.1*, Genevet et al., 2009) generated by recombination did not increase the mutant clone area either (Fig. 83C) and clones for *wts* behave as *hpo* ones (Anna Ainslie, personal communication). These observations, together with those on the ectopic activation of Yki and Hpo, indicate that the functions of the Hpo core kinase cascade and that of Yki in the abdominal epidermis are not related.

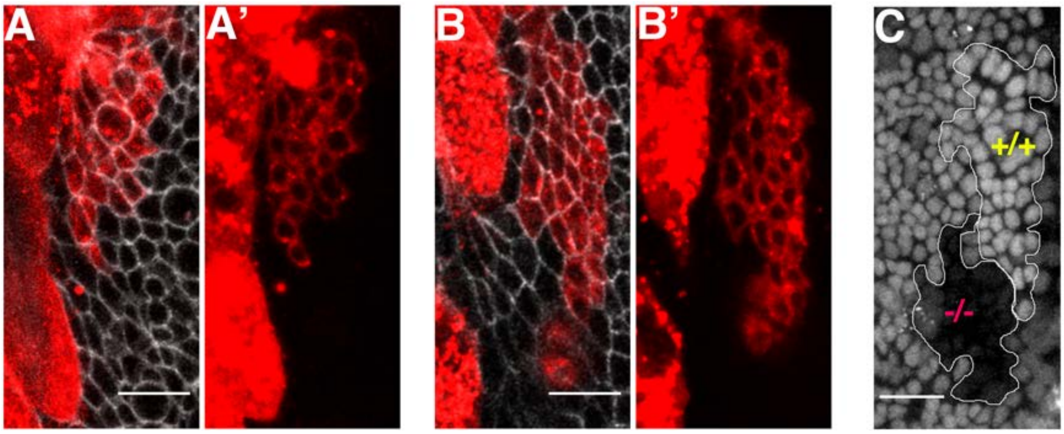

Fig. 83: *hpo* histoblasts behave as *wt*. A-A') Act5C>>Gal4 clones expressing UAS-CD8.mCherry alone (red) within the anterior edge of the A compartment at about 22 hours APF. **B-B')** Act5C>>Gal4 clones that express UAS-CD8.Cherry and UAS-hpoRNAi within the anterior edge of the A compartment at about 22 hours APF. Note that the cell size is indistinguishable from *wt* (A-A'). **C)** Mutant *hpo* clones and its twin outlined in white within the A compartment at about 24 hours APF. Sister clones areas appear of similar size. Anterior is to the left. Scale bar is 16 μm. Genotypes were *hsflp1.22; UAS-CD8.Cherry; Atpα::GFP/+* (A-A'); *hsflp1.22;UAS-CD8.Cherry/UAS-hpoRNAi;Atpα::GFP/+* (B-B'); and *hsflp1.22; FRT42D* $hpo^{5.1}$*/Ubi-RFP.nls FRT42D* (C).

-hpo Pupae Have Small Abdomens with Unperturbed Patterning

We last tested if *hpo trans* allelic combinations [preventing the early lethality associated with strong alleles of *hpo* (Udan et al., 2003; Wu et al., 2003; Genevet et al., 2009;)] led to alterations on abdominal size and shape. Interestingly, among the different *trans* allelic combinations tested (Fig. 84A and B), those of the loss-of-function allele *KC203* (Udan et al.,

2003) with the null allele *5.1* (Genevet et al., 2009) or the kinase-dead allele *42-47* (Wu et al., 2003) reached pharate stage successfully.

These pupae (Fig. 84C-to-F), as well as their pupal cases, were about half the size of controls (Fig. 84C). They displayed, however, a “hippo” phenotype (Udan et al., 2003) with slightly enlarged eyes, head, thorax and wings, folded wings and dark pigmentation (Fig. 84D-to-F). Remarkably despite the clear reduction in size, the abdomens were not dysmorphic, indicating a relative reduction of size in the abdomen when compared to other structures (Fig. 84D-to-F). Their patterning was not grossly disturbed either, indicating normal cell differentiation. Thus, *hpo* mutants primarily affected tissue size in the abdomen, within what it seems to be a systemic growth reduction. The abdomen was reduced in size along the A/P axis without being broader.

To elucidate the nature of reduction in segmental size, we monitored the cell outline morphologies of *hpoKC*^{203}/*hpo*$^{5.1}$ pupae employing *hpo*$^{5.1}$/+ heterozygous as a control and found that cell shapes where remarkably similar during expansion (Fig. 84G-H). Nevertheless,

LECs, but not histoblasts, were reduced in size from the onset of pupation, as well as the overall segmental territory (Fig. 84G-H). Notably, the histoblast spreading, as well as LECs delamination occurred normally (Fig. 84G-H).

At the steady state, the segmental size was about half a size of the control while the cell size and the disposition and number of patterned bristles was remarkably similar to heterozygous pupae (Fig. 84I-L). These observations suggest that tissue wide perturbations on Hpo activity have a systemic effect, probably, on cell number and, thus, tissue size.

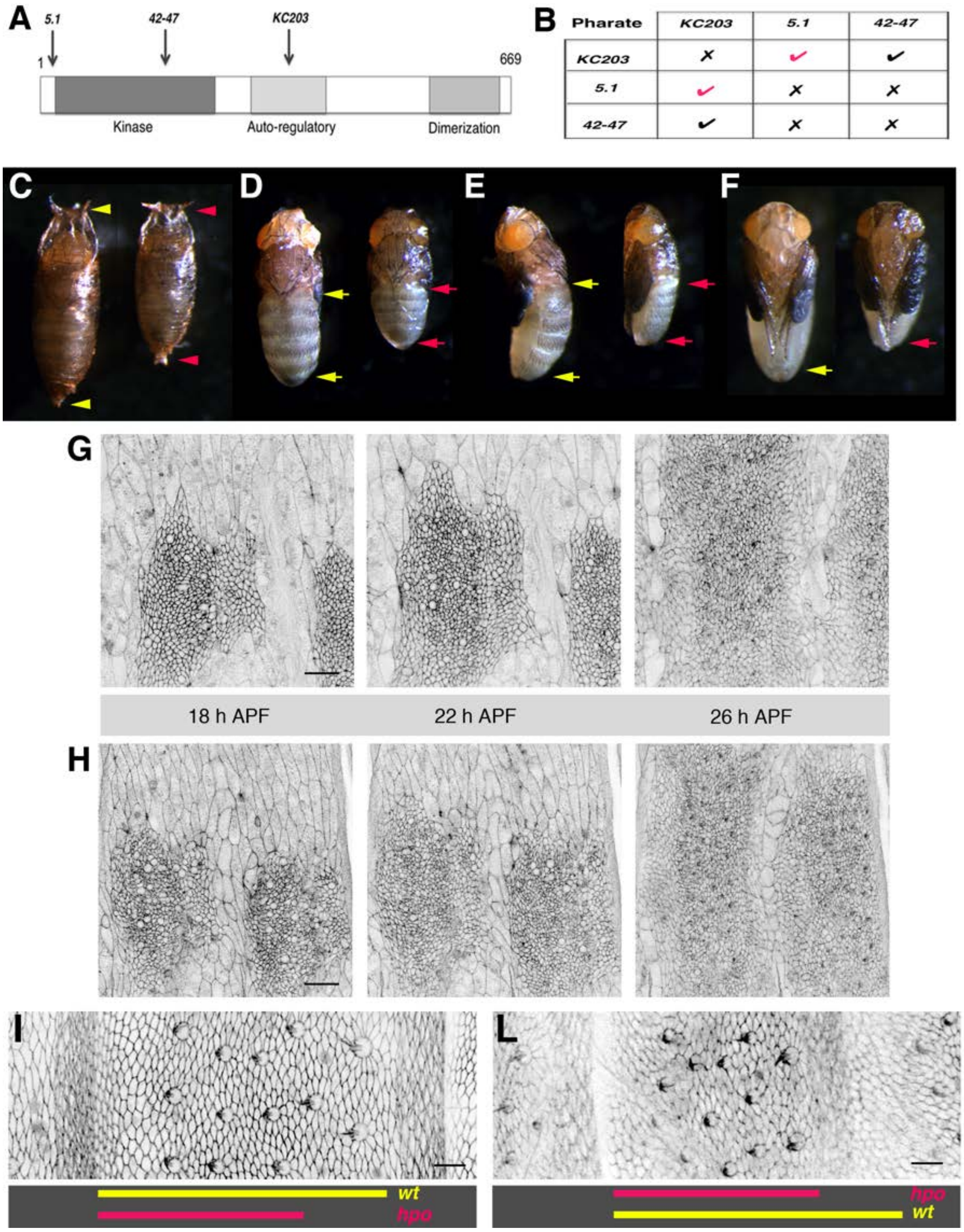
A
5.1
42-47
KC203
1
669
Kinase
Auto-regulatory
Dimerization
B
Pharate
KC203
5.1
42-47
KC203 ✗ ✓ ✓
5.1 ✓ ✗ ✗
42-47 ✓ ✗ ✗
C
D
E
F
G
18 h APF
22 h APF
26 h APF
H
I
wt
hpo
L
hpo
wt

Fig. 84: *hippo* pupae show systemic reduction of abdominal size.

(the legend of Fig. 84 is written in the next page)

Fig. 84: *hippo* pupae show systemic reduction of abdominal size. A) Schematic representation of the Hpo protein showing its main conserved domains according to Udan et al., 2003. The position of the different mutations tested are indicated by arrows. The null allele *5.1* is a deletion of most of the coding sequence. The kinase-dead allele *42-47* causes a deletion of 6 amino acids within the kinase domain. The hypomorph KC203 allele causes a premature stop codon within the auto-regulatory domain. **B)** Table highlighting the *trans* allelic *hpo* combination tested. All alleles were homozygous lethal. *hpo*$^{5.1}$/*hpo*^{KC203} reached the pharate adult stage, as well as *hpo*$^{42\text{-}47}$/*hpo*^{KC203}. **C-F)** Images of pharate adult *hpo*$^{5.1}$/+ (left) and *hpo*$^{5.1}$/*hpo*^{KC203}. Note that the *hpo* puparium (red arrowheads) is about half the size of the *hpo*$^{5.1}$/+ heterozygous one (yellow arrowheads) (C and D) Dorsal, (E) lateral and (F) ventral views of *hpo*$^{5.1}$/+ and *hpo*$^{5.1}$/*hpo*^{KC203} pupae. Note that the eyes, thorax and wings are slightly dysmorphic, while the abdominal region is isodiametrically reduced in size. Yellow arrows expand the abdominal region of *hpo*$^{5.1}$/+ pupae and red arrows the abdominal region of *hpo*$^{5.1}$/*hpo*^{KC203}. **G)** Cell outline morphology in an *hpo*$^{5.1}$/+ pupa during expansion. **H)** Cell outline morphology in an *hpo*$^{5.1}$/*hpo*^{KC203} pupa during expansion. Note that LECs 2D size is reduced. Note also that almost two hemisegments occupy the field of view in the *hippo* pupa compared to control. **I)** 50 hours APF cell arrangement visualized in a portion of the AIII segment of an *hpo*$^{5.1}$/+ pupa. **L)** 50 hours APF cell arrangement visualized in a portion of the AIII segment of an *hpo*$^{5.1}$/*hpo*^{KC203} pupa. Note that the segmental size is markedly reduces (compare the yellow and red lines below I and L), while the cell size, arrangement and disposition/number of pattern elements are remarkably similar. Scale bar is 20 μm (G-H) and 16 μm (I-L). For C-to-F anterior is up. For G-to-L anterior is to the left. Genotype were *hpo*$^{5.1}$/+;*Atp*α*::GFP/+* and *hpo*$^{5.1}$/*hpo*^{KC203};*Atp*α*::GFP/+*.

Synopsis

The Hpo/Yki signalling undergoes highly dynamic changes during the morphogenesis of the abdominal epithelium. The expression pattern of Yki and its transcriptional target *diap1* follows a precise spatiotemporal dynamics during expansion. Additionally, the expression of both genes specifically targets the SOP lineage.

Yki appears to be required for proper epithelial cell growth and survival, since both histoblasts and LECs apoptosis are affected by perturbation of its activity. Intriguingly, although these observations are in line with the function of the pathway in imaginal discs, the simultaneous activation of Yki in Histoblast and LECs seems to be insufficient to promote histoblast overgrowth. Moreover, the Yki upstream regulator Hpo does not appear to phenocopy Yki activation as it does in imaginal discs. Thus, Hpo may not function as a Yki inhibitor during abdominal epithelial morphogenesis.

Discussion

The tendency of motile organisms and cells to aggregate and align generating spatial patterns of various ranges of order is widespread in nature. From unicellular to multicellular organisms order is found at every scale. In community, such as in microscopic colonies of bacteria or in isolated motile mesenchymal cells as fibroblasts, individuals tend to aggregate and form locally aligned two-dimensional patterns in which cells arrange in multiple parallel arrays of various orientations (Elsdale, 1972; Elsdale & Wasoff, 1976). The same is found at an intermediate level in the organization of cells within tissues. In multicellular organism, mature tissues and organs reach high degrees of order in the arrangement of their constituent cells. Last, order is essential at the level of populations as in macroscopic schools of fish or small insects swarms (Giardina, 2008).

Order acquisition is thus a "Systems" problem. How is this achieved? Starting from broadly random scenarios, local cell alignments may emerge spontaneously through short-range interactions. Local order arises from local rules and activities; cell shape geometry, cell-cell contacts, positive or negative feedback based on neighbours' behaviours, local recruitment or density-driven transitions from disorganized to collective alignment/motion. Emergence of long-range alignments, however, would eventually demand coordinating spatial regularity and topographical information in wide fields: e.g. the presence of physical obstacles or chemical gradients [as in the formation of a single parallel array of fibroblasts or epithelial cells *in vitro* (Reig et al., 2014, Londono et al., 2010)].

During tissue and organ morphogenesis the coming out of a long-range order is subjected to multiple and multilevel developmental constrains. Complex series of temporal and spatial instructions must be integrated to account for reproducible and stereotyped mature tissue arrangements. A remarkable example is given by mature epithelial monolayers were cells are tighter together in specific morphologies via cell-cell adhesions showing highly organized planar patterns.

How the planar pattern of an epithelium is acquired is by no means a simple issue. Different epithelia may obey different rules depending on their origin, growing capabilities (post-mitotic or under active proliferation), multifaceted cellularity, asymmetries and/or identities. In each of them, as well, different layers of regulatory complexity could be involved, acting one on top of another. In particular, both, cell communication and physical/geometrical constrains must match each other tightly and dynamically for successful functional ordering.

Uniform order in an epithelium may arise as a single event in which all cells in response to a systemic signal simultaneously align to each other all around an epithelial field. Alternatively, the ordering process may be generated sequentially by coordinating the behaviour of interconnected short-range ordered groups in time and space. This would be followed by order spreading via information transfer or response to perturbations. These short-range ordered groups could be unique or multiple and be generated stochastically or at fixed positions and/or at specific times within the developing epithelial field.

While the cellular mechanisms influencing the geometry of cell arrangements have been extensively investigated (Hayashi and Carthew, 2004; Classen et al., 2005; Aigouy et al., 2010; Salbreux et al., 2012) little is known on the cellular mechanisms governing the orientation of cell arrangement with the tissue axis. How a common orientation of cell arrangement is reproducibly attained with the tissue axes? Which factors produce the orderly acquisition of the orientation of cell alignment within a monolayer? What type of cellular interaction can account for the uniform orientation of the cell arrangement in a uniaxial direction?

1. The uniform orientation of histoblast along the main A/P axis

The dorsal epithelium of each *Drosophila* abdominal segment is constituted by a mosaic of epidermal cells of elongated form coexisting with rounded bristles precursors. The epidermal histoblasts, upon morphogenesis completion, get uniformly oriented along the main A/P axis, aligning their positions in parallel to the A/P segmental boundary [axial uniform orientation of planar cell alignment (PCA)]. This uniform orientation is not altered by local variations in neighbours' number (packing topology) or the presence of the periodic roundish-shaped bristles populating the adult epithelium. Thus, a regular cell packing such that characterizing, for instance, the wing epithelium (Classen et al., 2005; Aigouy et al., 2010) is not an absolute pre-requisite for uniaxial PCA and, notably, does not explain the uniform orientation of all cells along the A/P axis. Then, how the axis orienting uniform PCA is established?

A dynamic analysis of the ordering process of the abdominal epithelium gives several hints on how uniformity of orientation is set up. The long-range acquisition of order is nor uniform, neither a phenomenon rising up simultaneously throughout the field but tightly spatiotemporally controlled. The initial patchy and irregularly oriented histoblasts tend to align their shapes from locations close to the A/P compartment boundary in each segment. The histoblasts adjacent to this region reorient their axis in a process that initiates as soon as the histoblasts nests start expansion by forming cell arrays of increased local order orienting towards the A/P boundary. This behaviour spreads in a wave-like manner to more anteriorly located cells, to finally mature into a uniform A/P uniaxial orientation of PCA involving every cell of the abdomen.

The attainment of histoblasts PCA orientation uniformity is accompanied by a progressive increase in cells junctional contacts and anisotropy. Coincidental or co-regulated, both events run hand-to-hand in spatial and temporal terms. This gain culminates in the markedly elongated shapes acquired by histoblasts in the mature segment. Is cell elongation a pre-requisite for uniform cell orientation and alignment? Are cell elongation and axis orientation influenced by the geometry of the tissue?

The sequential and directional character of the process of generation of the uniform pattern of cell orientation raises multiple issues. Are segmental boundaries and, particularly the A/P compartment boundary influencing the orientation of PCA? Why PCA orientation get established first at the A/P boundary? Is there any kind of instructive signal emanating from the compartment border? Or just the mechanical stress generated at this precise junction dictate when and where histoblasts will commence to align?

It has been proposed that intersegmental boundaries could act as organizing centres for coordinating cell behaviour in insect segments (Nubler-jung, 1987). A key question is to what extent they act as sources for an oriented long-range organization. The A/P compartment boundary in both the dorsal histoblasts and the wing disc is straight and smooth. Cells at both sides of the compartment boundary have similar shapes and expression levels of E-cadherin and Myosin II but different dynamic behaviour than those elsewhere in the field (Aliee et al., 2012; Landsberg et al., 2009; Major and Irvine, 2006; Monier et al., 2010; Fagotto et al., 2013). Histoblasts at the boundary are more constrained in their movements as a result of increased mechanical tension (Umetsu et al., 2014). However, while in the wing a supracellular cable of Myosin II has been shown (Landsberg et al., 2009) a similar enrichment at the A/P boundary in the abdomen has not been reported (Umetsu et al., 2014). This opens the door to other potential factors, still undefined, that would locally influence cell behaviour at the boundary.

A second issue is how PCA orientation spreads anterior-ward in the A compartment to cover the full landscape. Physical barriers at the anterior and posterior edges of the segments imposed by the inter-segmental boundaries could lead to the local compression of the fused nests at their periphery. This results in the local alignment of histoblast at the most anterior edge of the A compartment and the most posterior edge of the P compartment. However, this ordered alignment of mechanical origin does not spread out. Then, the directional spreading of the ordered territory from the A/P boundary must respond to specific positional signals. Do these correspond to pre-patterned information or does the actual dynamic deformation of the tissue associated to its stereotyped anisotropic growth has any input? This last possibility does not look to be the case as the stereotyped deformations/movements of the histoblast sheet as it expand and accommodate (Ninov et al., 2007; Bischoff and Cseresnyes, 2009) do not correlate with the spatiotemporal pattern of the orientation of PCA.

2. The Ds/Ft/Fj pathway and PCA

The stereotyped spatial and temporal precision observed in the progression towards uniformity of the oriented PCA in every segment and individual, suggests that PCA could be under inherited control. How this could be implemented was unknown.

The Ds/Ft/Fj pathway, known for its roles on tissue growth and planar polarity, has also recently been implicated in the control of tissue shape during the morphogenesis of the imaginal discs. Further, it has been shown that the pathway activity provides axial orientation guidance to a series of developmentally controlled cell behaviours, like cell divisions or rearrangements from early stages of development (Baena-Lopez et al., 2005; Aigouy et al., 2010; Mao et al., 2011; Bosveld et al., 2012; Sagner et al., 2012). We explored the expression patterns and functional characteristics of the different elements composing the pathway and uncovered a direct relationship between its function and the achievement of uniform axial order.

3. Expression pattern dynamics link the Ds/Ft/Fj pathway to the uniform axial orientation of the PCA

We characterized the expression pattern of the Ds/Ft/Fj components in the histoblasts since early stages of pupal development and found that Ds, Ft and Fj were not only early expressed in the histoblasts but that their patterns underwent stereotyped changes within the segmental field. The Ds and Fj opposing gradients along the A/P axis previously observed in the adult (Zeidler et al., 2000; Casal et al., 2004) are evident at the onset of histoblasts expansion. This complementary expression is less clear in the dorsal-most part of the nests where *fj* is kept at high levels up to the time of contralateral nest fusion. Ft, for whom no expression information in the abdomen was available up to now, is, at the initiation of nests expansion heterogeneously expressed. Highest Ft levels were found midway along the A/P axis in the anterior compartment gradually going down anteriorly and posteriorly up to the compartment and segment borders. Its expression was also somehow enriched dorsally (as for *fj*). Remarkably, Ft expression undergoes dramatic changes during expansion and tissue remodelling. Its maximum level of expression progressively gets displaced anteriorly up to a point that it reaches the anterior border of the A compartment. In this way, at steady state, Ft is expressed in a graded fashion from anterior to posterior mimicking the pattern of *fj* and largely opposing the stable gradient of Ds. This graded relative equilibrium between the three components of the pathway at steady state expanding the whole compartment is observed at the time of full axial uniform orientation of PCA (Fig. 85). We found that this relative balance between the pathway components is present early at the most posterior edge of the compartment, close to the A/P boundary, where the axial order is first taking place. This configuration spreads anterior along the A/P axis leading to relative changes in expression of Ds, Ft and Fj that closely parallel, spatial and temporally, the dynamics of the axial orientation of PCA. This suggests that the inherited capacity of the histoblasts to uniformly align to the A/P boundary rely on this pathway.

The Ds/Ft/Fj pathway during the morphogenesis of the abdominal epithelia comply a series of sequential steps involving changes in the expression of its components. These serve for the establishment of a dynamic pre-pattern that would guide the orientation of individual cells all throughout the whole epithelial field. There is no precedent for such a dynamic pre-pattern of the Ds/Ft/Fj pathway in other tissues. Nevertheless, the dynamic activity of the pathway has been recently monitored during wing development in relation with the asymmetries of the Core pathway components (Merkel et al., 2014). Ds and D get asymmetrically localized aligning to the P/D axis respecting the Ds and *fj* gradients in the pupae, while in the larvae their localization is less defined (Merkel et al., 2014). This suggests that the pathway may be also gradually reinforced. Yet, no information is available on a reciprocal dynamic of Ds and Ft expression over time. On the other hand, in the scutellum, the activity of the pathway appears to directly correlate with oriented cell rearrangements (Bosveld et al., 2012). Opposite gradients of Ds and *fj* influence Ds and D polarization but they appear to do so just in the central region of the hemi-scutellum during its remodelling and seem to affect local reorganizations. Again, no information on the expression dynamics of Ft or fj is available in this system.

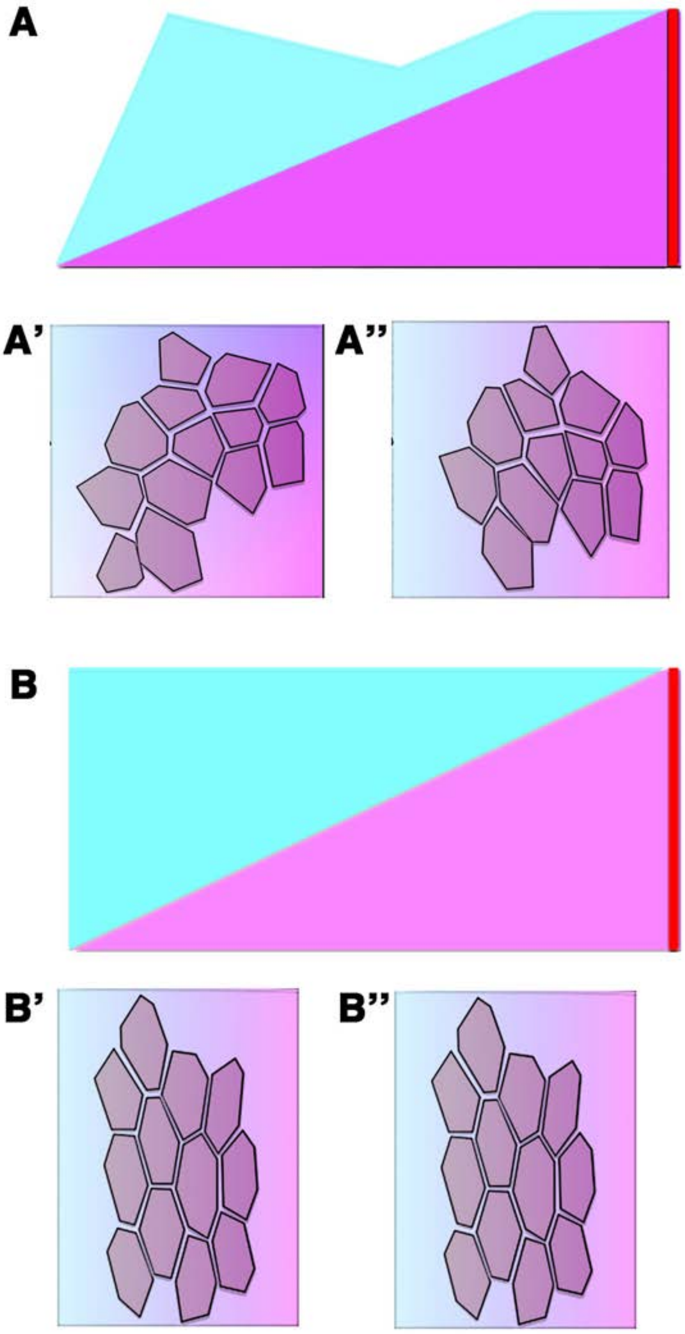

Fig. 85: Changes of Dachsous-Fat reciprocal expression and changes in PCA along the AP axis. Cartoons showing how changes in Ft expression (cyan) relative to Ds gradient (magenta) is related to an increase order in the orientation and strength of PCA in parallel to the AP boundary (red line). **A)** Ds and Ft gradients are not uniformly balanced across the tissue mid-way through histoblast PCA (26 h APF). More differences in reciprocal activity are confined anteriorly, where cells are not yet oriented parallel to A/P (A’) while early balance is attained close to the boundary where cells show early tendency to align parallel to it (A’’). **A)** Ds and Ft gradients are uniformly balanced trough the tissue when PCA is attained (47 h APF). No differences in reciprocal Ds and Ft activities are seen and cell show uniform orientation of PCA parallel to AP; Anterior-most (B’) or region closest to the A/P boundary (B’’) display same axis of orientation and high degree of mutual alignment.

Additionally, we found that, as wing, eye and thoracic cells of *Drosophila* (Ambegaonkar et al., 2012; Brittle et al., 2012; Bosveld et al., 2012; Merkel et al., 2014; Hale et al., 2015), Ds is asymmetrically localized in developing histoblast, pointing down its own gradient. Interestingly, however, conversely to the pupal thoracic scutellum (Bosveld et al., 2012) or the larval imaginal discs of the wing and eye (Brittle et al., 2012; Ambegaonkar et al., 2012), where Ds expression and subcellular asymmetry were found to be stronger in a subdomain of the developing tissues, Ds asymmetry was expressed by all histoblasts and over-time.

Our data indicate that Ds is and remains axial despite extensive proliferation, migration and rearrangements (Ninov et al., 2009; Bischoff and Ceserenyes, 2009; Umetsu et al., 2014) experienced by the histoblasts. This intriguing Ds polarity suggests that its restricted activity in a subset of cell junction could be instrumental to establish an axis for orienting PCA within the segment (Fig. 86).

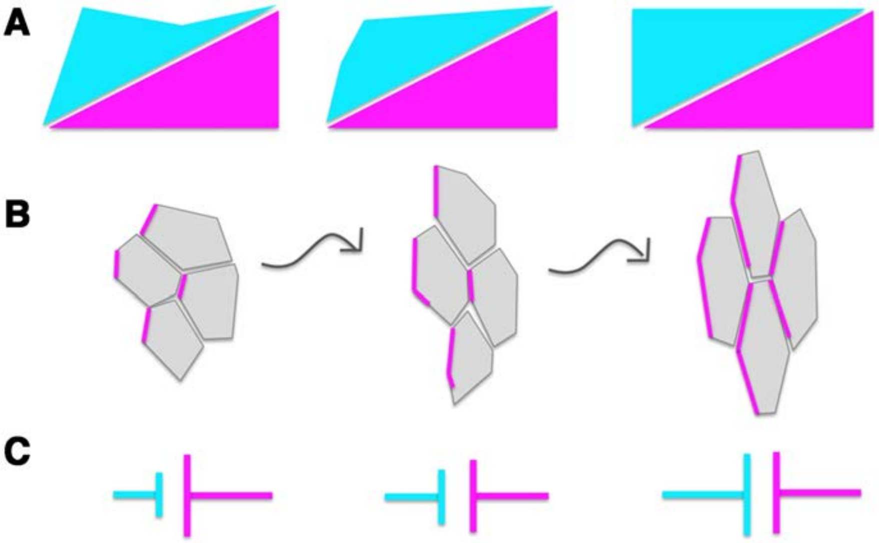

Fig. 86: Localized Ds-Ft interactions and changes in the orientation of PCA and cell shape anisotropy. A) Cartoons showing how the stable gradient of Ds (magenta) influences Ft expression (cyan) dynamic toward a gradient along AP opposed to it. **B)** Ds asymmetry is stable along AP oriented cell contacts and accompanies changes in cell alignment and elongation parallel to AP. **C)** Speculative reinforcement between Ds and Ft mutual interactions Ds and Ft over time. Asymmetry of Ds would promote Ft localization to opposite edges and adhesive interaction between Ds and Ft Cadherins will be reinforced over time. Ft would increasingly stabilize Ds asymmetry as a result of early Ds and Fj inputs onto it. Fj (not shown) cooperates to this process ensuring fidelity in Ds-Ft interaction over time.

Similarly, the atypical myosin D, a direct readout for proper Ds-Ft interaction (Mao et al., 2006; Brittle et al., 2012; Ambegaonkar et al., 2012; Merkel et al., 2014; Bosveld et al., 2012 and 2016), was showing an early tendency to be aligned with the gradient of Ds since early expansion. However, the endogenous levels of D eventually decay over time, while those of Ds, Ft and fj appear to just be remodelled. Decreases in D levels occur also in the pupal wing and in the thorax where endogenous D is expressed at stronger levels in the wing pouch over late LIII or in the scutellum, where appears regionally polarized (Brittle et al., 2012; Bosveld et al, 2012; Legoff et al., 2013). However, no explanation was provided for such a drastic change in D expression levels during normal development. One possibility is that D would be required to stabilize early Ds-Ft interactions, when their activity gradients and intercellular binding would be less stable.

4. The attainment of the uniform orientation of PCA requires the Ds/Ft/Fj pathway

Upon genetic perturbation of Ds, Ft or Fj activities a uniform pattern of PCA did not longer emerge at morphogenesis completion in any case. The uniform axial order of the tissue was somehow aborted in its progression, and multiple cell patches, displaying local alignments whose orientation was no longer related to the tissue axis were left behind. In spite of ordering failure, tissue growth and cell patterning and differentiation were fairly normal, pointing to a dedicated role of the pathway to the coordination of tissue orientation. Globally affecting Ds, Ft and Fj activities throughout the tissue indicates that the influence of the pathway in the orientation of PCA mainly rely on Ds and Ft cadherins. The lack of *fj* affected PCA orientation in a more restricted way in accord to its proposed regulatory role.

However, this analysis did not directly elucidate whether a link between the expression patterns of the pathway components and the uniform orientation of the PCA are axially bound. The main event in terms of expression dynamics linked to the progress of tissue expansion and remodelling is the Ft gradient development. This gradient formation is abolished or severely impaired in mutants for *ds* and *fj*. Ft expression remained heterogeneously expressed throughout most of the segment when Ds activity is perturbed and graded through most of the tissue but truncated at the most anterior end of the A compartment when Fj activity is abolished. As a result, and in a very precise way, PCA axial uniformity was abolished or restricted to those sectors of the compartment where the full configuration of the network was respected. So the exact balance between the components of the pathway at each position is essential for generating long-range order.

The cross-regulatory events between Ds, Ft and fj uncovered in the abdomen have been previously shown in the wing and in the eye imaginal discs, as in the abdomen, where they have been linked to planar polarity control (Yang et al., 2002; Ma et al., 2003; Strutt and Strutt, 2002; Casal et al., 2002).

Several considerations come from our functional analyses. In the absence of Ds/Ft/Fj function local alignment between neighbouring cells are unaffected and seem to spontaneously occur. Instead the pathway would be necessary to explain the emergence of uniform order providing dynamic topographical and temporal guidance. Next, the proposed role of the segmental boundaries as instructive physical constrains for the orientation of the cells (Nubler-jung, 1987) does not seem to hold in the long-range. The phenotype observed in the Ds/Ft/Fj mutants suggests that the influence of the boundary is just local and does not explain the long-range communal orientation of cells in large fields.

5. A cell adhesion code at the base of the establishment of PCA

Reorienting epithelial cells and changing their shapes demands a direct input into surface tension at cell junctions (Kafer et al., 2007; Lecuit and Lenne, 2007). Assuming that cells and tissues tend to minimize their surface free energy (Foty and Steinberg, 2005), the binding of adhesion molecules, causing cells to spread their cell-cell contacts, and the contractile activity of the actomyosin cell cortex counterbalancing adhesive forces, will be key determinants of cell and tissue shapes (Amack and Manning, 2012). Tensile patterns would therefore play instructive roles in the acquisition of long-range morphological order. Prevailing views emphasize the activities of motor proteins and cortex contractility in directing epithelial cell and tissue rearrangements (Lecuit et al., 2011; Heisenberg and Bellaiche, 2013).

In our case, the implementation of axial uniform orientation in response to Ds/Ft/Fj pathway implies that its activity must implement a dynamic topographically precise tensional guidance pattern evolving over time. A relevant candidate fulfilling the properties demanded to deploy such patterned information could be D. Ds and Ft cadherins interact heterophilically across cell interfaces and this interaction modulates the levels and intracellular asymmetry of the atypical myosin D (Matakatsu and Blair 2004; Brittle et al., 2012; Mao et al., 2006; Ambegaonkar et al., 2012; Bosveld et al., 2012 and 2016). D asymmetry has been instrumental to infer Ds/Ft heterodimeric interactions and activity as well as to extract the polarity vector of the Ds/Ft/Fj signalling (Bosveld et al., 2012 and 2016; Merkel et al., 2014; Brittle et al., 2012; Ambegaonkar et al., 2012; Carvajal-Gonzalez and Mlodzik, 2014). Yet, the molecular function of D has not been fully characterized and if it directly promotes contraction has not been evaluated. D influences oriented cell divisions in the centre of the wing where its asymmetry correlate with increase junctional tension that would indirectly orient mitotic spindles with the tissue axis (Mao et al., 2011) even though it seems dispensable for such an influence close to the hinge (Mao et al., 2013; Legoff et al., 2013) where, however, it appears strongly polarized (Brittle et al., 2012). D is also involved in polarized rearrangements in the scutellum in partnership with Ds (Bosveld et al., 2012).

D contractile activity could be at the root of the tensile needs of cell elongation or re-orientation necessary for orienting the PCA. We have found, however, that the subcellular polarization of D in response to the Ds/Ft/Fj pathway occurs very early and is temporally uncoupled of the axial uniform orientation of PCA. D polarized subcellular distribution was largely sustained in *ds* mutants but re-orient alongside the observed changes of cell shapes and orientation, following the PCA rather than instructing its directionality. Further, *d* loss of function in clones in an otherwise *wt* background did not affect the axial orientation of cell alignments (Mao et al., 2006; Mao et al., 2011) or cell shape (Legoff et al., 2013). Therefore, a bias in contractility at the cell cortex that could be generated by the asymmetric distribution of D seems dispensable for uniform PCA orientation. It is thus tempting to propose that the differential adhesion through heterophilic interactions between Ds and Ft may be at the root of the guidance posts employed by histoblasts to axially orient in the long-range. The Ds-Ft oriented adhesiveness would affect the capacity of the cells to change shape and to coordinately orient to maximize cell contacts.

It is known that differential adhesive properties between neighbours prevent cell intermingling. In clones, this lead to borders smoothness (Nardi and Kafatos, 1976; Nubler-Jung and Mardini, 1990; Lawrence et al., 1999) to minimize the contacts between cells that are not alike. Notably, we found that in the developing abdominal epithelia, major differences in roughness, perimeter and, to a lesser extent, on roundness are developed in mutant clones for members of the Ds/Ft/Fj pathway. For each component, the edges of the clones get smoother than for *wt*, particularly for *ft* where the clones were smooth all around their perimeter. Smoothness was also evident for *ds* and *fj,* although in these cases, it showed a directional bias. Smoother edges were found at the mutant clones' borders facing the flank of the A/P axis showing maximum expression of the affected gene: anterior for *fj* and posterior for *ds*. These facts further support the role of the combinatorial adhesive activity of the Ds/Ft/Fj pathway as the tissue proceeds towards the axial uniform orientation of PCA in generating directional information at cell junctions. These directional inputs lead to planar conflicts between cells with different adhesive properties, and these would result in clones with smooth borders at specific edges.

Indeed, we found strong deviations at clones' edges or within clones in mutant conditions from the oriented geometrical bias of *wt* cells at steady state. Contact angles and contact lengths between cells seem to specifically adjust depending on the clonal genotype and the relative location of the clone within the compartments.

In summary, we found that shaping the epithelial landscape during histoblasts expansion mostly respond to an adhesion code mediated by the Ds/Ft/Fj pathway topographically balanced along the A/P axis. During the expansion and remodelling of the abdominal epithelia, the expression pattern of Ft modulated by Ds and *fj* evolves into an A/P gradient spanning whole compartments. This expression refinement will result in the spreading, all over the epithelia, of a counterbalanced adhesion share between Ft and Ds that will delineate an axially oriented surface tension landscape instructive for PCA orientation. The most precocious areas to orient, which are located at the posterior edge of the A compartment would correspond to those domains where the compensated Ft A/P gradient originates. The directional cues dictated by the pathway put the epithelial cells on the right track, orienting their changing shapes. Cell aligning orientation would then proceed anterior along the body axis following the spreading of the tissue-wide Ft gradient.

6. Ds, Ft and Fj modulate cell-cell contact alignments and influence cell shape anisotropy

How is the axially directed uniform orientation of PCA implemented at cellular level? Shaping tissues may involve many different cellular and molecular activities. Coordinated cell-cell rearrangements, including cellular reallocations or neighbours exchanges, trigger tissue re-orientation (Aigouy et al., 2010; Suzanne et al., 2010) but can also lead to convergent extension (Keller, 2006). Alternatively, the apical constriction of epithelial cells may direct local bending of epithelial sheets (Pilot and Lecuit, 2005). Further, spatially controlled cell proliferation and growth, cell division orientation, and cell death can also give rise to global tissue changes (Hopyan et al., 2011; Mao et al., 2013; Campinho et al., 2013; Legoff et al., 2013). Together with the dramatic loss of uniform orientation of PCA we have found that *ds, ft* and *fj* mutant cells have reduced cell shape anisotropy. Such outcome suggests, considering the adhesive role of these cadherins, that missing or compromised Ds-Ft heterodimeric interactions may influence the strength of oriented cell-cell contacts and cells elongation. The tendency of histoblasts to elongate is a specific morphological characteristic of this epithelium. In other epithelia, such as the wing discs, the cells display only transient and regional elongations finally converging into a honeycomb-like pattern of isodiametric polygons (Classen et al., 2005; Aigouy et al., 2010).

Intriguingly, cell shape anisotropy in histoblasts appears to respond to the level of the pathway activity, while orientation of PCA seems to more dependent on gradient orientation as the different outcomes generated by Ds overexpression and *ds* loss of function suggest. Thus, a biunivocal relationship between cell anisotropy and PCA orientation does not hold. Even considering that changes in cell elongation are associated to, and may be necessary for the establishment of the axial uniform orientation of the PCA, they are not sufficient. Some other cellular character or behaviour must be taken in consideration during the uniform order acquisition of the epithelia.

During the expansion and remodelling of the abdominal epithelia, cell divisions are not spatially biased, as they are not cell division orientations either. The number of cell divisions decay during the remodelling period stopping completely half way into this stage, but not following any particular spatial pattern. Cell deaths are essentially anecdotic within the epithelial territory (Bischoff and Csereneyes, 2009) and differential growth cannot be distinguished between cells of distinct sectors or at different times. Last, cells D/V elongation is implemented quite uniformly except at the dorsal and ventral edges of the compartment where physical constrains do impede anisotropic cell changes. None of these parameters appear to be greatly affected (except clone area for *ft*) in clones for mutants of the different components of the pathway, where PCA was affected within (autonomously) and outside (non-autonomously) of the clone. In these clones, however, we noticed that several shape parameters were altered in mutant conditions. In particular, the capacity of cell intermingling was locally reduced indicating that, through time, the mutant cells minimized the contacts with the surrounding tissue in which the activity of the pathway was not perturbed. This effect was particularly pronounced throughout the A compartment in the posterior side of *ds* clones and all around *ft* clones. Clones lacking *fj* showed more pronounced contact minimization in the anterior side but such effect was somehow locally restricted to the antero-central domain of the anterior compartment. This directional behaviour was observed for *ds* and *fj* at the opposite side in which planar polarities defects were previously reported (Casal et al., 2002). No directional effect was found in terms of contact minimization for *ft*, for which planar polarity defects were reported in the posterior side (Casal et al., 2002). Notably, despite it has been shown that ds and ft have opposite non-autonomous effects in the A compartment of the abdomen (Casal et al., 2002) ft-ds double mutant clones do not display any clear non-autonomous effect in the polarity of the surrounding cells (Casal et al., 2006). It has been concluded that Ft and Ds are functionally equivalent for the propagation of planar polarity and that the lack of one would be compensated by surrounding *wt* cells (Casal et al., 2006). However our data clearly indicate that the action of Ds and Ft in orienting PCA, and indirectly PCP, is not equivalent, indicating that Ft is acting autonomously, at lest in PCA.

Furthermore, the fact that cell alignment and Ds-Ft trans-binding were recue all around *ft*, as well as the Ds-Ft interaction (*i.e.* D asymmetry), suggest that restored oriented alignment along AP is under the influence of Ds activity (Fig. 87).

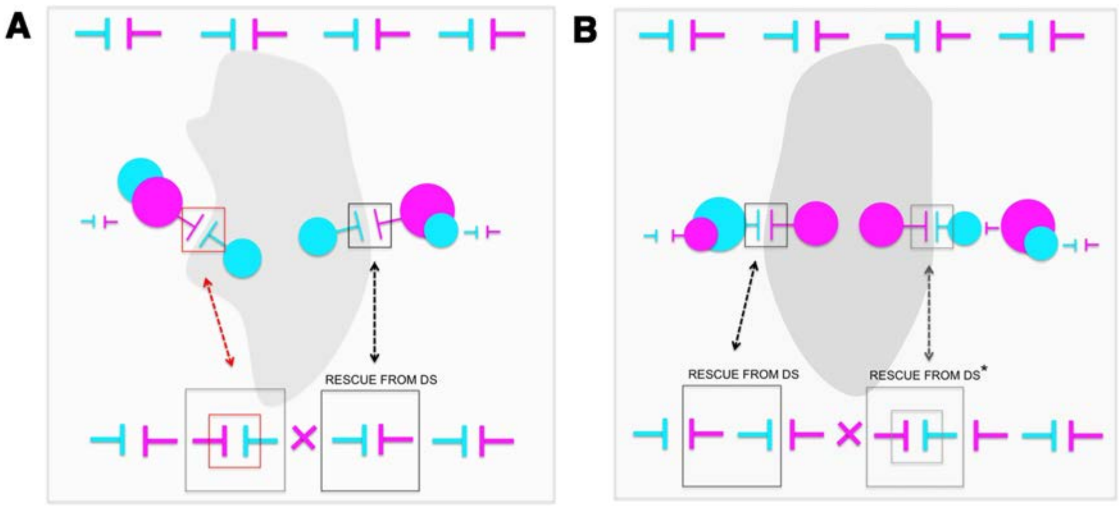

Fig. 87: The rescue of cell alignment in clones is mediated by Ds. A) Cartoons showing Ds (magenta) and Ft (cyan) interaction within, outside and at the boundary of a *ds* mutant clone. **B)** Cartoons showing Ds (magenta) and Ft (cyan) interaction within, outside and at the boundary of a *ft* mutant clone. Note that the directional activity of Ds is changed on *wt* cells facing the anterior side of a *ds* clones and within the posterior side of *ft* mutant clones. Asterisk indicates that, despite the rescue of alignment, D asymmetry and, occasionally, trichome polarity can be reversed. Within the *ds* mutant clone (A), the Ft cadherin is deprived of its binding partner. The available Ds for binding would come from the *wt* cells. On the posterior side of *ds* clones the alternated presence of Ds and Ft along A/P oriented cell interfaces remained intact. When *wt* cells face the posterior side of the clone, Ds outside would selectively recruit Ft from inside the clone to the opposite edge. However such propagation would be not able to extend inwards since no, or very little Ds is present. At the anterior side of the clone, Ft within the clone would be recruited by Ds, even though Ft is also present outside of the clone. In this scenario, Ds would bind Ft less efficiently, impinging on Ft-Ds heterodimeric interaction.

Within the *ft* mutant clone (B) the Ds cadherin is deprived of its binding partner. The available Ft for binding would come from the *wt* cells. On the posterior side of *ft* clones the alternated presence of Ds and Ft along A/P oriented cell interfaces remained intact up to the point at which the *wt* cells abut the clone border. Here Ft would be influenced by Ds from inside and outside the clone. Such input, however, would not propagate inward since no or very little Ft will be present. At the anterior side of the clone, Ds within the clone would recruit Ft from outside. In this scenario, Ds would bind Ft less efficiently, impinging on the Ft-Ds heterodimeric interaction.

We found that D was elevated within and at the boundary of *ft* clones, and, despite its high levels, D polarization was rescues all around the clone. This finding suggests that the rescue of the alignment is due to restored Ds-Ft heterodimeric interaction mediated by Ds (B). The absence of rescue in contact length suggests instead that Ds-Ft interaction strength is less stable than in wt cells, possibly due to differential expression levels at the clone boundary.

7. Does cells/tissue growth (the Hippo pathway) influence PCA orientation?

As just discussed, proliferation rates or cell divisions orientations appear to be unrelated to the process of tissue ordering associated to the morphogenesis of the abdominal epithelia. We also know that, in general, these parameters are unaffected when interfering in the Ds/Ft/Fj pathway. However, clones of cells mutant for *ft*, which loss their ability to extensively interact with *wt* cells, are also much bigger than controls, suggesting a role of Ft in growth regulation.

With the aim to investigate the potential influence that cell growth could have in the axial orientation of PCA, we have explored, both at the expression and functional level the activity of the Hippo pathway. However, while we found an enhanced expression of *diap1* in actively expanding cells at the edges of the histoblast nests and an intriguing expression of Yki and *diap1* in a particular cell of the SOP lineage later on, no indications of a role of the Hippo Kinase in proliferation have been found in the abdomen.

Along the consequences of inactivating of *yki* in clones in imaginal discs, which affects growth and survival autonomously (Huang et al., 2005), yki clones in the abdomen were highly fragmented and irregular and seem to be smaller than twins. Still, the overexpression of Yki did not lead to overgrowths but somehow prevent apoptosis of the larval epithelial cells. *hpo* mutants in clones do not lead to any growth defect. Thus, it is extremely unlikely that the Hippo pathway would have any input in cells alignment orientations. Growth still could have and impact, but our own data genetically accelerating the cell cycle by overexpressing simultaneously String and Cyclin E with no influence in ordering appear to discard this possibility.

8. The Ds/Ft/Fj pathway inputs in PCA and PCP

In the abdominal epidermis it has been genetically demonstrated that the Core and the Ds/Ft/Fj pathway have their own inputs in planar polarity (Casal et al., 2006; Lawrence et al., 2004). However the nature of the input of the Ds/Ft/Fj pathway in planar polarity remain largely mysterious.

In the adult abdominal epithelia, the planar polarity of individual histoblast is manifested in oriented cytoskeletal protrusions that in *wt* individuals always point posteriorly.

In this sense, PCP and PCA orientations are fully orthogonal all throughout the epithelial field. Both, the cell junctions and the trichomes organize in multiple rows uniformly oriented but perpendicular to each other.

Importantly, the first sign of trichomes growth is observed well beyond the time at which the axial uniform orientation of the PCA has been accomplished. Thus, the direction of cell alignment anticipates the orientation of cell polarity. In this way, mutant conditions for the components of the Ds/Ft/Fj pathway reveal that, irrespectively of the orientation of cell junctions, the trichomes directionality always orthogonally correlates with the cell longer axis. This cross relation is maintained even in the full absence of a functional pathway: e.g. *ds* and also *ft* cells retain their capacity to secrete trichomes and to polarize in the plane despite the absence of uniform PCA. In these mutant conditions, the trichomes polarity always respect the alignments sustained between neighbours, generating in many cases swirling patterns correlative to the maintenance of local groups of commonly oriented cells. We propose that the Ds/Ft/Fj pathway specifically controls the axis orientation of PCA and, indirectly, the orientation of PCP.

Yet, a role of the Ds/Ft/Fj pathway in PCP modulation cannot be fully discarded. It has been described that Ds modulates microtubule plus ends orientation in the pupal wing (Harumoto et al., 2010). Whether microtubules dynamics would lay upstream or downstream of Ds activity remains unclear. A speculative possibility would be that the orientation of the cortical microtubules may be altered as a consequence of misalignments in the orientation of PCA in the wing. This is a scenario that would deserve to be tested.

We found weak signs of asymmetry in Stbm localization during early histoblasts expansion. This polarization was never consistently oriented at this time. Just prior trichome eversion, however, Stbm could be found at all anteriorly oriented cell interfaces. Other members of the pathway have not been assessed. Remarkably, this scenario resembles the wing development. Here, Core components such as Stbm, Fz or Pk start showing signs of polarized localization from late larval stages (Classen et al., 2005; Sagner et al., 2012; Merkel et al., 2014). These asymmetries become more robust with time during the pupal period preferentially orienting toward the P/D axis following the morphogenetic movements that shape the wing (Aigouy et al., 2010; Merkel et al., 2014). It has been thus suggested that a cross talk may occur between the two pathways over the developmental course of pupation in the pupal wing (Merkel et al., 2014). Our data do not let to rule out an equivalent process, even if no signs of re-orientation where seen, at least with Stbm,

Intriguingly we found that the abnormal planar polarity orientation with the tissue axis was largely due to the altered axial cell arrangement within the plane of the abdominal epithelium.

The connection between the altered trichome polarity and the effect on the cell packing topology is unclear. It has been shown that the alteration in cell packing topology did not disturb planar polarity in the wing. Despite in Core mutants the honeycomb like pattern of the mature wing is disturbed by an increased fraction of non-hexagonal cells, trichomes orientation is not disturbed (Classen et al., 2005). In contrast, it was later proposed that local alterations of Ft activity in the pupal wing influenced trichomes polarity orientations by changes in cell packing topology (Ma et al., 2008). In light with our findings this apparent discrepancy could be potentially resolved by the observed phenotype of Ds/Ft/Fj in the abdomen. Changes in the orientation of cell packing rather than cell packing geometry *per se*, would affect the orientation of planar polarity. Possibly, the isodiametric wing cells may let any possible axial changes at the time of hair secretion hidden. It would be interesting to test this possibility again in light of our findings. However, no axial changes in cell topology have been yet reported in the wing.

9. Concluding Remarks

We have uncovered a new role for the Ds/Ft/Fj pathway implementing the uniform orientation of the planar alignment of histoblasts (PCA) in the epithelial field. The directional evolution of the expression of the different Ds/Ft/Fj pathway elements sets up a spatially and temporally controlled differential adhesion code between Ds and Ft. Differential adhesion imposed by Ds-Ft heterodimeric interaction at opposite edges of the cell perimeter would create a directional boundary to which the cell would align changing and orienting its shape. Over time this biased interaction responding to the Ds gradient would be reinforced in response to the activity of Ds and Fj onto Ft. This reinforcement would lead to orient the localization of Ft gradient as opposed to Ds. Cell shape changes and cell intermingling will ultimately guide the orientation of the long-range alignment of the epithelial cells

The developmentally controlled widespread local oriented coupling between Ds and Ft throughout morphogenesis will establish finely tuned adhesive contacts respecting the directionality of the expression gradients that will promote the cells “axialized” alignment. Whether this oriented input of the pathway may constitute a new universal mechanism for directional morphogenesis remains to be determined.

Conclusions

1. Upon morphogenesis completion, steady state abdominal epithelial cells display a uniform orientation of planar cell alignment (PCA) and pronounced cell shape anisotropy in parallel to the AP axis;

2. Cell-cell interactions are progressively oriented and gradually maximized in parallel to the A/P boundary from Posterior-to-Anterior within the segment;

3. The dynamic expression and axial activity of the Ds/Ft/Fj pathway along the AP axis resolves in the establishment of opposing gradients for Fj and Ft with Ds that expand full compartments from Posterior-to-Anterior;

4. Opposing gradients for Fj and Ft with Ds spatially and temporally correlate with uniform orientation of PCA.

5. The Ds/Ft/Fj pathway is essential for a uniform PCA to emerge but is largely dispensable for the autonomous expression of planar polarity;

6. An internal regulatory crosstalk within the Ds/Ft/Fj pathway directs the establishment of the axial Ft gradient and the attainment of the uniform orientation of the PCA;

7. Ds expression gradient and subcellular asymmetry are robustly oriented in parallel to the AP axis throughout abdominal morphogenesis;

8. Ds activity has an instructive role in the orientation of PCA through Ft;

9. D expression levels and subcellular asymmetry are modulated by both Ds and Ft and spatiotemporally correlate with an increased stability in Ds-Ft interaction across the tissue;

10. A cell adhesion code implemented by the heterodimeric interactions of Ds and Ft cadherins directs the cellular dynamics associated to the establishment of axial uniform orientation of PCA;

11. The regulation of Yki activity appears to be independent on the Hippo Kinase during histoblast growth and an input of Yki and Hpo on the orientation of PCA seems unlikely.

Bibliography

Abbott, L. A. and Lindenmayer, A. (1981). Models for growth of clones in hexagonal cell arrangements: applications in Drosophila wing disc epithelia and plant epidermal tissues. *J Theor Biol* **90**, 495-514.

Adler, P. N. (2002). Planar signaling and morphogenesis in Drosophila. *Dev Cell* **2**, 525-535.

Adler, P. N. (2012). The frizzled/stan pathway and planar cell polarity in the Drosophila wing. *Current topics in developmental biology* **101**, 1-31.

Adler, P. N., Charlton, J. and Liu, J. (1998). Mutations in the cadherin superfamily member gene dachsous cause a tissue polarity phenotype by altering frizzled signaling. *Development* **125**, 959-968.

Aigouy, B., Farhadifar, R., Staple, D. B., Sagner, A., Roper, J. C., Julicher, F. and Eaton, S. (2010). Cell flow reorients the axis of planar polarity in the wing epithelium of Drosophila. *Cell* **142**, 773-786.

Aliee, M., Roper, J. C., Landsberg, K. P., Pentzold, C., Widmann, T. J., Julicher, F. and Dahmann, C. (2012). Physical mechanisms shaping the Drosophila dorsoventral compartment boundary. *Curr Biol* **22**, 967-976.

Amack, J. D. and Manning, M. L. (2012). Knowing the boundaries: extending the differential adhesion hypothesis in embryonic cell sorting. *Science* **338**, 212-215.

Ambegaonkar, A. A., Pan, G., Mani, M., Feng, Y. and Irvine, K. D. (2012). Propagation of Dachsous-Fat planar cell polarity. *Curr Biol* **22**, 1302-1308.

Ashburner, M., Golic, K. G. and Hawley, R. S. (2005). *Drosophila: a laboratory handbook. Second edition.*

Axelrod, J. D. (2001). Unipolar membrane association of Dishevelled mediates Frizzled planar cell polarity signaling. *Genes Dev* **15**, 1182-1187.

Badouel, C., Gardano, L., Amin, N., Garg, A., Rosenfeld, R., Le Bihan, T. and McNeill, H. (2009). The FERM-domain protein Expanded regulates Hippo pathway activity via direct interactions with the transcriptional activator Yorkie. *Dev Cell* **16**, 411-420.

Baena-Lopez, L. A., Baonza, A. and Garcia-Bellido, A. (2005). The orientation of cell divisions determines the shape of Drosophila organs. *Curr Biol* **15**, 1640-1644.

Bainbridge, S. P. and Bownes, M. (1981). Staging the metamorphosis of Drosophila melanogaster. *J Embryol Exp Morphol* **66**, 57-80.

Bastock, R., Strutt, H. and Strutt, D. (2003). Strabismus is asymmetrically localised and binds to Prickle and Dishevelled during Drosophila planar polarity patterning. *Development* **130**, 3007-3014.

Bennett, F. C. and Harvey, K. F. (2006). Fat cadherin modulates organ size in Drosophila via the Salvador/Warts/Hippo signaling pathway. *Curr Biol* **16**, 2101-2110.

Bergstralh, D. T. and St Johnston, D. (2012). Epithelial cell polarity: what flies can teach us about cancer. *Essays Biochem* **53**, 129-140.

Bertet, C., Sulak, L. and Lecuit, T. (2004). Myosin-dependent junction remodelling controls planar cell intercalation and axis elongation. *Nature* **429**, 667-671.

Bilder, D., Li, M. and Perrimon, N. (2000). Cooperative regulation of cell polarity and growth by Drosophila tumor suppressors. *Science* **289**, 113-116.

Bilder, D. and Perrimon, N. (2000). Localization of apical epithelial determinants by the basolateral PDZ protein Scribble. *Nature* **403**, 676-680.

Bischoff, M. and Cseresnyes, Z. (2009). Cell rearrangements, cell divisions and cell death in a migrating epithelial sheet in the abdomen of Drosophila. *Development* **136**, 2403-2411.

Blankenship, J. T., Backovic, S. T., Sanny, J. S., Weitz, O. and Zallen, J. A. (2006). Multicellular rosette formation links planar cell polarity to tissue morphogenesis. *Dev Cell* **11**, 459-470.

Bodenstein, D. (1950). The postembryonic development of Drosophila. *Biology of Drosophila.*, 275-367.

Booth, A. J., Blanchard, G. B., Adams, R. J. and Roper, K. (2014). A dynamic microtubule cytoskeleton directs medial actomyosin function during tube formation. *Dev Cell* **29**, 562-576.

Bosveld, F., Bonnet, I., Guirao, B., Tlili, S., Wang, Z., Petitalot, A., Marchand, R., Bardet, P. L., Marcq, P., Graner, F., et al. (2012). Mechanical control of morphogenesis by Fat/Dachsous/Four-jointed planar cell polarity pathway. *Science* **336**, 724-727.

Bosveld, F., Guirao, B., Wang, Z., Riviere, M., Bonnet, I., Graner, F. and Bellaiche, Y. (2016). Modulation of junction tension by tumor suppressors and proto-oncogenes regulates cell-cell contacts. *Development* **143**, 623-634.

Brand, A. H. and Perrimon, N. (1993). Targeted gene expression as a means of altering cell fates and generating dominant phenotypes. *Development* **118**, 401-415.

Brittle, A., Thomas, C. and Strutt, D. (2012). Planar polarity specification through asymmetric subcellular localization of Fat and Dachsous. *Curr Biol* **22**, 907-914.

Brittle, A. L., Repiso, A., Casal, J., Lawrence, P. A. and Strutt, D. (2010). Four-jointed modulates growth and planar polarity by reducing the affinity of dachsous for fat. *Curr Biol* **20**, 803-810.

Brodsky, M. H. and Steller, H. (1996). Positional information along the dorsal-ventral axis of the Drosophila eye: graded expression of the four-jointed gene. *Dev Biol* **173**, 428-446.

Bryant, P. J., Huettner, B., Held, L. I., Jr., Ryerse, J. and Szidonya, J. (1988). Mutations at the fat locus interfere with cell proliferation control and epithelial morphogenesis in Drosophila. *Dev Biol* **129**, 541-554.

Calleja, M., Herranz, H., Estella, C., Casal, J., Lawrence, P., Simpson, P. and Morata, G. (2000). Generation of medial and lateral dorsal body domains by the pannier gene of Drosophila. *Development* **127**, 3971-3980.

Campinho, P., Behrndt, M., Ranft, J., Risler, T., Minc, N. and Heisenberg, C. P. (2013). Tension-oriented cell divisions limit anisotropic tissue tension in epithelial spreading during zebrafish epiboly. *Nat Cell Biol* **15**, 1405-1414.

Carthew, R. W. (2005). Adhesion proteins and the control of cell shape. *Current opinion in genetics & development* **15**, 358-363.

Carvajal-Gonzalez, J. M. and Mlodzik, M. (2014). Mechanisms of planar cell polarity establishment in Drosophila. *F1000Prime Rep* **6**, 98.

Casal, J., Lawrence, P. A. and Struhl, G. (2006). Two separate molecular systems, Dachsous/Fat and Starry night/Frizzled, act independently to confer planar cell polarity. *Development* **133**, 4561-4572.

Casal, J., Struhl, G. and Lawrence, P. A. (2002). Developmental compartments and planar polarity in Drosophila. *Curr Biol* **12**, 1189-1198.

Chacon-Heszele, M. F., Ren, D., Reynolds, A. B., Chi, F. and Chen, P. (2012). Regulation of cochlear convergent extension by the vertebrate planar cell polarity pathway is dependent on p120-catenin. *Development* **139**, 968-978.

Chen, C., Jack, J. and Garofalo, R. S. (1996a). The Drosophila insulin receptor is required for normal growth. *Endocrinology* **137**, 846-856.

Chen, W. S., Antic, D., Matis, M., Logan, C. Y., Povelones, M., Anderson, G. A., Nusse, R. and Axelrod, J. D. (2008). Asymmetric homotypic interactions of the atypical cadherin flamingo mediate intercellular polarity signaling. *Cell* **133**, 1093-1105.

Chen, Y., Chafin, D., Price, D. H. and Greenleaf, A. L. (1996b). Drosophila RNA polymerase II mutants that affect transcription elongation. *J Biol Chem* **271**, 5993-5999.

Chen, Y. and Struhl, G. (1996). Dual roles for patched in sequestering and transducing Hedgehog. *Cell* **87**, 553-563.

Cho, E., Feng, Y., Rauskolb, C., Maitra, S., Fehon, R. and Irvine, K. D. (2006). Delineation of a Fat tumor suppressor pathway. *Nat Genet* **38**, 1142-1150.

Cho, E. and Irvine, K. D. (2004). Action of fat, four-jointed, dachsous and dachs in distal-to-proximal wing signaling. *Development* **131**, 4489-4500.

Clark, H. F., Brentrup, D., Schneitz, K., Bieber, A., Goodman, C. and Noll, M. (1995). Dachsous encodes a member of the cadherin superfamily that controls imaginal disc morphogenesis in Drosophila. *Genes Dev* **9**, 1530-1542.

Classen, A. K., Anderson, K. I., Marois, E. and Eaton, S. (2005). Hexagonal packing of Drosophila wing epithelial cells by the planar cell polarity pathway. *Dev Cell* **9**, 805-817.

Collinet, C. and Lecuit, T. (2013). Stability and dynamics of cell-cell junctions. *Progress in molecular biology and translational science* **116**, 25-47.

Collu, G. M. and Mlodzik, M. (2015). Planar polarity: converting a morphogen gradient into cellular polarity. *Curr Biol* **25**, R372-374.

Cove, D. J. (2000). The generation and modification of cell polarity. *J Exp Bot* **51**, 831-838.

Curtin, J. A., Quint, E., Tsipouri, V., Arkell, R. M., Cattanach, B., Copp, A. J., Henderson, D. J., Spurr, N., Stanier, P., Fisher, E. M., et al. (2003). Mutation of Celsr1 disrupts planar polarity of inner ear hair cells and causes severe neural tube defects in the mouse. *Curr Biol* **13**, 1129-1133.

Das, G., Jenny, A., Klein, T. J., Eaton, S. and Mlodzik, M. (2004). Diego interacts with Prickle and Strabismus/Van Gogh to localize planar cell polarity complexes. *Development* **131**, 4467-4476.

Davidson, L. A. (2012a). Epithelial machines that shape the embryo. *Trends Cell Biol* **22**, 82-87.

Davidson, L. A. (2012b). No strings attached: new insights into epithelial morphogenesis. *BMC biology* **10**, 105.

Dogic, Z., Sharma, P. and Zakhary, M. J. (2014). Hypercomplex Liquid Crystals. *Annual Review of Condensed Matter Physics* **5**, 137-157.

Dong, J., Feldmann, G., Huang, J., Wu, S., Zhang, N., Comerford, S. A., Gayyed, M. F., Anders, R. A., Maitra, A. and Pan, D. (2007). Elucidation of a universal size-control mechanism in Drosophila and mammals. *Cell* **130**, 1120-1133.

Elliott, D. A. and Brand, A. H. (2008). The GAL4 system : a versatile system for the expression of genes. *Methods Mol Biol* **420**, 79-95.

Elsdale, T. and Bard, J. (1972). Cellular interactions in mass cultures of human diploid fibroblasts. *Nature* **236**, 152-155.

Elsdale, T., Pearson, M. and Whitehead, M. (1976). Abnormalities in somite segmentation following heat shock to Xenopus embryos. *J Embryol Exp Morphol* **35**, 625-635.

Fabre, C. C., Casal, J. and Lawrence, P. A. (2010). Mechanosensilla in the adult abdomen of Drosophila: engrailed and slit help to corral the peripheral sensory axons into segmental bundles. *Development* **137**, 2885-2894.

Fagotto, F. (2014). The cellular basis of tissue separation. *Development* **141**, 3303-3318.

Fagotto, F., Rohani, N., Touret, A. S. and Li, R. (2013). A molecular base for cell sorting at embryonic boundaries: contact inhibition of cadherin adhesion by ephrin/ Eph-dependent contractility. *Dev Cell* **27**, 72-87.

Fanto, M., Clayton, L., Meredith, J., Hardiman, K., Charroux, B., Kerridge, S. and McNeill, H. (2003). The tumor-suppressor and cell adhesion molecule Fat controls planar polarity via physical interactions with Atrophin, a transcriptional co-repressor. *Development* **130**, 763-774.

Feng, Y. and Irvine, K. D. (2009). Processing and phosphorylation of the Fat receptor. *Proc Natl Acad Sci U S A* **106**, 11989-11994.

Fichelson, P. and Gho, M. (2003). The glial cell undergoes apoptosis in the microchaete lineage of Drosophila. *Development* **130**, 123-133.

Fonck, E., Feigl, G. G., Fasel, J., Sage, D., Unser, M., Rufenacht, D. A. and Stergiopulos, N. (2009). Effect of aging on elastin functionality in human cerebral arteries. *Stroke* **40**, 2552-2556.

Franke, W. W. (2009). Discovering the molecular components of intercellular junctions--a historical view. *Cold Spring Harb Perspect Biol* **1**, a003061.

Fristrom, D. (1988). The cellular basis of epithelial morphogenesis. A review. *Tissue & cell* **20**, 645-690.

Fristrom, D. K. and Fristrom, J. W. (1993). The metamorphic development of the adult epidermis. pp. 843-897.

Fukata, M. and Kaibuchi, K. (2001). Rho-family GTPases in cadherin-mediated cell-cell adhesion. *Nature reviews. Molecular cell biology* **2**, 887-897.

Fuse, N., Hirose, S. and Hayashi, S. (1994). Diploidy of Drosophila imaginal cells is maintained by a transcriptional repressor encoded by escargot. *Genes Dev* **8**, 2270-2281.

Gao, B. (2012). Wnt regulation of planar cell polarity (PCP). *Current topics in developmental biology* **101**, 263-295.

Garcia-Bellido, A. and Merriam, J. R. (1971). Clonal parameters of tergite development in Drosophila. *Dev Biol* **26**, 264-276.

Garoia, F., Guerra, D., Pezzoli, M. C., Lopez-Varea, A., Cavicchi, S. and Garcia-Bellido, A. (2000). Cell behaviour of Drosophila fat cadherin mutations in wing development. *Mech Dev* **94**, 95-109.

Gemp, I. M., Carthew, R. W. and Hilgenfeldt, S. (2011). Cadherin-dependent cell morphology in an epithelium: constructing a quantitative dynamical model. *PLoS Comput Biol* **7**, e1002115.

Genevet, A., Polesello, C., Blight, K., Robertson, F., Collinson, L. M., Pichaud, F. and Tapon, N. (2009). The Hippo pathway regulates apical-domain size independently of its growth-control function. *J Cell Sci* **122**, 2360-2370.

Genevet, A. and Tapon, N. (2011). The Hippo pathway and apico-basal cell polarity. *The Biochemical journal* **436**, 213-224.

Giardina, I. (2008). Collective behavior in animal groups: theoretical models and empirical studies. *HFSP J* **2**, 205-219.

Gibson, M. C., Patel, A. B., Nagpal, R. and Perrimon, N. (2006). The emergence of geometric order in proliferating metazoan epithelia. *Nature* **442**, 1038-1041.

Golic, K. G. and Lindquist, S. (1989). The FLP recombinase of yeast catalyzes site-specific recombination in the Drosophila genome. *Cell* **59**, 499-509.

Goodrich, L. V. and Strutt, D. (2011). Principles of planar polarity in animal development. *Development* **138**, 1877-1892.

Goulev, Y., Fauny, J. D., Gonzalez-Marti, B., Flagiello, D., Silber, J. and Zider, A. (2008). SCALLOPED interacts with YORKIE, the nuclear effector of the hippo tumor-suppressor pathway in Drosophila. *Curr Biol* **18**, 435-441.

Gray, R. S., Roszko, I. and Solnica-Krezel, L. (2011). Planar cell polarity: coordinating morphogenetic cell behaviors with embryonic polarity. *Dev Cell* **21**, 120-133.

Gubb, D. and Garcia-Bellido, A. (1982). A genetic analysis of the determination of cuticular polarity during development in Drosophila melanogaster. *J Embryol Exp Morphol* **68**, 37-57.

Guerra, M., Postlethwait, J. H. and Schneiderman, H. A. (1973). The development of the imaginal abdomen of Drosophila melanogaster. *Dev Biol* **32**, 361-372.

Gumbiner, B. M. (2000). Regulation of cadherin adhesive activity. *The Journal of cell biology* **148**, 399-404.

Halder, G. and Johnson, R. L. (2011). Hippo signaling: growth control and beyond. *Development* **138**, 9-22.

Hale, R., Brittle, A. L., Fisher, K. H., Monk, N. A. and Strutt, D. (2015). Cellular interpretation of the long-range gradient of Four-jointed activity in the Drosophila wing. *Elife* **4**.

Hale, R. and Strutt, D. (2015). Conservation of Planar Polarity Pathway Function Across the Animal Kingdom. *Annual review of genetics* **49**, 529-551.

Hammer, Ø., Harper, D. and Ryan, P. (2001). PAST: Paleontological Statistics Software Package for education and data analysis. Palaeontolia Electronica 4.

Hansen, C. G., Moroishi, T. and Guan, K. L. (2015). YAP and TAZ: a nexus for Hippo signaling and beyond. *Trends Cell Biol* **25**, 499-513.

Harumoto, T., Ito, M., Shimada, Y., Kobayashi, T. J., Ueda, H. R., Lu, B. and Uemura, T. (2010). Atypical cadherins Dachsous and Fat control dynamics of noncentrosomal microtubules in planar cell polarity. *Dev Cell* **19**, 389-401.

Harvey, K. F., Pfleger, C. M. and Hariharan, I. K. (2003). The Drosophila Mst ortholog, hippo, restricts growth and cell proliferation and promotes apoptosis. *Cell* **114**, 457-467.

Hayashi, S., Hirose, S., Metcalfe, T. and Shirras, A. D. (1993). Control of imaginal cell development by the escargot gene of Drosophila. *Development* **118**, 105-115.

Hayashi, T. and Carthew, R. W. (2004). Surface mechanics mediate pattern formation in the developing retina. *Nature* **431**, 647-652.

Heisenberg, C. P. and Bellaiche, Y. (2013). Forces in tissue morphogenesis and patterning. *Cell* **153**, 948-962.

Hopyan, S., Sharpe, J. and Yang, Y. (2011). Budding behaviors: Growth of the limb as a model of morphogenesis. *Dev Dyn* **240**, 1054-1062.

Huang, J., Wu, S., Barrera, J., Matthews, K. and Pan, D. (2005). The Hippo signaling pathway coordinately regulates cell proliferation and apoptosis by inactivating Yorkie, the Drosophila Homolog of YAP. *Cell* **122**, 421-434.

Huber, F., Boire, A., Lopez, M. P. and Koenderink, G. H. (2015). Cytoskeletal crosstalk: when three different personalities team up. *Curr Opin Cell Biol* **32**, 39-47.

Irvine, K. D. and Wieschaus, E. (1994). Cell intercalation during Drosophila germband extension and its regulation by pair-rule segmentation genes. *Development* **120**, 827-841.

Ishikawa, H. O., Takeuchi, H., Haltiwanger, R. S. and Irvine, K. D. (2008). Four-jointed is a Golgi kinase that phosphorylates a subset of cadherin domains. *Science* **321**, 401-404.

Ito, K., Awano, W., Suzuki, K., Hiromi, Y. and Yamamoto, D. (1997). The Drosophila mushroom body is a quadruple structure of clonal units each of which contains a virtually identical set of neurones and glial cells. *Development* **124**, 761-771.

Jahne, B. (2004). *Practical Handbook on Image Processing for Scientific and Technical Applications, Second Edition*: CRC Press, Inc.

Jennifer, A. Z. and Richard, Z. (2004). Cell-pattern disordering during convergent extension in Drosophila. *Journal of Physics: Condensed Matter* **16**, S5073.

Jia, J., Zhang, W., Wang, B., Trinko, R. and Jiang, J. (2003). The Drosophila Ste20 family kinase dMST functions as a tumor suppressor by restricting cell proliferation and promoting apoptosis. *Genes Dev* **17**, 2514-2519.

Justice, R. W., Zilian, O., Woods, D. F., Noll, M. and Bryant, P. J. (1995). The Drosophila tumor suppressor gene warts encodes a homolog of human myotonic dystrophy kinase and is required for the control of cell shape and proliferation. *Genes Dev* **9**, 534-546.

Kafer, J., Hayashi, T., Maree, A. F., Carthew, R. W. and Graner, F. (2007). Cell adhesion and cortex contractility determine cell patterning in the Drosophila retina. *Proc Natl Acad Sci U S A* **104**, 18549-18554.

Keller, R. (2006). Mechanisms of elongation in embryogenesis. *Development* **133**, 2291-2302.

Kiehart, D. P., Galbraith, C. G., Edwards, K. A., Rickoll, W. L. and Montague, R. A. (2000). Multiple forces contribute to cell sheet morphogenesis for dorsal closure in Drosophila. *The Journal of cell biology* **149**, 471-490.

Koontz, L. M., Liu-Chittenden, Y., Yin, F., Zheng, Y., Yu, J., Huang, B., Chen, Q., Wu, S. and Pan, D. (2013). The Hippo effector Yorkie controls normal tissue growth by antagonizing scalloped-mediated default repression. *Dev Cell* **25**, 388-401.

Kopp, A., Blackman, R. K. and Duncan, I. (1999). Wingless, decapentaplegic and EGF receptor signaling pathways interact to specify dorso-ventral pattern in the adult abdomen of Drosophila. *Development* **126**, 3495-3507.

Kopp, A. and Duncan, I. (1997). Control of cell fate and polarity in the adult abdominal segments of Drosophila by optomotor-blind. *Development* **124**, 3715-3726.

Kopp, A., Muskavitch, M. A. and Duncan, I. (1997). The roles of hedgehog and engrailed in patterning adult abdominal segments of Drosophila. *Development* **124**, 3703-3714.

Kornberg, T. (1981). Compartments in the abdomen of Drosophila and the role of the engrailed locus. *Dev Biol* **86**, 363-372.

Kornberg, T., Siden, I., O'Farrell, P. and Simon, M. (1985). The engrailed locus of Drosophila: in situ localization of transcripts reveals compartment-specific expression. *Cell* **40**, 45-53.

Kylsten, P. and Saint, R. (1997). Imaginal tissues of Drosophila melanogaster exhibit different modes of cell proliferation control. *Dev Biol* **192**, 509-522.

Landsberg, K. P., Farhadifar, R., Ranft, J., Umetsu, D., Widmann, T. J., Bittig, T., Said, A., Julicher, F. and Dahmann, C. (2009). Increased cell bond tension governs cell sorting at the Drosophila anteroposterior compartment boundary. *Curr Biol* **19**, 1950-1955.

Lawrence, P. A., Casal, J. and Struhl, G. (1999). The hedgehog morphogen and gradients of cell affinity in the abdomen of Drosophila. *Development* **126**, 2441-2449.

Lawrence, P. A., Casal, J. and Struhl, G. (2002). Towards a model of the organisation of planar polarity and pattern in the Drosophila abdomen. *Development* **129**, 2749-2760.

Lawrence, P. A., Casal, J. and Struhl, G. (2004). Cell interactions and planar polarity in the abdominal epidermis of Drosophila. *Development* **131**, 4651-4664.

Lawrence, P. A., Struhl, G. and Casal, J. (2007). Planar cell polarity: one or two pathways? *Nat Rev Genet* **8**, 555-563.

Lecuit, T. (2005). Adhesion remodeling underlying tissue morphogenesis. *Trends Cell Biol* **15**, 34-42.

Lecuit, T. and Lenne, P. F. (2007). Cell surface mechanics and the control of cell shape, tissue patterns and morphogenesis. *Nature reviews. Molecular cell biology* **8**, 633-644.

Lecuit, T., Lenne, P. F. and Munro, E. (2011). Force generation, transmission, and integration during cell and tissue morphogenesis. *Annu Rev Cell Dev Biol* **27**, 157-184.

Lee, J. J., von Kessler, D. P., Parks, S. and Beachy, P. A. (1992). Secretion and localized transcription suggest a role in positional signaling for products of the segmentation gene hedgehog. *Cell* **71**, 33-50.

Legoff, L., Rouault, H. and Lecuit, T. (2013). A global pattern of mechanical stress polarizes cell divisions and cell shape in the growing Drosophila wing disc. *Development* **140**, 4051-4059.

Li, R. and Bowerman, B. (2010). Symmetry breaking in biology. *Cold Spring Harb Perspect Biol* **2**, a003475.

Lindsley, D. L. and Zimm, G. G. (1992). *The Genome of Drosophila melanogaster*.

Londono, C., Loureiro, M. J., Slater, B., Lucker, P. B., Soleas, J., Sathananthan, S., Aitchison, J. S., Kabla, A. J. and McGuigan, A. P. (2014). Nonautonomous contact guidance signaling during collective cell migration. *Proc Natl Acad Sci U S A* **111**, 1807-1812.

Ma, D., Yang, C. H., McNeill, H., Simon, M. A. and Axelrod, J. D. (2003). Fidelity in planar cell polarity signalling. *Nature* **421**, 543-547.

Madhavan, K. and Madhavan, M. M. (1995). Defects in the adult abdominal integument of Drosophila caused by mutations in torpedo, a DER homolog. *Roux's Archives of Developmental Biology* **204**, 330-335.

Madhavan, M. M. and Madhavan, K. (1980). Morphogenesis of the epidermis of adult abdomen of Drosophila. *J Embryol Exp Morphol* **60**, 1-31.

Madhavan, M. M. and Madhavan, K. (2004). Analysis of histoblasts. *Methods Mol Biol* **247**, 413-430.

Madhavan, M. M. and Schneiderman, H. A. (1977). Histological analysis of the dynamics of growth of imaginal discs and histoblast nests during the larval development of Drosophila melanogaster. *Roux's Archives of Developmental Biology* **183**, 269-305.

Mahoney, P. A., Weber, U., Onofrechuk, P., Biessmann, H., Bryant, P. J. and Goodman, C. S. (1991). The fat tumor suppressor gene in Drosophila encodes a novel member of the cadherin gene superfamily. *Cell* **67**, 853-868.

Major, R. J. and Irvine, K. D. (2006). Localization and requirement for Myosin II at the dorsal-ventral compartment boundary of the Drosophila wing. *Dev Dyn* **235**, 3051-3058.

Mao, Y. and Baum, B. (2015). Tug of war--the influence of opposing physical forces on epithelial cell morphology. *Dev Biol* **401**, 92-102.

Mao, Y., Rauskolb, C., Cho, E., Hu, W. L., Hayter, H., Minihan, G., Katz, F. N. and Irvine, K. D. (2006). Dachs: an unconventional myosin that functions downstream of Fat to regulate growth, affinity and gene expression in Drosophila. *Development* **133**, 2539-2551.

Mao, Y., Tournier, A. L., Bates, P. A., Gale, J. E., Tapon, N. and Thompson, B. J. (2011). Planar polarization of the atypical myosin Dachs orients cell divisions in Drosophila. *Genes Dev* **25**, 131-136.

Mao, Y., Tournier, A. L., Hoppe, A., Kester, L., Thompson, B. J. and Tapon, N. (2013). Differential proliferation rates generate patterns of mechanical tension that orient tissue growth. *EMBO J* **32**, 2790-2803.

Matakatsu, H. and Blair, S. S. (2004). Interactions between Fat and Dachsous and the regulation of planar cell polarity in the Drosophila wing. *Development* **131**, 3785-3794.

Matakatsu, H. and Blair, S. S. (2006). Separating the adhesive and signaling functions of the Fat and Dachsous protocadherins. *Development* **133**, 2315-2324.

Matakatsu, H. and Blair, S. S. (2008). The DHHC palmitoyltransferase approximated regulates Fat signaling and Dachs localization and activity. *Curr Biol* **18**, 1390-1395.

Maung, S. M. and Jenny, A. (2011). Planar cell polarity in Drosophila. *Organogenesis* **7**, 165-179.

McKenzie, E., Krupin, A. and Kelley, M. W. (2004). Cellular growth and rearrangement during the development of the mammalian organ of Corti. *Dev Dyn* **229**, 802-812.

Meng, Z., Moroishi, T. and Guan, K. L. (2016). Mechanisms of Hippo pathway regulation. *Genes Dev* **30**, 1-17.

Merkel, M., Sagner, A., Gruber, F. S., Etournay, R., Blasse, C., Myers, E., Eaton, S. and Julicher, F. (2014). The balance of prickle/spiny-legs isoforms controls the amount of coupling between core and fat PCP systems. *Curr Biol* **24**, 2111-2123.

Mohler, J. and Vani, K. (1992). Molecular organization and embryonic expression of the hedgehog gene involved in cell-cell communication in segmental patterning of Drosophila. *Development* **115**, 957-971.

Monier, B., Pelissier-Monier, A., Brand, A. H. and Sanson, B. (2010). An actomyosin-based barrier inhibits cell mixing at compartmental boundaries in Drosophila embryos. *Nat Cell Biol* **12**, 60-65; sup pp 61-69.

Morata, G. and Lawrence, P. A. (1975). Control of compartment development by the engrailed gene in Drosophila. *Nature* **255**, 614-617.

Nardi, J. B. and Kafatos, F. C. (1976). Polarity and gradients in lepidopteran wing epidermis. II. The differential adhesiveness model: gradient of a non-diffusible cell surface parameter. *J Embryol Exp Morphol* **36**, 489-512.

Ninov, N., Chiarelli, D. A. and Martin-Blanco, E. (2007). Extrinsic and intrinsic mechanisms directing epithelial cell sheet replacement during Drosophila metamorphosis. *Development* **134**, 367-379.

Ninov, N., Manjon, C. and Martin-Blanco, E. (2009). Dynamic control of cell cycle and growth coupling by ecdysone, EGFR, and PI3K signaling in Drosophila histoblasts. *PLoS Biol* **7**, e1000079.

Ninov, N. and Martin-Blanco, E. (2007). Live imaging of epidermal morphogenesis during the development of the adult abdominal epidermis of Drosophila. *Nat Protoc* **2**, 3074-3080.

Ninov, N., Menezes-Cabral, S., Prat-Rojo, C., Manjon, C., Weiss, A., Pyrowolakis, G., Affolter, M. and Martin-Blanco, E. (2010). Dpp signaling directs cell motility and invasiveness during epithelial morphogenesis. *Curr Biol* **20**, 513-520.

Nubler-Jung, K., Bonitz, R. and Sonnenschein, M. (1987). Cell polarity during wound healing in an insect epidermis. *Development* **100**, 163-170.

Nubler-Jung, K. and Mardini, B. (1990). Insect epidermis: polarity patterns after grafting result from divergent cell adhesions between host and graft tissue. *Development* **110**, 1071-1079.

Oda, H. and Tsukita, S. (2001). Real-time imaging of cell-cell adherens junctions reveals that Drosophila mesoderm invagination begins with two phases of apical constriction of cells. *J Cell Sci* **114**, 493-501.

Oh, H. and Irvine, K. D. (2008). In vivo regulation of Yorkie phosphorylation and localization. *Development* **135**, 1081-1088.

Oh, H. and Irvine, K. D. (2010). Yorkie: the final destination of Hippo signaling. *Trends Cell Biol* **20**, 410-417.

Oh, H., Reddy, B. V. and Irvine, K. D. (2009). Phosphorylation-independent repression of Yorkie in Fat-Hippo signaling. *Dev Biol* **335**, 188-197.

Olguin, P. and Mlodzik, M. (2010). A new spin on planar cell polarity. *Cell* **142**, 674-676.

Pantalacci, S., Tapon, N. and Leopold, P. (2003). The Salvador partner Hippo promotes apoptosis and cell-cycle exit in Drosophila. *Nat Cell Biol* **5**, 921-927.

Parsons, L. M., Grzeschik, N. A. and Richardson, H. E. (2014). lgl Regulates the Hippo Pathway Independently of Fat/Dachs, Kibra/Expanded/Merlin and dRASSF/dSTRIPAK. *Cancers (Basel)* **6**, 879-896.

Pearson, M. J. (1974). The abdominal epidermis of Calliphora erythrocephala (Diptera). I. Polyteny and growth in the larval cells. *J Cell Sci* **16**, 113-131.

Pflugfelder, G. O., Roth, H., Poeck, B., Kerscher, S., Schwarz, H., Jonschker, B. and Heisenberg, M. (1992). The lethal(1)optomotor-blind gene of Drosophila melanogaster is a major organizer of optic lobe development: isolation and characterization of the gene. *Proc Natl Acad Sci U S A* **89**, 1199-1203.

Piccolo, S., Dupont, S. and Cordenonsi, M. (2014). The biology of YAP/TAZ: hippo signaling and beyond. *Physiol Rev* **94**, 1287-1312.

Poodry, C. A. (1975). Autonomous and non-autonomous cell death in the metamorphosis of the epidermis ofDrosophila. *Wilhelm Roux's archives of developmental biology* **178**, 333-336.

Priya, R. and Yap, A. S. (2015). Active tension: the role of cadherin adhesion and signaling in generating junctional contractility. *Current topics in developmental biology* **112**, 65-102.

Puspoki, Z. and Unser, M. (2015). Template-free wavelet-based detection of local symmetries. *IEEE Trans Image Process* **24**, 3009-3018.

Rawls, A. S., Guinto, J. B. and Wolff, T. (2002). The cadherins fat and dachsous regulate dorsal/ventral signaling in the Drosophila eye. *Curr Biol* **12**, 1021-1026.

Reig, G., Pulgar, E. and Concha, M. L. (2014). Cell migration: from tissue culture to embryos. *Development* **141**, 1999-2013.

Ren, F., Zhang, L. and Jiang, J. (2010). Hippo signaling regulates Yorkie nuclear localization and activity through 14-3-3 dependent and independent mechanisms. *Dev Biol* **337**, 303-312.

Rezakhaniha, R., Agianniotis, A., Schrauwen, J. T., Griffa, A., Sage, D., Bouten, C. V., van de Vosse, F. N., Unser, M. and Stergiopulos, N. (2012). Experimental investigation of collagen waviness and orientation in the arterial adventitia using confocal laser scanning microscopy. *Biomech Model Mechanobiol* **11**, 461-473.

Roberts, W. M., Howard, J. and Hudspeth, A. J. (1988). Hair cells: transduction, tuning, and transmission in the inner ear. *Annu Rev Cell Biol* **4**, 63-92.

Robertson, C. W. (1936). The metamorphosis of Drosophila melanogaster, including an accurately timed account of the principal morphological changes. *Journal of Morphology* **59**, 351-399.

Rogulja, D., Rauskolb, C. and Irvine, K. D. (2008). Morphogen control of wing growth through the Fat signaling pathway. *Dev Cell* **15**, 309-321.

Roseland, C. R. and Schneiderman, H. A. (1979). Regulation and metamorphosis of the abdominal histoblasts of Drosophila melanogaster. *Roux's Archives of Developmental Biology* **186**, 235-265.

Roth, S. and Lynch, J. A. (2009). Symmetry breaking during Drosophila oogenesis. *Cold Spring Harb Perspect Biol* **1**, a001891.

Saburi, S. and McNeill, H. (2005). Organising cells into tissues: new roles for cell adhesion molecules in planar cell polarity. *Curr Opin Cell Biol* **17**, 482-488.

Sagner, A., Merkel, M., Aigouy, B., Gaebel, J., Brankatschk, M., Julicher, F. and Eaton, S. (2012). Establishment of global patterns of planar polarity during growth of the Drosophila wing epithelium. *Curr Biol* **22**, 1296-1301.

Salbreux, G., Barthel, L. K., Raymond, P. A. and Lubensky, D. K. (2012). Coupling mechanical deformations and planar cell polarity to create regular patterns in the zebrafish retina. *PLoS Comput Biol* **8**, e1002618.

Santamaria, P. and Garcia-Bellido, A. (1972). Localization and growth pattern of the tergite Anlage of Drosophila. *J Embryol Exp Morphol* **28**, 397-417.

Sauret-Gueto, S., Schiessl, K., Bangham, A., Sablowski, R. and Coen, E. (2013). JAGGED controls Arabidopsis petal growth and shape by interacting with a divergent polarity field. *PLoS Biol* **11**, e1001550.

Schock, F. and Perrimon, N. (2002). Cellular processes associated with germ band retraction in Drosophila. *Dev Biol* **248**, 29-39.

Schwander, M., Kachar, B. and Muller, U. (2010). Review series: The cell biology of hearing. *The Journal of cell biology* **190**, 9-20.

Seifert, J. R. and Mlodzik, M. (2007). Frizzled/PCP signalling: a conserved mechanism regulating cell polarity and directed motility. *Nat Rev Genet* **8**, 126-138.

Sharma, P. and McNeill, H. (2013). Regulation of long-range planar cell polarity by Fat-Dachsous signaling. *Development* **140**, 3869-3881.

Sharma, S. and Mukhopadhyay, G. (2009). Shape-dependent force between magnetic nanoparticles in a colloidal ferro-fluid. *J Nanosci Nanotechnol* **9**, 5448-5450.

Shimada, Y., Usui, T., Yanagawa, S., Takeichi, M. and Uemura, T. (2001). Asymmetric colocalization of Flamingo, a seven-pass transmembrane cadherin, and Dishevelled in planar cell polarization. *Curr Biol* **11**, 859-863.

Shirras, A. D. and Couso, J. P. (1996). Cell fates in the adult abdomen of Drosophila are determined by wingless during pupal development. *Dev Biol* **175**, 24-36.

Shuai, M., Klittnick, A., Shen, Y., Smith, G. P., Tuchband, M. R., Zhu, C., Petschek, R. G., Mertelj, A., Lisjak, D., Copic, M., et al. (2016). Spontaneous liquid crystal and ferromagnetic ordering of colloidal magnetic nanoplates. *Nat Commun* **7**, 10394.

Silva, E., Tsatskis, Y., Gardano, L., Tapon, N. and McNeill, H. (2006). The tumor-suppressor gene fat controls tissue growth upstream of expanded in the hippo signaling pathway. *Curr Biol* **16**, 2081-2089.

Simon, M. A. (2004). Planar cell polarity in the Drosophila eye is directed by graded Four-jointed and Dachsous expression. *Development* **131**, 6175-6184.

Simon, M. A., Xu, A., Ishikawa, H. O. and Irvine, K. D. (2010). Modulation of fat:dachsous binding by the cadherin domain kinase four-jointed. *Curr Biol* **20**, 811-817.

Singh, J. and Mlodzik, M. (2012). Planar cell polarity signaling: coordination of cellular orientation across tissues. *Wiley Interdiscip Rev Dev Biol* **1**, 479-499.

Sisson, B. E., Ziegenhorn, S. L. and Holmgren, R. A. (2006). Regulation of Ci and Su(fu) nuclear import in Drosophila. *Dev Biol* **294**, 258-270.

Sopko, R. and McNeill, H. (2009). The skinny on Fat: an enormous cadherin that regulates cell adhesion, tissue growth, and planar cell polarity. *Curr Opin Cell Biol* **21**, 717-723.

St Johnston, D. and Nusslein-Volhard, C. (1992). The origin of pattern and polarity in the Drosophila embryo. *Cell* **68**, 201-219.

Struhl, G., Barbash, D. A. and Lawrence, P. A. (1997a). Hedgehog acts by distinct gradient and signal relay mechanisms to organise cell type and cell polarity in the Drosophila abdomen. *Development* **124**, 2155-2165.

Struhl, G., Barbash, D. A. and Lawrence, P. A. (1997b). Hedgehog organises the pattern and polarity of epidermal cells in the Drosophila abdomen. *Development* **124**, 2143-2154.

Struhl, G. and Basler, K. (1993). Organizing activity of wingless protein in Drosophila. *Cell* **72**, 527-540.

Strutt, D. (2009). Gradients and the specification of planar polarity in the insect cuticle. *Cold Spring Harb Perspect Biol* **1**, a000489.

Strutt, D., Johnson, R., Cooper, K. and Bray, S. (2002). Asymmetric localization of frizzled and the determination of notch-dependent cell fate in the Drosophila eye. *Curr Biol* **12**, 813-824.

Strutt, D. and Strutt, H. (2007). Differential activities of the core planar polarity proteins during Drosophila wing patterning. *Dev Biol* **302**, 181-194.

Strutt, D. I. (2001). Asymmetric localization of frizzled and the establishment of cell polarity in the Drosophila wing. *Molecular cell* **7**, 367-375.

Strutt, H., Mundy, J., Hofstra, K. and Strutt, D. (2004). Cleavage and secretion is not required for Four-jointed function in Drosophila patterning. *Development* **131**, 881-890.

Strutt, H. and Strutt, D. (2002). Nonautonomous planar polarity patterning in Drosophila: dishevelled-independent functions of frizzled. *Dev Cell* **3**, 851-863.

Strutt, H. and Strutt, D. (2008). Differential stability of flamingo protein complexes underlies the establishment of planar polarity. *Curr Biol* **18**, 1555-1564.

Strutt, H. and Strutt, D. (2009). Asymmetric localisation of planar polarity proteins: Mechanisms and consequences. *Semin Cell Dev Biol* **20**, 957-963.

Strutt, H., Warrington, S. J. and Strutt, D. (2011). Dynamics of core planar polarity protein turnover and stable assembly into discrete membrane subdomains. *Dev Cell* **20**, 511-525.

Tabata, T., Eaton, S. and Kornberg, T. B. (1992). The Drosophila hedgehog gene is expressed specifically in posterior compartment cells and is a target of engrailed regulation. *Genes Dev* **6**, 2635-2645.

Takeichi, M., Nakagawa, S., Aono, S., Usui, T. and Uemura, T. (2000). Patterning of cell assemblies regulated by adhesion receptors of the cadherin superfamily. *Philos Trans R Soc Lond B Biol Sci* **355**, 885-890.

Tapon, N., Harvey, K. F., Bell, D. W., Wahrer, D. C., Schiripo, T. A., Haber, D. and Hariharan, I. K. (2002). salvador Promotes both cell cycle exit and apoptosis in Drosophila and is mutated in human cancer cell lines. *Cell* **110**, 467-478.

Taylor, J., Abramova, N., Charlton, J. and Adler, P. N. (1998). Van Gogh: a new Drosophila tissue polarity gene. *Genetics* **150**, 199-210.

Tepass, U., Tanentzapf, G., Ward, R. and Fehon, R. (2001). Epithelial cell polarity and cell junctions in Drosophila. *Annual review of genetics* **35**, 747-784.

Thomas, C. and Strutt, D. (2012). The roles of the cadherins Fat and Dachsous in planar polarity specification in Drosophila. *Dev Dyn* **241**, 27-39.

Thompson, D. A. W. (1945). *On growth and form / by D'Arcy Wentworth Thompson*. Cambridge :: University Press ;.

Thoreson, M. A., Anastasiadis, P. Z., Daniel, J. M., Ireton, R. C., Wheelock, M. J., Johnson, K. R., Hummingbird, D. K. and Reynolds, A. B. (2000). Selective uncoupling of p120(ctn) from E-cadherin disrupts strong adhesion. *The Journal of cell biology* **148**, 189-202.

Thummel, C. S. (2001). Molecular mechanisms of developmental timing in C. elegans and Drosophila. *Dev Cell* **1**, 453-465.

Tree, D. R., Shulman, J. M., Rousset, R., Scott, M. P., Gubb, D. and Axelrod, J. D. (2002). Prickle mediates feedback amplification to generate asymmetric planar cell polarity signaling. *Cell* **109**, 371-381.

Turner, C. M. and Adler, P. N. (1995). Morphogenesis of Drosophila pupal wings in vitro. *Mech Dev* **52**, 247-255.

Tyler, D. M. and Baker, N. E. (2007). Expanded and fat regulate growth and differentiation in the Drosophila eye through multiple signaling pathways. *Dev Biol* **305**, 187-201.

Udan, R. S., Kango-Singh, M., Nolo, R., Tao, C. and Halder, G. (2003). Hippo promotes proliferation arrest and apoptosis in the Salvador/Warts pathway. *Nat Cell Biol* **5**, 914-920.

Umetsu, D., Dunst, S. and Dahmann, C. (2014). An RNA interference screen for genes required to shape the anteroposterior compartment boundary in Drosophila identifies the Eph receptor. *PLoS One* **9**, e114340.

Usui, T., Shima, Y., Shimada, Y., Hirano, S., Burgess, R. W., Schwarz, T. L., Takeichi, M. and Uemura, T. (1999). Flamingo, a seven-pass transmembrane cadherin, regulates planar cell polarity under the control of Frizzled. *Cell* **98**, 585-595.

Vichas, A. and Zallen, J. A. (2011). Translating cell polarity into tissue elongation. *Semin Cell Dev Biol* **22**, 858-864.

Villano, J. L. and Katz, F. N. (1995). four-jointed is required for intermediate growth in the proximal-distal axis in Drosophila. *Development* **121**, 2767-2777.

Vinson, C. R. and Adler, P. N. (1987). Directional non-cell autonomy and the transmission of polarity information by the frizzled gene of Drosophila. *Nature* **329**, 549-551.

Vogg, M. C., Wenger, Y. and Galliot, B. (2016). How Somatic Adult Tissues Develop Organizer Activity. *Current topics in developmental biology* **116**, 391-414.

Wang, J., Mark, S., Zhang, X., Qian, D., Yoo, S. J., Radde-Gallwitz, K., Zhang, Y., Lin, X., Collazo, A., Wynshaw-Boris, A., et al. (2005). Regulation of polarized extension and planar cell polarity in the cochlea by the vertebrate PCP pathway. *Nat Genet* **37**, 980-985.

Wang, Y. and Nathans, J. (2007). Tissue/planar cell polarity in vertebrates: new insights and new questions. *Development* **134**, 647-658.

Wedlich, D. (2002). The polarising role of cell adhesion molecules in early development. *Curr Opin Cell Biol* **14**, 563-568.

Wheelock, M. J. and Johnson, K. R. (2003). Cadherin-mediated cellular signaling. *Curr Opin Cell Biol* **15**, 509-514.

Whiteley, M., Noguchi, P. D., Sensabaugh, S. M., Odenwald, W. F. and Kassis, J. A. (1992). The Drosophila gene escargot encodes a zinc finger motif found in snail-related genes. *Mech Dev* **36**, 117-127.

Willecke, M., Hamaratoglu, F., Sansores-Garcia, L., Tao, C. and Halder, G. (2008). Boundaries of Dachsous Cadherin activity modulate the Hippo signaling pathway to induce cell proliferation. *Proc Natl Acad Sci U S A* **105**, 14897-14902.

Wong, L. L. and Adler, P. N. (1993). Tissue polarity genes of Drosophila regulate the subcellular location for prehair initiation in pupal wing cells. *The Journal of cell biology* **123**, 209-221.

Wootton, R. J. (1992). Functional Morphology of Insect Wings. *Annual Review of Entomology* **37**, 113-140.

Wright, L. G., Chen, T., Thummel, C. S. and Guild, G. M. (1996). Molecular characterization of the 71E late puff in Drosophila melanogaster reveals a family of novel genes. *J Mol Biol* **255**, 387-400.

Wu, J. and Mlodzik, M. (2009). A quest for the mechanism regulating global planar cell polarity of tissues. *Trends Cell Biol* **19**, 295-305.

Wu, S., Huang, J., Dong, J. and Pan, D. (2003). hippo encodes a Ste-20 family protein kinase that restricts cell proliferation and promotes apoptosis in conjunction with salvador and warts. *Cell* **114**, 445-456.

Wu, S., Liu, Y., Zheng, Y., Dong, J. and Pan, D. (2008). The TEAD/TEF family protein Scalloped mediates transcriptional output of the Hippo growth-regulatory pathway. *Dev Cell* **14**, 388-398.

Xu, T. and Rubin, G. M. (1993). Analysis of genetic mosaics in developing and adult Drosophila tissues. *Development* **117**, 1223-1237.

Xu, T., Wang, W., Zhang, S., Stewart, R. A. and Yu, W. (1995). Identifying tumor suppressors in genetic mosaics: the Drosophila lats gene encodes a putative protein kinase. *Development* **121**, 1053-1063.

Yang, C. H., Axelrod, J. D. and Simon, M. A. (2002). Regulation of Frizzled by fat-like cadherins during planar polarity signaling in the Drosophila compound eye. *Cell* **108**, 675-688.

Yap, A. S., Niessen, C. M. and Gumbiner, B. M. (1998). The juxtamembrane region of the cadherin cytoplasmic tail supports lateral clustering, adhesive strengthening, and interaction with p120ctn. *The Journal of cell biology* **141**, 779-789.

Zallen, J. A. (2007). Planar polarity and tissue morphogenesis. *Cell* **129**, 1051-1063.

Zallen, J. A. and Blankenship, J. T. (2008). Multicellular dynamics during epithelial elongation. *Semin Cell Dev Biol* **19**, 263-270.

Zallen, J. A. and Wieschaus, E. (2004). Patterned gene expression directs bipolar planar polarity in Drosophila. *Dev Cell* **6**, 343-355.

Zeidler, M. P., Perrimon, N. and Strutt, D. I. (2000). Multiple roles for four-jointed in planar polarity and limb patterning. *Dev Biol* **228**, 181-196.

Zhang, L., Ren, F., Zhang, Q., Chen, Y., Wang, B. and Jiang, J. (2008). The TEAD/TEF family of transcription factor Scalloped mediates Hippo signaling in organ size control. *Dev Cell* **14**, 377-387.

Zhu, H. (2009). Is anisotropic propagation of polarized molecular distribution the common mechanism of swirling patterns of planar cell polarization? *J Theor Biol* **256**, 315-325.